KINETIC CHARACTERIZATION OF SITE-DIRECTED MUTANTS OF THE CONSERVED ACTIVE-SITE PHENYLALANINE OF URACIL-DNA GLYCOSYLASE FROM *Escherichia coli*

By

RYAN W. SHAW

A DISSERTATION PRESENTED TO THE GRADUATE SCHOOL
OF THE UNIVERSITY OF FLORIDA IN PARTIAL FULFILLMENT
OF THE REQUIREMENTS FOR THE DEGREE OF
DOCTOR OF PHILOSOPHY

UNIVERSITY OF FLORIDA

2003

Copyright 2003

by

Ryan W. Shaw

This work is dedicated to Carl Sagan, whose writings inspired me to choose science as my vocation.

ACKNOWLEDGMENTS

I am in eternal gratitude to my parents whose love and support helped push me through the trials of life and graduate school. I would also like to thank Linda Bloom for getting me involved in the very rewarding research training at ASU and giving me a opportunity in her lab.

TABLE OF CONTENTS

Page

LIST OF TABLES

LIST OF FIGURES

Abstract of Dissertation Presented to the Graduate School
of the University of Florida in Partial Fulfillment of the
Requirements for the Degree of Doctor of Philosophy

KINETIC CHARACTERIZATION OF SITE-DIRECTED MUTANTS OF THE CONSERVED ACTIVE-SITE PHENYLALANINE OF URACIL-DNA GLYCOSYLASE FROM *Escherichia coli*

By

Ryan W. Shaw

December 2003

Chair: Linda B. Bloom
Major Department: Biochemistry and Molecular Biology

Uracil is removed from DNA by the highly conserved uracil-DNA glycosylase (UDG), which hydrolyzes the *N*-glycosidic bond of deoxyuridine (dU), starting the base excision and repair pathway. This specific and powerful catalyst can lower the activation barrier of deoxyuridine (dU) cleavage by almost 16 kcal/mol, yet UDG exhibits no detectable *N*-glycosidic bond cleavage of other structurally similar bases. In an effort to better understand how UDG is such a powerful and specific catalyst, mutational analysis was performed on a conserved active-site phenylalanine (Phe77) that π-stacks with the uracil ring of the substrate.

The Phe77 mutations did not change the specificity of UDG as the mutants showed no detectable activity toward normal DNA. Under single-turnover conditions the F77A and F77Y mutations had a mild 2.0 and 1.6 kcal/mol destabilizing effects (respectively) on the activation barrier of glycosidic bond cleavage, while changing Phe77 into

asparagine has a surprisingly large 4.2 kcal/mol destabilizing effect. The alanine mutation was relatively more detrimental on UDG's activity toward dsDNA rather than ssDNA substrates, indicating Phe77 contributes to dU binding in duplex DNA.

The glycosylase's ability to bind dU in double-stranded DNA was monitored through changes in its intrinsic tryptophan (Trp) fluorescence. As wild-type UDG binds dU-containing DNA its Trp fluorescence quenches and then recovers as the enzyme releases the products after catalysis. The F77N and F77Y mutations had little effect on the Trp quenching kinetics, while the F77A mutant's Trp signal was disrupted and uninterpretable. This indicated that at least the F77N and F77Y mutations had not affected the flipping and dU binding of UDG. All UDG variants studied showed a phase of Trp fluorescence recovery that happened at approximately the same rate as the steady-state rate of catalysis.

These results indicate the active-site phenylalanine has a small, but significant, contribution to transition state stabilization. The large effect of the F77N mutation could possibly be attributed to this polar group perturbing the nonpolar environment of the normal UDG active site. These results have implications for proposed UDG reaction mechanisms and demonstrate how seemingly small changes in an enzyme's active site can affect a finely tuned catalyst.

CHAPTER 1
BACKGROUND AND SIGNIFICANCE

Uracil in DNA: An Ancient Problem

Roughly three billion years ago life took a major step forward by reassigning the task of genetic information storage from ribonucleosides to deoxyribonucleosides [1-4]. Presumably, some time after this transition, organisms evolved to use deoxythymidine (dT) instead of deoxyuridine (dU) in their genomes [5-8]. The organisms that evolved to use dT were bestowed the advantage of being able to distinguish between a proper coding adenine base-pairing partner from the mutagenic dU formed from deamination of cytosine, thus supplying an added level of genomic stability [8]. Of course, this advantage is only realized if the organism has evolved a way of repairing deaminated cytosine before the next round of DNA replication fixes the C:G→T:A transition mutation. Thus it appears that the ability to excise and repair dU was an extremely important part of the evolution of modern DNA genomes.

Today's DNA-based organisms have to deal with uracil that arises in DNA via three sources: spontaneous deamination of cytosine; polymerase incorporation of deoxyuridine triphosphate (dUTP); and enzymatic deamination of cytosine. Each of these scenarios is discussed in detail.

Spontaneous Deamination of Cytosine

Cytosine is the most unstable of the four natural bases because of the vulnerability of the exocyclic amine at position C4 of the pyrimidine ring to hydrolysis. This hydrolytic deamination reaction has been proposed to follow two mechanisms [9, 10].

The supposed major, or "direct," reaction involves protonation at the N3 position of cytosine followed by direct nucleophilic attack by hydroxyl ion and the subsequent elimination of the amino group at the C4 position. Another cytosine deamination mechanism is proposed to occur by an addition–elimination mechanism. Water first adds to the C5=C6 double bond to form an unstable 5,6-dihydrocytosine. The C4 amino group is then replaced by a carbonyl; and dehydration of the resulting dihydrouridine produces uracil. This alternative seems unlikely because 5-methylcytosine should resist deamination for both steric and electrostatic reasons; but instead is deaminated 3-4 times more rapidly [11-13].

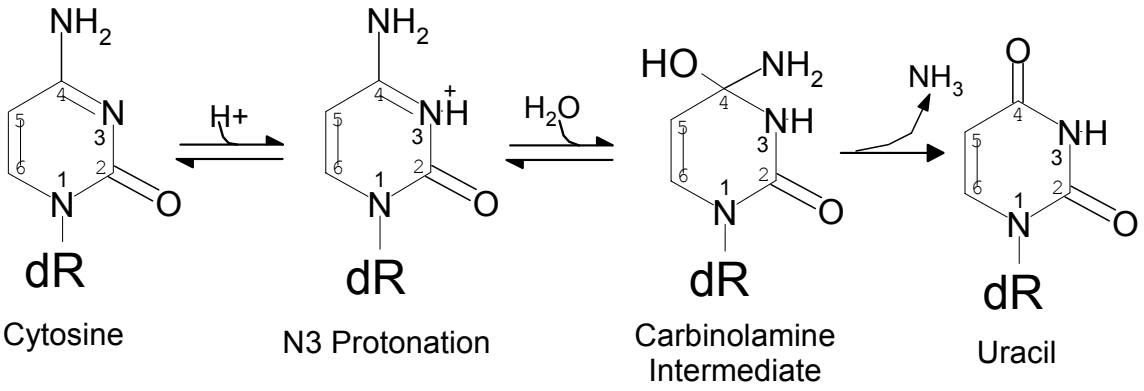

Figure 1-1. Major reaction mechanism for the spontaneous deamination of cytosine to uracil. This reaction pathway is the "direct route" to hydrolytic deamination (see text).

Cytosine deamination rates have been measured in a number of ways. The earliest studies followed the conversion of cytosine to uracil as function of pH, temperature, and DNA secondary structure. Cytosine in single-stranded DNA, poly(dC), or poly(dCMP) was equally susceptible to deamination in aqueous solution buffered at pH 7.4 and incubated at 95˚C ($k \approx 2 \times 10^{-7}$ sec^{-1}) [11]. From these measurements Lindahl and

Nyberg [11] extrapolated a spontaneous deamination rate of < 1 X 10^{-12} for the reaction at 37˚C, and an activation energy of 29 kcal/mol.

This extrapolation was confirmed *en vivo* by a sensitive genetic assay based on C→T reversion frequency of a site-specific mutation in the *lacZ*$_{\alpha}$ gene of bacteriophage M13mp2 [14]. Influence of temperature, incubation time, and repair by UDG on reversion rates was measured. The genetic-based assay gave rates for cytosine deamination of 1 x 10^{-10} s^{-1} in single-stranded DNA and 7 x 10^{-13} s^{-1} in double-stranded DNA. These rates convert to half-lives of 200 years and 30,000 years for cytosine in single- and double-stranded DNA, respectively. At first glance, these half-lives might suggest that spontaneous deamination is not a serious threat to genomic stability. However, if one multiplies the half-life for the deamination reaction by the number of cytosines in the large human genome (in both ssDNA and dsDNA), approximately 100 uracil lesions per cell per day would accumulate if not repaired. As stated earlier, if U:G mispairs resulting from spontaneous deamination are not repaired before the next round of replication, they result in transition mutations (C:G→T:A).

The approximate 150-fold stabilization of cytosine in duplex over single-stranded DNA is thought to reflect the shielding that the hydrogen bond formed by the N1 donor proton of guanine gives to the N3 of cytosine. This would protect the N3 from protonation, thus preventing hydrolytic deamination via the direct mechanism. In support of this hypothesis, deamination rate constants for a C:C mispair (0.4 x $10^{-10}s^{-1}$) and a T:C mispair (1.3 x $10^{-10}s^{-1}$) approximate those of single-stranded DNA, emphasizing the importance of proper base-pairing and the resultant hydrogen bonding in protecting the N3 position of cytosine [15]. Also in agreement with this interpretation, the presence of

O^6-alkylguanine can catalyze "cross-strand deamination" where methylation of O6 of a guanine opposite cytosine favors protonation of that cytosine at N3 from the donor guanine, which promotes deamination [16, 17].

Therefore, it is now generally accepted that cytosine deamination most likely occurs via a single-stranded intermediate. This implies that cells that have a significant proportion of their genomes in single-stranded conformations (such as a cell undergoing rapid division or genes that are under a high level of transcription) would be vulnerable to higher deamination rate and possible transition mutations if those cytosine deaminations are not repaired. This is reflected in the higher UDG activity found in reproductive organs, such as the testis, and other tissues that are undergoing rapid proliferation as compared to tissues that are not.

The role of transcription in mutation generation was tested in *E. coli* by Beletskii and Bhagwat [18] who found that induction of transcription can cause up to a 10-fold increase in the frequency of C to U deaminations in the nontranscribed strand (which could be reduced by the presence of UDG). Transcription has also been shown to induce mutations in yeast [19]; and has been proposed to lead to transcription-associated strand asymmetry in mammals, which is manifest as an excess of G and T over A and C on the coding strand of most genes [20]. This transcription-associated strand asymmetry is thought to be a byproduct of transcription-coupled repair in germline cells and is yet another way cytosine deamination continues to shape our genomes.

Chemical Stimulation of Cytosine Deamination

Cytosine deamination can be induced by a number of chemical species commonly found *in vivo*. Sodium bisulfite, a common component in beverages, has been found to catalyze a time-dependent first-order conversion of cytosine to uracil, but at high

concentrations (1-3 M) [21]. Under physiologically relevant conditions (10 mM bisulfite, pH 7.4, 37˚C), induced deamination of cytosine in single-stranded DNA (ssDNA) has been found to be only slightly elevated (3.5×10^{-10}) [22]. More recent studies have shown that the ssDNA binding protein in *E. coli* protected ssDNA by as much as 4-fold from sodium bisulfite induced cytosine deamination as compared to naked ssDNA [23]. Thus it appears that sodium bisulfite induced cytosine deamination is only a minor source of dU in DNA *in vivo*.

The mutagen glyoxal, which is also widely present in various beverages and foods, was reacted with DNA or deoxynucleosides under physiological conditions (pH 7.4, 37˚C) and a considerable amount of dU was detected in the DNA [24]. When equimolar amounts of glyoxal and DNA (calculated as nucleotides) were reacted for 24 h, 1% of the dC (0.19 mol% as DNA base) was converted to dU in the DNA. The *in vivo* mutation spectrum in the chromosomal *lacI* gene induced by treatment of a wild-type *E. coli* strain with glyoxal was analyzed [25]. This study found that mutation frequency increased with increasing concentration of glyoxal added to the culture medium. Sequencing of the glyoxal-induced mutants revealed the ratio of base-pair substitutions was increased; and 78% of the base-pair substitutions occurred at G:C sites, with G:C→A:T transitions being predominant, followed by G:C→T:A transversions. However, this mutation may occur either by a dC→dU conversion or by base pairing between glyoxal-G adduct and dT, so it is unclear just how much of a role cytosine deamination has in these transitions. Highlighting this ambiguity, the same research group [26] found that *in vitro* glyoxal treatment of a *supF* gene in a vector that was immediately transfected into mammalian COS-7 cells induces single base substitutions that were predominately transversions, with

only 13% being G:C→A:T transitions. Whether glyoxal is relevant as an *in vivo* source of dU through cytosine deamination needs further study.

Nitric oxide (NO·) is an important physiological messenger that is involved in many processes in vivo, including blood vessel relaxation, inhibition of platelet aggregation, and neurotransmission [27]. Nitric oxide reacts with oxygen, for example, to form the nitrosating agent nitrous anhydride, N_2O_3, which can nitrosate primary amine functionalities on DNA bases, leading to deamination of cytosine, 5-methylcytosine, adenine, and guanine [28, 29]. The G:C→A:T transition has frequently been observed as the primary type of mutation formed upon NO· treatment [29]. However, this mutation could result from the deamination of cytosine, guanine, or 5-methylcytosine. Caulfield et al. [30] have studied the relative rates of NO·-induced deamination of dC and dG in different DNA structures. The relative reactivity varied between 2′-deoxyribonucleosides, single- and double-stranded DNA. In all cases, dG was approximately twice as reactive as dC. It appears then, that NO·-induced G:C→A:T mutations were more likely to proceed through a xanthine (deaminated guanosine) intermediate than through uracil formation. An *in vivo* measurement of NO·-induced deamination is needed to further clarify this route of mutagenesis.

Ultraviolet Light Stimulation of Cytosine Deamination

Ultraviolet (UV) light can stimulate cytosine deamination through forming cytosine hydrates, cytosine glycol, and cyclobutane pyrimidine dimers (i.e., C<>C, T<>C, C<>T) [31, 32]. Cytosine hydrate is the principal monomeric photoproduct in DNA, where addition of water at C6 leads to saturation of the C5=C6 double bond forming 6-hydroxy-5,6-dihydrocytosine [33]. From studies conducted on a poly(dG-[^{3}H]dC) substrate, approximately 4% of the cytosine hydrate formed will deaminate to form uracil hydrate,

which is a poor substrate for UDG [34]. After incubation to allow for the slow *trans*-elimination of water, about one-half of the uracil hydrate had converted to uracil (half-life of 6 h at 37˚C), thus U:G mispairs can result from UV irradiation of cytosine-containing DNA without pyrimidine dimer formation.

However, among the variety of sequence changes in DNA produced by UV-mutagenesis, C→T transitions at dipyrimidine cytosine-containing sites are exceptionally frequent, and have been associated with translesion DNA synthesis by POL V at cyclobutane pyrimidine dimers [35-37] or at (6–4) photoproducts [38-40]. It has been known for some time that the rates for deamination of cytosines within cyclobutane pyrimidine dimers (CPDs) are far greater than those for deamination of monomeric cytosines in dsDNA (a million-fold) or even ssDNA (at least 10,000-fold), however there has been some doubt that cytosine deamination in CPDs happens on a time scale fast enough to be integral to the forming of C→T transition mutations [35, 36, 41, 42]. In studies with natural DNA duplexes, the measured half-lives of cytosines in cyclobutane dimers vary from 5 to 100 h ([43], Table 2). Details for the two most recent *in vitro* studies are given below.

Barak et al. [36] UV-irradiated plasmid DNA under defined *in vitro* conditions to measure the deamination of the cyclobutane pyrimidine dimers by assaying the formation of uracils in the DNA using a bioassay. The bioassay consisted of deamination of a plasmid carrying an indicator gene, followed by photoreactivation with photolyase to monomerize the dimers, and assaying uracils in DNA by their ability to cause derepressive mutations in an indicator strain that was *ung*$^{-}$. Sequence analysis revealed that 93% of the mutants carried GC→AT transitions. These mutations were generated at

37 ˚C with first-order kinetics, at a rate of ≈ 3.9 x 10^{-5} s^{-1}, corresponding to a half-life of 5 h. Physiological salt conditions (150 mM potassium chloride or glutamate buffered to pH 7.5) increased the half-life to 12 h. The temperature dependence of the rate constant yielded an activation energy of 13.6 +/- 3.3 kcal/mol, which is about 15 kcal less than values found for deamination of cytosine in ssDNA [11, 14], and close to previously *in vivo* determined values of 17 kcal/mol [44].

The second in vitro study, by Peng and Shaw [43], focused on a CCCC target sequence so that UV-induced deamination to uracil specifically in C<>C cyclobutane dimers in dsDNA could be measured. Their method is essentially the same as the bioassay described above (incubation at 37˚C, pH 7.4 followed with photolyase treatment), except a M13 phage-based dsDNA construct was UV-irradiated. Upon transfection into *ung*$^{-}$ *E. coli* cells, the reversion frequencies in the CCCC target sequence nearly doubled every day of incubation post-UV exposure; and after 8 days, the reversion frequencies had increased by two orders of magnitude in *ung*$^{-}$ cells, relative to *ung*$^{+}$ cells. Sequencing of the revertants revealed that all mutations were single C→T or tandem double CC→TT mutations; and an increasing percentage (> 84% after 4 days) of tandem double CC→TT mutations was found with longer post-UV incubation times. Tandem CC→TT mutations appeared with a pseudo-first-order rate constant of ≈ 10^{-6} s^{-1}, which suggested to the authors that a concerted deamination of both residues in a tandem C<>C dimer was occurring. This finding is interesting because tandem CC→TT transitions in UV-irradiated cellular DNA are relatively frequent and have been cited as a signature of UV damage in skin cancer [45].

The deamination in a C<>C dimer occurred with a half-life of ≈ 5 days, which is 26-fold slower than that measured by Barak et al.[36]. Peng and Shaw reasoned their value was slower because the data of Barak et al. included deamination at all possible cyclobutane pyrimidine dimers and that deamination of cytosine in C<>T and T<>C dimers may be faster than in a C<>C dimer. However, both studies suggest that deamination of cytosine-containing dimers is too slow to play an important role in UV mutagenesis in *E. coli*, but could have a role in mammalian cells, where the mutagenic process is slower.

Burger et al. [46] determined the *in vivo* deamination rates for cytosines in CPDs in an assay similar to the *in vitro* methods described above except whole *ung*$^{-}$ *E. coli* were UV-irradiated, held in buffer for varying times and temperatures to allow for cytosine deamination in CPDs, and then exposed to light for photoreversal of CPDs to establish monomer uracils where deamination had occurred. Measuring tRNA suppressor mutations at a specific codon gave a CPD induced cytosine deamination rate of 0.0091 min^{-1}, or a half-life for deamination of 1.27 h. These studies, like those of Peng and Shaw, also revealed a large proportion of CC→TT tandem transitions, with the average rate for second deaminations being 7.6-fold greater than the average rate for first deaminations, indicating a mechanism of concerted deamination in C<>C dimers. Burger and colleagues concluded that changing a cytosine-containing CPD to a uracil-containing CPD via cytosine deamination, could be an integral part of UV-induced C→T mutations. *In vivo* studies that directly assess the fate of CPDs separately from other mutagenic processes are needed to verify these preliminary results so the role of cytosine deamination in UV mutagenesis can be thoroughly defined.

Enzyme-Induced Cytosine Deamination

The first evidence that inadvertent enzymatic cytosine deamination could also contribute to C→T transition mutations was demonstrated for DNA (cytosine-5)-methyltransferases [47, 48]. Several prokaryotic methyltransferases have been shown to increase the rate of C→U (≈ 10^4-fold increase) and 5-methyl-C→T deamination at the cytosine targeted for methylation *in vitro* in the absence of the cofactor S-adenosylmethionine and the reaction product S-adenosylhomocysteine [47, 49-51]. Mutations causing inactivation of the cofactor binding activity of the *Hpa*II methyltransferase, thus mimicking conditions of limiting *S*-adenosylmethionine concentration, could convert the DNA methyltransferase into an enzyme with higher C → U deamination frequency, even in the presence of physiological concentrations of S-adenosylmethionine and S-adenosylhomocysteine [52]. Several DNA methyltransferases have been found to bind G:U mismatches with higher affinities than for their normal G:C targets, interfering with their repair by UDG [53]. This finding suggests that the occurrence of mutational hot spots at CpG sites may not always be due to spontaneous deamination of 5-methylcytosine to form thymine, but might also be initiated by enzymatic deamination of cytosine to uracil. The fact that C→T transition mutations at mutational hot spots at CpG sites in humans are correlated to genetic disease and cancer [54, 55] underscores the importance of these findings and the role cytosine deamination may play in this mutation pathway.

While investigating the origin of mutations that are actually highly beneficial to human health, researchers have now found a novel source of mutagenic and potentially carcinogenic DNA damage; enzymatic deamination of cytosine in DNA by cytidine deaminase family proteins. Activation-induced cytidine deaminase (AID), a

B-cell-specific protein, has been shown in a number of *in vivo* studies to deaminate dC residues to dU in DNA [56-58]. This function of AID is believed to be the first step in the somatic hypermutation of the immunoglobulin variable region (IgV) and class switch recombination. This diversification is the key to the function of the immune system which depends on the combinatorial production of a wide range of immunoglobulin molecules. AID deaminates dC with a weak preference for the DNA sequence WRCY or its inverse, RGYW, (W = A or T, R = purine, Y = pyrimidine), as this "Rogozin" motif is a hotspot for somatic hypermutation in UNG knockout mice [59]. However, little is known about how AID is specifically targeted to IgV genes and how it is controlled. This is a very interesting problem, as uncontrolled AID deamination activity may prove to be the carcinogenic trigger of some B-cell lymphomas.

The AID homologue, apolipoprotein B RNA editing complex 1 (APOBEC1), was originally discovered as the catalytic component of an RNA editing complex which deaminates C6666→U in apolipoprotein B RNA in gastrointestinal tissue, thereby generating a premature stop codon [60]. Like AID and other cytidine deaminating proteins, APOBEC1 has been found to be able to deaminate dC to dU in DNA [58, 61]. Interestingly, deamination is targeted to single-stranded DNA and was influenced by DNA sequence with deamination being especially disfavored when a purine is located immediately 5′ of the cytosine. The observation that ectopically expressing APOBEC1 predisposes transgenic mice to cancer [62] suggests that APOBEC1-mediated DNA deamination could well be of physiological relevance.

In summary, DNA (cytosine-5)-methyltransferases, AID, and APOBEC proteins, enzymes with obviously beneficial cellular functions, may produce widespread genome

instability if not controlled properly. Intriguingly, the local DNA sequence context of the dC residue targeted for mutation differs between APOBEC family members. Research into the catalytic mechanisms, distribution and control of these enzymes could provide valuable insight into tissue-specific mutation spectra and carcinogenesis.

Polymerase Incorporation of Deoxyuridine Triphosphate

Polymerases from prokaryotes and eukaryotes will accept deoxyuridine triphosphate (dUTP) and incorporate deoxyuridine monophosphate (dUMP), which also base pairs with adenine, with the same efficiency as deoxythymidine triphosphate (dTTP) [63-66]. Therefore, the amount of uracil incorporated into DNA during replication depends largely on the dUTP:dTTP ratio in the intracellular pool [67-70]. This dUTP:dTTP ratio depends on the route of dTTP biosynthesis used by the organism.

For some bacteria like *E. coli*, dUTP is an intermediate in the biosynthesis of dTTP due to the action of deoxycytidine triphosphate (dCTP) deaminase. *Escherichia coli* can also synthesize dUTP by phosphorylation of deoxyuridine diphosphate (dUDP) after reduction of the ribose diphosphate (rUDP) by ribonucleoside diphosphate reductase [10]. Therefore, *E. coli* have two biosynthetic sources of dUTP, with about 80% coming from the action of dCTP deaminase, and 20% from dUDP phosphorylation [71]. Mammalian cells have a deoxycytidine monophosphate deaminase instead of a dCTP deaminase, so deoxyuridine monophosphate is the biosynthetic precursor to dTTP, and elevated levels of dUTP are avoided. The only intracellular biosynthesis of dUTP in mammals comes from the accidental phosphorylation of dUMP or rUDP in the reductase reaction [72, 73].

The level of dUTP is tightly controlled in most organisms by a deoxyuridine 5′-triphosphate nucleotidehydrolase (dUTPase) that catalyzes the hydrolysis of dUTP to

dUMP and pyrophosphate [68, 74, 75]. Despite the action of their dUTPases, it has been estimated that up to 4000 and ~10^4 deoxyuridines are erroneously incorporated into *E. coli* and human genomes, respectively, after DNA replication [10]. Uracil incorporation instead of thymine is not a directly mutagenic change, but results in altered binding affinities of transcription factors and other regulatory proteins. Mutant *E. coli* lacking or impaired in dUTPase activity was either unviable or failed to grow exponentially, became filamentous at nonpermissive temperatures where the mutant dUTPase no longer functioned, and exhibited a hyper-recombination phenotype [64, 69, 76]. The phenotype of these mutants was attributed to findings in earlier studies in which dUMP incorporation during DNA replication caused the accumulation of short DNA fragments that impaired replication [63, 77]. Fragment generation was found to be dependent on the action of UDG on the uracil-containing DNA.

It is not surprising then that many organisms can tolerate high levels of incorporated uracil in their genomes when UDG activity is not present. For example, T4 bacteriophage DNA containing as much as 30% of its thymine replaced by uracil was still viable as long as an ung$^-$ host was used for propagation [68, 78]. *E. coli* deficient in both UDG and dUTPase activities had as much as 20% of the thymine stably replaced by uracil and were still able to grow exponentially at a rate comparable to wild-type cells [64]. UDG knockout (*ung*$^{-/-}$) mice demonstrated an elevated steady-state level of uracil in their genomic DNA [79]. The number of strand breaks per cell in *ung*$^{-/-}$ fibroblast cells was markedly increased by preincubation with UDG, and used to estimate an increased steady-state level of ≈ 2000 uracil residues per genome. Two thousand uracils would be a very small fraction of the total number of bases in the murine genome, and is

tolerated as evidenced by the lack of deleterious effects associated with the *ung*$^{-/-}$ genotype. It will be interesting to see if the dUMP percentage will increase over many subsequent generations of *ung* null mice; and if so, what the final level of tolerance would be for uracil in a mammalian genome. With the *ung* null mice it may also be possible to determine the gene sequences and transcription factors that absolutely require the methyl group of thymine for recognition. One fact that is already clear from these studies is the powerful influence UDG activity exerts on the composition of genomic DNA.

Whether uracil is enzymatically incorporated or arises by cytosine deamination, uracil in DNA is a constant and serious problem. The integrity of the genome depends on expedient removal of uracil from all DNA contexts. The recognition and removal of dU by UDG and other uracil glycosylases is only the first step toward the correction of this problem.

Base Excision and Repair Pathway

It has been stated that, "For a strict reductionist, the replication of DNA by DNA polymerase is what life is all about" [80 pg. 54]. If that is true, then for a strict perfectionist, DNA repair by the DNA Base Excision and Repair (BER) pathway is what *staying* alive is all about. Strictly speaking, some enzymes involved with base excision and repair serve also to induce mutations needed to produce genetic variability. However, in this review the focus will be on the *repair* role these enzymes have in maintaining the integrity of the genome.

The BER pathway is by far the most important DNA repair pathway (reviews, [81-86]). The BER pathway must process endogenous DNA damage that occurs at a frequency of about 20,000 events per human cell per day. The loss or damage of DNA

bases that causes relatively minor disturbances to the helical DNA structure are the substrates for repair by this base-excision pathway.

The bases of DNA, like any unsaturated heterocycle, are vulnerable to attack by water, reactive oxygen species, and a multitude of endogenous and environmentally derived alkylating agents [13, 87, 88]. Hydrolytic deamination, depurination, and depyrimdination reactions occur when water attacks electrophilic centers in DNA bases. The hydrolysis of the *N*-glycosidic bond of purines alone is estimated to happen at an *in vivo* steady-state rate of > 4500 abasic site lesions (≈ 2 million in a 20 h period) in the human genome that fall mostly on BER for correction [89]. In contrast, pyrimidine *N*-glycosidic bonds are more stable and hydrolyze at only 5% the rate of purines [13]. These Apurinic/Apyrimidinic (AP or abasic) sites are mutagenic and cytotoxic because they can block replication and can lead to DNA strand breaks if not repaired [90, 91].

BER glycosylases target the most common products of oxidation and alkylation damage. The electrophilic carbons of DNA bases can react with oxygen, forming 7,8-dihydro-8-oxoguanine (8-oxoG), formamidopyrimidines, and pyrimidine glycols (all of which are mutagenic and cytotoxic) [88, 92]. Oxidative metabolism forms many reactive species, some of which can alkylate DNA bases. Lipid peroxidation can form fatty-acid radicals, aldehydes, and other species that can react with DNA bases causing etheno adducts and other types of alkylation damage catalyzed by oxygen-derived radicals. The natural cofactor *S*-adenosylmethionine (SAM) is a methyl group donor and is a weak alkylating agent that can react with ring nitrogens in purines [13]. All these common damages are relatively efficiently removed by dedicated glycosylases, strongly suggesting that they occur at significant rates *in vivo* [83].

Base Excision Repair: Many Paths from Damage to Repair

Recognition of these DNA damages by a specific glycosylase is the first step of the BER. The glycosylase then excises the damage by cleaving the *N*-glycosyl bond linking the base to the deoxyribose phosphate, creating an abasic site. Monofunctional glycosylases, such as UDG, must rely on a Class II AP endonuclease for 2′-phosphodiester hydrolysis of the abasic site followed by a deoxyribophosphodiesterase (dRPase) that excises the abasic sugar-phosphate by cutting the 3′-phosphodiester bond to create a single nucleotide gap (see Fig. 1-2 for the specific names of the *E. coli* and Human enzymes involved in uracil-initiated BER).

If the glycosylase is bifunctional (also known as Class I AP endonuclease or AP lyases) with an additional β-lyase activity, it will cleave 3′ to AP sites by a β or β-δ elimination mechanism, generating a single-strand break. The β-elimination leaves an α,β-unsaturated aldehyde (*trans*-4-hydroxy 2-pentenal 5-phosphate) attached to the 3′-phosphate; and if the reaction proceeds to the δ-elimination, just a 3′-phosphate along with a 5′-phosphate terminus (Fig. 1-2). A Class II AP-endonuclease removes the α,β-unsaturated aldehyde or 5′-phosphate by hydrolyzing the 5′-phosphodiester bond, forming a single-nucleotide gap. The nicked DNA is finally repaired when DNA polymerase fills the gap and DNA ligase reseals the nick between the new nucleotide and the 5′-phosphate of the neighboring DNA.

A subset of bifunctional DNA glycosylases also possesses a DNA dRPase activity. The most active dRPase of this subset in E. coli is 2,6-dihydroxy-5N-formamidopyrimidine (a ring-opened purine) DNA glycosylase (Fpg) [93], which was also the first enzyme found to efficiently remove 8-oxoG from DNA. In an interesting example of functional convergence, the human 8-oxoguanine DNA glycosylase

Figure 1-2. Uracil-initiated base excision and repair (see next page). The general pathway from uracil damage to repair with the key (most active) enzymes for *E. coli* (left) and Human (right) that accomplish each step. Enzymes with homology (sequence and/or functional) are parallel to each other and common alternative names are in parentheses. The DNA repair patch can be a single nucleotide to hundreds, depending on conditions (see text). Abbreviations: Dug = dsDNA Uracil Glycosylase; TDG = Thymine DNA Glycosylase; MBD4 = Methyl-CpG Binding Domain protein; SMUG = Single-strand selective Monofunctional Uracil DNA Glycosylase; Endo = endonuclease; Exo = exonuclease; Pol = polymerase; HAP = Human AP-endonuclease (a.k.a. APE, AP-Endonuclease); dRPase = deoxyribophosphodiesterase; Fpg = Formamidopyrimidine DNA Glycosylase; OGG1 = 8-oxoguanine DNA glycosylase; RF-C = Replication Factor C; PCNA = Proliferating Cell Nuclear Antigen; FEN-1 = Flap Endonuclease; XRCC1 = X-ray Cross-Complementation protein; LIG = ligase.

Uracil-initiated Base Excision Repair

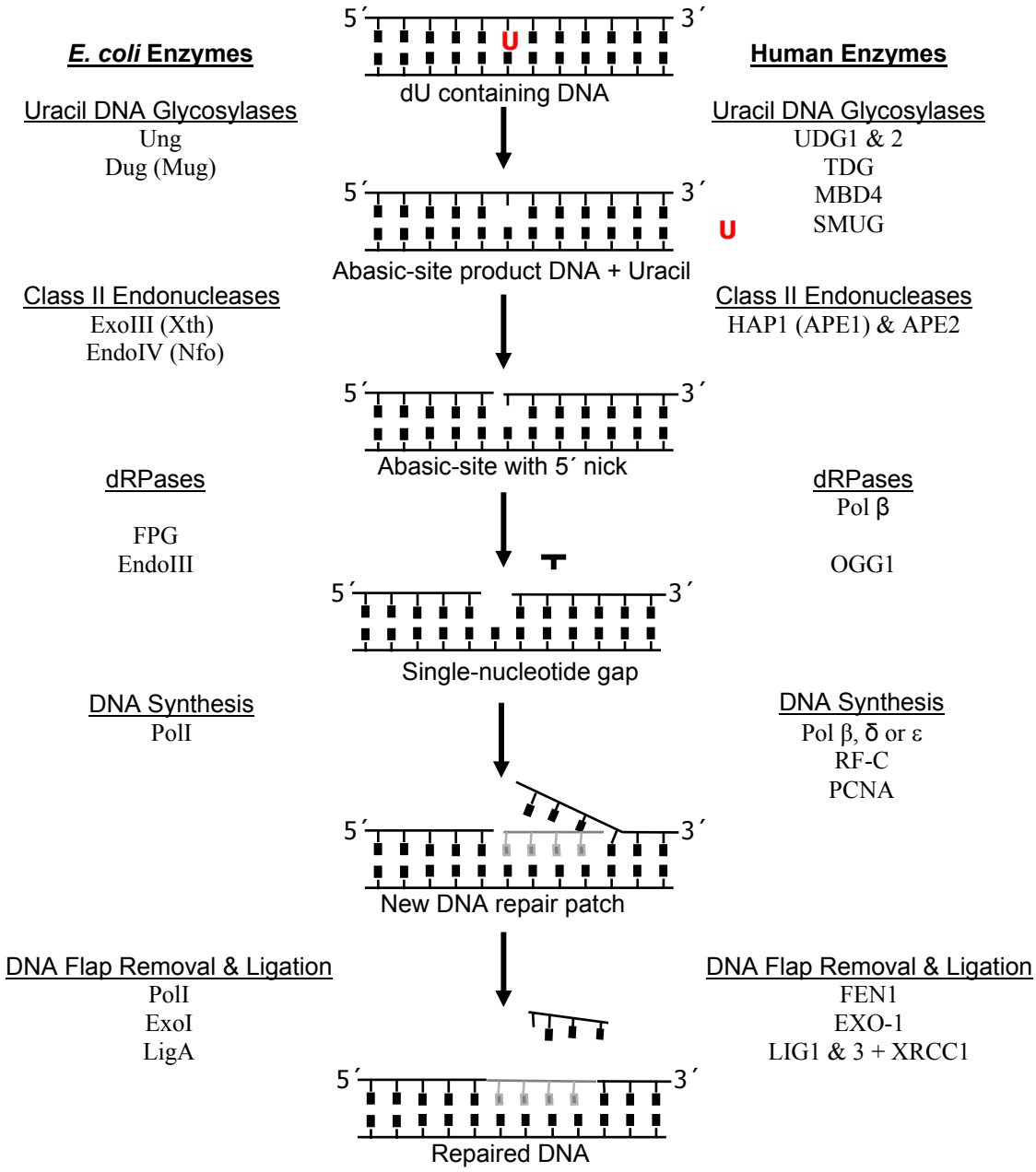

(OGG1) which also removes 8-oxoG, also has dRPase activity, even though it is in a different structural family than Fpg [94]. However, in humans the major dRPase activity is contained in the polymerase that fills the nick, DNA Polymerase β (Pol β) [95]. In *E. coli* there are two major Class II AP endonucleases; Exo-III and Endo-IV. Exo-III comprises ≈ 90% of the total cellular AP endonuclease activity in *E. coli* under normal physiological conditions ([96]; review, [97]). However, during periods of oxidative and nitrosative stress, Endo-IV is induced to protein levels that are comparable to Exo-III [98, 99].

Human AP-Endonuclease 1, HAP1, (a.k.a. APE1, APEX, and REF1) is the mammalian homologue of Exo-III and is also the predominant Class II AP endonuclease comprising >95% of the total cellular AP site incision activity in human cell extracts [100-102]. A mammalian counterpart to Endo-IV has not yet been identified. However, a second subfamily of Exo-III-like proteins was discovered with human APE2 [103], which differs from APE1 at the N- and C-terminal ends, but retains many of the essential active-site residues. The role of APE2 in BER or other DNA repair pathways has yet to be elucidated.

The BER Patch-Size Debate

In addition to short-patch BER, there is a long-patch pathway (2-19 nt) where the polymerase (Pol I in *E. coli*; and Pol β, ε, or δ in humans) replicates past the abasic site, pushing out a "flap" of nucleotides that is later cleaved by a flap-endonuclease (FEN-1) [104]. One possible trigger for long-patch BER may be when the deoxyribose phosphate group is resistant to excision by the dRPase of Pol β [105] or the initial glycosylase may determine the BER pathway [106]. There is considerable debate as to the size of the DNA repair patch and the frequency of short-patch versus long-patch repair synthesis. It

appears that with in vitro-reconstituted BER systems, the repair-patch size could be highly influenced by the relative concentration of BER enzymes and the size of the oligonucleotide substrate, as short substrates bias BER toward short patch repair. It was reasoned that short oligonucleotides may not provide a platform long enough for the interaction of DNA polymerase and other BER proteins to carryout long patch BER [107, 108].

The most recent study of BER path size in *E. coli* by Sung and Mosbaugh [108] used a closed circular duplex DNA plasmid substrate containing a site-specific uracil or ethenocytosine (εC) residue treated with cell extracts supplemented with various proteins involved in BER. Their results indicate that nick ligation by DNA ligase is the slowest step in the *E. coli* BER pathway; and that both uracil and ethenocytosine-initiated BER events were Pol I dependent and produced short, long, and very-long DNA repair synthesis patches. Increasing the ratio of ligase:polymerase caused an increase in short-patch repair. There also was temporal influence on patch size, with longer patches (> 20 nucleotides) dominating the patch size spectrum at longer times.

While human BER can be reconstituted with only four proteins *in vitro* (a DNA glycosylase, Ape1, Pol β and Ligase1), the BER pathway (including all of the subpathways and the various DNA glycosylases) consists of roughly 32 core genes [109]. For example, in the mammalian BER pathway, strand displacement synthesis can precede with several different polymerases that effect patch size [110]. Ligation is also a complex coordination of protein-protein interactions such as those between XRCC1 and DNA ligase III or Pol β [111, 112], Pol β and DNA ligase I [113], and PCNA and DNA ligase I [114].

Previous reports found up to 90% of BER happens by a Pol β-dependent short patch pathway in humans [115, 116]. Using a reconstituted human enzyme BER system composed of a 51 nucleotide duplex substrate with a U:G mispair, uracil-DNA glycosylase, HAP1, Pol β, and DNA ligase I, Srivastava et al. [117] identified the dRP lyase activity associated with Pol β as the rate determining step. Uracil-initiated BER on a duplex M13mp2 DNA template has also been studied in human glioblastoma U251 cells, colon adenocarcinoma LoVo cells, and with mouse embryonic fibroblast cell extracts [118, 119]. DNA repair patch size with these cell extracts was primarily distributed between 1 and 8 nucleotides in length with 1 nucleotide repair patch constituting approximately only 20% of the repair events.

Recently, the complete reconstitution of 8-oxoG repair pathway was found to require only hOGG1, HAP1, Pol β and DNA ligase I [120]. In agreement with Sung and Mosbaugh's results with *E. coli* extracts, the presence of DNA ligase I confined the repair patch at 8-oxoG to 1 nucleotide, even in the presence of high levels of Pol β and FEN1. These results are in conflict with recent *in vivo* measurements of repair patch size on plasmids with a site-specific 8-oxoG abasic site that found up to 80% of the repair was mediated by the long patch pathway (2-6 nucleotides) [121]. Further work needs to be done with these BER systems to clarify the DNA damage to repair patch size relationship. An understanding of this relationship is important because it could lead to insights into mutation spectrums associated with disease states. As will be discussed in the next section, the repair patch itself may be a source of mutations if the nascent DNA is not replicated with high fidelity.

Fidelity of Uracil-Initiated BER

The question of whether the repair process itself can cause mutations has been addressed in *E. coli*. Using an M13mp2 lacZα DNA-based reversion assay the error frequency and mutational specificity associated with uracil-initiated base excision repair were measured [122]. *Escherichia coli* have two principle Uracil-DNA glycosylases, Udg that is encoded by the *ung* gene and Double-stranded Uracil-DNA glycosylase, dsUdg or Dug (a.k.a. Mismatch Uracil DNA glycosylase or Mug) encoded by the *dug* gene. In reactions utilizing ung^+ and dug^+ *E. coli*, approximately 80% of the uracil-DNA was repaired, whereas about 20% repair (≈5.5 fold slower) was observed using an ung^- dug^+ strain. Fidelity measurements of DNA repair replication gave a base substitution reversion frequency of approximately 5.5×10^{-4}. Mutations occurred almost exclusively at the target uracil with T→G and T→A transversions being 70% and 29% of the mutations, respectively. Interestingly, uracil-mediated BER initiated by Dug alone was more mutagenic than Ung-initiated BER. Based on the incorporation rate of 1 uracil per 1200 nucleotides in *E. coli*, Sung et al. calculated that Ung-proficient BER could generate approximately two mutations per cycle of semiconservative DNA replication, providing that some sort of error correction did not occur prior to mutation fixation.

The idea of error correction for newly synthesized DNA after repair is intriguing because if the majority of repair patches are under 20 nt then it is highly unlikely that methyl-directed mismatch repair would be effective [123]. The extra mutation suppression of mismatch repair may be a reason for *E. coli* to employ very long patch repair (>200 nt). The interplay between BER patch size and BER DNA replication fidelity is a fascinating area that should yield insight into some of the major processes that drive and shape the evolution of DNA genomes.

For the majority of human BER the gap-filling step is catalyzed by Pol β, which does not have an intrinsic editing function and consequently makes rather frequent errors, at a level of 1 per 4000 nucleotide incorporation events [124]. The fidelity of uracil-initiated BER was studied using homozygous mouse embryonic fibroblast Pol β proficient (+/+) and deficient (-/-) cells to determine the error frequency and mutational specificity associated with the completed repair process [119]. The base substitution reversion frequency was only slightly elevated in Pol β (-/-) cells (7.2×10^{-4}) as compared to Pol β (+/+) cells (5.7×10^{-4}). The most common DNA repair synthesis errors were single base deletion or incorporation of dTMP which occurred predominantly at the position of the U:G target. These results agree well with the misincorporation frequency of uracil-initiated BER DNA synthesis measured in human glioblastoma and adenocarcinoma LoVo cell extracts ($\approx 5.3 \times 10^{-4}$) [118]. So regardless of the polymerase involved, there seems to be a universal upper limit to the fidelity of uracil-initiated repair in either *E. coli* or human cells. This is interesting in comparison with the results of Nilsen and coworkers who reconstituted uracil-initiated human BER on nucleosome core particles.

Human BER of damaged DNA packaged in nucleosome core particles (the basic repeating unit of chromatin) has been reconstituted *in vitro* with the human uracil-DNA glycosylases UNG2 and SMUG1, and the rest of the standard BER enzymes: HAP1, Pol β, and Ligase 3 [125]. Both glycosylases were able to remove uracil from nucleosomes, albeit with 3 to 9-fold reduced efficiency as compared to naked DNA.

Excision of site-specific U:A base pairs was essentially uniform along the length of the DNA substrate, indicating UNG2 could access the damage irrespective of the DNA's

rotational position on the core particle. The effect nucleosome core particles have on the activity of UNG2 highlights the fact that accurate measurements of BER rates and fidelity need to be performed in the proper context if they are to represent well the *in vivo* processes.

The influence of chromatin on the rate of cytosine deamination and the rate of uracil-initiated BER are important questions for the future. It is evident that the mutagenic potential of different types of DNA damage depends on the amount of initial damage and cell's capacity to execute repair. Given the established link between defects in DNA repair and human disease, research in BER will remain an important focal point in DNA metabolism.

Uracil DNA Glycosylase: An Ancient Enzyme

After finding that cytosine in DNA deaminates to uracil at significant rates under physiological conditions, Lindahl and coworkers went looking for an activity that would remove uracil from DNA. In 1974 they purified and characterized Uracil-DNA glycosylase from *E. coli* (*e*UDG) [126], the first of many DNA glycosylases to be discovered, and the beginning of a new field in DNA metabolism, DNA base excision repair. Since then, homologous UDGs from viral, bacterial, archaea bacterial, and eukaryotic sources have been discovered forming the Ung family of UDGs, while underscoring the importance of this protein to all forms of life with DNA genomes.

The high level of primary amino acid sequence conservation from prokaryotes to eukaryotes, and construction of an evolutionary tree of the Ung family glycosylases has demonstrated that the proto-Ung ancestor arose around 3 billion years ago (Shaw, Young and Benner, unpublished data). This coincides with theories that envision the proto-Ung enzyme as a major selective pressure in the switch from uracil to thymine in DNA

genomes [8]. The study of the biochemical properties and protein structure of UDG is a window through 3 billion years that this ancient molecule has shaped life.

Sequence and Structure Conservation in the UDG Superfamily

Currently there are seven known families of proteins that can remove uracil from DNA grouped according to their differences in substrate recognition and amino acid sequence [127]. Five of these are classed into a UDG superfamily with the sixth classified as a mismatch-specific DNA glycosylase (MIG) family and the seventh being the strangest member, the MjUDG family, named after the hyperthermophilic archaea *Methanococcus jannaschii* [127]. MjUDG is strange in that it can also remove 8-oxoG, has an [4Fe-4S]-binding cluster and has features in common with MIG and *E. coli* Exo-III. The UDG superfamily consists of: the Ung related class (family 1) [128]; the Double-stranded or Mismatch specific Uracil-DNA Glycosylase, Dug (a.k.a Mug)/TDG, related class (family 2) [129]; the Single-stranded specific, SMUG, related class (family 3) [130]; the thermostable UDG related class (family 4, TmUDG) [131]; and the UDG-B family (family 5) [132, 133]. These five different UDG families show a limited sequence similarity, but they share both a common structural fold and two active site motifs.

Primary sequence and secondary structural alignments revealed the UDG superfamily has an ancestral core fold that consists of a central parallel four-strand β-sheet with a 2-1-3-4 strand connectivity, which alternates with four α helices (Fig. 1-3) [134-136]. A substrate-binding pocket is formed by the regions located after strand 1 and 4. Another characteristic structural feature of the UDG superfamily is a central conserved motif that corresponds to a sharp turn between strand 3 and the adjacent helix 3, which is required for the enzyme conformation needed to accommodate DNA. It was proposed that this core fold resembles the basic fold of a family of bacterial periplasmic

sugar-binding proteins, which bind substrate at a cleft in the C-terminal end composed of β-sheets [135]. Some examples of these sugar-binding proteins include the *E. coli* D-ribose-binding protein and L-arabinose-binding protein. Similar folds were also found in domains of *E. coli* topoisomerase I and yeast topoisomerase II , which suggested coevolution of a fold common to UDG and topoisomerase that functions in the formation and recognition of extra-helical nucleotides [135].

In the loop preceding the conserved helix 1 (Fig. 1-3) there lies a conserved aromatic residue. Sequence alignment of 70 family 1 members showed this amino acid is absolutely conserved as phenylalanine in the Ung family of UDGs (Shaw, Young, and Benner, unpublished data). This active site amino acid is usually Phe in the Smug family of proteins as well. In the Dug/TDG family the aromatic is frequently tyrosine, but is sometimes replaced by an aliphatic residue in a small subset of these UDGs [136]. Since this conserved phenylalanine lines the bottom of the active sites of every UDG structurally examined to date, it suggested a universal mechanism of uracil binding in the majority of the UDG superfamily and is the focus of this dissertation.

Two conserved active site motifs of the UDG superfamily provide the specific binding site for uracil [132, 137]. The highly conserved active site sequences in UNG-type UDGs contain a catalytic aspartate, GQ*D*PY, and histidine, *H*PSPLSA, and are referred to as motifs-A and -B, respectively. The precise role of these catalytic residues will be discussed in the following sections. These motifs have topological equivalents in the other four UDG families which retain very similar conformations to family 1 UDGs. In UDG families 2 and 3 (Dug/TDG-related and SMUG-related) the catalytic aspartate in motif-A is replaced by asparagine. In family 4, the motif-A

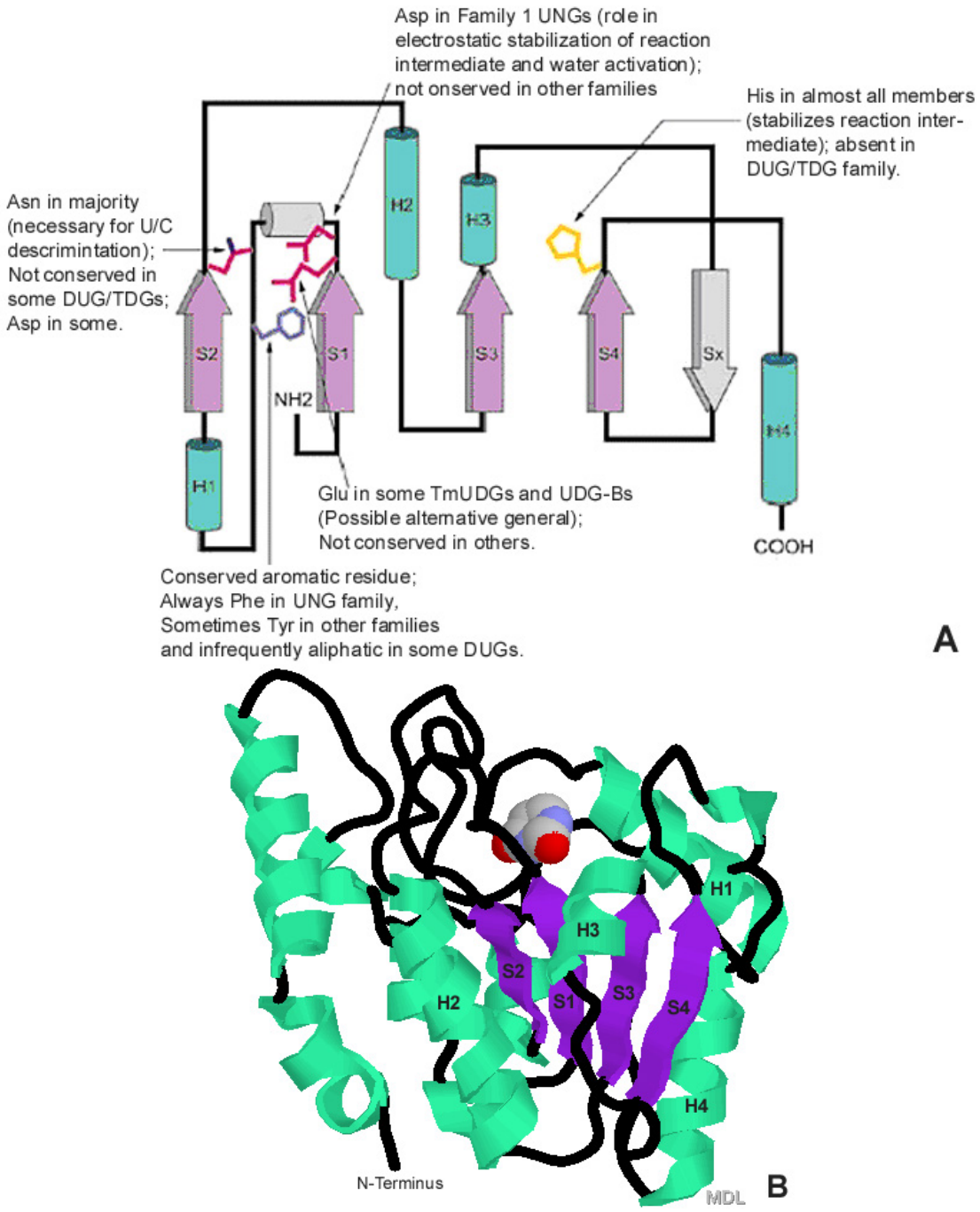

Figure 1-3. Structural fold of the UDG superfamily. (A) The secondary structure topology map of the UDG superfamily (adapted with permission from [136]). The core conserved elements (purple arrows = β-sheet; green cylinders = α-helix) and unique features of different families, including structures observed only in the DUGs (a.k.a. MUGs) (shown in gray). (B) The tertiary structure of *E. coli* UDG with secondary structural element cartoons colored as in *A* generated with Protein Explorer from PDB ID 5EUG. Uracil is shown space-filled bound to the active-site.

aspartate is replaced by a glutamate; and family 5 appears to lack a polar residue, as there is a alanine at this position.

Interestingly, mutation of this alanine to aspartate impairs the activity in Pyrobaculum areophilum UDGb, a family 5 member [132]. The conserved histidine in family 1 motif-B is also conserved in the other UDG families except for family 2, where it is again replaced in by an asparagine. The lack of the catalytic residues in Dug-related UDGs may be an adaptation to allow the more efficient at removal of 3,N_4-ethenocytosine (εC) [138].

The highly conserved asparagine that discriminates between uracil and cytosine in the UNG family 1 UDGs is also conserved as either an Asn or an Asp in the majority of the UDG superfamily enzymes, with the exception of a family 3 SMUGs and a few members of the other families, most notably some Dug/TDGs. It has been proposed that the substitution of Asn in UDG family members with broader substrate specificity probably allows for the removal of alkylated bases such as etheno-cytosine [136]. This is supported by the fact that mutational replacement of Asn by Asp in hUDG results in its acquiring cytosine glycosylase activity [139].

Although the UDG superfamily is nearly ubiquitous among life forms with DNA genomes, the individual families have distinct phyletic distributions that are sometimes limited, such as family 3 SMUGs in eukaryotes. Other examples include eukaryotes encoded UNG and TDG-family enzymes that are closely related to their bacterial orthologs, yet are not found in archaea [136]. The unfolding evolutionary puzzle for the UDG families involves multiple events of lateral gene transfer and lineage-specific gene

loss; the fringe of a fascinating picture of the role this enzyme has had on the shaping of genomes and the development of life.

Basic Biochemical Characteristics of UNG Family UDGs

Family 1 UDGs are monofunctional, cleaving the N_1'-glycosidic bond of deoxynucleosides as UDG does not recognize uracil in RNA [126]. UDG from *E. coli* is most active against deoxyuridine, from either single-stranded or double-stranded DNA, while residues in oligonucleotides at the 3′ and 5′-terminal position are poorly catalyzed [140]. The glycosidic bond cleavage step is essentially irreversible in aqueous solution, as there was no detectable incorporation of radio-labeled uracil in DNA by incubation of UDG with the abasic DNA product in the presence of high concentrations of Uracil [141].

In a thorough study of the DNA moieties that *e*UDG uses during catalysis, Jiang et al. found the optimal substrate for the enzyme is a five-nucleotide ssDNA with uracil centrally located (ApApUpApA) [142]. Jiang and Stivers [143] also revealed that free 2′-deoxyuridine nucleoside, once thought not to be a UDG substrate, is actually the minimal substrate for *e*UDG. Although this minimal 2′-deoxyuridine nucleoside substrate is about a million fold less reactive than the optimal substrate, it still showed a significant rate of *N*-glycosidic bond cleavage as compared to the nonenzymatic reaction. This study also found that adding a tetrahydrofuran (D) abasic site nucleotide to both the 5′ and 3′ sides of the minimal substrate (DpUpD) caused over an 8000 fold increase in the specificity constant (k_{cat}/K_M) for the substrate, whereas adding the full nucleotides (ApUpA) gave a ≈ 13,000 fold enhancement in k_{cat}/K_M relative to the minimal substrate. Finally, addition of the nucleotide in the fourth position was found to increase the reactivity of trimer substrates with rigid furanose rings or nucleotides in the +1 and -1

positions by 1300-270,000-fold (i.e., DpUpD→DpUpDpA or ApUpA→ApUpApA). Jiang and Stivers proposed a mechanism in which the binding energy of the 3′-nucleotide is used drive the rigid +1 and -1 A or D substituents into their binding pockets, resulting in a net catalytic benefit of 4.3 to 7.5 kcal/mol. The specificity constant increases 3.6 billion fold from minimal to optimal substrate, tracking how UDG uses energetic cooperativity between distant site binding interactions to enhance catalysis an incredible amount.

A variety of C5-substituted uracil bases were tested as substrates for *e*UDG [144]. Only fluorouracil residues are recognized and removed by *e*UDG, whereas the larger chloro-, methyl-, bromo-, and iodo-substituted uracils are not. This establishes the upper limit on the size of C5 substituents permitted by UNG at some value between the fluoro and chloro-substituted derivatives (1.35 vs. 1.80 Å [145, 146]). Although there is only a small difference in the van der Waals radius between the hydrogen and fluoro groups (1.2 vs. 1.35 Å,) uracil was removed faster than fluorouracil by a factor of 10.

There are reports that claim that UDG from both *E. coli* and humans can remove 5-hydroxyuracil and 5,6-dihydroxyuracil, cytosine-derived products of oxidative DNA damage [147-149]. However, the data in these studies was inconsistent and of very poor quality. The results of Zastawny et al. [148] contradict the study by Hatahet et al. [147] stating that 5-hydroxyuracil is not a substrate for *e*UDG while 5,6-dihydroxyuracil is, which itself seems internally inconsistent. Even if these results are not experimental artifacts, the data of Liu et al. [144] indicates the activity of UDG toward these substrates should be very miniscule and of little consequence *in vivo*.

Numerous studies have shown that UDG from various sources can remove uracil in duplex DNA across from all bases, natural or synthetic, with a slight preference for mispairs [140, 150, 151]. Surface plasmon resonance was utilized to monitor the real-time biomolecular interaction of site-directed mutants of the herpes simplex virus type 1 UDG (vUDG) lacking catalytic activity with single- and double-stranded oligonucleotides, with or without uracil [152]. Interaction with G:U mismatches was significantly stronger (≈ 30 fold lower K_D) than that with A:U base pairs and there was negligible interaction between the mutants and DNA lacking uracil. This is in agreement with data for hUDG that showed uracil in the U:G context was excised at a slightly elevated rate as compared to base paired uracil [134].

These studies are in disagreement with a kinetic analysis of *e*UDG [153] that showed deoxyuridine nucleotide flipping and DNA affinities were largely unaffected by the base pair context (nucleotide flipping will be discussed in more detail later). Strangely, this data is corroborated by another study with a catalytically incompetent vUDG that showed, in contrast to the earlier study with surface-plasmon resonance, that nearest neighboring bases had more effect on substrate catalysis and affinities than base pairing partners, which had negligible effects [154]. In the same study that rigorously defined the size limits of the UDG active site, the researchers found uracil is removed when paired with adenine, 2-aminopurine, nebularine, and 2,6-diaminopurine only slightly less efficiently than when in wobble base pairs with guanine and hypoxanthine (deoxyinosine) [144]. The authors suggested that the reduced thermal stability of the wobble base pairs could promote the extrusion of the target uracil into the binding pocket, thereby facilitating removal, albeit to a small degree. Thus it appears that the

earlier studies have overestimated the energetic benefit that a wobble U:G base pair would provide towards UDG catalysis. The localization of hUDG at replication foci and its demonstrated role in removing uracil incorporated during replication [155] requires a protein that is efficient in removing U from U:A base pairs. This fact argues that UDG cannot be too preferential towards U:G mispairs if it is to also be efficient enough for its role during replication. The energetics of nucleotide flipping has been investigated further in experiments that will be discussed in the upcoming section on the nucleotide flipping mechanism of UDG.

Product Inhibition of UDG

One product of glycosidic bond cleavage, free uracil base, noncompetitively inhibits UDG from both *E. coli* and humans, although at high concentrations (50% inhibition at 2mM free uracil) [156, 157]. More recent measurements of *e*UDG's affinity for free uracil gave a K_D value of around 50 μM [158, 159].

The second product of glycosidic bond cleavage, abasic site containing DNA has been shown to competitively inhibit hUDG. Parikh et al. measured a K_D of 7 nM for abasic site containing DNA [134]. This group also solved a crystal structure that contained a hUDG bound to abasic-site containing DNA at the abasic site. The hUDG bound abasic site was without uracil and flipped-out of the DNA double helix into the enzyme active site, thus demonstrating that UDG will rebind its product.

This is in contrast to studies with catalytically incompetent mutant vUDG which have shown either negligible binding or an apparent K_D of 1.5 to 4 μM for abasic site containing DNA [152, 154]. *E. coli* UDG was found to bind a 19mer abasic site containing dsDNA with an apparent K_D of about 90 nM [159]. One possible explanation for the range of abasic site affinities is that *N*- and *C*-terminal additions or deletions to the

conserved structural core help modulate UDG's binding to abasic product. It has been discovered that human mitochondrial uracil-DNA glycosylase preform (UNG1) is processed to two forms, one of which is resistant to inhibition by abasic sites [160]. The enzyme used in the research by Parikh et al. was a deletion mutant with both ends of the polypeptide truncated, thus it appears that the tight abasic site binding could be an artifact of their enzyme preparation. It was proposed that this tight abasic site binding by hUDG protects the cells from the deleterious DNA damage and signals the following BER enzymes to target the abasic site for quick repair [134]. This hypothesis seems tenuous given the above facts.

Designed Chemical Inhibition of UDG

There is much interest in specific inhibitors of uracil DNA glycosylase that could possibly serve as antiviral agents for primate lentiviruses (human immunodeficiency viruses 1 & 2), pox viruses, and type I herpes virus. These viruses require a UDG activity for viral DNA replication and genome maintenance, and/or escape from latency ([161-165], review [166]). UDG inhibitors could also have potential for inhibiting the counterproductive repair of damaged bases produced during chemotherapy treatments [167]. Early studies with pyrrolidine abasic site analogs (4-azafuranose) showed that many glycosylases could be inhibited by this set of molecules with the exception of UDG [168]. The failure of pyrrolidine abasic site analogs to inhibit UDG was explained by the discovery that *e*UDG would remain bound to an 11-mer oligonucleotide containing a cationic 1-aza-deoxyribose residue only if in complex with a uracil anion [159]. The 1-aza-deoxyribose was designed to be a stable mimic of the high-energy oxacarbenium ion reaction intermediate (discussed later) and is the tightest binding UDG inhibitor to date, with a K_D^{Ap} of 110 pM in the presence of saturating anionic uracil.

Inhibitor design has also been directed towards Herpes Simplex Virus 1 UDG (vUDG), due to its importance in infectivity and reactivation [161]. One group used 6-(p-n-octylanilino)uracil to "selectively" inhibit vUDG with a high IC_{50} of 8 μM [169, 170]. More effective inhibitors for vUDG were found in the molecules of 2′-fluoro-2′-deoxyuridine (dfU) and furan homouridine (Fig. 1-4) [171]. When dfU and furan homouridine were incorporated into double-stranded 25mers they competitively bound vUDG with apparent affinities of 4 and 160 nM, respectively. The measured affinity of vUDG for dfU approximates the binding affinity of *e*UDG for the same inhibitor ($K_D^{Ap} \approx 50$ nM [159]). So the dfU inhibitor binds about 500 fold less tightly than the 1-aza-deoxyribose inhibitor, but has the benefit of not needing saturating amounts of uracil anion present. This dfU inhibitor has proven to be a valuable tool, being used extensively in the kinetic characterization of *e*UDG (Chapter1 pg. 48).

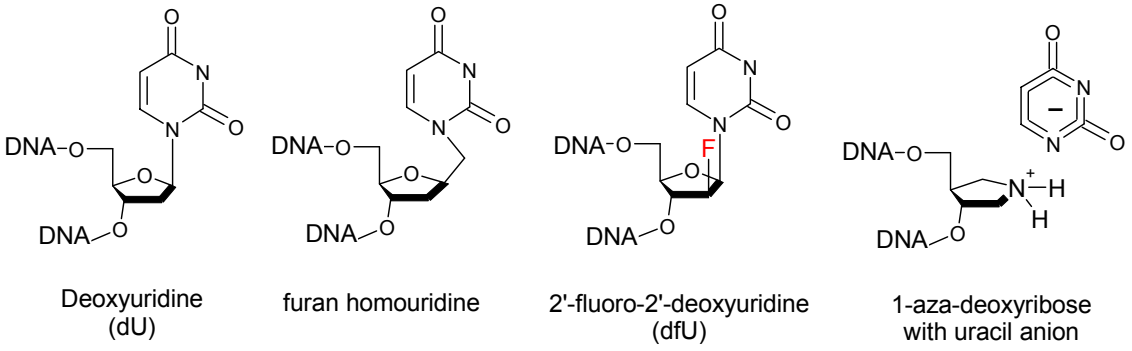

Figure 1-4. Structures of the most successful chemical inhibitors of Ung UDGs. The structures and tightest binding inhibitors of Ung family UDGs yet synthesized. Only inhibitors that are part of an oligo have shown a significant affinities: furan homouridine ($K_D^{Ap} \approx 160$ nM); 2′-fluorodeoxyuridine ($K_D^{Ap} \approx 50$ nM); and 1-aza-deoxyribose with uracil anion ($K_D^{Ap} \approx 110$ pM). The structure of the natural substrate (dU) is shown for reference.

Proteinaceous Inhibitor of UDG

One very interesting relic (if in fact it is that old) of the pre-deoxythymidine days of DNA based genomes is the Bacillus subtilis bacteriophage (PBS-1 and -2), which uses deoxyuridine instead of deoxythymidine to encode its genome [172]. This supposed relic has survived because it has evolved a uracil DNA-glycosylase inhibitor protein (Ugi), an early gene product that protects the PBS genome from digestion by Ung family glycosylases [173-175]. Ugi is specific for Ung family UDG's, binding at the active site and forming an essentially irreversible complex with UNG, while being unable to inhibit MUG and SMUG.

The effectiveness of this proteinaceous inhibitor has naturally sparked intense interest into the mechanism of its binding to Ung in the form of many mutational and crystallographic studies [135, 176-180]. These studies have shown that Ugi interacts with conserved regions of Ung involved in DNA binding, and directly mimics protein–DNA interactions observed in the enzyme–flipped oligonucleotide complex. The incredible specificity of Ugi for Ung family UDGs has facilitated *in vivo* studies where Ugi is used to knock-out Ung activity. Since Ugi is specific for Ung, it leaves Dug (a.k.a. Mug) and other uracil glycosylase activities intact, making Ugi an invaluable tool in alternative uracil glycosylase research.

The continued existence of a phage that uses uracil instead thymine is a perplexing subject. What selective advantage could come from using uracil in a genome? Especially considering that the organism is faced with the daunting task of knocking out a very active, nearly ubiquitous enzyme that can easily destroy it. It is entertaining to think that maybe once there were many PBS-like phages that exerted a strong negative selective pressure early during evolution. This negative selection pressure may have added toward

the need to evolve a powerful enzyme like UDG to counteract these phages. Therefore, UDG may have acted like a restriction endonuclease in the defense of the host, supplying a strong selective advantage.

This scenario solves the problem that Poole et al. first proposed [8] of which came first, UDG or thymidine? Without a repair system there is no obvious benefit to evolve to use dT instead of dU. If the repair system comes before the machinery for dT synthesis arises, then the organism has to deal with the removal of proper coding uracil along with the mutagenic deaminated cytosines. Because the possibility that both dT synthesis and dU removal abilities evolved simultaneously is very small, Poole and colleagues propose that the problem could have been alleviated by a proto-ung ancestor, much like Dug (a.k.a. Mug), that was not very active and therefore would not remove too many of the proper coding uracils (which would cause serious harm to the organism). However, this is still a negative selective force, which is hard to reconcile unless there was an obvious gain, such as protection from phages. It is easier to see how the potential deleterious effects of coding uracil removal (such as mutation and toxic abasic-site formation) would be tolerated if there was the tremendous advantage of immunity from what could have been the majority of parasites of that time. The PBS phage would then be one of the lucky few parasites that were able to counteract UDG with its inhibitor protein and survive (while others adapted to use dT). To answer these fascinating questions we would need to be able to trace the genetic lineage of the PBS phage to see when it arose. The Ugi protein has given biochemists much to think about, from its mechanism of very specific irreversible inhibition, to its implications in evolution.

Structural Characterization of UNG family UDGs

Structural work on the highly conserved Ung-family glycosylases has focused on the herpes simplex virus type 1 (vUDG), the human (hUDG), and the *E. coli* enzymes (*e*UDG). Structure-based sequence alignments of herpes simplex virus type 1 UDG, *e*UDG, and human UDG give a 39% sequence identity between vUDG and hUDG, and a 56% sequence identity (73% similarity) between *e*UDG and hUDG [179, 181]. At this time there are 20 unique crystal structures of Ung family UDGs in the Research Collaboratory for Structural Bioinformatics (RCSB) Protein Data Bank. These structures of the herpes virus, *E. coli*, and human enzymes have shown that the overall root-mean-squared (rms) distances for C^{α} positions of *E. coli* UDG with human and viral UDG are 0.9 Å and 1.5 Å, respectively (figure 1-5)[135, 181]. Comparing the human and viral UDGs gives rms for C^{α} positions of 1.3 Å, which means the human and *E. coli* enzymes are more structurally similar to each other than to vUDG, but all have an almost identical core structure.

The crystal structure of vUDG provided the first view of a monofunctional glycosylase and revealed the alternating α-β-α fold that has become the structural hallmark of the UDG superfamily [182] (Fig. 1-3). The structure showed that free uracil was bound in the active site and allowed the discernment of key enzyme–uracil interactions. Three types of interactions define a strikingly specific pocket for binding uracil: specific H-bonding, aromatic π-stacking, and tight steric constraints (Fig. 1-5 and 1-6).

Direct hydrogen bond partners are available to every polar atom of the uracil ring. The O2 carbonyl of the bound pyrimidine receives a hydrogen bond from the amide hydrogen of the peptide bond joining a conserved Gly–Gln sequence (Gly143–Gln144 in

hUDG; Gly62–Gln63 in *e*UDG; Gly86–Gln87 in vUDG). This interaction helps fix the orientation of the base in the pocket, but does not distinguish cytosine from uracil.

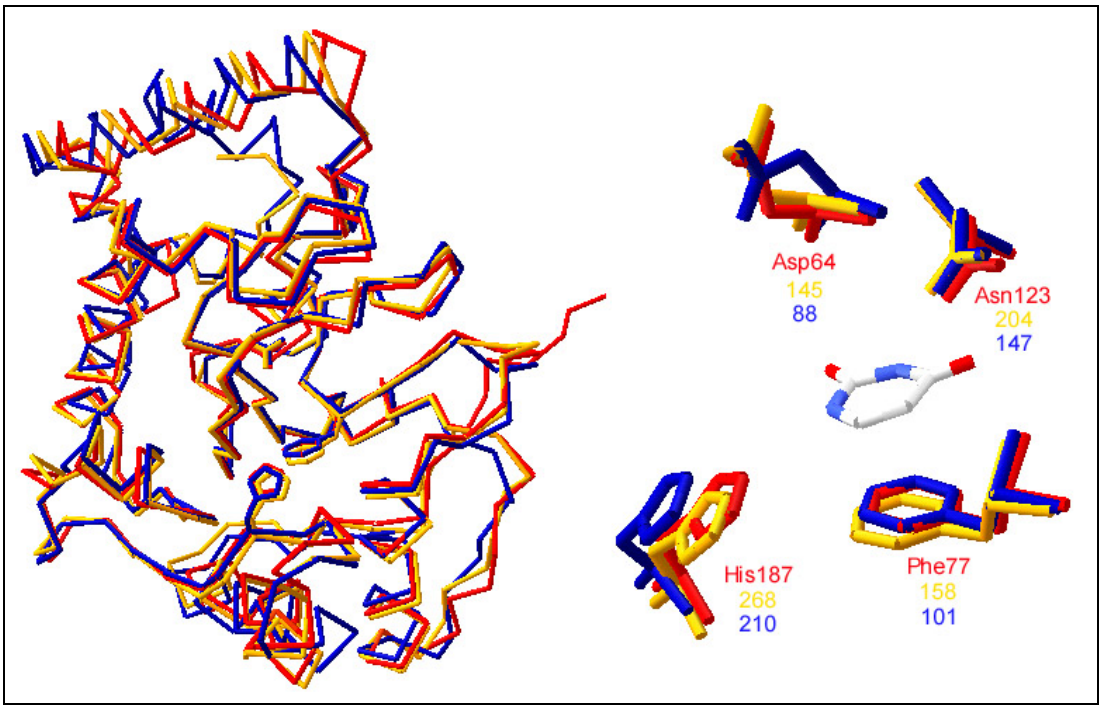

Figure 1-5. Peptide backbone alignment of bacterial, human and viral UDGs. On the left is a α-carbon trace of *e*UDG (PDB ID 1EUG in red) aligned with those of vUDG (PDB ID 1UDG in blue, RMSD 1.3 Å, 206 target pairs) and hUDG (1AKZ in yellow, RMSD. 0.9 Å, 213 target pairs). On the right is an overlay of the key catalytic amino acids colored and their residue number colored as on left surrounding uracil (CPK coloring). Figure generated with the Swiss PDB Viewer.

The electrophilic catalytic histidine (of motif B) also makes important contacts to the O2 of uracil through an H-bond at the N^{ε} (His268 in hUDG; His187 in *e*UDG; His210 in vUDG). This hydrogen bond has been found to become very polarized during the glycosidic bond cleavage transition state that is critical for stabilizing the uracil anion [158] (this is discussed in detail in the upcoming section on UDG reaction mechanism). This same group also makes another H-bond from the N^{ε} of the catalytic histidine to the N1 of uracil (Fig. 1-6).

To distinguish uracil from cytosine there is an asparagine at the front of the uracil-binding pocket (Asn 204 in hUDG; Asn 123 in *e*UDG). The orientation of this amide head group is critical, because in the opposite rotamer, the amide group could form parallel hydrogen bonds with the unprotonated N3 ring nitrogen and exocyclic N4 amino groups of cytosine. It has been proposed that the solvent structure of the binding pocket fixes the orientation of the asparagine side chain because surprisingly, the amide head group of the asparagine makes no direct hydrogen bonding interactions with the rest of the protein that would unambiguously fix its orientation [137].

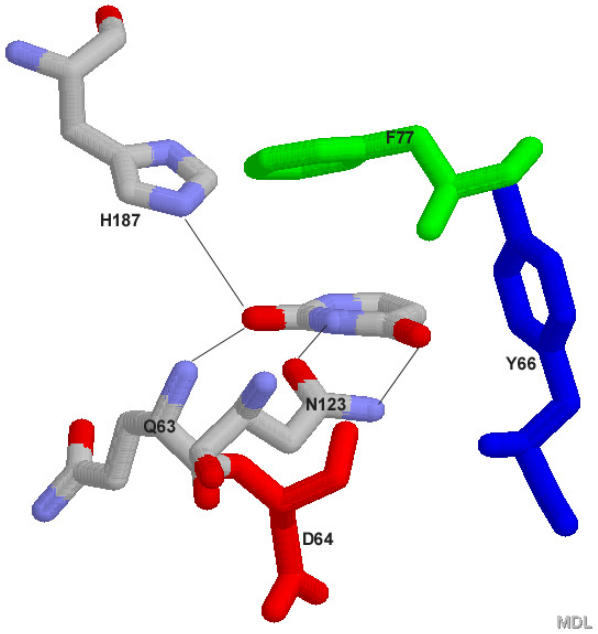

Figure 1-6. The key uracil–UDG active-site interactions. Model of *e*UDG active-site with uracil bound. Hydrogen bonding groups colored in CPK with implied H-bonds drawn in with narrow straight lines. The conserved Phe (green) and Tyr (blue) from rigid walls with the catalytic Asp (red) positioned under the uracil. Generated from PDB ID 2EUG with Protein Explorer.

A face-to-face π-π stacking interaction is made between the conserved phenylalanine (Phe-77 in *e*UDG; Phe-158 in hUDG; Phe101 in vUDG) and the bound uracil. The nature of this interaction and the energy contributed to uracil binding is the

focus of this work. Another aromatic residue, the conserved tyrosine (Tyr66 in *e*UDG; Tyr147 in hUDG), makes a van der Waals contact against the C5 of uracil, which prevents binding of thymine as the methyl group (or any group larger than fluorine) would sterically clash with the phenol ring. These rings form the rigid walls, buttressed by the bulk of the protein, of the extraordinarily specific UDG active site.

UDG Accesses DNA by Flipping Nucleotides

Shortly after the structure of vUDG was published the crystal structure of a catalytically inhibited double mutant hUDG was solved and showed the enzyme in a product bound state [183]. This structure revealed that the enzyme had rotated, or flipped, the abasic site deoxyribose 180° from the major groove, extruding it from the double helix with the free uracil base captured in the active site pocket. Two highly conserved structural motifs are involved in nucleotide flipping and uracil recognition. The "finger" motif of His-Pro-Ser-Pro-Leu-Ser forms a stiff loop with the leucine side chain forming the tip. This finger enters the DNA helix from the minor groove and occupies the space left by the flipped deoxyuridine. The uracil base is then captured and the *N*-glycosidic bond is cleaved with the Gly-Gln-Asp-Pro-Tyr-His active site motif (motif A) in which the aspartate is reputed to electrostatically stabilize the carbenium reaction intermediate and activate a water to act as a general base to capture the carbocation (discussed on pg. 57).

This cocrystal structure provided an answer to the question of how UDG was able to carry out a nucleophilic attack at the anomeric center, which is buried in the grooves of DNA. Methyltransferases were the first nucleotide flipping enzymes observed [184, 185] and UDG was the first glycosylase to be shown to use nucleotide flipping, which has

subsequently been found to be a general strategy used by enzymes to gain better access to nucleotides in DNA.

The "Pinch, Push, Pull" Mechanism

An ensuing hUDG–product-DNA cocrystal structure [134], this time with the fully active unmutated human enzyme, allowed for comparison of unbound and product bound states of the enzyme leading the authors to propose a "Pinch-Push-Pull" model for substrate recognition. In this model UDG kinks the DNA phosphate backbone while reading along purine N3 atoms in the minor groove with the leucine finger, which stops the enzyme when it runs into the N3 of guanine in a U:G wobble mispair (which juts into the minor groove). This pause in DNA scanning allows UDG to use rigid Ser-Pro loops to compress, or "pinch," the DNA phosphates flanking a given site providing initial damage detection without the need for flipping every nucleotide [134]. During the DNA pinching process, the DNA both 5′ and 3′ of the flipped-out nucleotide is B-form, and the distance between the phosphates flanking the uracil nucleotide is compressed by ≈ 4 Å with three rigid enzyme loops, which causes the DNA to kink almost 45˚. It was proposed that this kink of the DNA backbone destabilizes the DNA duplex and provides almost all of the force needed for nucleotide flipping (discussed in detail in kinetics section). Superimposing straight, undamaged B-DNA onto the uncomplexed UDG structure revealed that free UDG cannot bind B-DNA without pinching and thereby bending the DNA backbone.

The next proposed steps can happen in either order as the structurally derived nucleotide flipping model lacked the information to assign the temporal order in the flipping mechanics. The leucine finger motif could enter the DNA helix from the minor groove to "push" the nucleotide and the uracil is "pulled" into the active site via specific

hydrogen bonding, or the deoxyuridine is pulled into the active site and the finger fills the void in the DNA, thus achieving nucleotide flipping. The strong UDG "pull" was proposed to allow effective catalysis of single-stranded DNA, where the pinch and push components are negligible [186].

However, this model fails to explain how the DNA–protein interactions are sufficient for UDG scanning of long segments of DNA when the enzyme–DNA interface is small and has few direct and water-mediated DNA phosphate contacts with basic or polar amino acid side chains. The model also does not explain how UDG finds uracil that is base paired with adenine with only slightly less efficiency than uracil in a U:G mispair.

Human UDG Cocrystal Structure with Substrate Mimic

A final piece of the UDG structural puzzle came with the hUDG–substrate-DNA structure of the enzyme bound to an unhydrolyzable substrate analog, 2′-deoxypseudouridine (dψU) which has a C-C glycosidic bond instead of the normal C-N bond [187]. This model shows UDG rotates the uracil ring ≈ 90° on its N1–C4 axis to a position almost halfway between *anti* and *syn* (χ angle = 177˚; figure 1-7). Steric clashes between the uracil C6 hydrogen and the deoxyribose O4′, and between uracil O2 and the deoxyribose C2′ hydrogen, work together to significantly stretch the glycosylic bond in this enzyme-induced deoxyuridine deformation. In the dψU–UDG uncleaved substrate complex, the π-π interaction with the stacking active site Phe is less ideal because the C1–C6 (N1–C6 in normal uracil) edge is tilted about 20° more toward the sugar. This stretches the hydrogen bonds between the uracil and conserved active site moieties more than in the cleaved-product complex. Thus, the cleaved uracil can travel further (≈ 0.8 Å) into the active site to achieve greater complementarity with the enzyme

than the uncleaved dψU DNA substrate complex can. Therefore, none of the specific active site–uracil interactions evident in the product complex are optimized until after the glycosylic bond is cleaved.

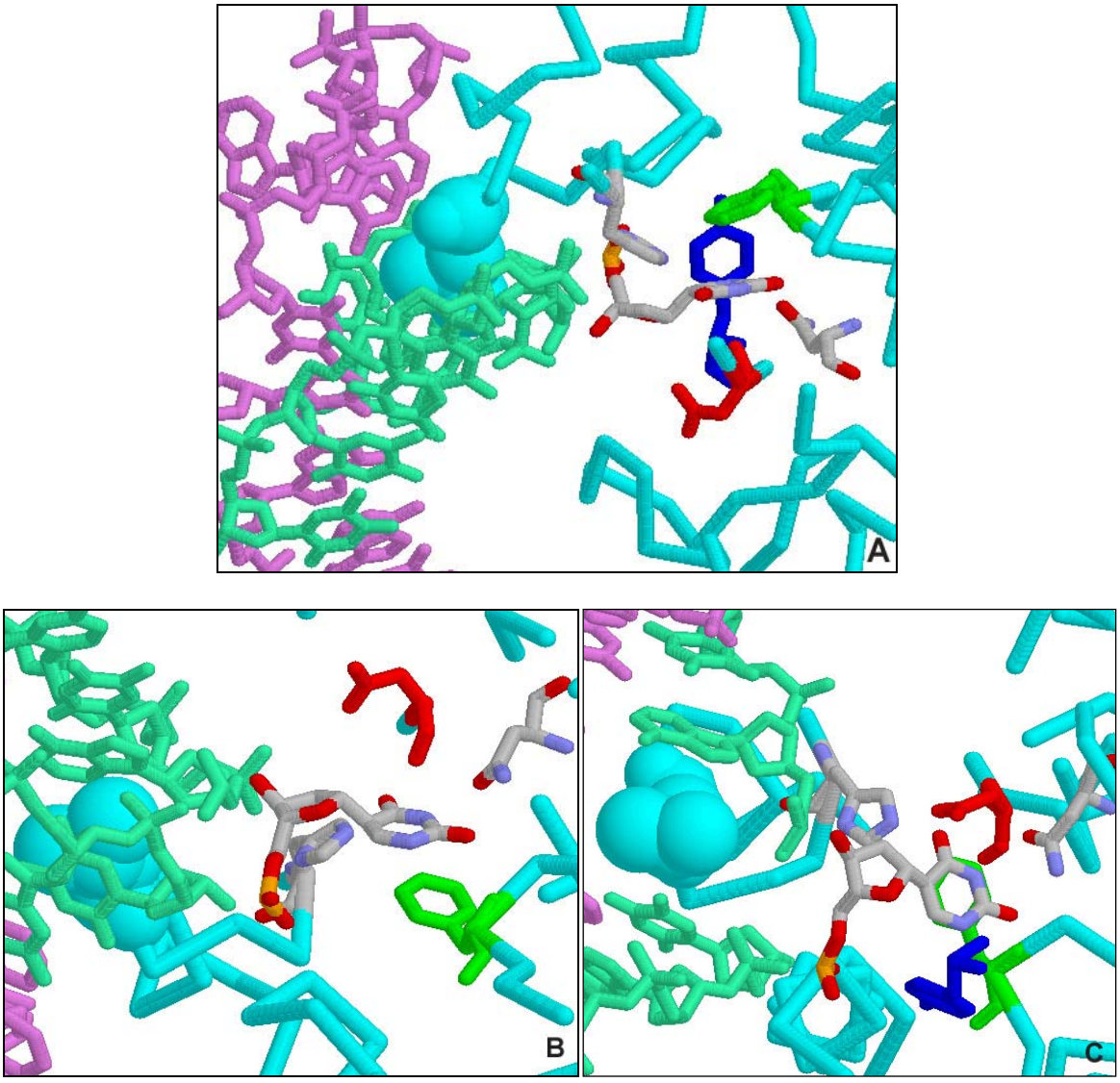

Figure 1-7. Human UDG bound to substrate mimic dψU. Different views of hUDG bound to a duplex DNA containing dψU (CPK color scheme). Active-site residues: Phe (green), Tyr (blue), Asp (red), His and Asn (CPK) are depicted in stick form while the leucine finger is shown space-filled to its Van der Waals radii. (A) Zoomed out view with Tyr in background; (B) view from other side and with the Tyr omitted for clarity; (C) is the view from the top with the uracil ring on top of the conserved Phe. Generated from PDB ID 1EMH with Protein Explorer.

The sum of these distortions, implemented by the rigid aromatic residue walls (Phe and Tyr discussed above) in conjunction with the tight anchoring of the DNA phosphates both 5′ and 3′ of the substrate mimic, induce a deformation that results in an approximate tetrahedral geometry at C1 (the glycosylic bond is bent ≈ 50° out of the plane of the uracil ring) instead of the normal trigonal planar geometry at N1 (Fig. 1-7). The distortion was not limited to the glycosidic bond, but also involved the flattening of the deoxyribose ring from an O2′-endo conformation (normally found in B-DNA) into a C3′-exo conformation. These observations led to the proposal of a structure-based reaction mechanism in which the substrate distortion aligned atomic orbitals for maximal hyperconjugative overlap facilitating electron transposition needed for bond cleavage.

Structure-Based Reaction Mechanism

Parikh and colleagues [187] proposed a structure-based reaction mechanism that resolves what they termed as the apparent "orthogonal paradox" where the three electron pairs to be transposed in glycosidic bond cleavage are held in orthogonal orbitals. In deoxyuridine the σ*-orbital of the C1′ of deoxyribose is orthogonal to the π-orbital of the C2=O carbonyl bond of the uracil base, thus preventing orbital overlap. Normally, nucleotides in DNA assume an *anti*-conformation, with the σ*-orbital involved in the anomeric effect. The anomeric effect refers to the observation that electronegative substituents in the anomeric position (C1′ in sugars) prefer to be axial even though they are expected to be equatorial from steric considerations [188-191]. Parikh et al. propose that the first stereoelectronic effect utilized by UDG is an enhancement of the anomeric effect with the flattening of deoxyribose to a mild C3′-exo, which enables more p-σ* overlap with O4′ (Fig. 1-8).

The orthogonal paradox is then remedied by a second stereoelectronic effect that is achieved via the glycosylic bond rotation and pyramidalization of N1. Together, these distortions create electron orbital overlap between the glycosylic bond and the C2=O and C4=O carbonyl π-systems, to take advantage of a hypothetical σ-π aromatic effect.

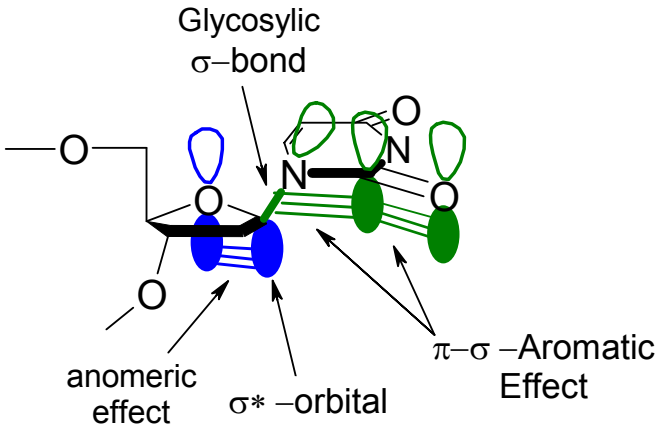

Figure 1-8. Hypothetical stereoelectronic effects utilized by UDG. Deformation of dU in the active site of UDG enhances the anomeric effect (blue) which stabilizes the carbocation on C1 and aligns π-orbitals of uracil (green) with the *N*-glycosylic bond so electrons can flow onto the uracil ring, cleaving the glycosylic bond. Adapted from [187].

The σ-π aromatic effect was first developed to explain the attributes of pyridoxal phosphate-dependent enzyme catalysis [192], and is manifest as the enhanced cleavage of σ-bonds that are aligned perpendicular to the aromatic pyridinium ring to optimize σ-π orbital interactions. UDG forces stereoelectronic cooperativity between the anomeric and σ-π aromatic effects, aligning pairs of atomic orbitals participating in each electron transposition so the electrons can flow from the deoxyribose C1′ to the uracil O2, creating a carbocation at C1′ and uracil anion while cleaving the glycosidic bond. Therefore, Parikh et al. suggest that the UDG transition state is "highly dissociative" with bond cleavage followed by collapse of the reactive intermediates. In the discussion of the

UDG transition state, a comparison of the features of this structure-based reaction mechanism will be made with the proposed transition state for the *E. coli* enzyme. This comparison is valid due to the high level of conservation between the human and prokaryote enzymes along with the nearly identical reaction rates measured for both enzymes when assayed under the same conditions [142].

Conformational Switching by UDG

Superimposing the dψU–UDG or product–UDG cocrystal structures with UDG's structure alone shows the enzyme undergoes a "conformational clamping," (induced fit) upon binding these oligos. Studies of *e*UDG showed the enzyme's intrinsic tryptophan fluorescence was quenched upon addition of dfU inhibitor containing DNA substrate, but not with normal DNA, and was proposed to be caused by the conformational change in the enzyme's structure (discussed in detail in next section)[153]. For *e*UDG alone, there are structural data on 20 crystallographically independent molecules, free as well as complexed with various DNA substrates or Ugi, which have helped define this conformational clamping.

Difference distance matrices relating DNA-free and DNA-bound molecules constructed for the *E. coli* and human enzymes delineate four essentially rigid body regions of the molecule, within each of which the internal movements are minimal [193]. These four rigid regions can be further grouped into two topographical domains that upon DNA binding rotate relative to each other, but stay relatively rigid in themselves. For *e*UDG domain 1 contains amino acids 6-76 and 112-150, while domain 2 consists of amino acids 77-105 and 155-220 with amino acids106-111 and 151-154 being linker regions between the domains (Fig.1-9). The transformation from the open to the closed form causes a rotation in the range 8-10˚ between the essentially rigid bodies of the

domains along an axis passing through the extensive interface located in the middle of the central β-sheet between the two domains. Main-chain hydrogen bonds connect the two central strands (I and III) in the closed form, displacing a bridging water in the open form.

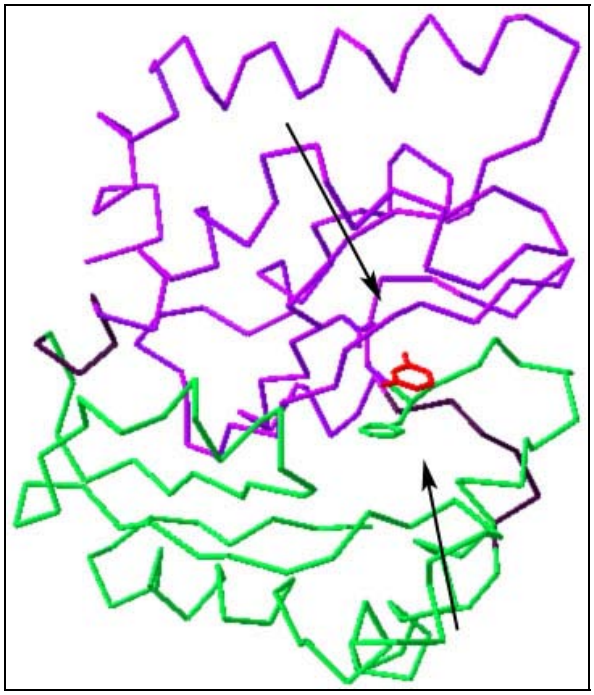

Figure 1-9. Structural domains of UDG. The UDG structure can be divided into domain I (purple) and domain II (green) that rotate about 10˚ on an axis formed by linker regions (black) toward each other. This motion results in a clamping (arrows) on the substrate or product (red). Generated from PDB ID 2EUG with Swiss PDB Viewer.

The only other particularly pronounced movement during DNA binding involves a α-helix in topographical domain 2. This helix consists of amino acids 166-171 in *e*UDG and is on the protein surface with its N-terminus forming part of the DNA-binding region. The helix as a whole rotates about an axis nearly parallel to its own α-helical axis by an angle of about 8˚, while the helical parameters remain unchanged. This movement, along with concerted movements of the topological domains upon binding substrate

mimic or product DNA, causes rotations that close in on the nucleic acid molecule. The exact relationship (if there is one) between these domain movements and the associated quenching of UDG's tryptophan fluorescence has yet to be defined.

The Kinetics of *E. coli* UDG

From a chemical standpoint, the Ung family UDGs offer a chance to examine a remarkable catalyst. It is estimated that *e*UDG enhances the rate of spontaneous *N*-glycosidic bond hydrolysis by a factor of $\approx 10^{12}$ fold and has a catalytic proficiency (defined as the single-turnover maximum bond cleavage rate divided by the uncatalyzed reaction rate) of 10^{18} $mol^{-1}L$. Even more amazing is the fact that substrate binding and flipping contribute less than 2 kcal/mol of energy towards this catalysis [153]. The secrets of UDG's awesome power have been revealed in a number of studies with the *E. coli* enzyme and engineered mutants that have used a wide range of techniques.

DNA Interaction and Nucleotide Flipping Kinetics of UDG

The development of stopped-flow fluorescence has allowed a detailed investigation into the mechanism of nucleotide flipping of *e*UDG. Stivers et al. have determined the minimal kinetic mechanism for *e*UDG DNA binding and nucleotide flipping, and have measured a flipping rate that indicates the enzyme amazingly seems virtually unaffected by DNA helix stabilizing forces [153]. The authors of this study used the fluorescent base 2-aminopurine (2-AP; adenine analog that base pairs with thymine) as a probe to measure the nucleotide flipping rates and binding constants of *e*UDG. The DNA substrates utilized in their assays contained the deoxyuridine analog 2′-β-fluoro-2′-deoxyuridine (dfU), that was centrally located in the DNA substrate sequence and either base stacked with a 5′-2-AP or base paired with 2-AP in a complimentary strand. It was found that the *N*-glycosidic bond of the dfU nucleotide was hydrolyzed at a rate

10^7-fold slower than a regular dU nucleotide, which allowed for the measurement of binding and flipping via the fluorescence of the 2-AP, which becomes more fluorescent as base stacking between it and adjacent bases is disrupted. Stivers et al. determined that uracil flipping was not rate limiting and that UDG destabilizes the DNA before the flipping step, leading to flipping that is independent of base-pair stability and largely independent of base-stacking stabilizing forces.

In addition, Stivers et al. [153, 194] discovered that the fluorescence of *e*UDG's tryptophan residues decreased specifically with substrate flipping, giving them an intrinsic reporter for flipping induced isomerization of UDG. They monitored protein isomerizations caused by dU and dfU containing substrates, and control DNA substrates that had thymine in place of uracil. They found that there is no change in tryptophan fluorescence when the control undamaged DNA is the substrate, suggesting that UDG does not completely flip non-uracil bases. This intrinsic substrate-induced Trp fluorescence change of UDG provided direct evidence for an active mechanism of nucleotide flipping.

Stivers and coworkers also were able to measure the nonspecific DNA binding affinity of *e*UDG with stopped-flow pulse-chase experiments, where the enzyme and DNA were preincubated and the rate of the decomposition of the enzyme–nonspecific DNA complex was monitored by an increase in fluorescence as *e*UDG rebound a trap substrate DNA containing 2-AP next to dfU. A disassociation constant of 1.5 μM was measured, which does not support a DNA scanning mechanism for damaged base recognition. How then, does UDG find uracil within a large genome?

The problem of finding uracil within a genome has been likened to finding a needle in a haystack. If one considers that uracil differs from thymine by only a methyl group and base pairs with adenine with the same Watson-Crick geometry as an A:T base pair, then the problem is better described as finding a few special needles in a whole pile of millions of needles!

A processive extrusion mechanism for initial damaged site recognition where UDG migrates along DNA flipping every nucleotide isoenergetically by exchanging one extra helical base for the next does not seem likely due to a fast off rate of 560 s^{-1} determined with fluorescent spectroscopy for non-specific DNA [153]. Previous processivity measurements of UDG on 25mer concatemeric dsDNA substrates indicated that the enzyme is semi-processive at physiological salt concentrations [195, 196]. A semi-processive mechanism would indicate that the enzyme "hops" along the DNA, sampling bases at the points the enzyme makes contacts. Thus, in the absence of alternatives, *base sampling* seems the most likely process by which Ung family UDGs locate uracil bases in DNA.

Raman spectroscopy has also been used to investigate the pathway for attaining the final extrahelical state [197]. The binding of undamaged DNA to *e*UDG results in decreased intensity of the DNA Raman bands, which the authors attributed to an increased level of base stacking. This is consistent with the structural models that show that UDG pinches the DNA backbone causing a compression that would decrease the space in between neighboring bases, and increase base-stacking in the DNA. Duplex DNA containing dfU in complex with eUDG shows similar increases in the level of DNA base stacking. In addition, a strong sharp negative peak in the Raman spectra of UDG

was assigned to Phe77. This peak decreased in intensity when UDG and dfU substrate mimic were mixed, indicating the uracil was base-stacking with the active-site phenylalanine and that UDG could flip dfU all the way into its active site. Comparison of spectra taken in the presence and absence of substrate analog dfU, showed an additional conformational change in UDG that is not observed with undamaged DNA, consistent with the conformational clamping of the enzyme onto the damaged nucleotide. Therefore the Raman spectral data confirm many of the UDG–DNA interactions found by X-ray crystallography.

Mutational Analysis of Nucleotide Flipping by UDG

The proposed "pushing" component of the nucleotide flipping was first tested by mutation of the leucine "finger" in hUDG to alanine, which reduced the mutants activity to <1% that of wild-type [134](Fig. 1-7). The analogous mutations in *e*UDG, L191A and L191G, retained roughly 10% and 1% of the enzymatic activity, respectively [177, 198, 199]. As expected, Jiang et al. found that the L191A and L191G mutants were deficient in substrate binding, but unexpectedly, the mutations also compromised the enzyme's ability to conformationally switch, demonstrated by a lack of tryptophan quenching [194]. Interestingly, mutation of the leucine finger to valine or phenylalanine had a negligible effect on the catalytic efficiency of *e*UDG, indicating side chains of different shape and size are tolerated as long as they extend beyond a methyl group and do not hydrogen bond with the DNA appreciably [177].

Further, it was demonstrated that incorporating a bulky pyrene across from uracil within duplex DNA rescues the L191A and L191G mutations, restoring the L191A to wild-type activity levels [198, 199]. The rescuing of these mutants by pyrene was due to the restoration of substrate binding capacity to wild-type levels, as measured with the dfU

substrate analog [199]. The authors also found that pyrene can rescue the association and off-rate defects of the Leu191 deletion mutants along with the ability of the mutants to undergo the induced fit conformational change, as evidenced by a restoration in tryptophan quenching. It was proposed that the pyrene wedge accomplished the same functions as the leucine finger, namely, causing the deoxyuridine across from it to be stably extrahelical, or flipped, and facilitation of the conformational change into the substrate induced fit. This lead to the proposal that Leu191 plays a role in the early stage of the flipping process by acting as a pushing wedge to help form the extrahelical state of the substrate, and then functions in the late stages of nucleotide flipping as a plug to increase the lifetime of the substrate in the active site pocket [194].

The "pinching" component of the nucleotide flipping mechanism of UDG was also probed by mutational analysis. The DNA recognition and pinching loops in *e*UDG contain conserved serines (S88, S189, and S192) that H-bond with the DNA phosphodiester backbone [134]. The most important for enzyme activity are S88 and S189, with the double S88A/S189A mutant exhibiting an 8200-fold damaging effect on k_{cat}/K_M as compared to wild-type *E. coli* UDG [200]. The S88A/S189A double mutant shows a 65-fold detrimental effect substrate affinity, which due to defects in both the rate of substrate binding (on rate defects) and the ability of the enzyme to stay bound to substrate (off rate defects). In addition, the serine double mutant, like the Leu191 deletion mutants, has 35% less Trp fluorescence quenching upon binding dfU, indicating this double mutation impairs the enzyme's conformational change [194]. However, removal of these individual serine side chains does not prevent or dramatically slow attainment of the closed conformation as judged by the similar Trp fluorescence

decreases with wtUDG, suggesting cooperative action of these groups in the overall process of attaining the conformationally closed state.

As compared to the leucine finger mutants, pyrene rescue shows a distinctly different effect for the serine pinching mutants, fully rescuing on-rate defects but not the off-rate defects. This indicated to Jiang and Stivers that the S88A/S189A mutations cannot be rescued by pyrene because the pyrene wedge is not able to fulfill the stabilizing interactions of these groups in the substrate bound state. This research has defined the role of these serines, and amazingly, how critical two hydrogen bonds can be to substrate binding and manipulation by UDG and possibly other glycosylases.

Finally, asparagine and histidine mutations (N123G, H187G) were engineered to remove hydrogen-bonding groups that "pull" on the uracil by bonding to O2, O4, and N3. Only the removal of Asn123 shows a strong damaging effect on base flipping [194], which confirmed earlier observations by this research group that His187 forms a strong H-bond with the Uracil O2 *only* during the transition state of glycosidic bond cleavage (discussed further below) [158]. The absence of a tryptophan fluorescence change suggests the N123G mutant could not achieve the induced fit conformational change with the substrate.

This research has provided an intimate view of the three step process of nucleotide flipping and substrate recognition. To summarize, a positively charged DNA binding cleft orients the initial DNA–UDG collision complex and allows the conserved serines pinching loops to disrupt the DNA duplex. The pinching destabilizes the DNA prior to nucleotide flipping making flipping largely independent of DNA structure. The pinching also provides almost all of the force needed to flip the nucleotide from the DNA helix,

with a small pushing contribution from the leucine finger. The leucine finger stabilizes the extrahelical nucleotide allowing more efficient capture of the uracil base in the active site. Once flipped, the enzyme undergoes a conformational change that clamps down upon the nucleotide, docking the substrate within UDG.

Current Kinetic Mechanisms for *E. coli* UDG

Two groups have proposed complete kinetic pathways for *E. coli* UDG, both of which are very similar. One pathway is composed of steps that are rigorously defined with many techniques with multiple types of substrates (i.e., the dfU inhibitor and differing oligos) [159], but which makes testing the self-consistency of a global mechanism impossible [201]. The other kinetic pathway has been defined with a single substrate, therefore allowing for global, computer-simulated fit of all kinetic data to a single minimal reaction mechanism and a unique set of microscopic rate constants [202]. Conversely, the more accurate global analysis of the mechanism came at the expense of the quality of data obtained from a minimal set of measurements (and some of the data had a low signal:noise ratio). My discussion of these kinetic pathways will emphasize the major differences, while the complete set of rate constants will be presented in Chapter 8 (Fig. 8-1).

The mechanisms consist of the same steps with the exception of an additional protein isomerization step included in the pathway by Wong et al. These steps are represented as follows: formation of the initial UDG–DNA collision complex ($E+S \leftrightarrow ES$); deoxyuridine flipping ($ES \leftrightarrow EF$); first UDG isomerization leading to Trp quenching ($EF \leftrightarrow EqF$); irreversible glycosidic bond cleavage ($EqF \rightarrow EqP$); reverse protein isomerization or leucine finger retraction (only in the model by Wong et al.) ($EqP \leftrightarrow EP$); product release ($EqP \leftrightarrow E+D+U$ or $EP \leftrightarrow E+D+U$ where D = abasic site

DNA). So in the mechanism by Stiver's group, relaxation of UDG from the conformationally clamped state happens concomitantly with product release, whereas Wong et al. claim that protein relaxation (Trp fluorescence recovery) and product release are separate steps.

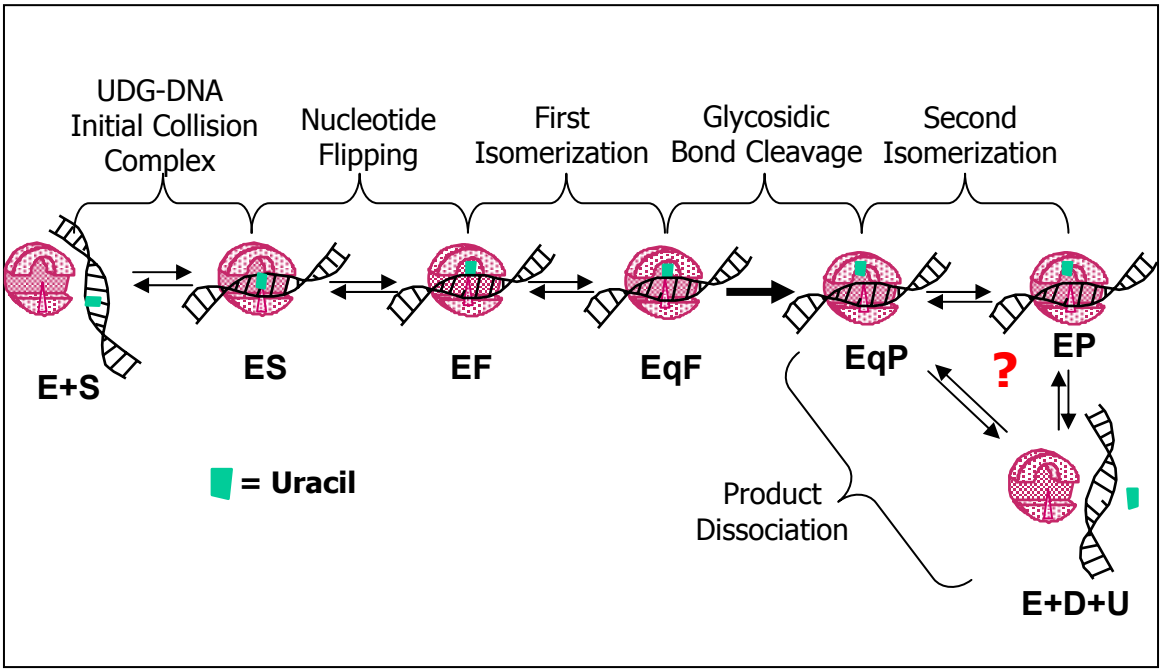

Figure 1-10. Cartoon of the current kinetic mechanisms proposed for *E. coli* UDG. Two groups [194, 199, 202] have suggested reaction pathways for the UDG catalytic cycle that are the same except for a second isomerization step added before product dissociation in the model Wong et al. See text for details.

The proposed mechanism by Stivers' group has been constantly evolving. Both the on rate ($E+S \leftrightarrow ES$) and flipping rate ($ES \leftrightarrow EF$) previously reported were significantly faster than currently reported rates (550 $\mu M^{-1}s^{-1}$ and 1240 s^{-1} versus 220 $\mu M^{-1}s^{-1}$ and 700 s^{-1}, respectively). Curiously, Stivers' group did not have a separate step for isomerization prior to the publication by Wong et al. Both groups propose a three-step mechanism for deoxyuridine flipping and justify the temporal placement of the enzyme's

conformational change after nucleotide flipping with measurements of the maximum rate of the 2-AP fluorescence evolution that range 40-60% faster than the maximal Trp quenching rate.

The use of the substrate analog (dfU) allowed Jiang and Stivers [199] to make some important measurements that could not be performed by Wong and coworkers. First they noted that the hyperbolic concentration dependence of the observed rate for UDG binding to substrate analog indicates a change in the rate-limiting step from concentration-dependent association of the enzyme with the DNA to concentration-independent isomerization of the enzyme-DNA complex. The dfU containing DNA was also used to measure the off-rate of UDG from substrate and was found to be single exponential, which indicated that the multistep process of DNA dissociation has one major rate-limiting transition state. Another important observation was that the off rates measured using tryptophan and 2-AP fluorescence were identical, indicating to Jiang and Stivers that the same rate-limiting step is detected in both experiments; requiring the reverse isomerization of UDG to be slow compared to the reverse step of base flipping and DNA dissociation.

The computer-simulated fit of the kinetic data by Wong and colleagues [202] showed that substrate DNA is bound at least one order of magnitude faster than expected for a diffusion-control limited process, and much faster than the value measures by Jiang and Stivers. This lead the authors to suggest that UDG utilizes some form of a facilitated diffusion search mechanism for locating U:A base pairs. This hypothesis is based on measurements made with 2-AP as a reporter on UDG association with DNA, which in my opinion lacked a high enough signal to noise ratio.

Wong and coworkers' model was also based on single turnover reaction rates measured with rapid chemical quench. These authors found that irreversible *N*-glycosidic bond cleavage occurs at a rate of 38 s^{-1}, and that UDG has a K_D^{Ap} of 38 nM for deoxyuridine containing DNA. Utilizing the UDG inhibitor protein (Ugi) as a nondestructive quench, Wong et al. measured a net product forming partitioning factor of 33%. Finally, simulation of a minimal kinetic mechanism by Wong et al. required an additional step for a conformation change, which they claim reflects the retraction of the inserted leucine finger, and occurs after excision but prior to release of product at the steady-state turnover rate of 0.5 s^{-1}. However, there is no direct evidence for this second conformational change and as stated by the authors themselves, "[t]he assignment of the tryptophan signal to Leu insertion is somewhat more presumptive…," [202 pg. 19430] because the Trp fluorescence change could result from any structural change that effects their environment. Indeed, there are three tryptophans (out of the 6 total) that are the most likely source of the signal change are above the active site Phe (Fig. 8-8), removed from the leucine finger [181].

Rigorous interpretation of these pathways is dependent on the correlation of Trp fluorescence signal change to an actual structural event in UDG. Despite this shortcoming, these two kinetic pathways have provided valuable insight into the mechanics of this powerful catalyst and excellent benchmarks to compare future results with. It will be interesting to see if the nucleotide flipping rates of other glycosylases will measure up to UDG. If the flipping rates are comparable between glycosylases that could mean that there is a universal limit in forming extra-helical nucleotides. The question if

other glycosylases undergo a similar substrate-induced conformational clamping is also interesting, considering the diverse sets of damaged bases removed.

Features of the Transition State for UDG Glycosidic Bond Cleavage

One way to directly determine the transition-state structure for a chemical reaction is the use of kinetic isotope effects (KIEs). A KIE is a ratio of the reaction rates (k_{light}/k_{heavy}) for a substrate with light and heavy isotope substitutions at specific atom(s) that may change in vibrational environment between the reactant state and the transition state of the reaction [203, 204]. Therefore KIEs reflect changes in bonding modes between a reactant state and the transition state, providing direct information about the extent of bond breakage and geometry in the transition state.

Werner and Stivers measured a large normal ($k_{light}/k_{heavy} > 1$) α-deuterium KIE of 1.201 indicating that the anomeric carbon had become sp^2-like in the transition state, resulting from a loosening of the out-of-plane bending mode for the anomeric proton in the planar transition state as compared to the tetrahedral reactant state [141]. The sp^2 character of the C1′ carbon was further implied by large stereospecific 2′-β-deuterium KIEs of 1.102 and 1.106, which were proposed to originate from hyperconjugation of the 2′-substituents to the electron deficient *p*-orbital on the anomeric carbon of the nascent oxacarbenium ion. These large β-secondary and α-secondary KIEs along with a small primary ^{13}C KIE of 1.010, strongly suggested that the UDG reaction transition state is highly dissociative, with uracil departure and nucleophilic attack occurring in distinct steps (although a concerted but asynchronous mechanism is also possible). These results, together with several NMR and pH titrations of UDG active site groups, have led to the proposal of the following events during the glycosidic bond cleavage by *e*UDG.

In the ground state, UDG distorts the deoxyribose sugar into an unusual 3′-exo conformation that aligns the 2′-hydrogens for maximum hyperconjugative orbital overlap with the just formed *p*-orbital of the oxacarbenium ion in the transition state. Evidence for this distortion comes from the two, 2′-*β*-deuterium KIEs that are large and nearly equal, indicating that the dihedral angles for $H2'_S$ and $H2'_R$ in the transition state are approximately the same and therefore aligned. The crystal structure of deoxypsuedouridine bound to the active site of hUDG also showed that the enzyme had deformed the sugar conformation from the usual 2′-endo conformation found in B-DNA into a "mild 3′-exo conformation" (discussed in the structure-based reaction mechanism) [187] . This hyperconjugation helps to stabilize the developing carbocation on the C1′. This preorganization of the substrate also minimizes motion in the ground state of reactive atoms during achievement of the transition state.

As the reaction proceeds to the transition state, the electrophilic catalyst His187 forms a strong hydrogen bond with the uracil O2 which serves to pull electron density away from N1 of uracil and stabilize the negative charge that develops at that carbonyl. Nuclear magnetic resonance and pH titrations together have shown that His187 does not donate a proton to uracil, but remains neutral during the catalytic cycle [158, 205]. The Raman studies also show a N1=C2-O is zwitterionic in character in the ground state, which suggests that the uracil 02–His187 interaction contributes substantially to make uracil a good leaving group [197]. These interactions decrease the nucleophilic reactivity of N1 and hinders reformation of the glycosidic bond.

When the carbocation is formed on the deoxyribose, electrostatic interactions with the uracil anion, Asp64, and nearby phosphate groups of the product DNA are used for its

stabilization. The magnitude of the electrostatic stabilization of the UDG transition state has been studied through transition-state mimics and site-directed mutations of both Asp64 and His187, which supposedly holds the uracil anion in the UDG active site with the H-bond to uracil O2. Evidence for the important role of these amino acids is supplied by mutation studies that found the D64N and H187Q mutants exhibit 6,600- and 3,500-fold decreases in the maximum single-turnover rates, which correspond to contributions of 5.3 and 4.8 kcal mol^{-1}, respectively [206]. These groups have been tested further by measuring the effect mutation of these residues has on the binding of the 1-azadeoxyribose transition state intermediate analog (Fig. 1-4). The apparent magnitudes of the electrostatic stabilization of the transition state provided by these charges is 2.9 kcal/mol and 3.4 kcal/mol on the basis of the 118- and 318-fold damaging effect of removing Asp64 and His187, respectively, with the D64N/H187Q double mutant having an additive 7.2 kcal/mol (154,000-fold) damaging effect to binding of the 1-azadeoxyribose transition state mimic [207].

In a computational study of the UDG reaction, the major driving force for glycosidic bond cleavage was suggested to be "substrate autocatalysis" [208]. Dinner et al. used hybrid quantum-mechanical/molecular-mechanical (QM/MM) approach with the coordinates of the hUDG–dψU crystal structure and found the dominant contribution to lowering the transition state activation barrier comes from the DNA substrate phosphate groups (21.9 kcal/mol). These phosphates are buried on substrate binding opposite the uracil base, and are hypothesized to stabilize the rate-determining transition state by repelling the uracil anion leaving group and stabilizing the carbocation. This QM/MM computational study also found that the protein backbone accounts for an additional 4.7

kcal/mol, and importantly that that conformational strain and stereoelectronic effects contribute at most 5 kcal/mol to catalysis.

Jiang et al. addressed this proposal by comparing the damaging effects of stereospecific methylphosphonate (MeP) substitutions, that ablate the negative charges of phosphodiester groups, on the kinetic parameters of UDG and 1-azadeoxyribose oxacarbenium ion analogue affinity [142]. These experiments revealed that in total, all of the combined phosphodiester interactions with the substrate contribute only 6-8 kcal/mol toward lowering the activation barrier (3-fold less than the computed value). Although these results are not as large as calculated by the QM/MM approach, the significant role of the substrate's negative backbone in lowering the barrier for glycosidic bond cleavage means part of UDG's catalytic power does come from substrate autocatalysis.

Finally, in the last step of the glycosidic bond cleavage, a nucleophilic water attacks C1′ carbocation and the sugar relaxes back to a normal C2′ endo configuration in the product complex. This water molecule is found in the dψU–hUDG crystal structure to be held by the catalytic Asp in a position that does not allow the water to act as a direct in-line general base; but the water would be close enough to capture the carbocation [187]. The proton from the water nucleophile has been proposed to be bonded to Asp64 [208], but there currently is no experimental evidence for its fate.

The stepwise mechanism[1] of dU glycosidic bond cleavage by UDG is rare among enzymes and highlights the mechanistic differences between enzyme-catalyzed hydrolysis of purine and pyrimidine bases. Purine *N*-ribohydrolases have the advantage

[1] It should be pointed out that the observed KIEs were composite values through irreversible bond cleavage and therefore a concerted asynchronous hydrolysis mechanism has not been completely ruled out by experiment.

that the purine leaving group can easily be activated by protonation at N7 ($pK_a \approx 2$) [209], whereas protonation of a pyrimidine is unfavorable due to the high pK_a's of its carbonyls [158, 206]. Uracil DNA glycosylase has solved the chemical problem of activating a pyrimidine base to become a good leaving group by stabilization of charged transition state intermediates, instead of protonation of uracil. To stabilize the uracil anion UDG uses a set of H-bonds that pull the negative charge towards the carbonyl oxygens. The enzyme then uses this stabilized anion with the catalytic Asp to help stabilize the carbocation on the deoxyribose in an "electrostatic sandwich." It is fascinating how UDG uses charges on the substrates and products to achieve and enhance catalysis.

UDG is remarkable in that it can work with equal facility on double-stranded and single-stranded dU DNA, but has no activity towards RNA. The half life of the nonenzymatic cleavage of dU at pH 7 and 37˚ C is 23 years [210], which *e*UDG reduces to about 5 ms (under saturating enzyme single-turnover conditions). This 10^{12}-fold (16 kcal/mol) reaction rate enhancement and incredible specificity make UDG an amazing catalyst, worthy of all the attention devoted towards it.

Project Relevance

Hopefully, the preceding literature review made it apparent that UDG is one of the most thoroughly investigated enzymes, and the most thoroughly characterized DNA repair glycosylase. However, out of all the engineered mutations to UDG, no one has yet mutated the active site phenylalanine (Phe77 in *e*UDG). Because of its absolute conservation in family-1 UDGs, and its stacking interaction with uracil, we hypothesized that Phe77 may be an important part of the catalytic core of UDG. This section of the

introduction lists questions we thought mutating Phe77 could address, and the relevance of UDG research because of its biological importance in mutation avoidance.

Relevance of Mutating Phenylalanine 77 of *E. coli* UDG

The mutation of Phe77 of *e*UDG will reveal how critical this amino acid is to the functioning of the enzyme and supply some insight into the following questions: *How important are the steric constraints in the proper functioning of the UDG active site?* The structure-based reaction mechanism suggested that enforcing a tetrahedral geometry on the substrate lowered the energy barrier for glycosidic bond cleavage by inducing conformational strain and stereoelectronic effects in the substrate. Replacement of the phenyl side chain with a methyl group would be expected to loosen the steric constraints within the active site. If catalysis is critically dependent on the geometry of the substrate within the active site we could see a large damaging mutational effect.

Do the π-π orbital base stacking interactions between Phe and uracil help pull the base into the active-site? Although π-π orbital interactions are weak in solution, the assumed (based on the transition state) low dielectric constant inside the UDG active site may amplify this interaction. The active site His187 has an anomalously low pK_a [206], so there is a precedent for strange effects within the UDG active site. The importance of base stacking interactions in enzyme mechanism has precedence in DNA polymerases [211].

Crystal structure models of free enzyme as compared to the substrate and product structures show UDG clamps down upon substrate or product, becoming more compact, with movements that bring key hydrogen bonding groups into better position. So, if we just think on a mechanical level, we can ask if there is a mechanical trigger: *Does uracil stacking with Phe trigger the protein to isomerize into the closed confirmation?*

The role of Phe77 could be complex; necessitating consideration of altered substrate geometry and π-orbital stacking effects; or the role could be as simple as excluding water from the active site to keep a low dielectric environment for the reaction. A simple site-directed mutagenesis experiment will not be enough to answer the aforementioned questions, but it is a beginning.

The Importance of UDG as a Genome Guardian

Ung$^-$ strains of *E. coli* exhibit 3- to 5-fold increase in spontaneous mutation frequencies throughout their whole genomes ([212], with up to a 35-fold in G:C→A:T transitions at some specific sites [44, 213-215]. Unexpectedly, -1/-2 nt frameshifts are also elevated in *ung*$^-$ strains, which challenges the assumption of a simple relationship between glycosylase and mutation spectra [212]. The loss of UDG not only effects replication-associated mutation fixation (i.e., when a deaminated C is fixed into a transition), but has been associated with an increase in transcription-associated -1 nt frameshift mutations in Saccharomyces cerevisiae [19]. Thus even nongrowing cells require expedient removal of uracil caused by cytosine deamination to avoid transcriptional base substitutions that would generate mutant proteins and phenotypic changes [216].

The absence of a substantially higher mutation frequency in *UNG* knockout mice has led to the proposal that the primary function of UDG in mammalian cells is the removal of uracil paired with adenine from dUTP incorporation during DNA replication [79]. Seemingly in agreement, UNG expression is cell cycle-dependent [217], increasing substantially following DNA replication, and UNG has been found to colocalize at replication foci [155, 217, 218]. However, contrary to the knockout study, human cells expressing the phage PBS2-encoded inhibitor of UDG show a marked increase in

C:G→T:A spontaneous mutations [219], indicating that UNG does contribute to the removal of uracil in U:G mispairs resulting from cytosine deamination. More recent work has created an amended model in which hUDG is responsible for both pre-replicative removal of deaminated cytosine and post-replicative removal of misincorporated uracil at the replication fork, with hSMUG1 as a broad specificity backup [220]. It seems premature to claim *UNG* knockout mice do not have a higher mutation frequency because it may take a great many generations of mice before mutations reach a detectable level. It is naïve to think that a few litters of mice can reliably report on selective pressures that have shaped life for billions of years.

Hence, many imperfections in the DNA repair process may have very subtle effects, with no appreciable phenotype. It is well established that gross loss of DNA repair capacity leads to severe conditions such as xeroderma pigmentosum, an autosomal recessive disorder where inactivating mutations cause extreme skin cancer predisposition [221]. Yet, it is now discernable that modest changes in repair capacity, detected in both population studies and animal models, are also associated with an increased risk of cancer, particularly when coupled with environment [109].

The cell extracts from *UNG* null mice have revealed a fifth distinct uracil-DNA glycosylase activity [79], emphasizing that correction of uracil in DNA is a major biological problem that demands considerable overlapping activities to retain a high level of DNA quality control. Impairment of any one of these redundant uracil-DNA repair activities, while not displaying an overt phenotype, weakens the overall fitness of the organism. Understanding the subtleties of uracil-initiated BER is the first step in uncovering the nuances of major forces that affect our health and evolution.

CHAPTER 2
EXPERIMENTAL METHODS

Cloning and Expression of Wild-Type UDG from *E. coli*

The gene that encodes UDG in *E. coli* has been given the designation *ung* [222, 223]. The *ung* gene was PCR cloned from *E. coli*. strain B genomic DNA and spliced in frame at a start codon into the pLex expression vector (Invitrogen), which controls protein expression with a trp repressor (J. Lopez). In this expression construct, transcriptional control is achieved by expression of the λCI repressor that is driven by the trp promoter. When tryptophan is added to the medium it forms a complex with the trp repressor that binds the trp promoter and stops transcription of λCI repressor controlling the transcription of the target gene, which is then expressed to high levels driven by the promoter for bacteriophage lambda.

The pLex vector containing *ung* was transformed into the competent strain supplied by Invitrogen. These cells were grown at 30˚C to an optical density (OD) of 0.5 at 550 nm in induction media made according to the manufacturer's directions lacking tryptophan. Protein expression was then induced by adding tryptophan to 100 μg/ml final concentration and increasing the incubator temperature to 37˚C. After four hours of protein expression, the cells were harvested by centrifugation (10 min at 5000 X g) and the media decanted followed immediately with storage at -70˚C.

Purification of Wild-Type Recombinant UDG from *E. coli*

The purification procedure was adapted from several published methods (see Fig. 2-1 for reagents and purification details) [156, 223, 224]. The protein purity of

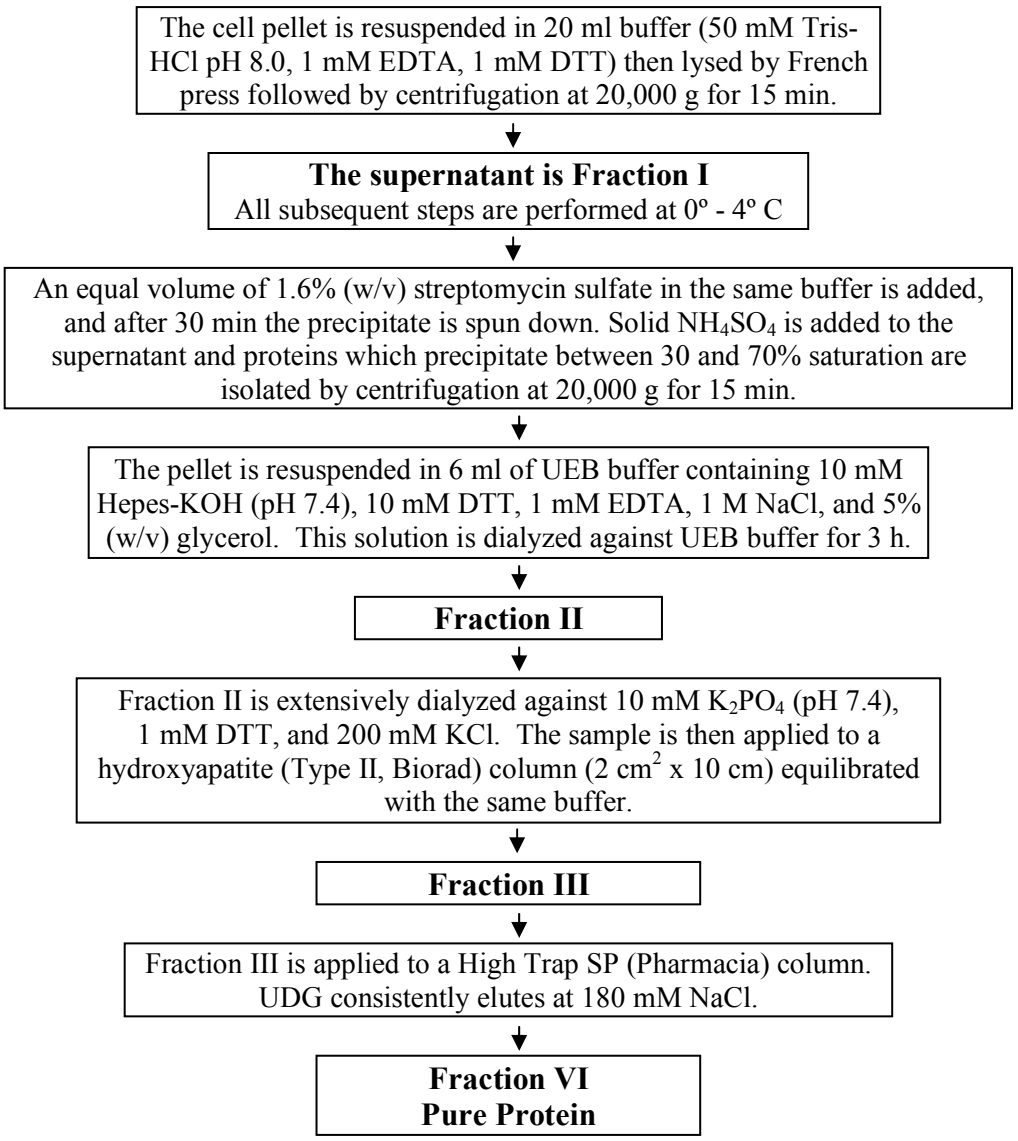

Figure 2-1. Purification flowchart for wild-type *E. coli* UDG. This procedure was adapted from refs [156, 223, 224].

fraction VI was assessed by silver-stained SDS-PAGE. The gels showed only two bands, one that traveled at the same molecular weight as the control UDG purchased from New England Biolabs, and one that appeared to be double the 25.5 kD molecular weight calculated for UDG from its amino acid sequence. By increasing the amount of reductant (5 mM DTT final) and decreasing the temperature (from 100 to 75˚ C) that SDS denaturing was performed at, the high molecular weight band was almost completely eliminated, which suggested it was a dimer caused by a sulfhydryl bond between the single surface cysteine of the proteins. The assumption that the upper band of the approximate molecular weight of 50 kD was in fact a dimer of UDG was later confirmed by Western blot (see purification of His-tagged UDG section).

To confirm that the protein in fraction VI was in fact UDG, *N*-terminal amino acid sequencing was performed by the ICBR protein chemistry core facility at the University of Florida. The first 17 residues from our preparation were sequenced and showed that the *N*-terminal methionine was removed, as it is normally *in vivo* for UDG from *E. coli*, and the sequence was identical to the published UDG sequence[222]. The absence of signals for contaminating proteins during the *N*-terminal amino acid sequencing provided a lower estimate of the preparation's purity as greater than 95% pure, with a final yield of about 50 mg UDG purified from 4 liters of cells.

Pure fraction VI enzyme was dialyzed against UDG storage buffer (35 mM Bicine-KOH, 45 mM KCl, 1 mM EDTA, 1 mM β-mercaptoethanol, 50% (v/v) glycerol pH 8.0) containing only 5% (w/v) glycerol, which was supplemented after dialysis to attain the necessary 50% (v/v) glycerol final. Enzyme concentration was determined by measuring its absorbance at 280 nm using the experimentally determined extinction coefficient of

38,000 $M^{-1}cm^{-1}$ [126, 156] for both the native and denatured protein. This enzyme stock was aliquotted and stored at -70˚ C. However, stocks also kept at -20˚C showed no appreciable loss of activity after years of storage.

Construction and Expression of His-Tagged Wild-Type and Mutant UDGs

Phenylalanine 77 of the *ung* gene was changed to an alanine, asparagine, and a tyrosine by standard site-directed mutagenesis in three constructs. After the mutations in these constructs were confirmed by sequencing of both strands, the wild-type and mutant constructs were cloned into pET14b expression vector (Novagen) at the Nde1 and EcoR1 restriction sites (a gift from Dr. Joyce Feller). This expression vector adds a six histidine affinity tag attached with a thrombin cleavage site to the amino terminus of the polypeptide to aid in purification. The pET14b(wt), pET14b(F77A), pET14b(F77N), and pET14b(F77Y) constructs were then transformed into the recombination deficient host *E. coli* BL21(DE3)plysS for expression. The extra level of transcriptional control offered by the BL21(DE3)plysS construct was necessary due to the fact that BL21(DE3) only host did not grow well, which was assumed to be due to leaky expression of the construct that was somehow toxic to the cells. Host BL21(DE3)plysS cells express low levels of T7 lysozyme which inhibits leaky transcription by T7 RNA polymerase often found in the BL21(DE3) only cells.

Transformed cells were plated on LB agar plates supplemented with 100 μg/ml ampicillin and 1% (w/v) glucose according to the manufacturer's instructions, and incubated overnight at 37 ˚C. Single colonies from the plates were used to inoculate 100 ml of 2XYT starter cultures supplemented with 100 μg/ml ampicillin and 1% glucose. The starter cultures were grown until they reached an OD_{600} of 0.4, at which point they were immediately transferred to 4 ˚C. After overnight incubation at 4 ˚C the starter

cultures were centrifuged at 6000 × g and washed with 10 ml of ice cold Luria broth supplemented with 100 μg/ml ampicillin to wash away any secreted β-lactamase. After the culture was washed two times it was resuspended and used to inoculate two 2 L culture flasks containing 1 L 2XYT media supplemented with 100 μg/ml ampicillin. These cultures were grown until they reached an OD_{600} of 0.6, at which point they were induced with 1 mM (final concentration) IPTG. After 4 hours of induction, the cells were centrifuged at 6000 × g and immediately placed in the -70˚C freezer. Typical yields ranged between 6-9 g of cells per L culture.

Purification of His-tagged Wild-Type and Mutant UDGs

Frozen cells (≈ 20 g) were placed in 50 ml conical tubes and resuspended by vigorous shaking in ice cold binding/wash buffer (20 mM $NaPO_4$, 0.5 M NaCl, 5% (w/v) glycerol, 1% cell lytic B (Sigma) pH 7.2). Cells were ruptured by French press (three passes at 4000 lbs/inch pressure) and the insoluble material was centrifuged at 25,000 × g. The supernatant was extracted and 1.6 % (w/v) streptomycin sulfate was added with stirring on ice. After at least 30 min of stirring on ice, the precipitate was centrifuged at 25,000 × g. The supernatant was diluted with binding buffer and applied to two 5 ml High Trap chelating columns (Amersham-Pharmacia) that had been previously loaded with nickel and washed and equilibrated with binding buffer according to manufacture's directions. After loading of the protein, the chelating columns were washed with buffer until the absorbance at 280 nm (A_{280}) and conductivity returned to the original baseline levels of buffer only. His-tagged protein was washed and eluted with elution buffer (20 mM $NaPO_4$, 0.5 M NaCl, 5% (w/v) glycerol, 0.5 M imidazole pH 7.2). The washes consisted of 10% elution buffer for 5 column volumes followed by 20% elution buffer until A_{280} stabilized at a new baseline (usually around 10 column volumes),

followed by a linear gradient over 2 column volumes of 50% to 80% elution buffer. His-tagged UDG, visible as a large UV absorbance above the buffer background, eluted around 55-65% elution buffer (≈ 300 mM imidazole).

Eluted His-tagged enzyme was concentrated by stirred cell (Amicon) and dialyzed against (10 mM Bicine-KOH, 100 mM KCl, 1 mM EDTA, 1 mM β-mercapto ethanol, 5% (v/v) glycerol pH 8.0) five 1 L buffer changes at 4˚C. After dialysis, the appropriate volume of 20X UDG storage buffer and glycerol were added (see wtUDG purification protocol), and the proteins stored at -70˚C. Protein purity and identity was assessed by Sypro Red™ (Amersham-Pharmacia)-stained SDS-PAGE and western blot, respectively. Twelve percent SDS-polyarcylamide gels were prepared, run, and stained with Sypro Red™ according to manufacturer's directions, except all stainings were incubated overnight. These gels were then destained for 30 min and scanned with the Typhoon fluorescence/ phosphoimager (Molecular Dynamics) with the following instrument settings: Green (532 nm) laser, normal sensitivity, and photomultiplier tubes at 700 V. Serial dilutions of the wild-type protein were always included on the gel with the mutant protein to ascertain if the gel stain/scanning instrument were working to their peak detection limit. The protein was judged to be >95% pure by densitometric analysis of the scanned gels.

The gels, like those of the non-His-tagged protein, showed two bands; one band that migrated even with the control UDG, and one that appeared to be a dimer. The approximate molecular weight of these bands as judged in relation to protein standards was about 28 kD for the monomer and 55 kD for the dimer, which is the expected size of the complete protein with His-tag (25.5 kD for UDG + 2.2 kD for the His-tag) calculated

from amino acid sequence. The presence of the 6× His-tag was confirmed by Western blot with a murine monoclonal antibody specific for that epitope (Sigma). The presence of the His-tag was detected in both the 28 and 55 kD bands, confirming that the dimer was indeed UDG.

Protein concentrations were determined by A_{280} with the same extinction coefficient as used for the wt enzyme (38,000 M^{-1} cm^{-1}), since both the active site and His-tag mutations did not add or subtract tryptophan residues from the protein. The concentration determined by UV absorbance correlated well with the detection limit of the Sypro Red™ dye (≈ 5 ng). Typical yields were about 15 mg of pure protein/L of culture.

Oligodeoxynucleotide Synthesis and Purification

Substrate oligos, 25 nucleotides in length, were designed with their respective complimentary strand and analyzed with the program DNA-Man for possible secondary structure that might interfere with UDG–substrate interactions. Each DNA differs by only one base that is centrally located in the oligo. The abbreviations of the DNA substrates are based on the central substrate (U = deoxyuridine), undamaged (T = thymine), abasic-site product mimic (X = tetrahydrofuran), and substrate mimic (ψ = deoxypsuedouridine) nucleotides flanked by their nearest neighbors, two adenines. The compliments are designated small "c" followed by the one letter designation for the base that pairs with the nucleotide of interest. The shorthand designation for the substrate AUA annealed to the compliment in which the central uracil forms a proper Watson-Crick base pair is AUA/A. This nomenclature will be used to designate the duplex DNA substrates throughout this paper (i.e., in AUA/G, G = guanine and is complimentary to AUA and forms a uracil:guanine mispair (Table 2-1).

Table 2-1. The DNA substrates used in this study.	
Abbreviation	Sequence 5′ to 3′
AUA	ACC GTG TGA TAA **AUA** AGG CGT TAA A
ATA	ACC GTG TGA TAA **ATA** AGG CGT TAA A
AXA	ACC GTG TGA TAA **AXA** AGG CGT TAA A
AΨA	ACC GTG TGA TAA **AΨA** AGG CGT TAA A
cA	T TTA ACG CCT **TAT** TTA TCA CAC GGT
cG	T TTA ACG CCT **TGT** TTA TCA CAC GGT
cG-Rh	T TTA ACG CCT **TGT** TTA TCA CAC GGT-NH_2-Rh

The abbreviations of the DNA substrates are based on the central substrate (U = deoxyuridine), undamaged (T), product mimic (X = tetrahydrofuran), and substrate mimic (Ψ = deoxypsuedouridine) nucleotides flanked by their nearest neighbors. The compliments are designated small "c" followed by the one letter designation for the base that pairs with the nucleotide of interest (i.e., in cA, A = adenine and is complimentary to AUA and forms a uracil/adenine base pair.

These substrates were synthesized with an Applied Biosystems 390 synthesizer using nucleoside phosphoramidites and reagents purchased from Glen Research (Sterling, VA). After deprotection in concentrated NH_4OH overnight at 65 ˚C, the NH_4OH was evaporated by rotary vacuum and the oligos were mixed with 50% (w/v) glycerol and applied directly to a denaturing 20% polyacrylamide, 8 M Urea, TBE (100 mM Tris-HCl, 38 mM Borate, 1 mM EDTA) gel for purification, with no more than 50 nmol DNA loaded per lane. The bands corresponding to the desired product were visualized with UV-shadowing, cut from the gel and electro-eluted with four buffer changes in sterile 0.5X TBE. The fractions were then passed over an anion exchange resin (Sigma) loaded spin column (Biorad), washed with DNA storage buffer (10mM Bicine-KOH, 10mM KCl, and 1mM EDTA) supplemented with 0.2 M KCl and then eluted with the same buffer containing 2 M KCl. Using 3 kD nominal molecular weight cut-off Amicon micro concentrators (Milipore) the buffer was exchanged (four buffer changes) with DNA storage buffer and the oligos were concentrated. DNA concentrations were determined

by UV absorption at 260 nm, using the calculated extinction coefficients for the constituent nucleotides [225]. These DNA stocks were aliquotted and stored at -20˚C in storage buffer.

Radio-Labeling of DNA Substrates

To detect the substrate, approximately 5% of the 25mer substrate oligo AUA was radio-labeled at its 5′ end with ^{32}P in a reaction mixture containing kinase buffer (35 mM Bicine-KOH, 100 mM KCl, 8 mM $MgCl_2$, 1 mM DTT pH 8.0) 6.44 μmols of DNA, and 120 μCi of [γ-^{32}P]ATP (Amersham-Pharmacia) through a reaction catalyzed by 1 unit of T4 polynucleotide kinase (New England Biolabs). After an overnight incubation at 25˚C the kinase was then heat deactivated by heating at 75˚C for 15 min. The substrates are then annealed in DNA storage buffer to their compliments to form duplex DNA by heating to 75˚C for five minutes followed by slow cooling over a period of no less than 3 hours. These 5′-end-labeled single-stranded or duplex oligos were used in the assay without further purification.

Steady-State Glycosidic Bond Cleavage Assay

The cleavage assay was adapted directly from a protocol developed by Varshney and van de Sande[140]. The assay takes advantage of the fact that abasic sites formed by the action of UDG can be cleaved by heating under alkaline conditions. The abasic site deoxyribose is in equilibrium between closed hemiacetal and ring-opened aldehyde tautomers, of which the open aldehyde is susceptible cleavage via a β-elimination reaction [226].

The steady-state bond cleavage assay was performed in UDG reaction buffer (35 mM Bicine-KOH, 45 mM KCl, 1 mM $MgCl_2$, 1 mM β-mercaptoethanol, 40 ng/ml BSA pH 8.0) and all reactions were performed at 25˚C. Reactions were initiated with

addition of 0.1 nM to 1 nM UDG and terminated by adding 5 µL of the reaction to 15 µL of 0.1 M KOH and immediately chilling the tubes on ice. Once all the samples are collected, the tubes are incubated at 75˚C for 30 minutes to completely catalyze phosphodiester backbone cleavage.

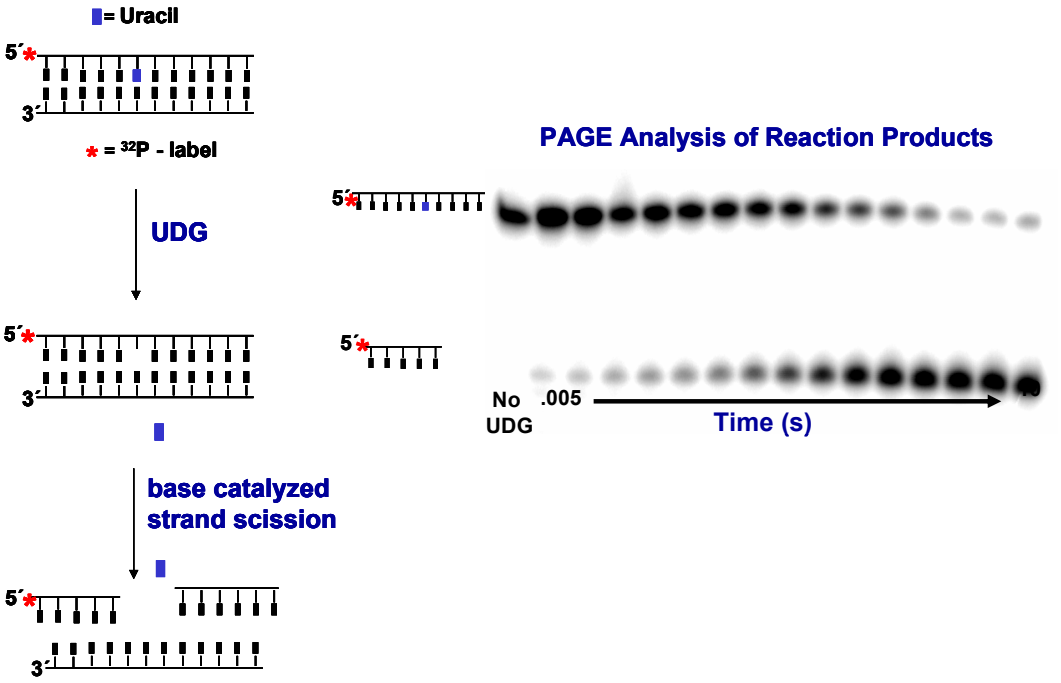

Figure 2-2. Glycosidic bond cleavage assay diagram with an example gel. Abasic site product formed by UDG is cleaved in half by a β-elimination reaction and are separated by denaturing PAGE based on size. A control reaction without UDG is quatitated as background and subtracted from the data.

After abasic site cleavage, the samples are chilled, centrifuged to collect the condensate, and an equal volume of loading buffer (95% formamide with about 0.05% bromophenol blue/xylene cyanol and 10 mM EDTA) was added. The 5′-radio-labeled products are half the length of uncatalyzed reactants and can easily be separated by electrophoresis on a 20% polyacrylamide denaturing (8 M urea, 1X TBE) sequencing gel. The β-emissions of the radio-label allow the amount of DNA in the product and reactant

bands to be measured by a Storm 840 phosphoimager (Molecular Dynamics). Only DNA that retains the 5′-label is visualized (Fig. 2-2).

The data are analyzed with the program Image Quant (Molecular Dynamics), which enables the user to define an area and quantitate the volume of counts in that area. Loading error is corrected by taking the ratio of products over the total counts in a given lane. Kinetic parameters were obtained by plotting the reaction velocities as a function of enzyme concentration and using nonlinear least squares regression curve-fitting to the Michaelis-Menten (Equation 2-1)

$$v_0 = \frac{V_{MAX} * [S]}{K_M + [S]} \qquad (2-1)$$

where v_o and V_{max} are the initial and maximal reaction velocities and K_M is the Michaelis constant. The assay is performed so that products stay under 10% of the total substrate concentration to maintain the system pseudo first-order with respect to substrate. All data plot creation and nonlinear least squares regression curve-fitting in this study is performed solely with the graphing program Sigma Plot™ (SPSS Inc.).

Rapid Chemical Quench Glycosidic Bond Cleavage Assay

The cleavage assay described for the steady-state measurements in the above section was readily adapted for use with a rapid quench machine. We employ a three syringe rapid quench machine made by KinTek™ (Fig. 2-3) [227]. The KinTek RQF-3 functions by using buffer to push the substrate and the enzyme that are loaded in the sample lines, into a reaction line which then mixes with the chemical quench in the exit line that is then ejected into a sample tube. This rapid-quench machine enables measurements of presteady-state kinetics on a millisecond timescale.

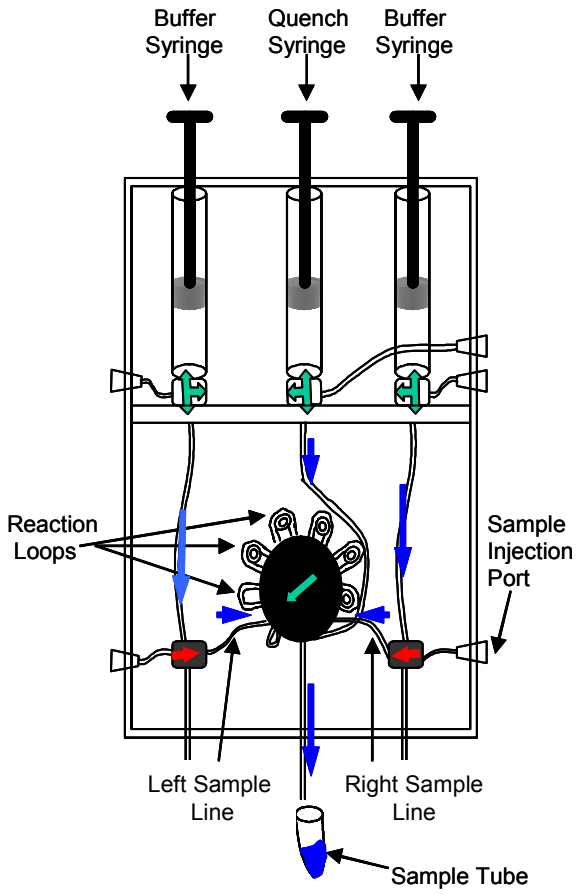

Figure 2-3. Diagram of the KinTek RQF-3. Through the sample injection ports enzyme is loaded on the left and substrate on the right. The reactants are pushed (direction of flow indicated by the blue arrows) into a reaction loop for a specified reaction time programmed into the instrument and then mix with the quench and are ejected into a sample tube.

All the buffers and substrates are identical to those described in the steady-state reactions and again potassium hydroxide is used as a quench. It was determined that at 0.5 M the UDG reaction is completely quenched (data not shown). The increased concentration of quench is necessary due to the fact that the rapid quench machine injects equal volumes of enzyme and substrate solutions together, and the amount of enzyme used in these reactions is far greater than in the steady-state reactions.

Maximum Single-Turnover Uracil Excision Measurements

To measure the rate of the chemical reaction catalyzed by UDG in absence of the effects of substrate binding maximum single-turnover uracil excision measurements were performed with the rapid-quench cleavage assay. In these reactions the concentration of enzyme was 10 to 100-fold in excess over substrate (usually 10 μM UDG to 0.1 μM substrate). Data points were collected on a time scale of 0-100 ms. The concentration of products formed over time ($[P]_t$) are graphed versus time and fit by nonlinear regression to a single exponential according to Equation 2-2,

$$[P]_t = y_0 + A(1 - e^{-k_{obs}t}) \qquad (2-2)$$

where A and k_{obs} denote the amplitude and the apparent rate constant of the exponential rise.

Presteady-State Product Burst Measurements.

The burst of product formation prior to attainment of steady-state enzyme turnover was measured by reacting limiting UDG (0.1 μM) with excess substrate 5′-^{32}P labeled AUA/A (0.5 μM and 1.0 μM). Reactions were performed on the KinTek RQF-3 rapid quench machine with reaction times focusing on the burst (under 2 s) to obtain sufficient data density to discern the separate phases of the reaction. Plots of the reaction products versus time are then fit by nonlinear regression to a single exponential (Eq. 2-2) followed by a line shown in Equation 2-3,

$$[P]_t = A(1 - e^{-k_{obs}t} + k_{ss}t) \qquad (2-3)$$

where k_{ss} represents the linear steady-state rate constant and the other variables are defined as in Eq. 2-2.

Single-Turnover Titrations.

Single-turnover titrations, where the enzyme concentration was held constant at 100 nM and the substrate was varied from 0.1 to 3 μM, were performed on the KinTek RQF-3 rapid quench machine. Typically, seven or more time points were collected spanning the full range of the reaction to over 85% completion. Reaction time courses were then fit with Eq. 2-2 by nonlinear regression. The observed reaction velocities (k_{obs}) from a set of reactions with substrate varied are then graphed as a function of enzyme concentration. The linear region of the dependence of k_{obs} on enzyme concentration is fit by linear regression to give approximations of the apparent second-order rate constant for association of the enzyme with the substrate (k_{on}, obtained from the slope), and the rate of dissociation of enzyme from substrate (k_{off}, the *y*-intercept value) [227]. The ratio of k_{off} over k_{on} will give the true dissociation constant (K_D) for the substrate. The plateau of k_{obs} versus enzyme concentration represents k_{max}, the maximal single-turnover glycosidic bond cleavage rate.

Steady-State Fluorescent Anisotropy Equilibrium Binding Measurements

Fluorescence anisotropy was used to measure binding affinities of UDG and mutants for various DNA oligomers. The fluorescent probe X-rhodamine (λ_{ex}^{max} = 585 nm, λ_{em}^{max} = 610 nm, τ = 5 ns; Molecular Probes) was coupled to the DNA via an isothiocyanate linkage to an amide linker synthesized into the DNA as a phosphoramidite. After labeling (according to manufacturer's instructions), the free unreacted dye is removed from the sample by purification on a gel filtration column filled with desalting resin (Biorad). The oligo labeled with Rhodamine was the compliment 25mer, cAUA-G (Table 2-1). This compliment was annealed to either substrate mimic, product mimic, or undamaged oligos (in 10% excess) to form the duplex DNA with the

target nucleotide centrally located in the sequence and the rhodamine 11 nucleotides away at the 5′-end.

Titrations were performed in a quartz cuvette in the standard UDG reaction buffer with 50 or 100 nM rhodamine labeled substrate and enzyme varied. Optical spectra were taken on a Photon Technology Inc. fluorimeter in dual channel mode, band pass set to 5 nm, and with excitation and emission monochromaters set to 580 and 610 nm, respectively. Each concentration step was measured in a separate cuvette, and the anisotropy change between the DNA only and DNA + UDG was recorded. Control measurements where UDG storage buffer only was added were subtracted as background from the data.

Kinetic parameters from this data were obtained by plotting the anisotropy values as a function of enzyme concentration and using nonlinear least squares regression curve-fitting to obtain the apparent dissociation constant (K_D). The fluorescence data is fit with Equation 2-4,

$$\Delta r = \Delta r_{\max} \frac{(K_D + [UDG]_0 + [DNA]_0) - \sqrt{(K_D + [UDG]_0 + [DNA]_0)^2 - 4[UDG]_0[DNA]_0}}{2[DNA]_0} \quad (2-4)$$

where Δr is the difference between starting (free anisotropy) and bound anisotropy, Δr_{max} is the maximal anisotropy signal change from the asymptotic value of the fit, K_D is the apparent dissociation constant for the interaction, and $[UDG]_0$ and $[DNA]_0$ are the initial concentrations of enzyme and DNA ligand, respectively.

Tryptophan Fluorescence Stopped-Flow Kinetic Measurements

The kinetics of the enzyme conformational change during catalysis was monitored through changes in UDG's tryptophan fluorescence in real time on an Applied Photo Physics Stopped-flow instrument (Surry, U.K.) in the two-syringe mode and equipped

with a 150W xenon arc lamp. Protein Trp fluorescence was excited at 290 nm and a 320 nm cuton filter (CVI) was used to monitor emission. All measurements were preformed in UDG reaction buffer lacking BSA at 25˚C. In the titrations enzyme was held constant while substrate was varied.

Between 4-8 kinetic traces were taken with the instrument set for a split time base in over-sampling mode. In over-sampling mode the data set is limited to 500 pts per half of the split time base, but each point in the slow portion of the time base is the average of the maximum number of acquisitions possible by the detector. This helps increase the signal:noise over long time courses. These kinetic traces were then averaged themselves to further increase the signal-to-noise ratio.

The fluorescent traces of the UDG F77N and F77Y mutants were fit entirely with an exponential decay followed by an exponential rise according to Equation 2-5,

$$f_t = A_1(1 - e^{(-t/\tau 1)}) + A_2(e^{(-t/\tau 2)}) + f_0 \qquad (2-5)$$

where f_t equals the change in Trp fluorescence over time, A is the amplitude of the signal change, τ is the inverse of the apparent rate constants for the exponential decay and recovery phases, and f_0 is the starting fluorescence. The F77A UDG data sets were not permissive to this analysis and had to be separated into their constituent quenching and recovery phases, which were graphed and analyzed by non-linear regression with a standard exponential decay for the fluorescence quenching phase given by Equation 2-6,

$$f_t = f_0 + A(e^{-k_{obs}t}) \qquad (2-6)$$

where the change in Trp fluorescence over time (f_t) and the other variables are as in Eq. 2-5. The exponential rise of fluorescence recovery was fit with Eq. 2-2, where f_t is substituted for $[P]_t$. Likewise, the Trp fluorescence traces of wt(His-tagged)UDG needed

to be separated into quenching and recovery phases due to the sigmoidal nature of the Trp-recovery. The quenching phase was fit with Eq. 2-7 while the recovery phase was fit with Equation 2-7,

$$f_t = f_0 + \frac{A}{1 + e^{-\left(\frac{t - t_0}{k_{obs}}\right)}} \qquad (2-7)$$

where the change in Trp fluorescence over time (f_t) follows a four parameter sigmoid with the variables defined as in Eq. 2-5.

For all proteins the observed rates obtained from the fitting of the fluorescence quenching were graphed versus substrate concentration. As with the analysis of the single-turnover titration data, observed rate constants that lie on the linear portion of the concentration dependence of the reaction rates were fit separately by linear regression to provide initial estimates of the rate constants k_{on} and k_{off} from the slope and y-intercept of the fit, respectively. These parameters were then used as constraints for a general hyperbolic expression representing two (or more)-step reversible binding, Equation 2-8,

$$k_{obs} = \frac{K[S]k_{quench} + k_{off}}{(K[S] + 1)} \qquad (2-8)$$

where k_{quench} is the maximum quenching or recovery rate, K is a composite equilibrium constant for the reversible steps, and k_{on} is determined from the product of K and k_{quench}. These refined values of k_{off} and k_{on} are used to calculate the equilibrium dissociation constant for substrate (k_{off} over k_{on}).

CHAPTER 3
CHARACTERIZATION OF WILD-TYPE UDG

Steady-State Kinetics of Wild-Type UDG

To provide the basis for comparison of the Phe77 mutagenesis effects, wild-type UDG (wtUDG) from *E. coli* was purified and its steady-state kinetic parameters measured. These kinetic parameters were determined using the glycosidic bond cleavage assay (with the 5′-radio-labeled substrate AUA/A; Table 2-1) first developed by Varshney and van de Sande [140]. The root of this method stems from the chemistry of Maxim and Gilbert DNA sequencing, which takes advantage of the base-labile abasic site formed by the removal of uracil by UDG, to cleave the phosphodiester backbone of the product DNA for facile separation from unreacted substrates on denaturing PAGE.

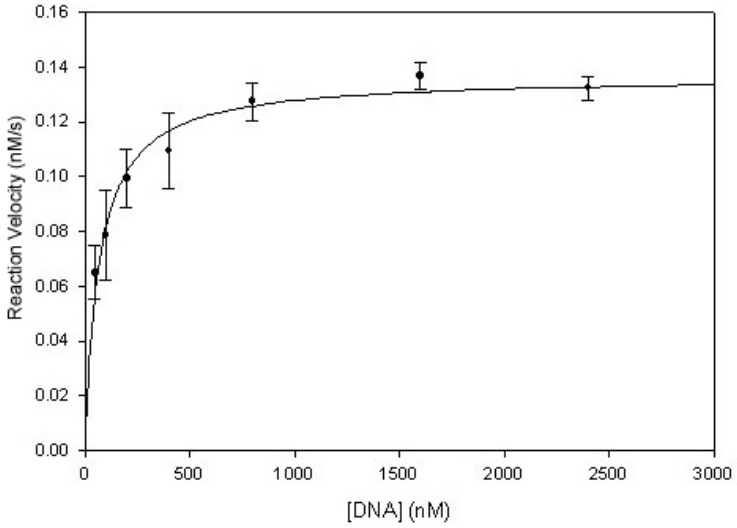

Figure 3-1. Determining the steady-state kinetic parameters for wtUDG by glycosidic bond cleavage assay. Increasing concentrations of substrate (AUA/A; 0-4 μM) were reacted with 100 pM UDG. The reactants and products were separated by denaturing PAGE and quantified by phosphoimager. The data were fit with nonlinear regression to the Michaelis-Menten equation (2-1), which gave a k_{cat} of 1.4 s^{-1} and a K_M of 70 nM.

These polyacrylamide gels are then dried and the counts of the separated reactants and products quantified by phosphorimaging (for an example of a phosphorimage see Fig. 3-6). By calculating the percent reaction of the total counts in each lane sample loading errors are avoided.

Increasing concentrations of AUA/A (0.05-1.6 μM; Table 2-1 for complete sequence) were reacted with 100 pM enzyme in UDG reaction buffer. The reaction velocity data are presented in the Michaelis-Menten Plot (Fig. 3-1) and the kinetic parameters k_{cat} and K_M determined by fitting Eq. 2-1 to the data by nonlinear regression are reported in Table 3-1. The steady-state k_{cat} of 1.4 s^{-1} and K_M of 70 nM agree well with previously published values [206]. The catalytic turnover of ssAUA by wtUDG also agrees well with measurements on similar substrates from other studies [205]. The differences between the steady-state reaction with single- and double-stranded DNA substrates is explained by the difference in the rate-limiting step of product release since the turnover of UDG is severely limited by slow product release first documented by Drohat et al. [205].

Equilibrium Binding Measurements for wtUDG

The equilibrium binding of wtUDG to various DNA ligands was measured using a fluorescence anisotropy based binding assay. Fluorescence anisotropy measures the change in rotational depolarization of a reporter fluorophore linked to a ligand, such as DNA in this case, when another molecule (UDG) binds the ligand [228]. When a large molecule like UDG binds fluorescently-labeled DNA the rotational fluorescence depolarization of the DNA decreases (the large molecule slows the tumbling of the smaller one) which is calculated as an increase in the anisotropy of the fluorescent DNA. Fluorescence anisotropy is a sensitive method to measure binding affinities with the

advantage of having all analytes free in solution, as compared to other techniques such as surface plasmon resonance. This technique has been applied previously in measuring the affinity of herpes simplex 1 virus UDG for various DNA ligands [154].

Titrations of undamaged DNA mispair (ATA/G; see Table 2-1 for oligo sequences), substrate mimic deoxypseudouridine (AψA/A), and tetrahydrofuran abasic site product mimic (AXA/G), were performed by adding increasing UDG to a fixed concentration of ligand in standard UDG reaction buffer. Polarized intensities were measured at each concentration of UDG and used to calculate the change in anisotropy. These data are plotted as a function of enzyme concentration and fit by nonlinear regression to Eq. 2-4 (Fig. 3-2 – 3-5). The results of the fits are listed in Table 3-1.

In agreement with previous studies, we found that wtUDG has a low affinity for DNA lacking deoxyuridine (undamaged), with an apparent dissociation constant (K_D^{Ap}) of about 8 μM [153, 202]. These results are a rough estimate of the lower limit of the K_D for normal DNA because it was not possible to completely saturate this ligand. Due to limitations in the amount of enzyme available, only one titration set was taken to the highest UDG concentration.

Surprisingly, wtUDG did not have a significant affinity for the substrate mimic dψU containing DNA ligand ($K_D^{Ap} \approx 5.5$ μM). This was unexpected since dψU is an isosteric isomer of deoxyuridine achieved solely by interchange of N1 and C5 in the uracil ring, creating a C–C glycosylic bond (Fig. 3-3). This substrate mimic has all the features of the natural substrate, such as the carbonyls and ring nitrogen, yet wtUDG has not much more affinity for this mimic than it does for undamaged DNA.

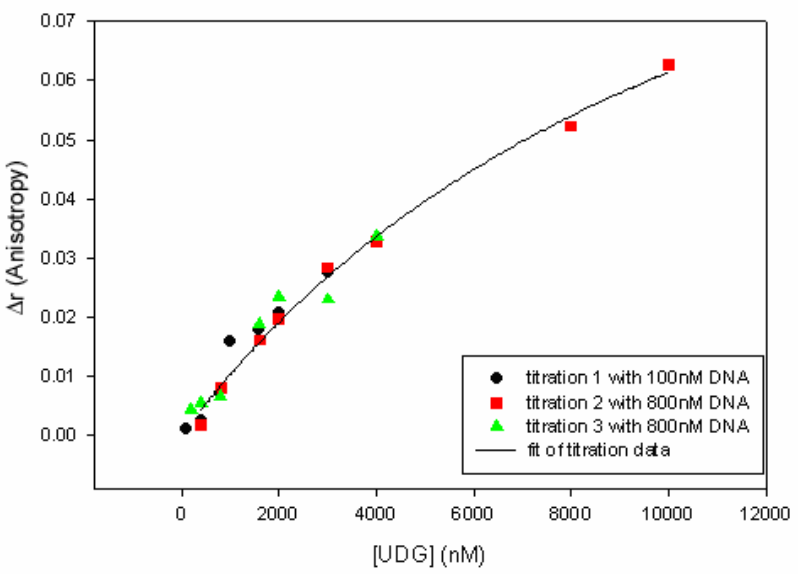

Figure 3-2. Determination of the dissociation constant for undamaged DNA binding to wtUDG using fluorescence anisotropy. Increasing concentrations of enzyme (0-12 μM) were added to the duplex DNA ATA/G (0.1 or 0.8 μM) labeled with an X-rhodamine fluorescent probe. The change in fluorescence depolarization of the probe (Δr) is plotted versus enzyme concentration. The data were fit with nonlinear regression to Eq. 2- 5, which gave a K_D^{Ap} of ≈ 8 μM.

Table 3-1. Kinetic parameters of wtUDG

Substrate or ligand	k_{cat} (s^{-1})	K_M (nM)	K_D^{Ap} (μM)	k_{max} (s^{-1})
ssAUA	12 ± 1.2	390 ± 40		170 ± 10
AUA/A	1.4 ± 0.2	70 ± 50		130 ± 20
ATA/G			8.0 ± 2	
AψA/G			5.5 ± 2	
AXA/G			0.12 ± 0.002	

Reaction rates were measured by glycosidic bond cleavage assay and K_D by fluorescence anisotropy titration. The errors reported are the standard deviation between data sets.

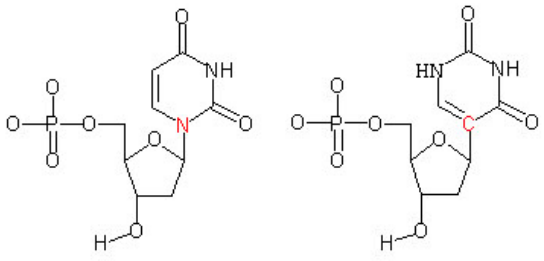

Figure 3-3. Structure of deoxyuridine (left) and deoxypseudouridine (right).

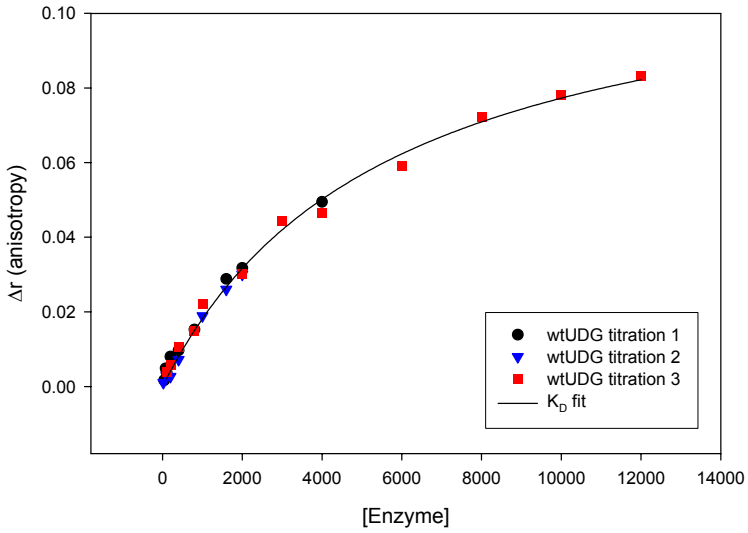

Figure 3-4. Determining the dissociation constant for substrate mimic DNA binding to wtUDG using fluorescence anisotropy. Increasing concentrations of enzyme (0-12 μM) were added to the duplex DNA AψA/G (100 nM) labeled with an X-rhodamine fluorescent probe. The change in fluorescence depolarization of the probe (Δr) is plotted versus enzyme concentration. The data were fit with nonlinear regression to Eq. 2-4, which gave a K_D^{Ap} of ≈ 5.5 μM.

One group has measured an apparent K_D for natural dU containing dsDNA as low as 38 nM [202], which is about 125-fold tighter than the affinity for dψU measured here. Since the difference between an average C-C bond (1.53 Å) and an average C-N bond (1.47 Å) is small and the C-C bond is actually slightly longer, it is amazing that this slight change to the glycosidic bond caused such a drastic effect on binding by UDG. Previous work used a 2′-fluoro-2′-deoxyuridine (dfU) substrate analog, which was shown to be cleaved 10^7-fold slower and bound reversibly to *E. coli* UDG with a K_D^{Ap} of 50-100 nM [153, 159]. Therefore the feature of dψU that does not allow UDG to bind it is not an uncleaveable glycosidic bond, that is, unless the *N*-glycosidic bond in the dfU substrate analog can stretch to accommodate the distortion the enzyme's active site imposes on it. The hUDG–dψU-DNA cocrystal structure [187] shows the C-C glycosidic bond of dψU

is twisted about 90˚ toward the *syn* conformation and stretched 0.08 Å by the H-bonding and steric constraints placed upon it by the UDG active site. Seemingly, a dfU–UDG complex would be under an equivalent amount of strain. There seems to be some other structural difference in the dψU substrate mimic that makes UDG binding unfavorable, possibly the sp^2-like character of the C1 of dψU. A detailed inquiry into the nature of the dfU–UDG complex and how it accommodates the strain the UDG active site imposes on it is needed to resolve this paradox. (Further evidence for the inability of dψU to dock with the UDG active site is also supplied by an absence in Trp fluorescence quenching, presented later.)

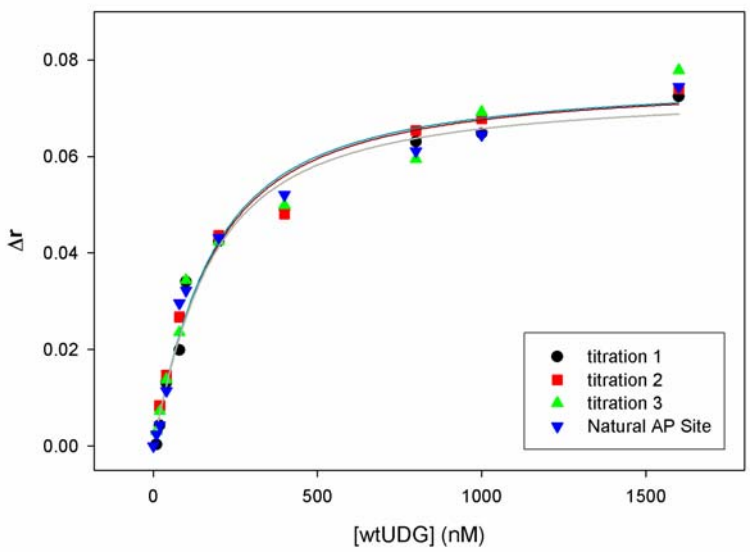

Figure 3-5. Determining the dissociation constant for product mimic DNA binding to wtUDG using fluorescence anisotropy. Increasing concentrations of enzyme (0-1.5 μM) were added to the duplex DNA AXA/G (100 nM) labeled with an X-rhodamine fluorescent probe. The change in fluorescence depolarization of the probe (Δr) is plotted versus enzyme concentration. The data were fit with nonlinear regression to Eq. 2-4, which gave a K_D^{Ap} of ≈ 115 nM.

The apparent affinity of wtUDG for an abasic site analog containing duplex DNA was found to be approximately 120 nM. As a control, natural abasic site product was

created *in situ* by incubation of UDG with dU containing substrate for several minutes. Due to the high activity of wtUDG, the substrate was fully converted to natural abasic site product. Anisotropy measurements were immediately conducted with the natural abasic site product to measure the affinity of UDG for this ligand. Within error, this control gave the same apparent K_D, indicating that the tetrahydrofuran abasic site analog closely approximates the natural product (plotted as ▼ in the above graph).

The crystal structure of hUDG with product DNA shows that the enzyme can flip abasic sites [134], therefore this moderate affinity for the abasic site containing DNA by *e*UDG probably reflects the same process. This result agrees well with the K_D^{Ap} of 100 nM for a similar duplex tetrahydrofuran containing oligo (11nt) measured via a competitive binding assay [207]. Since the rate-limiting step in the steady-state turnover of UDG is product release, it makes sense that the enzyme has the highest affinity for product containing DNAs.

Presteady-State Uracil Excision Kinetics of wtUDG

The final set of wtUDG catalytic activity bench marks measured were the presteady-state kinetics (a.k.a., transient-state kinetics) of uracil excision by UDG from the single stranded (ssAUA) and duplex DNA substrates (AUA/A). Examination of an enzyme reaction pathway by transient-state kinetics helps resolve reaction steps buried within steady-state parameters. In the presteady-state the enzyme can be a stoichiometric reactant, which allows individual reaction steps can be measured directly [227]. In addition, the concentration dependence of the rates and amplitudes of the reaction in the transient-state will also reveal mechanistic information.

Maximum Single-Turnover Catalytic Velocity Measurements for wtUDG

The maximum single-turnover catalytic rate of uracil excision by wtUDG was measured with rapid chemical quench-flow (rapid quench). As the name implies, reactants are mixed and aged for the specific reaction time followed by mixing with a solution that instantaneously stops the reaction. Rapid quench is conducted with a machine that can mix reactants at high velocities allowing measurement of reactions in the millisecond time-scale.

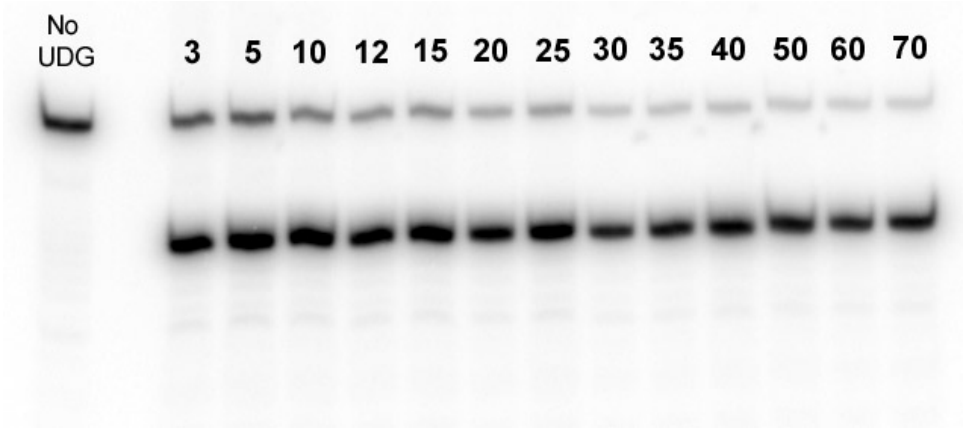

Figure 3-6. Typical denaturing PAGE used to separate and quantify radio-labeled reactants and products of a glycosidic bond cleavage assay. This is data for the single-turnover time course of a wtUDG reaction with AUA/A. The first lane separated from the rest is a no enzyme control that is the uncut oligo treated exactly as the reactant lanes. In the reactant lanes the lower bands are cleaved products that are half the size of reactants. The reaction time is indicated above each lane in milliseconds (at the shortest time of 3 ms the reaction is already about 60% complete).

The goal of measuring the maximum single-turnover velocity of an enzyme is to measure the rate of chemistry of the reaction, or the rate of a limiting step prior to chemistry, if such a step exists. This is accomplished by using saturating amounts of enzyme with a set limited amount of substrate so that all substrate is bound. This effectively eliminates the enzyme–substrate association step, so that the following steps can be assayed directly.

The maximum single-turnover of UDG for the substrates ssAUA and AUA/A were performed by using a 40:1 ratio of enzyme to substrate. Higher concentrations of enzyme did not increase the reaction rate, indicating that the substrate was saturated by UDG (data not shown). The maximum rate of uracil excision from ssAUA was found to be 170 s^{-1}. This rate is close to the 160 s^{-1} measured for a similar single-stranded substrate [206].

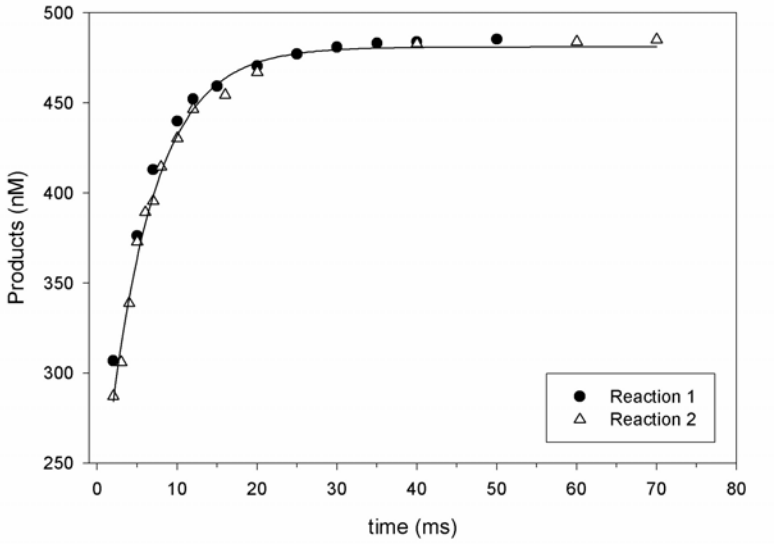

Figure 3-7. Maximum single-turnover catalytic rate of wtUDG with the substrate ssAUA. The rapid quench glycosidic bond cleavage assay was used to measure the maximum catalytic rate of wtUDG (20 μM) reacted with ssAUA (0.5 μM). The data from two separate experiments are shown above fit with Eq. 2-2. to obtain a k_{max} of 170 s^{-1}.

The maximum single-turnover catalytic rate of uracil excision from the double-stranded DNA substrate AUA/A was found to be 130 s^{-1}, which matches closely to the previously measured rate of 115 s^{-1} [206]. Comparing this maximum single-turnover number (k_{max}) to the enzyme's steady-state turnover number (k_{cat}), provides an estimate of the extent to which product release is rate limiting for a given substrate in the steady-state. If k_{max} equals k_{cat} then the chemistry step (or a prior step) is rate limiting for

that substrate, while a k_{max} much larger than k_{cat} indicates that a slow step after the chemistry step is rate limiting for the enzyme's turnover in the steady-state. The k_{max} for the substrates measured here is much larger than the k_{cat}, so as previously noted by Drohat et al. a step after chemistry limits UDG's steady-state turnover of both the single and double-stranded DNA substrates.

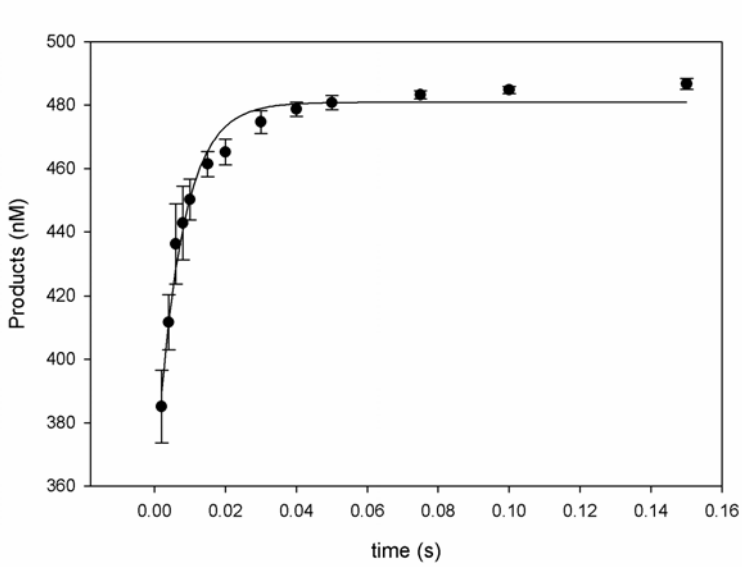

Figure 3-8. Maximum single-turnover catalytic rate of wtUDG with the double-stranded substrate AUA/A. The rapid quench glycosidic bond cleavage assay was used to measure the maximum catalytic rate of wtUDG (20 μM) reacted with dsAUA (0.5 μM). Three separate experiments were averaged to obtain the standard deviation (error bars). The above data are fit with Eq. 2-2 which gives a k_{max} of 120 s^{-1}.

Presteady-State Burst Kinetics of wtUDG

Often the rates and amplitudes of an enzymatic reaction will show a concentration dependence in the transient-state that can reveal mechanistic information. A burst of products will be formed when mixing substrate in excess of a limiting concentration of enzyme if product is able to accumulate at the enzyme's active site [201, 227]. This build-up of enzyme bound products will be released when a denaturing quench stops the

reaction, and the sum of bound products, in addition to product already released during normal turnover, will form the burst. Product accumulation is caused by a reaction step which comes after chemistry that is slower than any previous steps (i.e., rate limiting).

Assuming that substrate binding is much more rapid than catalysis, and the enzyme active sites are saturated, the amplitude of the burst or lack thereof, can supply valuable information about the reaction mechanism. The amplitude of the burst is dependent on the rate of product formation relative to both the rate of product release and the rate of the reverse reaction from products back to substrates. If the reaction equilibrium in the active site favors product formation, and the rate of the catalysis is much faster than product release, the burst amplitude should be one per enzyme active site. If the burst amplitude is less than one, then the rate of product release and/or the rate of the reverse reaction are lowering the burst amplitude (i.e., as product release becomes faster less product can build up in the active site). However, these scenarios are distinguishable: if the rate of product release increases (as the burst amplitude decreases) so will the rate of the transition into the steady-state; and if the back reaction is competing with product formation, the decrease in burst amplitude will accompany an *increase* in burst rate (this is because the overall rate is the sum of the forward and reverse rates; thus if the back reaction rate increases the *burst phase* rate must increase also). Importantly, if there is no burst, then either a step before chemistry or the chemical reaction itself is rate limiting.

Presteady-state burst kinetics of uracil excision by wtUDG were measured for the substrate AUA/A. The reactions were performed by rapid-chemical-quench with the substrate concentrations that were five- and ten-fold greater than the enzyme's. Time courses focused within the first second of the reactions to obtain sufficient data density in

these critical reaction phases. The data are plotted in Figure 3-9 and the rate constants are displayed in Table 3-2.

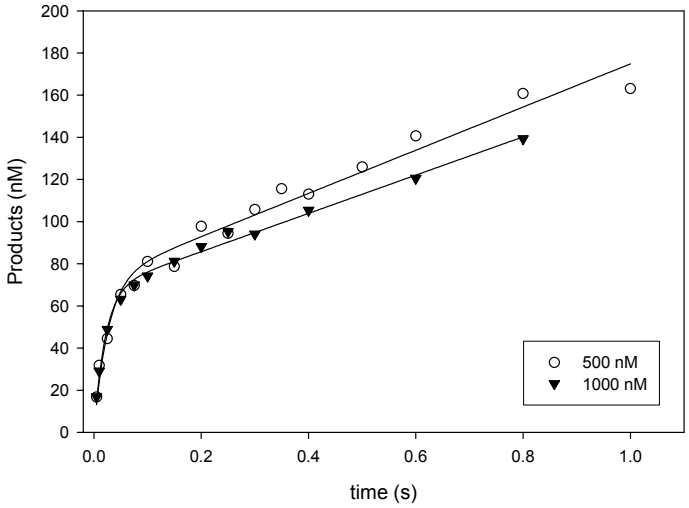

Figure 3-9. Measurement of the presteady-state burst of product formation by wtUDG uracil excision. The above plot are data obtained by rapid-quench reactions performed with duplex substrate AUA/A (0.5 and 1.0 μM) in excess over UDG (0.1 μM). The data are fit to a sum of single-exponential and linear phases by Eq. 2-3.

Table 3-2. Presteady-state kinetic parameters of UDG

	500 nM AUA/A	1000 nM AUA/A
Burst Amplitude	72 nM	67 nM
Burst rate	51 s^{-1}	52 s^{-1}
Steady-state rate	1.35 s^{-1}	1.06 s^{-1}

The data in Fig. 3-9 were fit with Eq. 2-3 to calculate the magnitude and rate of the product burst when limiting amounts of UDG are reacted with substrate in excess.

In agreement with the maximum single-turnover kinetics, presence of a presteady-state burst of products indicates that a step following chemistry is rate limiting in UDG's reaction mechanism. The amplitudes of the bursts of the 500 and 1000 nM reactions were equivalent (72 and 67 nM, respectively) within the error of the parameter estimation by nonlinear regression. The burst amplitude is a rough approximation of the

concentration of the steady-state enzyme–product complex ($[E\text{-}P]_{ss}$) [227] so about 70% of the UDG had product in its active site. Since at least 70% of the enzyme bound substrate in the first turnover this puts an upper limit on the K_D for substrate of around 150 nM.

The burst rates were also almost identical ($k_{obs} \approx 50\ s^{-1}$), indicating that the difference in substrate concentration did not affect the internal equilibrium of the reaction in the UDG active site. There was a discrepancy in the steady-state rates between reactions. The slope of the 500nM AUA/A reaction gave the expected rate of $1.35\ s^{-1}$, almost equivalent to the steady state k_{cat} previously measured. However, the slope of the 1000nM AUA/A reaction was slightly below the expected steady-state rate ($k_{cat} = 1.06\ s^{-1}$). This might be due to the higher DNA concentration increasing the ionic strength of the reaction buffer, or product inhibition. Because these experiments use large amounts of expensive reagents and they are not crucial to the overall goal of this work, the discrepancy between these results was not investigated further.

This work confirms previous UDG kinetics results by other groups and confirms that our reagents, equipment, and techniques are properly measuring the kinetics of UDG. These kinetic measurements of wtUDG provide a basis to compare the effect of adding a His-tag to the enzyme as discussed in the next chapter.

CHAPTER 4
COMPARISON OF WILD-TYPE AND HIS-TAGGED UDGS

Due to reported difficulty of working with *ung*$^-$ strains of *E. coli* [229], a 6X His-tag was engineered onto the N-terminus of wild-type and mutant versions of UDG so that the mutant forms of the protein could be purified from the endogenously expressed UDG. This strategy has been utilized previously by Drohat et al. [206] successfully to purify other active site mutants of *E. coli* UDG. Therefore, to ensure that the His-tag did not impair the activity of the enzyme a series of comparisons were performed between wt- and His-tagged UDGs.

Steady-State Kinetics of His-tagged UDG

Kinetic comparisons began with the measurement of the steady state kinetic parameters of His-tagged UDG (HisUDG). These parameters were measured using the glycosidic bond cleavage assay with the same substrate (AUA/A) and conditions as used with the wild-type enzyme. The steady state kinetic parameters obtained from the Michaelis-Menten plot (Fig. 4-1) are reported in Table 4-1. Both the steady-state reaction rate and the K_M are equivalent within the error of the measurement. The results demonstrate that the 6X His-tag, which contains a thrombin cleavage site and is 20 amino acids in length, has no appreciable effect on the steady-state properties of UDG.

Equilibrium Binding Measurements for His-tagged UDG

To ensure that the His-tag did not significantly perturb the interactions of UDG with DNA ligands, anisotropy titrations were performed with HisUDG under the same conditions as used previously with wtUDG. Anisotropy titrations with undamaged DNA

mispair (ATA/G) and substrate mimic deoxypseudouridine (AψA/A) ligands, were performed by adding increasing His-tagged UDG to a fixed concentration of ligand. As before, the background corrected data are plotted versus enzyme concentration and fit by nonlinear regression to Eq. 2-4. The titration results are shown in Figures 4-2 and 4-3 and collected in Table 4-2.

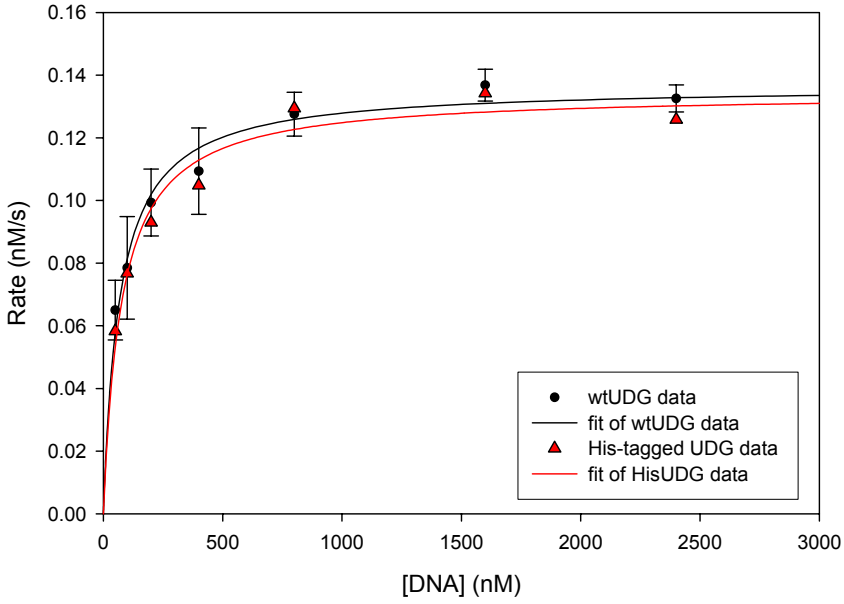

Figure 4-1. Michaelis-Menten plots of wild-type and His-tagged UDG steady-state reactions measured by glycosidic bond cleavage assay. Increasing concentrations of substrate (0-3.2 μM) were reacted with 100 pM enzyme. The data were fit with nonlinear regression to Eq. 2-1. Fit results are reported in Table 4-1.

Table 4-1. Steady-state kinetic parameters for wtUDG and His-tagged UDG		
	wtUDG	His-tagged UDG
k_{cat}	1.36 s^{-1}	1.34 s^{-1}
V_{max}	0.14 nM/s ± 0.002	0.13 nM/s
K_M	68 nM ± 50	76 nM

The error for wtUDG is the standard deviation between three data sets. The error for the His-tagged UDG parameters was estimated from the uncertainty of the fit with Eq. 2-1 to be less than 5%.

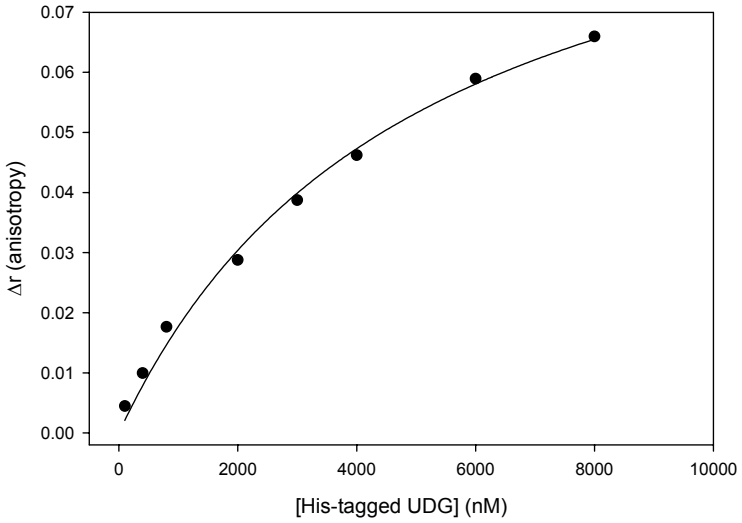

Figure 4-2. Determination of the dissociation constant for undamaged DNA binding to His-tagged UDG using fluorescence anisotropy. Increasing concentrations of enzyme (0-8 μM) were added to the duplex DNA ATA/G (50 nM) labeled with an X-rhodamine fluorescent probe. The change in fluorescence depolarization of the probe (Δr) is plotted versus enzyme concentration. The data were fit with nonlinear regression to Eq. 2-4, which gave a K_D^{Ap} of ≈ 5 μM.

The addition of a His-tag did seem to slightly lower the K_D^{Ap} of UDG for undamaged DNA (from 8.0 μM to 5.5 μM). However, due to the fact that it wasn't possible under these conditions to saturate this DNA ligand with wild-type and tagged UDG, there is a large uncertainty in the fitting parameters. Therefore this difference is almost within the error of the measurement and should not be over interpreted. Regardless, there is no extreme perturbation of the enzyme's interaction with an undamaged 25mer duplex DNA, as it demonstrates the low affinity this enzyme has for DNA lacking uracil.

His-tagged UDG also did not show an appreciable affinity (K_D^{Ap} of ≈ 3.4 μM) for the substrate mimic deoxypsuedouridine in the context of a duplex 25mer DNA. This confirms that the supposed substrate mimic does not form a long-lived complex with either form of UDG. Thus, taken together, these equilibrium binding measurements

demonstrate that the His-tagged and wild-type enzymes interact with DNA in an equivalent fashion.

Table 4-2. Equilibrium binding comparison of wt- and His-tagged UDGs.

Ligand	K_D^{Ap}(μM) HisUDG	K_D^{Ap} (μM) wtUDG
ATA/G	5.5 ± 0.2	4.0 ± 0.2
AψA/G	3.4 ± 0.03	5.5 ± 0.1

Results from fits of data in Figures 4-2 & 3 with Eq. 2-4. Reported errors are the uncertainties of the theoretical fits for the HisUDG data.

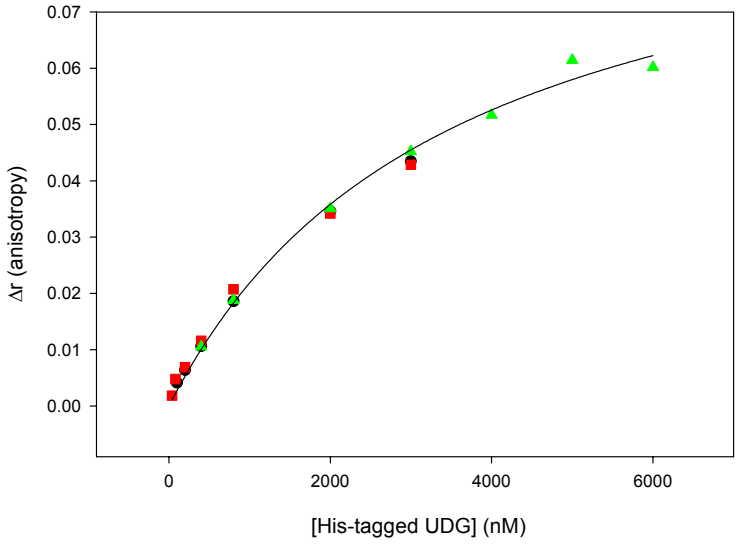

Figure 4-3. Determination of the dissociation constant for substrate mimic DNA binding to His-tagged UDG using fluorescence anisotropy. Increasing concentrations of enzyme (0-6 μM) were added to the duplex DNA AψA/G (0.1 μM) labeled with an X-rhodamine fluorescent probe. Three separate titrations were performed (represented by ▲, ■, and ●). Fit of the three data sets gave a K_D^{Ap} of ≈ 3.4 μM.

Presteady-State Reaction Kinetics Comparison of wt- and His-Tagged UDGs

Transient state kinetics measurements were performed with HisUDG as the final step in the comparison between wild-type and tagged proteins. To ensure that the rate of the chemical step for UDG was unchanged by the His-tag, the maximum single-turnover rate of uracil excision was measured for HisUDG. The data for parallel reactions of

100nM AUA/A substrate reacted with 10 μM of normal and tagged enzymes are plotted in Figure 4-4. These reaction data overlapped very closely giving an identical catalytic rate for both proteins. These results demonstrate that the wild-type and His-tagged enzymes give the same single-turnover catalytic rate when assayed in parallel under the same conditions.

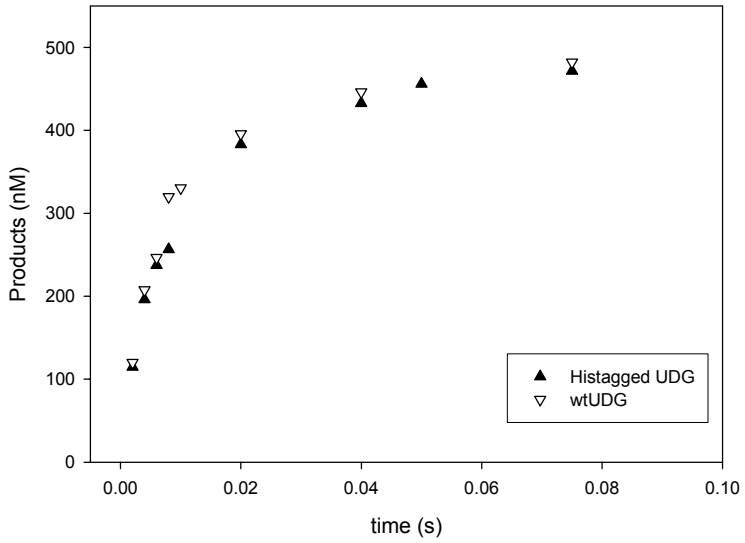

Figure 4-4. Single-turnover uracil excision rate comparison of His-tagged and wtUDGs. The duplex substrate AUA/A (0.5 μM) is reacted with excess UDG (5.0 μM) in a rapid-quench uracil excision assay.

Presteady-state product burst formation kinetics were measured for wild-type and His-tagged UDG as described in Chapter 3. Comparing presteady-state burst rates and amplitudes provides a way to determine if the His-tag has perturbed the internal equilibrium of product formation of the enzyme. The presteady-state burst kinetics (discussed on pg. 92) reports on substrate binding, product formation, and product release, giving detailed information about the functioning of the enzyme and providing confirmation for the single-turnover measurements.

The burst kinetics were measured for reactions containing 0.5 μM substrate (AUA/A) and 0.1 μM enzyme, either wild-type or His-tagged. Four data sets for each enzyme, tagged or unmodified, were collected by rapid-quench, with three of these performed in parallel on the same day with the same reagents. The plotted data are displayed in Figure 4-5, while the parameters for the nonlinear regression fit of the data with Eq. 2-3 are displayed in Table 4-3.

For some unknown reason these particular experiments were difficult to repeat and the standard deviation between data sets was large. Nevertheless, within the error of these experiments the burst kinetics of the wt- and His-tagged UDGs were the same. This indicates that the enzymes' active sites saturate with substrate at the same rate, and therefore the His-tag in no way interferes with UDG's ability to locate, flip, and cleave dU from the dsDNA substrate AUA/A under these conditions.

This completes the comparison of wild-type and His-tagged UDGs. Having confirmed that the His-tag did not perturb the natural behavior of the enzyme, the His-tag allowed for the purification of the Phe77 mutants from endogenous wtUDG. Obtaining mutant enzymes that were completely free from contaminating wtUDG is absolutely critical for the accurate measurement of the mutational effects, because even trace amounts of fully active UDG could badly distort results due to its high activity.

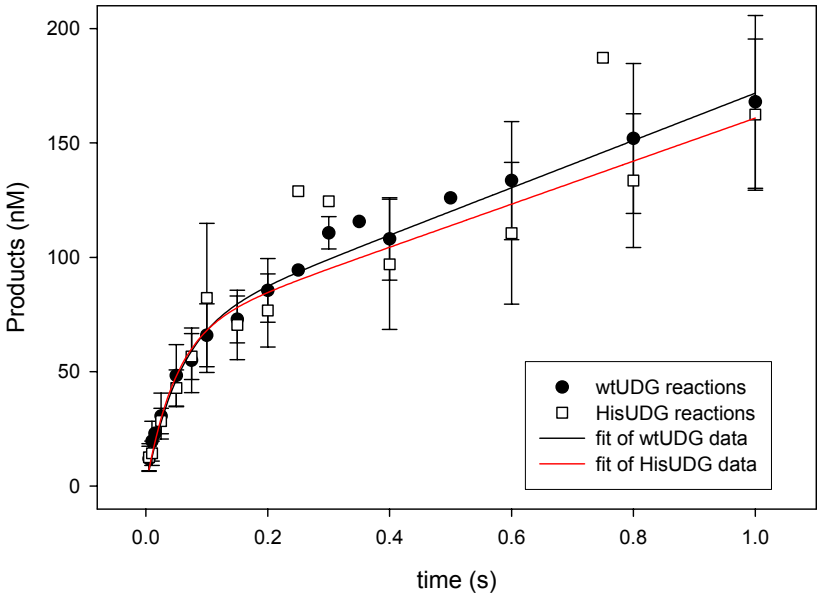

Figure 4-5. Comparison of product burst formation for wild-type and His-tagged UDG. Excess duplex 25mer AUA/A (0.5 μM) was reacted with the enzymes (0.1 μM) by rapid-quench as described in Chapter 2 pg. 78. The data are fit with Eq. 2-3 with the error bars representing the standard deviation between four data sets each for wt- and HisUDG. Fit results are reported in Table 4-3.

Table 4-3. Burst kinetics of wild-type and His-tagged UDG

Enzyme	wtUDG	His-tagged UDG
Burst Amp	68	67
Burst Rate	19 s^{-1}	21 s^{-1}
Steady-state Rate	1.03 s^{-1}	0.94 s^{-1}

The data displayed in Fig. 4-5 were fit with Eq. 2-3 to obtain the rate constants displayed in this table. The upper limit of the error in the rates is ± 20%.

CHAPTER 5
STEADY-STATE KINETIC CHARACTERIZATION OF PHE77 MUTANTS

To examine the role of the conserved active site phenylalanine 77 in the functioning of *E coli* UDG, three site-directed mutants were constructed. The three mutants probe the role of the phenyl side chain in different ways. The phenylalanine to alanine mutant (F77A) completely removes phenyl ring while retaining a hydrophobic amino acid at that position. The phenylalanine to asparagine mutant (F77N) puts in a side chain that has about half the bulk and one π-bond of the phenyl ring. The resonance in the amido group of the asparagine keeps that moiety planar like the phenyl ring. The asparagine mutation also replaces the hydrophobic phenyl with a hydrophilic hydrogen bond donor and acceptor. The final mutation of phenylalanine to tyrosine keeps the phenyl group but adds an electron withdrawing substituent to the ring. This small perturbation of the π-electron ring system of the phenyl side chain will probe the importance of the reported π-π stacking interaction between the uracil ring and UDG. In addition, the hydrophilicity of the phenol group is intermediate between the very hydrophilic amido and hydrophobic methyl groups of the asparagine and alanine mutants, thus these mutations cover a spectrum of polarity (i.e., except for charged groups) within the UDG active site.

Steady-State Kinetics of Uracil Excision Catalyzed by Phe77 Mutants

Characterization of the effect mutating Phe77 has on UDG's function began with measurement of each mutant's steady-state kinetic parameters. Although the effects of the Phe77 mutations would likely be underrepresented in the steady-state due to the

rate-limiting step of product release found for the wild-type enzyme, these steady-state experiments provided the initial rate estimates for the mutational effects, and established limits that helped in the design of the subsequent transient-state kinetics experiments. The results in this section also show that each mutant still has uracil excision activity, with no detectable glycosylase activity toward undamaged DNA (Fig. 5-1).

Steady-state kinetics were measured using the glycosidic bond cleavage assay with the same sets of substrates and conditions as used previously with wild-type UDG and His-tagged UDG (HisUDG). Images of the gels (1 of 3 for each data set) used in the quantification of the uracil excision by the Phe77 mutants from the substrate AUA/A are shown in Figure 5-1. The steady-state kinetic parameters of uracil excision from ssAUA and AUA/A substrates for all three mutants are plotted in Figure 5-2 and reported in Table 5-1.

The gels in Figure 5-2 show bands that correspond to uncleaved 25mer substrate and 12mer products caused by excision of uracil. The fact that all the mutants retain uracil excision activity is not surprising given that a few other putative UDGs from other homologous families (DUG/TDG family pg. 25) do not have a phenylalanine in that position in their active sites.

These gel images show only one prominent product band that corresponds to products the same size as those created with wtUDG and strand scission by base. This indicates that the mutants are still remarkably specific for uracil. This discrimination between pyrimidines is not totally unexpected as the active sites of the mutants still retain the tyrosine and asparagine that exclude thymine and cytosine, respectively.

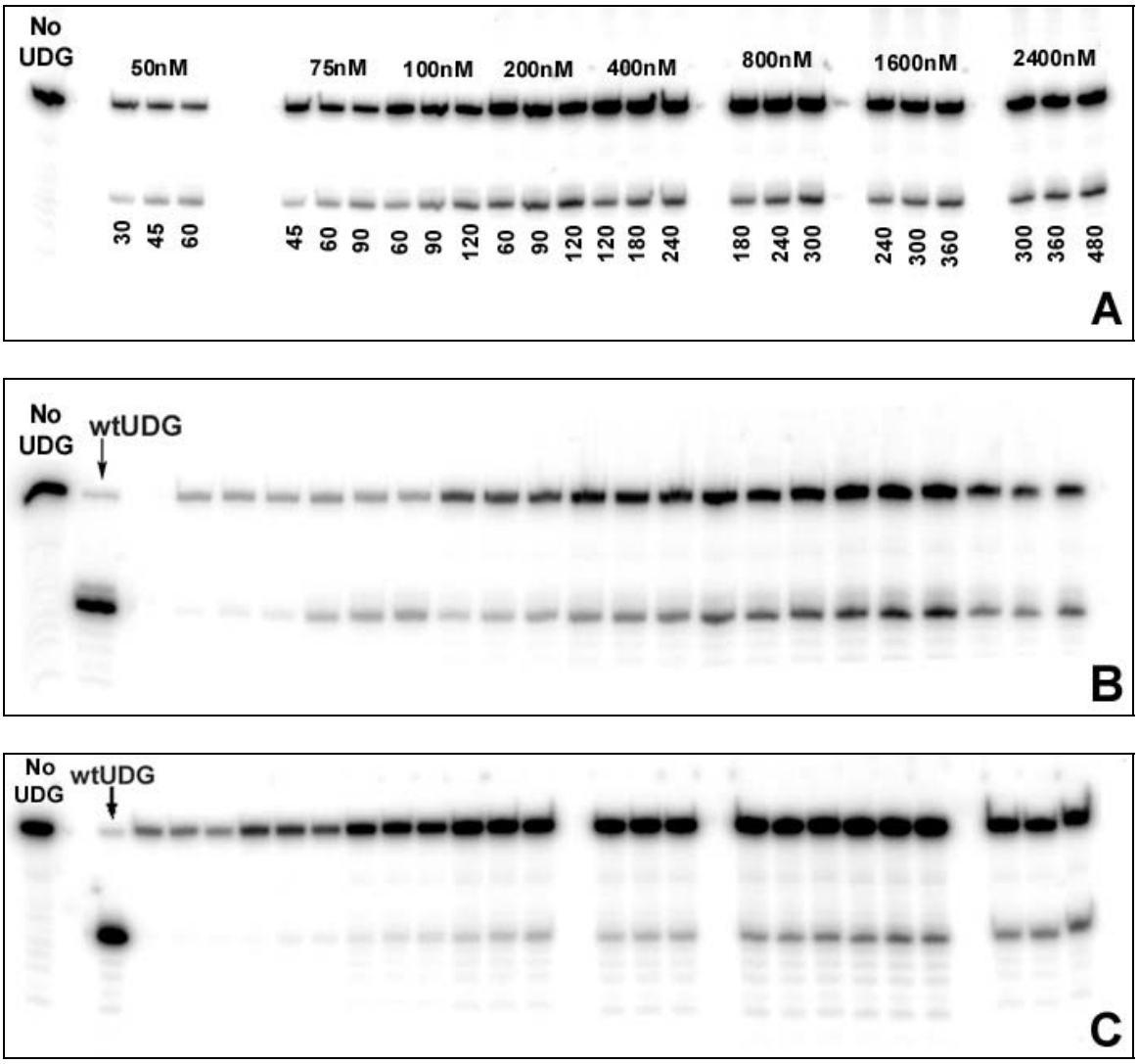

Figure 5-1. Phosphorimages of 20% polyacrylamide gels used to separate uracil excision products and unreacted substrate (AUA/A) for reactions with Phe77 mutants. Panels A, B, and C show a series of steady-state reactions with the F77A, F77N, and F77Y mutants, respectively. The first lane of each gel is a no enzyme control, where the DNA is heated with 0.2 M KOH exactly as the reactions. The numerous minute bands that migrate lower on the gel in this control lane are from nonspecific nicking of the DNA caused by the treatment. In panel A the concentrations of substrate used in this assay are listed above the reactants. Each substrate concentration has a set of three lanes that are time points taken during the course of the reactions (reaction time in seconds is displayed under each lane). In panels B and C there are wtUDG control reactions that show > 95% cleavage of the substrate into the single product band half the size of the substrate 25mer.

Therefore it appears, within the limits of this detection method, that the discrimination between cytosine and uracil is not dependent on the supposed π-π stacking interaction between the phenylalanine and the uracil base. Removing the steric constraint of the phenyl group does not appear to have affected the H-bonding interaction between conserved Asn124 and the uracil base which allows discrimination from cytosine (Chapter1 pg. 39). However, this interaction may still be disrupted, possibly contributing to the slower turnover number of the F77A mutant, but not disrupted to the extent where the enzyme cannot distinguish uracil from cytosine.

The kinetic constants reported in Table 5-1 show large errors in the K_M's for the mutant and wild-type enzymes. However, these errors are normal, and even below the common error range in measured K_M's (± 40-50 %) for this enzyme with the glycosidic bond cleavage assay and other techniques [206]. One source of this error is that it becomes increasingly difficult to accurately measure steady-state kinetics the slower the enzyme is, because of the constraints imposed by working within the steady-state assumption ([Enzyme]<<<[Substrate] and <10% products).

The increase in error with increasing substrate concentration is an example of a common problem in the steady-state measurements of the uracil excision rate of wtUDG and the mutants in this study. In order to fully saturate the enzymes with substrate, high concentrations of DNA substrate were needed. This high substrate concentration increased the background level of ^{32}P, which in turn decreases the accuracy of quantifying the products that are restricted to less than 10%. (Another concern was differences in the amount of background radioactive contaminants from one batch of [γ-^{32}P] ATP to the next, which was found to vary significantly (data not shown)).

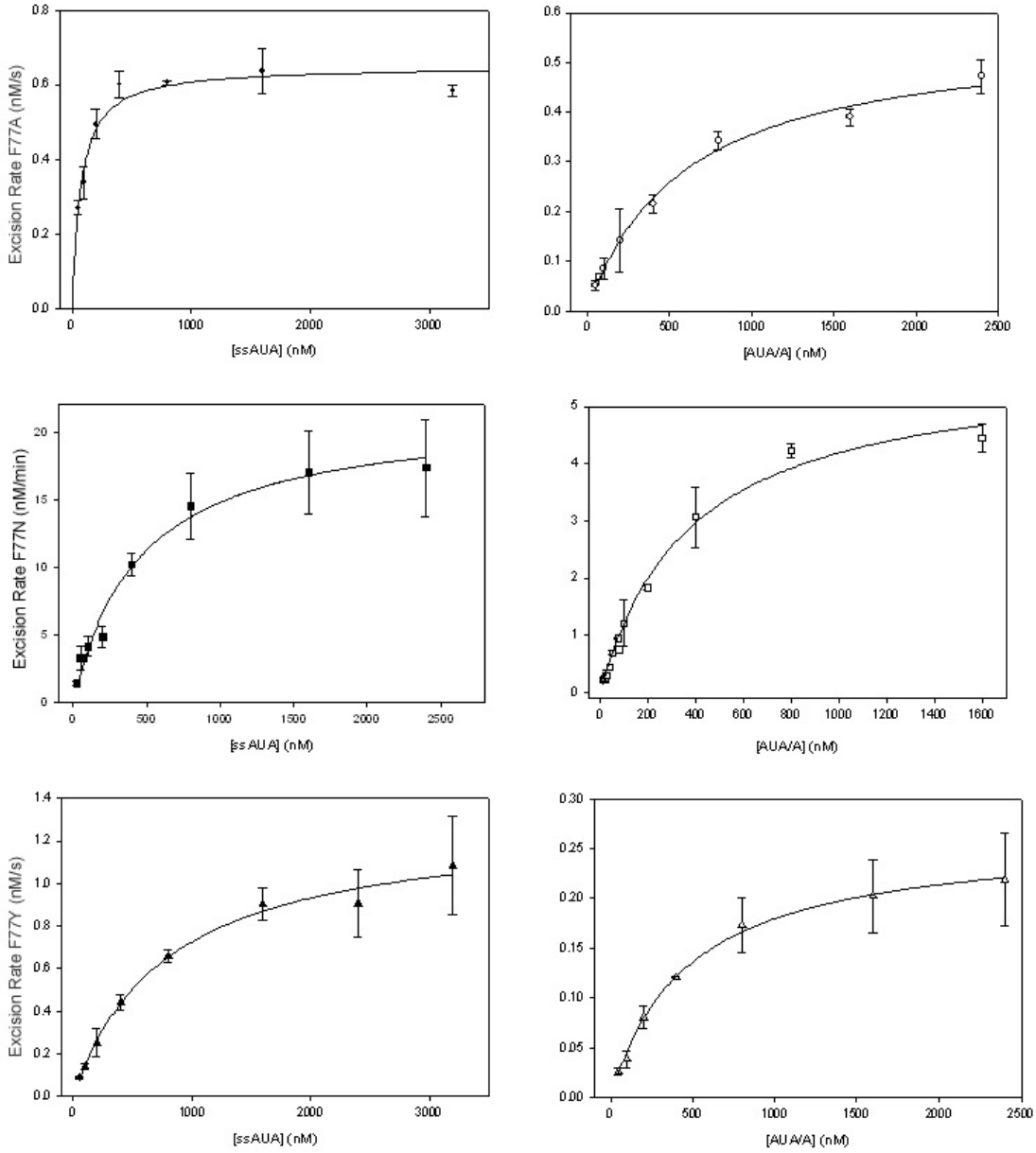

Figure 5-2. Steady-state kinetics of uracil excision by Phe77 mutants. The glycosidic bond cleavage assay was used to measure the uracil excision rates for each mutant on both ssAUA (left column of graphs, closed symbols) and AUA/A (right column, open symbols). The results for F77A are in the top row (●,○), for F77N in the middle (■,□), and in the bottom row of graphs for F77Y (▲,Δ). Each graph shows the average of three independent experiments with the error bars representing the standard deviation between each rate measurement within each data set. The solid lines are a nonlinear regression of the data with Eq. 2-1 to determine the steady-state kinetic parameters listed in Table 5-1.

Table 5-1. Steady-state parameters for His-tagged wtUDG and phenylalanine mutants

Enzyme	[Protein] (nM)	Substrate	V_{max} (nM/s)	K_M (nM)	k_{cat} (s^{-1})	k_{cat}/K_M	K_M^{mut}/K_M^{wt}	$k_{cat}^{wt}/k_{cat}^{mut}$	$(k_{cat}/K_M)^{wt}/(k_{cat}/K_M)^{mut}$
wtUDG	0.1	ssAUA	1.2 ± 0.1	390 ± 40	12	0.031			
	0.1	AUA/A	0.14 ± 0.02	70 ± 50	1.4	0.02			
F77A UDG	0.2	ssAUA	0.65 ± 0.05	70 ± 15	3.3	0.05	0.2	3.7	0.6
	10	AUA/A	0.57 ± 0.05	600 ± 200	0.06	1.0×10^{-4}	8.6	23	200
F77N UDG	10	ssAUA	0.36 ± 0.09	460 ± 190	0.036	7.8×10^{-5}	1.2	330	400
	10	AUA/A	0.096 ± 0.007	380 ± 70	0.0096	2.5×10^{-5}	5.4	150	800
F77Y UDG	0.4	ssAUA	1.4 ± 0.36	870 ± 380	3.5	4.0×10^{-3}	2.2	3.4	8
	0.4	AUA/A	0.21 ± 0.03	550 ± 370	0.5	1.0×10^{-3}	7.9	2.8	20

These constants are derived from the fits of data displayed in Fig. 5-2 with Eq. 2-1. The reported errors are the standard deviations for three independent experiments for each substrate and enzyme combination. The last three columns show the ratio of rate constants for wild-type (wt) to mutant (mut) enzyme parameters. Wild-type UDG used in the steady-state reactions with AUA/A was His-tagged.

Nevertheless, the results from this set of experiments are supported by Trp fluorescence measurements discussed in Chapter 7, so some speculation about the steady-state data will be hazarded here. The F77A and F77Y mutations have a relatively mild effect on the turnover number of the enzyme in comparison with the effects mutation of the key catalytic groups His187, the electrophilic H-bond donor, and Asp64, the putative carbocation stabilizing group (Chapter 1 pg. 57). For the single-stranded substrate ssAUA the F77A and F77Y mutations slightly reduced k_{cat} by 3- to 4-fold (Table 5-1). The turnover number for the activity of F77Y on the double-stranded AUA/A was impaired by an equivalent factor (3-fold) as compared to its activity on the ssDNA (relative to wtUDG activity). Conversely, the k_{cat} of F77A for the dsDNA substrate AUA/A is reduced 23-fold relative to wtUDG, which is significantly greater than the 3-fold effect this mutation has on the enzyme's turnover of ssAUA. This preference for ssDNA substrate is also reflected in the almost 9-fold greater K_M F77A has for AUA/A relative to wtUDG.

This is in contrast to the H187Q and D64N mutations which showed a different effect between the ssDNA and dsDNA substrates, with the general trend of the activity towards single-stranded substrates being more impaired. Drohat et al. [206] found the H187Q mutation had 300- and 60-fold damaging effects on k_{cat} with similar (19mer oligo with uracil between two adenines) single-stranded (ssAUA-like) and double-stranded (AUA/A-like) DNA substrates, while the D64N mutation caused 830- and 100-fold damaging effects on k_{cat} in reactions with those same substrates, respectively. The authors proposed that because the steady-state turnover of dsDNA substrates is rate-limited to a greater extent by the product-release step than the turnover of ssDNA

substrates, mutational effects should be greater for the steady-state catalysis of ssDNA substrates (i.e., because ssDNA turns over faster).

The fact that the F77A and F77Y mutants do not show this trend of more impairment of their steady-state turnover numbers toward ssDNA substrates than dsDNA substrates indicates these mutations have complex effects which include substrate binding and possibly other steps. The very large 200-fold reduction in the specificity constant (k_{cat}/K_M) towards AUA/A versus only a 0.6-fold reduction for ssAUA substrates (as compared to wild-type) caused by the alanine mutation could mean that the recognition and/or binding of uracil when it is in duplex DNA is impaired for F77A UDG.

The largest compromising mutational effects are seen for the F77N mutation. The 300- and 150-fold reduction in k_{cat} on the catalysis of ssAUA and AUA/A, respectively, are in the neighborhood of the aforementioned effects the mutation of the key catalytic groups, H187Q and D64N, have on the enzyme's activity. The ratio of the specificity constant (k_{cat}/K_M) of wtUDG with the specificity constant of F77N UDG for the substrates ssAUA and AUA/A, reveal that F77N UDG is 400- and 800-fold less specific for substrate relative to wtUDG. In general, the effects of the Phe77 mutations on both k_{cat} and K_M indicate that these mutational effects are likely a mixture of effects on chemistry and substrate recognition.

Equilibrium Binding Measurements with Phe77 Mutants

To measure the affinity of the Phe77 mutants for undamaged DNA containing a mispair (ATA/G), substrate mimic deoxypseudouridine containing DNA (AψA/A), and tetrahydrofuran abasic site product mimic containing DNA (AXA/G), fluorescence anisotropy titrations were undertaken exactly as had been performed with wtUDG. Increasing amounts of mutant protein were titrated into a fixed concentration of ligand

and the change in the depolarization of the rhodamine fluorescent probe attached to the DNA ligand was recorded. As before, the background corrected data are plotted versus enzyme concentration and fit by nonlinear regression to Eq. 2-4. Due to limited amounts of enzyme, most measurements were performed only once. The errors of these measurements are reported as standard uncertainties of the theoretical fits, which assumes that the uncertainties in the individual measurements are approximated by the standard uncertainty of the points from the fitted curve. Because each point of these data sets is a wholly separate measurement from the others, this assumption is a valid approximation of the data accuracy. The titration results are shown in the plots in Figures 5-3 through 5 and listed in Table 5-2.

Table 5-2. Equilibrium binding constants for His-tagged UDG and Phe77 mutants

Enzyme	K_D^{Ap} Undamaged DNA (ATA/G) (μM)	K_D^{Ap} Substrate Mimic DNA (AψA/G) (μM)	K_D^{Ap} Product Mimic DNA (AXA/G) (nM)
wt(His-tag)	5.5 ± 0.2	3.4 ± 0.03	120 ± 2
F77A	6.0 ± 0.4	7.5 ± 0.07	150 ± 1
F77N	3.5 ± 0.04	0.94 ± 0.05	120 ± 1
F77Y	5.0 ± 1.3	4.2 ± 0.04	150 ± 2

Apparent dissociation constants are derived from the fit of the anisotropy data with Eq. 2-4. The shorthand designation for the DNA ligands is in parentheses (Table 2-1). The reported errors are the uncertainties of the theoretical fits.

All of the Phe77 mutants show approximately the same affinity (≈ 5.0 μM) for the undamaged duplex 25mer ATA/G (Fig. 5-3A, -4A, and -5A; Table 5-2). Thus, the mutants retain the low affinity for undamaged DNA exhibited by the wild-type enzyme. This is not surprising, as the mutations are internal and probably do not disturb the conserved serine-proline loops implicated in DNA backbone pinching or other surface residues in the DNA binding cleft.

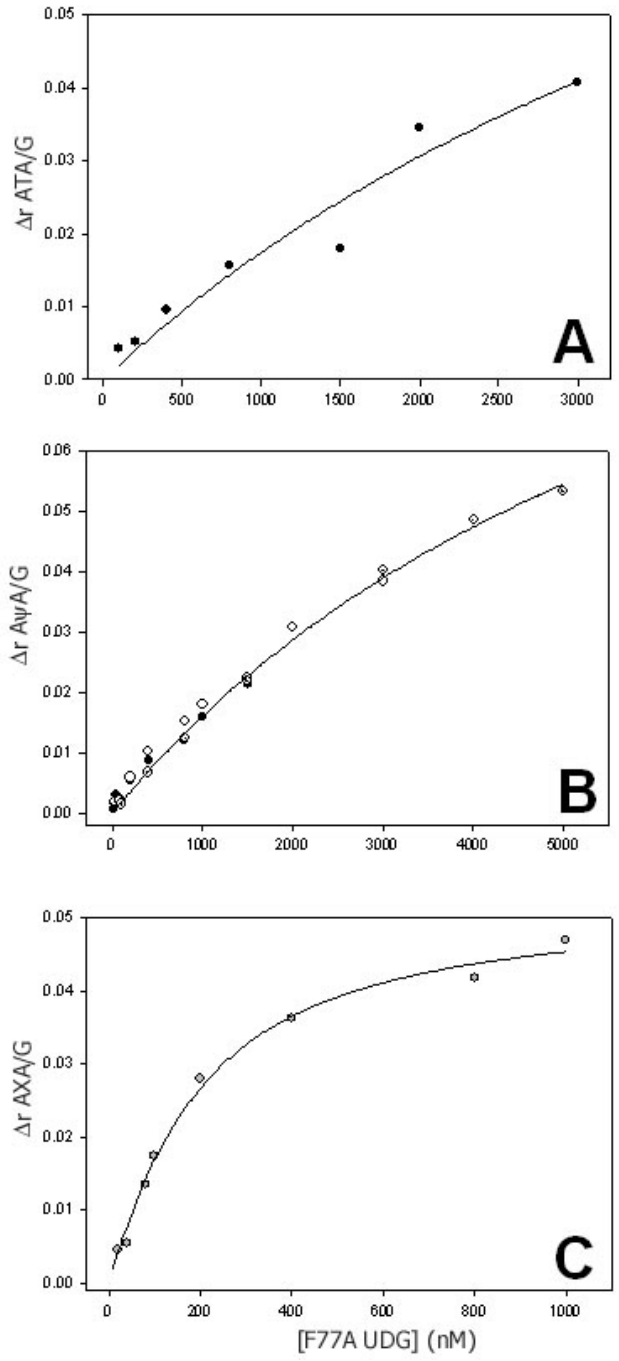

Figure 5-3. Determining the affinity of F77A UDG for various DNA ligands by fluorescence anisotropy. Increasing concentrations of enzyme (0-5 μM) were added to 0.1 μM of the fluorescently labeled DNA ligands ATA/G (A), AψA/G (B), and AXA/G (C). The change in fluorescence anisotropy (Δr) is plotted versus enzyme concentration and the data were fit with nonlinear regression to Eq. 2-4. The titration of AψA/G (B) was replicated while the other titrations were not. The apparent dissociation constants (K_D^{Ap}) derived from the fits are reported in Table 5-2.

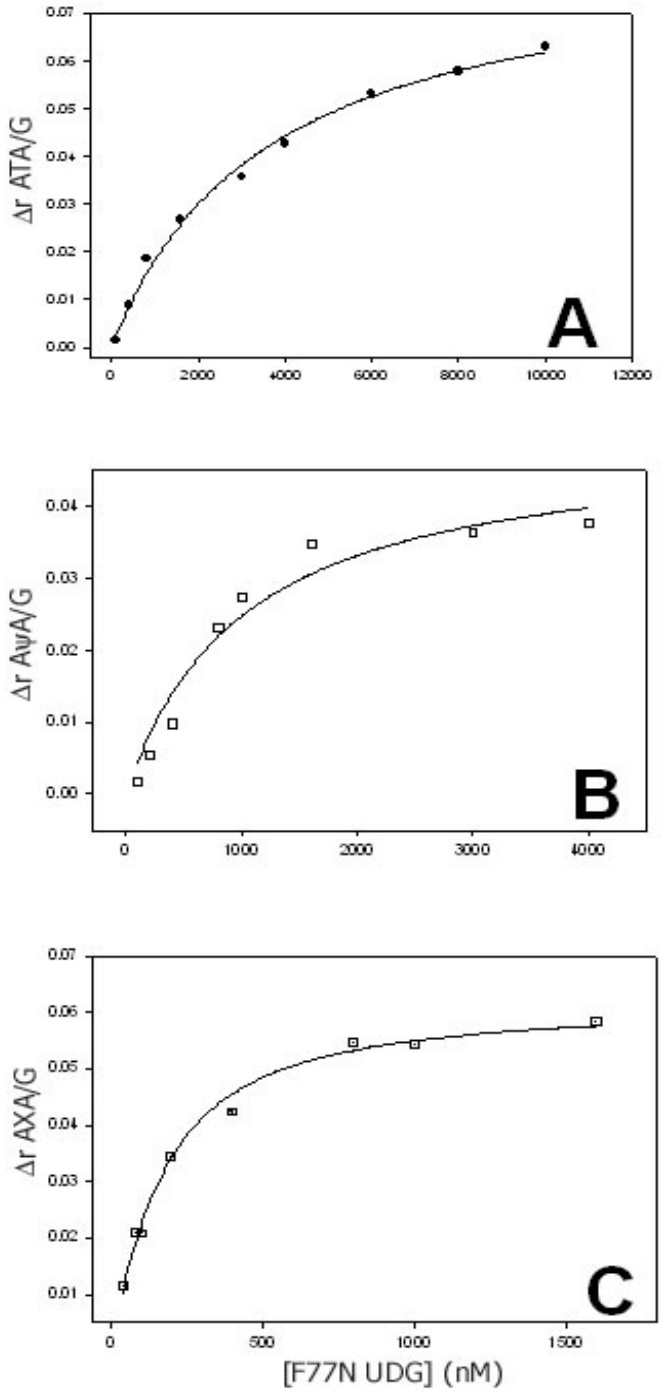

Figure 5-4. Determining the affinity of F77N UDG for various DNA ligands by fluorescence anisotropy. Increasing concentrations of enzyme (0-10 μM) were added to 0.1 μM of the fluorescently labeled DNA ligands ATA/G (A), AψA/G (B), and AXA/G (C). The change in fluorescence anisotropy (Δr) is plotted versus enzyme concentration and the data were fit with nonlinear regression to Eq. 2-4. The apparent dissociation constants derived from these fits are reported in Table 5-2.

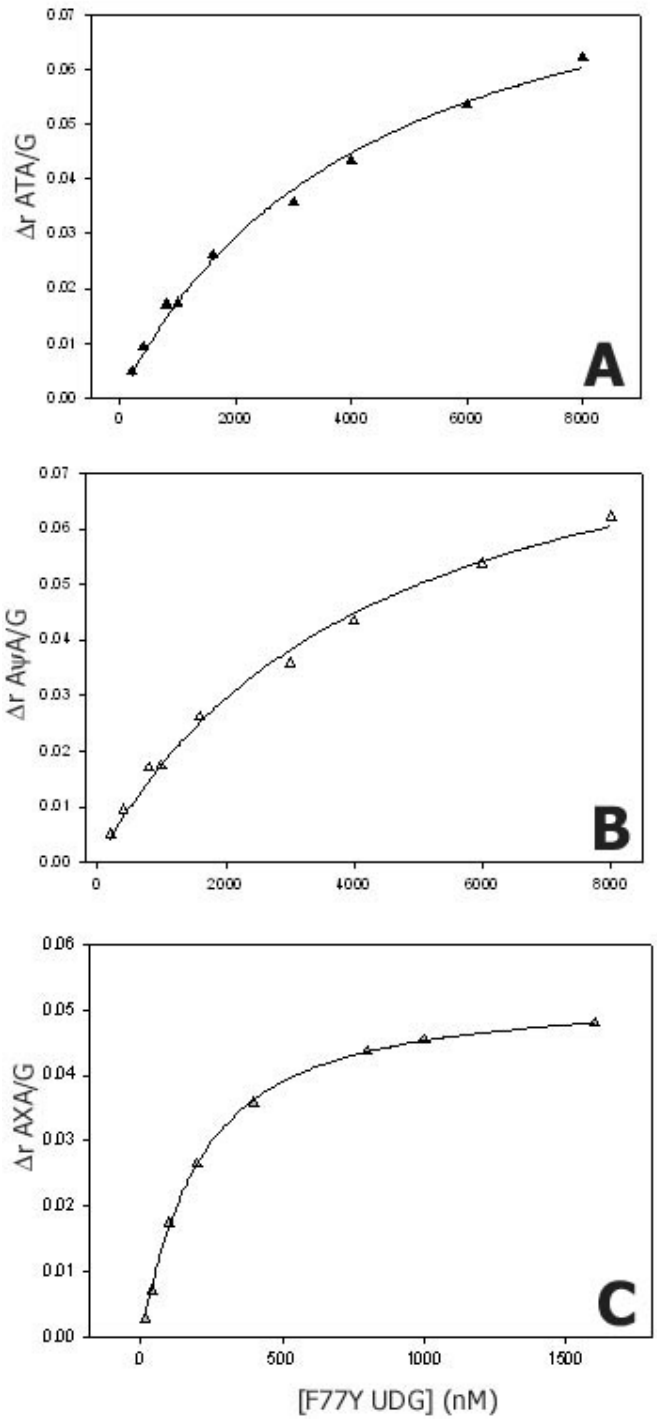

Figure 5-5. Determining the affinity of F77Y UDG for various DNA ligands by fluorescence anisotropy. Increasing concentrations of enzyme (0-8 μM) were added to 0.1 μM of the fluorescently labeled DNA ligands ATA/G (A), AψA/G (B), and AXA/G (C). The change in fluorescence anisotropy (Δr) is plotted versus enzyme concentration and the data were fit with nonlinear regression to Eq. 2-4. The apparent dissociation constants derived from these fits are reported in Table 5-2.

It was hypothesized that replacing Phe77 with alanine might allow this mutant enzyme to have a higher affinity for the substrate mimic containing dsDNA (AψA/G). The reasoning was that if the strain induced by the wtUDG active site upon the dψU was the cause for the enzyme's low binding affinity for this ligand, then replacing the bulky phenyl group with a smaller methyl side chain might allow some of the sterically induced strain to be relaxed, leading to better binding by the F77A mutant. Exactly the opposite was discovered when an apparent dissociation constant of ≈ 7.5 μM was measured for the interaction between F77A UDG and the ligand AψA/G (Fig. 5-3B; Table 5-2). This K_D is twice that of the His-tagged wtUDG, indicating that although both proteins have a relatively weak interaction with the supposed substrate mimic DNA, Phe77 does seem to contribute to UDG's interaction with this nonhydrolysable substrate analog.

Intriguingly, the F77N mutant shows a K_D^{Ap} of ≈ 1 μM for the AψA/G DNA ligand (Fig. 5-4B), which is about three times lower than that of His-tagged wtUDG. One possible reason for this may be that the engineered asparagine's side chain forms extra hydrogen bonds with the substrate mimic that are not present in the wild-type enzyme. Another possibility is that the F77N mutation has distorted the active site in a manner that accommodates the dψU better; of course, there is always a possibility for structural deformation whenever mutations are introduced. Apparently, the F77Y mutation does not change UDG's affinity for dψU containing dsDNA, as its K_D^{Ap} is approximately that of HisUDG (≈ 5 μM; Fig. 5-5B; Table 5-2). This is not surprising as the tyrosine is expected to be in almost the same orientation as the normal phenylalanine is in the wild-type protein.

The interaction of the Phe77 mutants with abasic site product mimic DNA (AXA/G) was approximately equivalent to wtUDG with an apparent K_D of around 130 nM (Fig. 5-3C, -4C, and -5C; Table 5-2). Thus, just as the mutant UDG–undamaged DNA interaction seems undisturbed by the mutations, so does the mutant UDG–abasic product interaction. The same reasoning can be applied here as before; the mutations are internal and probably do not affect the leucine finger that inserts into the DNA. The leucine finger is proposed to aid in nucleotide flipping and to increase the lifetime of the enzyme–flipped nucleotide state [194, 198].

These results, together with the steady-state glycosidic bond cleavage assay data, indicate that the Phe77 mutations have done little to affect UDG's normal interactions with undamaged and product DNAs. The data indicate, as expected, that the mutations effect UDG's catalytic cycle at steps after initial DNA binding (as indicated by a normal –relative to wtUDG– K_D for ATA/G) and before abasic site product release (as indicated by a normal K_D for AXA/G). This leaves nucleotide flipping, protein isomerizations, the chemical step, and uracil base product release as possible points of inhibition by the mutations. To discern the level of involvement of these mutations in these possible steps, a measurement of the rate of the chemical step is needed. Although the mutants are slower than normal UDG, they are still active enough that measurement of the chemical step required the use of the rapid-chemical-quench machine. Our adventure into the presteady-state kinetics of the Phe77 mutants begins in the next chapter.

CHAPTER 6
PRESTEADY-STATE KINETICS OF THE PHE77 MUTANTS

Because the rate-limiting step of the wtUDG catalytic cycle is product release, the much faster nucleotide flipping and chemical steps are hidden within the steady-state turnover number. This also applies to mutations that effect steps before the rate-limiting step. For example, if a mutation slowed the glycosidic bond cleavage step by 10-fold relative to wtUDG to about 10 s^{-1}, this large mutational effect is still not as slow as the rate-limiting product release step, which limits k_{cat} to 1.4 s^{-1}. Therefore the full effect of the mutation on the enzyme would be underestimated.

An obvious solution to this problem is to measure the kinetics of the reaction steps preceding the rate-limiting step directly. Previous research on the reaction mechanism of wtUDG has defined at least three steps after association with DNA and prior to the rate-limiting product release step (Chapter 1 pg. 54). These three steps are nucleotide flipping (ES↔EF), protein isomerization (EF↔EqF), and glycosidic bond cleavage (EqF↔EqP. The experimental strategy implemented to measure the nucleotide flipping and protein isomerization steps involves stopped-flow fluorescence and will be discussed in Chapter 7. The rate of the chemical step can be measured directly using the rapid chemical-quench version of the glycosidic bond cleavage assay discussed in the characterization of wild-type and His-tagged UDGs (Chapters 3 & 4).

Single-Turnover Titration of Wild-type UDG

The single-turnover rate of uracil excision was measured for His-tagged UDG and the Phe77 mutant enzymes to directly measure the rate of chemistry of the reaction.

These experiments were carried out essentially as described in Chapter 3 (pg. 90), except for the following change in experimental strategy. Previous single-turnover experiments for the characterization of wtUDG were performed with a single saturating amount of enzyme with a limiting amount of substrate so that all substrate is immediately enzyme bound. However, because the validity of dψU as a true substrate mimic is questionable ($K_D^{Ap} \approx 4$ μM; Chapter 5 pg. 82), another approach was needed to measure the wtUDG and Phe77 mutant's affinity for substrate. Therefore, instead of using a single saturating amount of enzyme, the substrate (0.1 μM AUA/G) was reacted with increasing amounts of enzyme (0.2 – 6.0 μM) to reveal the dependence of the reaction rate on the enzyme concentration. The observed rate of reaction (k_{obs}) can then be plotted as a function of enzyme concentration. Considering a bimolecular reaction, this plot should be linear under enzyme (or substrate) concentrations that make the on rate (k_{on}) of enzyme–substrate association comparable to the rate of dissociation (k_{off}) of the enzyme–substrate complex [227]. From the linear plot of k_{obs} versus enzyme concentration the apparent rate constants k_{on} and k_{off} can be approximated from the slope and y-intercept, respectively. It is important to note that because K_D is the ratio of the composite dissociation constant of the enzyme–substrate complex (k_{off}) with the composite substrate binding constant (k_{on}), it is independent of the number of intervening steps. Therefore the ratio of k_{off} over k_{on} will give the overall dissociation constant for the substrate AUA/G. If we take into account the previous kinetic work with *E. coli* UDG which showed the substrate association, flipping, and conformational clamping steps are faster (over 3-fold) than the glycosidic bond cleavage step (Chapter 1 pg. 31), then at enzyme concentrations in which substrate is saturated the rate of product formation should plateau at the

maximum rate of the chemical step (k_{max}). To distinguish these types of presteady-state experiments that use varied amounts of enzyme from the maximal single-turnover uracil excision measurements presented in the earlier chapters that used a single saturating enzyme concentration, the following experiments are designated "single-turnover titrations" (but the rate constants for maximal uracil excision all have the same designation, k_{max}).

The first single-turnover titration uracil excision measurement was performed for His-tagged wtUDG. The single-turnover reactions of increasing HisUDG (0.2 – 5 μM) with a constant amount of substrate (0.1 μM AUA/G) were accomplished using the standard rapid-quench adapted glycosidic bond cleavage assay (Chapter 2 pg. 48). Between six and eight data points were taken per concentration of enzyme on a timescale appropriate to capture the majority of the reaction for the given enzyme concentration and activity. These reaction time courses are graphed as a function of time and fit with Eq. 2-2 to obtain the observed reaction rate at each concentration of enzyme. The data for the HisUDG single-turnover reactions with 100 nM AUA/G are presented in Figure 6-1A. The observed rates from the time course fits are then plotted as a function of enzyme concentration (Fig. 6-1B). The rate constants in the linear portion of the reaction dependence on enzyme concentration are fit by linear regression to obtain k_{on} (the slope) and k_{off} (the y-intercept). A horizontal line drawn through the plateau (i.e., saturation) in the values of k_{obs} represents the maximal single-turnover excision rate constant (k_{max}). For wild-type His-tagged UDG k_{on} is 73 $\mu M^{-1}s^{-1}$ and k_{off} is 0.72 s^{-1}, which gives a K_D of 10 nM for the substrate AUA/G.

Under saturating enzyme concentrations, His-tagged UDG cleaves the glycosidic bond of dU in this 25mer dsDNA U:G mispair substrate with a $k_{max} \approx 125\ s^{-1}$. The observed rate constants for the single-turnover titration of HisUDG and their fit by linear regression are displayed in Figure 6-1B, and collected in Table 6-1. The rate constants from the previous single-turnover experiments (at one enzyme concentration) with AUA/A and ssAUA are also shown (Table 6-1) for comparison. These values are essentially the same as the results for the single-turnover titrations with AUA/G, therefore the redundant data is not displayed.

The maximum rate of uracil excision ($k_{max} = 125\ s^{-1}$) from the single-turnover reactions with the substrate AUA/G agrees well with the previous single-turnover excision rate obtained at a single saturating enzyme concentration ($k_{max} = 130\ s^{-1}$) for the substrate AUA/A. This confirms a previous observation by Stivers et al. [153] that UDG amazingly seems virtually unaffected by the base-pairing context in which the uracil resides. Whether the uracil is in a proper Watson-Crick base pair with adenine or in a wobble mispair with guanine, has little effect on the activity of UDG (in the limit that nucleotide flipping from either context is faster than bond cleavage). This remarkable observation has been postulated to be due to the enzyme being able to destabilize the DNA structure upon binding with its DNA pinching motifs [134] so that there is essentially no energetic difference between a properly paired and mispaired base [153].

The dissociation constant for HisUDG's interaction with true substrate ($K_D \approx 10$ nM) obtained from the fit of the observed single-turnover uracil excision rate constants is about 300 times lower than the K_D measured for the substrate mimic dψU containing DNA measured via fluorescence anisotropy (Table 3-1 pg. 58). This is

another strong indication that the substrate mimic does not interact with UDG the way the natural substrate does.

The 10 nM K_D for double stranded substrate (AUA/G) measured in this work is close to dissociation constants measured for UDG in previous studies with similarly sized dsDNA substrates. In several studies, that used 2-AP as a fluorescent reporter of the helical structure of a double stranded DNA, the apparent dissociation constant for the substrate mimic dfU ranged from 50 nM for a 19mer dsDNA substrate with a central dfU:G mispair to 130 nM for a 11mer dsDNA with a dfU:A proper base pair [153, 194]. The experimental approach to measure the K_D of the true substrate in this work is based on the approach used by Wong et al. [202], in which they also performed a series of single-turnover reactions with varying amounts of enzyme and 10 nM of a dsDNA substrate; therefore the concentrations of substrate and enzyme were 10-fold less than those used this experiment. Wong et al. reported a K_D^{Ap} of 38 nM for the natural substrate deoxyuridine base paired with 2AP in a 25mer dsDNA, which is close to the value measured in this work and the work of Jiang and Stivers mentioned above.

However, Wong and coworkers measured a maximal concentration independent uracil excision rate of 38 s^{-1} which is over three times smaller than the k_{max} value found by Drohat et al. [206] and the value reported here. The source of these differences could come from the ionic strength and pH of the buffer (30 mM Tris-HCl pH 7.4, 1 mM EDTA, 1 mM dithiothreitol, 5% (w/v) glycerol) used in the experiments of Wong et al. The lower pH of 7.4 is below the optimal pH for *E. coli* UDG (pH 8.0) [156], the pH of the buffers used in our work. In addition, the lower ionic strength and absence of a divalent cation in the buffer of Wong and coworkers could also result in changes in the

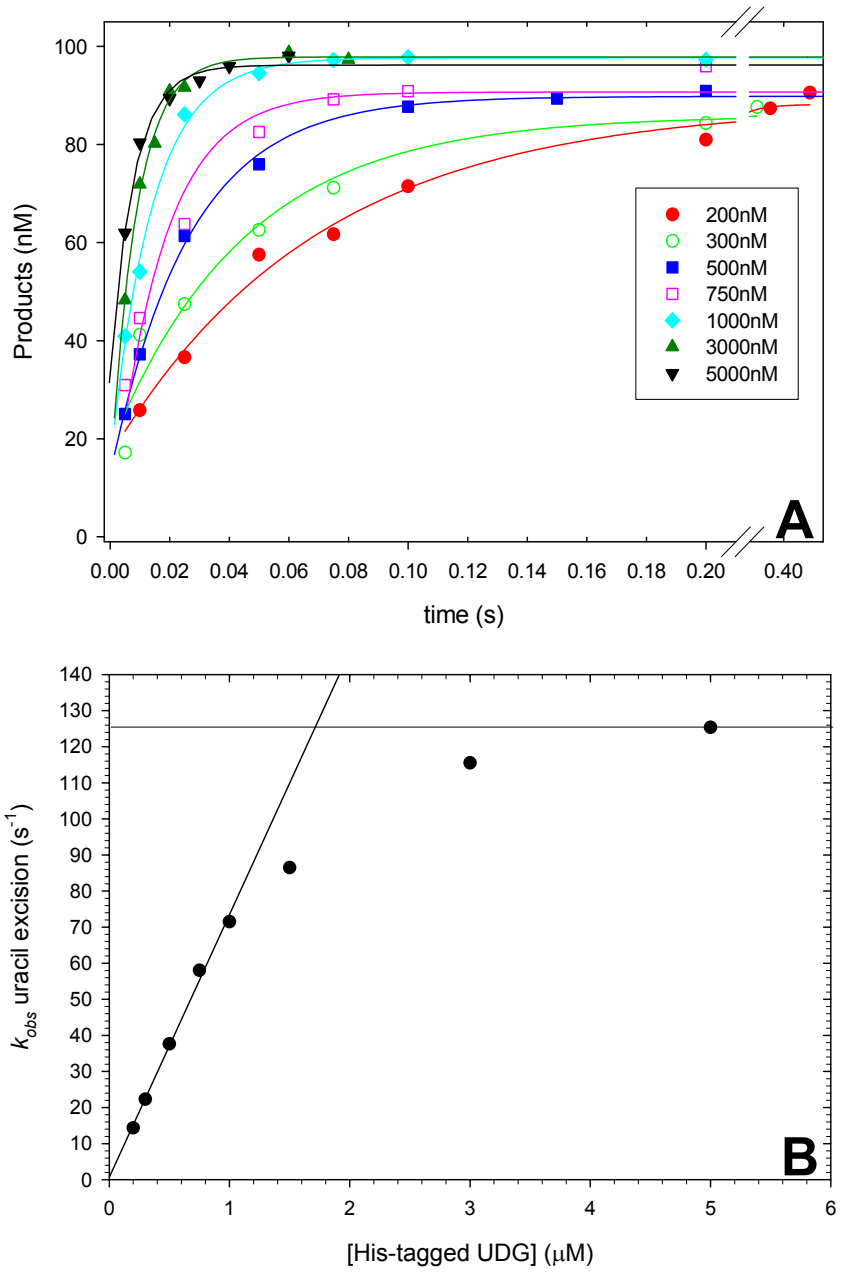

Figure 6-1. Single-turnover uracil excision reaction titration of AUA/G with HisUDG. (A) The reaction time course data acquired by the rapid-quench glycosidic bond cleavage assay (pg. 76) for the conversion of 0.1 μM AUA/G into the products of uracil excision by increasing amounts of HisUDG (0.2-5.0 μM; see figure legend). The data are fit with Eq. 2-2 to yield the observed rate constants for uracil excision. (B) The linear regression fit of the observed rate constants to obtain the apparent rates for k_{on} and k_{off}. The maximal single-turnover excision rate (k_{max}) is the concentration independent rate attained at saturation and represented by a horizontal line (reported in Table 6-1).

Table 6-1. Parameters for single-turnover uracil excision by wtUDG and Phe77 mutants.

Enzyme	k_{max} (s^{-1}) AUA/G	k_{on} ($\mu M^{-1}s^{-1}$)	k_{off} (s^{-1})	K_D (nM)	$k_{max}^{wt}/k_{max}^{mut}$	k_{max}/k_{cat}	k_{max} (s^{-1}) AUA/A	k_{max} (s^{-1}) ssAUA
wt(His-tagged)	125 ± 15	73 ± 1	0.72 ± 0.01	10 ± 1		90	130 ± 10	170 ± 20
F77A*	≥ 3	0.46 ± 0.05	0.066 ± 0.03	130 ± 12	≤ 40	50	1.2 ± 0.1	1.3 ± 0.1
F77N	0.08 ± 0.02	0.05 ± 0.005	$7.0 \times 10^{-4} \pm 1.0 \times 10^{-4}$	13 ± 1.3	1600	8	0.05 ± 0.01	0.08 ± 0.01
F77Y	7 ± 2	6.0 ± 0.3	0.16 ± 0.08	27 ± 2	18	14	5.2 ± 2	9.1 ± 1

The substrates AUA/A and ssAUA were assayed only at a single saturating (usually 10 μM) concentration of enzyme. The dissociation constants (K_D) are for the AUA/G data (see text). The reported errors for the AUA/G data set are the uncertainties in the fit of the titration set and the errors reported for the AUA/A and ssAUA data sets are the standard deviation of three data sets.
* k_{obs} for F77A did not saturate so only the lower limit of k_{max} could be estimated.

properties of UDG–substrate interaction. These buffer differences alone could explain the lower k_{max} measured by Wong et al., however a second notable difference between experimental procedures was that Wong and coworkers used a quench that contained 6 M NaOH *and* 4 M guanidine thiocyanate (as compared to the 0.5M KOH, 2mM EDTA quench used in our rapid-quench assays). As Wong et al. noted in their publication, the addition of 4 M guanidine thiocyanate to the quench resulted in at least one other supposed β-elimination DNA cleavage product, complicating the quantification of reaction products. Attempts in our lab to use the 6 M NaOH, 4 M guanidine thiocyanate quench resulted in both distortion of the migrating DNA bands during the separation step by denaturing PAGE, and significant degradation of the DNA during the base catalyzed phosphodiester backbone cleavage step (data not shown). These complications could lead to significant errors in the quantification of the DNA reactant and product bands.

Given all the differences between the methods implemented in the measurements of the properties of *E. coli* UDG, it may be best to conclude that any direct comparisons between the kinetic constants determined by these various methods should not be over-interpreted. The fact that despite the variations in experimental protocol, the measured maximum single-turnover uracil excision rates are only 3-fold different, and dissociation constants for dsDNA substrates are all within ≈ 5-fold of each other, implies that the variety of techniques are accurately assessing the same parameters of UDG. This large body of research is a strong foundation for the comparison of mutational effects.

Single-turnover Titrations of Phe77 Mutant UDGs

With single-turnover uracil excision titration results for wt(His-tagged)UDG complete, the Phe77 mutant UDGs were assayed in the same manner. This allowed direct comparisons between the single-turnover uracil excision kinetics of the UDG variants and the wild-type enzyme. The data are shown in Figures 6-2 to 6-4 and the kinetic constants are collected in Table 6-1.

The concentration independent maximal single-turnover uracil excision rates (k_{max}) of the Phe77 mutants show that the chemical step, or possibly steps prior to chemistry but subsequent to substrate binding, or both, are impaired by the substitution of Phe77. The ratio of the wild-type (His-tagged) and mutant maximal single-turnover uracil excision rates ($k_{max}^{wt}/k_{max}^{mut}$; Table 6-1) reveal that the F77N mutant is the most impaired, excising uracil almost 1600-fold more slowly relative to wild-type UDG for the same substrate, AUA/G. The F77A and F77Y mutants show only mildly reduced maximal single-turnover uracil excision rates as compared to wild-type (≤ 40 and 18 fold, respectively), indicating that these mutations do not strongly influence the chemistry of glycosidic bond cleavage. Given the existence of other putative UDG superfamily members that lack the

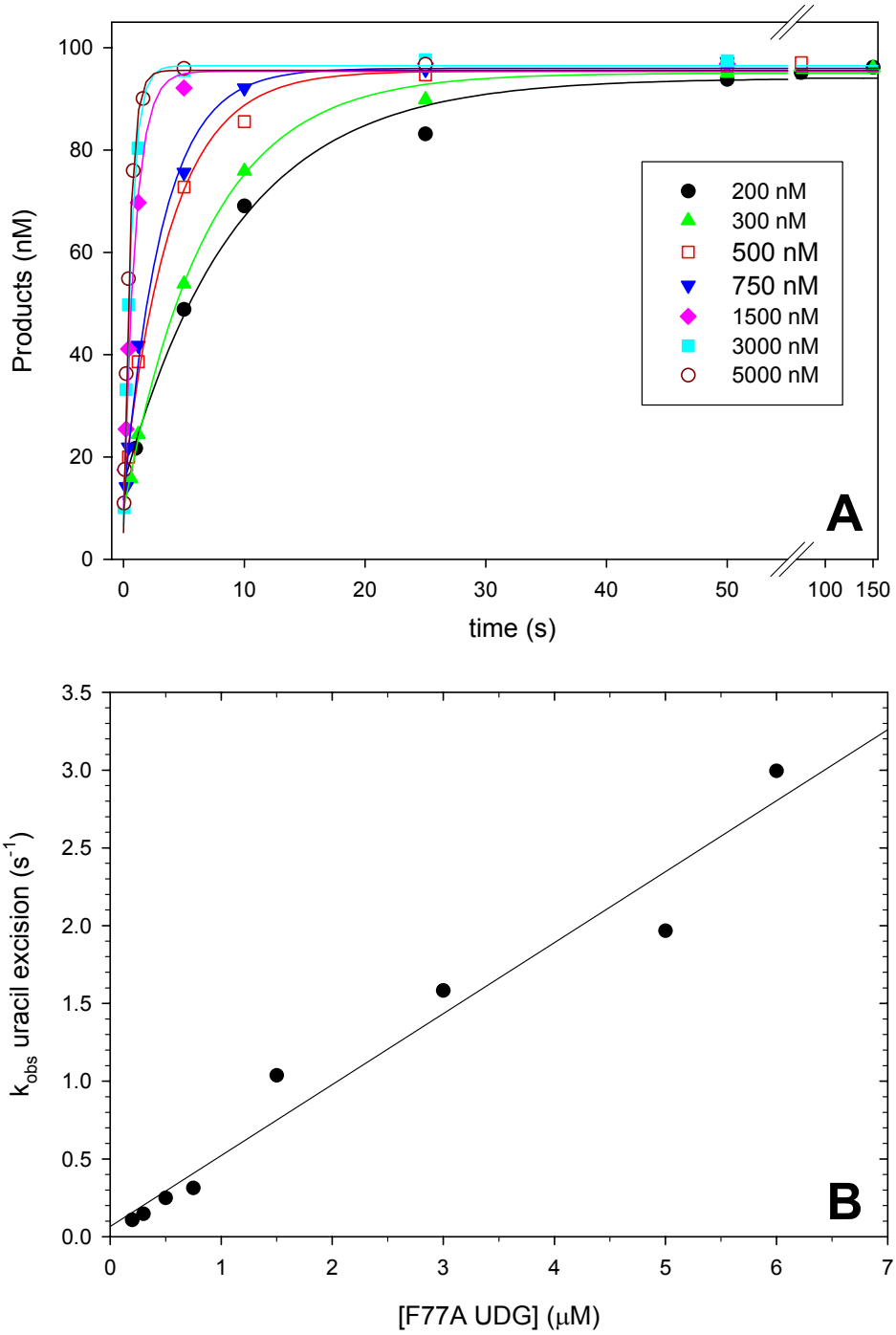

Figure 6-2. Single-turnover uracil excision reaction titration of AUA/G with F77A UDG. (A) The reaction time course data for the conversion of 0.1 μM AUA/G into the products of uracil excision by increasing amounts of F77A UDG (0.2-5.0 μM; see figure legend). The data are fit with Eq. 2-2 to yield the observed rate constants for uracil excision. (B) The fit of the observed rate constants by linear regression to obtain and the dissociation constant (K_D) for the interaction of F77A UDG with AUA/G (Table 6-1).

active site phenylalanine or naturally have a tyrosine instead (Chapter 1 pg. 14), it is not unexpected that the F77A and F77Y mutants retain most of their activity. Yet, if one considers that the F77Y mutation only adds a hydroxyl group, it is fascinating that this mutation exerts an effect on this powerful catalyst. Conversely, it can also be considered remarkable that complete removal of a phenyl group that makes van der Waals contacts with the substrate does not create a greater perturbation of the mechanics of UDG.

As in the earlier analysis of wtUDG (Chapter 3) the k_{max} and the steady-state k_{cat} rate constants of the Phe77 mutants can be compared to determine if the rate-limiting step in the enzymes' reaction pathways are either at the chemical step or before, or a step after chemistry, such as product release. Interestingly, all the mutants have k_{max}/k_{cat} ratios that are greater than unity, implying that although the concentration independent single-turnover uracil excision rates are slower relative to wild-type for these mutants, the rate-limiting step in the steady-state is not the glycosidic bond cleavage step. This indicates that Phe77 could have roles before and after glycosidic bond cleavage, because both chemistry and a step, or steps, after bond cleavage are handicapped relative to the wild-type enzyme. This is evident for F77A UDG in the differences between single- and double-stranded DNA substrates when the reactions are either pseudo-first-order in enzyme or substrate.

Although it is unclear that the F77A mutant was saturating the substrate at the highest concentrations of enzyme attainable (Fig. 6-2B), the single-turnover titration of the substrate AUA/G still establishes a lower limit for k_{max} of $\approx 3\ s^{-1}$. Comparison of this value with the steady-state turnover numbers of F77A UDG for ssAUA ($k_{cat} = 3.3\ s^{-1}$) and AUA/A ($k_{cat} = 0.06\ s^{-1}$; Table 6-1) reveals that at high enzyme concentrations the

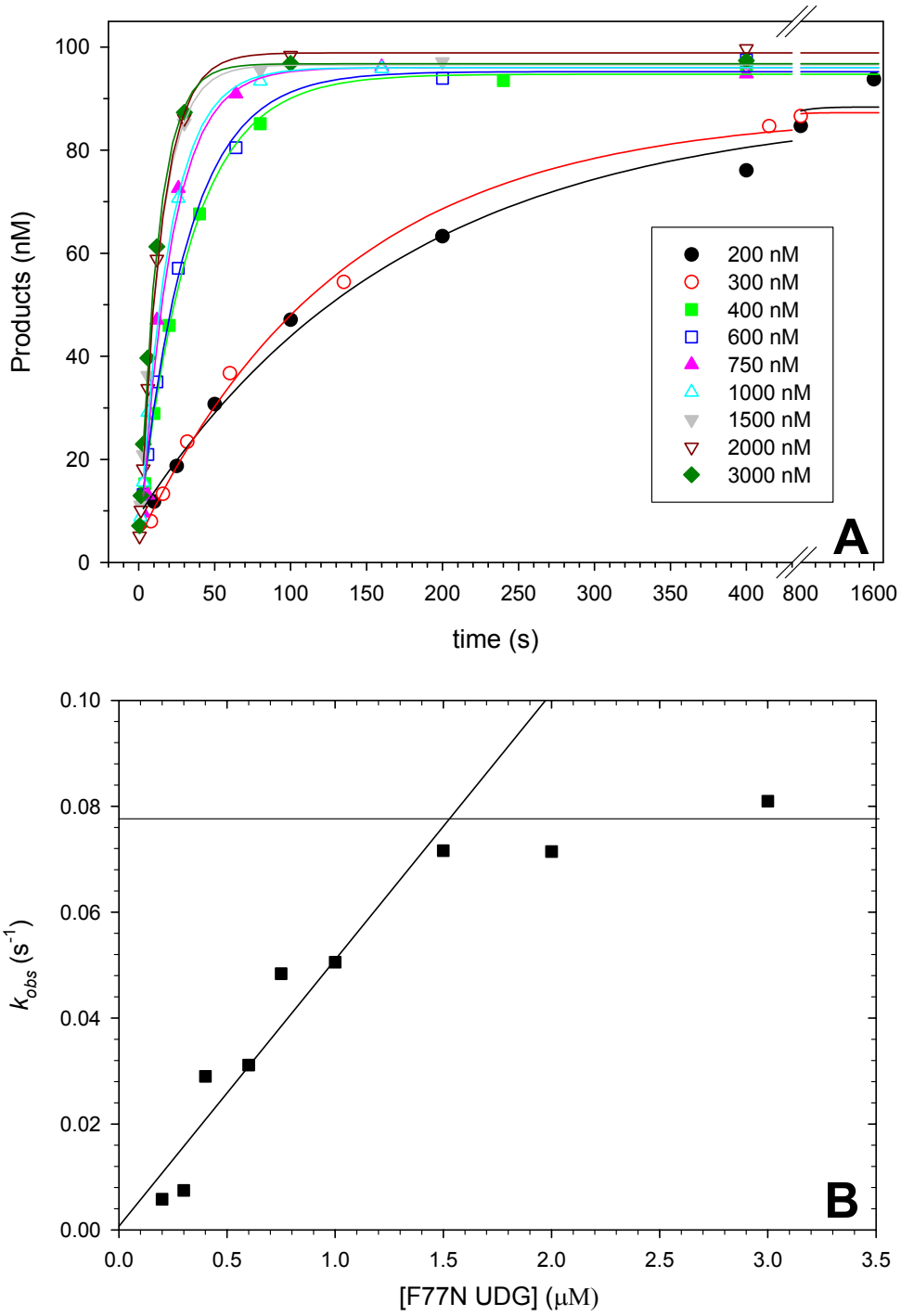

Figure 6-3. Single-turnover uracil excision reaction titration of AUA/G with F77N UDG. (A) The reaction time course data for the conversion of 0.1 μM AUA/G into the products of uracil excision by increasing amounts of F77N UDG (0.2-3.0 μM). The data are fit with Eq. 2-2 to yield the observed rate constants for uracil excision. (B) The linear regression of the observed rate constants as described in Fig. 6-1 (Table 6-1).

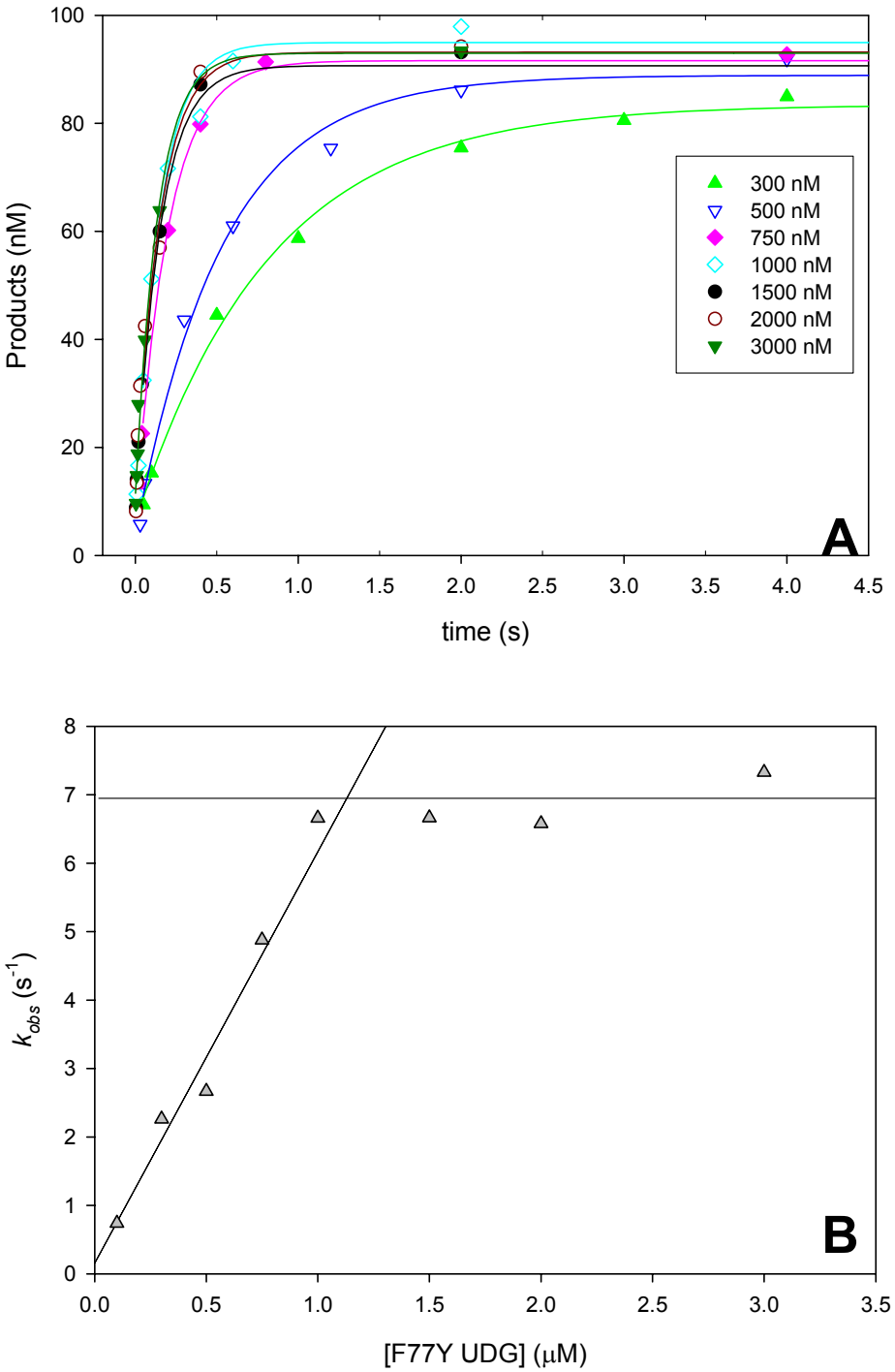

Figure 6-4. Single-turnover uracil excision reaction titration of AUA/G with F77Y UDG. (A) The reaction time course data for the conversion of 0.1 μM AUA/G into the products of uracil excision by increasing amounts of F77Y UDG (0.3-3.0 μM). The data are fit with Eq. 2-2 to yield the observed rate constants for uracil excision. (B) The fit of the observed rate constants by linear regression for the composite rate constants for the interaction of F77Y UDG with the substrate AUA/G as described in Fig 6-1 (Table 6-1).

catalytic deficiency towards dsDNA substrate is alleviated to give a rate close to the steady-state turnover of ssDNA. Therefore it appears that the alanine mutation has decreased the on rate of UDG for dsDNA, impairing its ability to bind this substrate. Once enough F77A UDG is present to overcome this deficiency in AUA/A association, the rate-limiting step becomes glycosidic bond cleavage or a subsequent step in the reaction pathway. Backing evidence for this assumption comes from the over 10-fold larger K_D (as compared to wild-type) of F77A UDG for substrate and the approximately equal single-turnover uracil excision rates for the substrates ssAUA and AUA/A (Table 6-1). Since this effect is specific for dsDNA it strongly implies that the alanine mutation has affected UDG's ability to either flip the nucleotide or conformationally clamp onto dU in a duplex DNA context. Removing the phenyl group has shown that this conserved amino acid does contribute to UDG's affinity for dU.

The F77N mutant has k_{max}/k_{cat} ratio that is 5:1 for the substrate AUA/A, which is the closest to unity of all the mutants. This raises the possibility that glycosidic bond cleavage is rate-limiting for this enzyme in the steady-state reactions if it was not saturated with substrate. This possibility should be kept under consideration since higher concentrations of F77N UDG were needed in the steady-state reactions with AUA/A to create enough products to accurately quantitate on a reasonable timescale.

The slower single-turnover uracil excision kinetics of the Phe77 mutants clearly demonstrates that Phe77 aids in lowering the activation barrier for catalysis, either by facilitating substrate binding or chemistry. This result can be expected for a highly conserved active-site residue. What is unexpected is that the conserved Phe77 may also play a role in destabilizing the enzyme–product complex to aid in product release, as

indicated by comparison of the slower steady-state turnover of the Phe77 mutants as compared to their maximal concentration independent uracil excision rates. Comparing the activity of F77A UDG with single- and double-stranded substrates has also enabled the dissection of its contribution to substrate binding. The results show that Phe77 does contribute a favorable interaction that facilitates binding of dU in a duplex DNA context. Therefore the conserved Phe can be justly designated as a *pulling* residue under the terminology of the proposed "pinch, push, and pull" mechanism (Chapter 1 pg. 23).

Presteady-State Burst Kinetics of F77A and F77Y UDG

The discovery that the glycosidic bond cleavage step was not rate-limiting for the F77A and F77Y UDG mutants allowed for the possibility that these UDG variants may display a presteady-state burst of products. As discussed in Chapter 3, a burst of products will be formed when mixing a limiting concentration of enzyme with substrate in excess, if product dissociation is slow and enzyme bound product is able to accumulate. Wild-type UDG creates a large burst of products due to the large difference in the rates of the bond cleavage and product release steps, with bond cleavage being 90-fold faster than product release (Fig. 3-9). Therefore to determine if the F77A and F77Y mutations would still allow a product burst to form, limiting concentrations of enzyme were reacted with 0.5 μM of the substrate AUA/A as previously performed for wtUDG and His-tagged wtUDGs according to the protocol for the rapid quench glycosidic bond cleavage assay described in Chapter 2.

Both F77A and F77Y mutants show discernable bursts in the transient kinetics of their reactions with dsDNA substrate (Figures 6-5 and 6-6). The slope of the linear portion of the fit with Eq. 2-3 through the data sets for the F77A reaction gives a rate for the reaction of ≈ 1.5 nM/s, which gives a steady-state turnover number of 0.03 s^{-1},

equivalent to the previously measured steady-state rate of catalysis by F77A at these substrate concentrations. Likewise, the rates obtained by the same analysis of the F77Y data are equivalent to the steady-state rate of uracil excision for this enzyme (0.46 and 0.48 nM/s, for the 50 and 200 nM reactions, respectively).

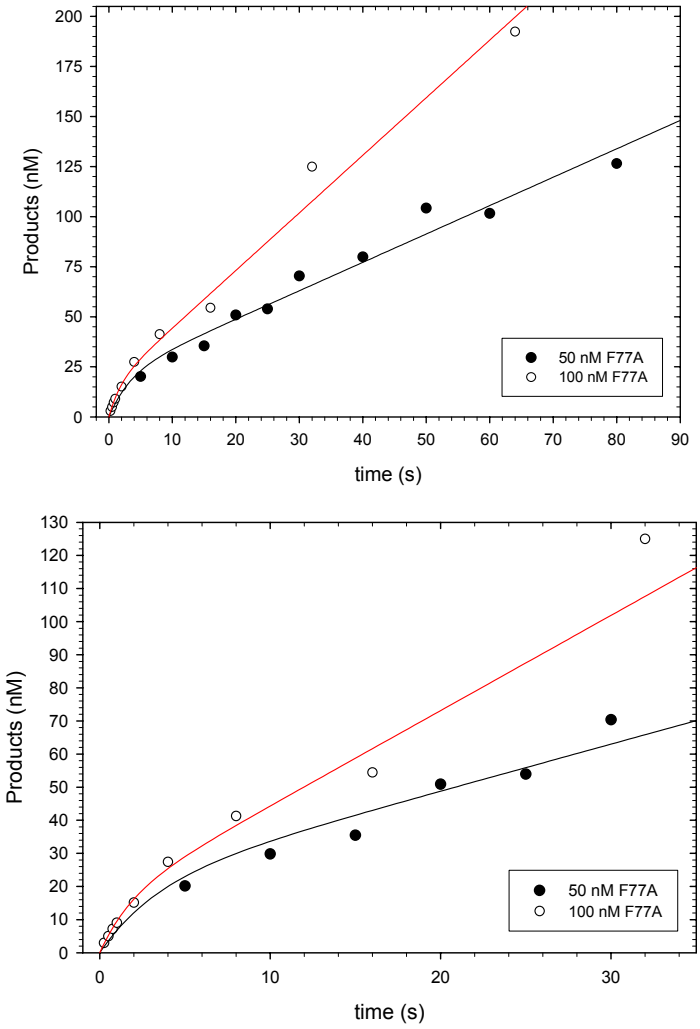

Figure 6-5. Presteady-state burst of products by F77A UDG. Limiting amounts of F77A UDG (50 and 100 nM) were reacted with excess dsDNA substrate (0.5 μM) AUA/A according to the protocol for the rapid quench glycosidic bond cleavage assay described in Chapter 2. The data are fit with Eq. 2-3 to give the burst-and steady-state rate of the reactions (reported in Table 6-2).

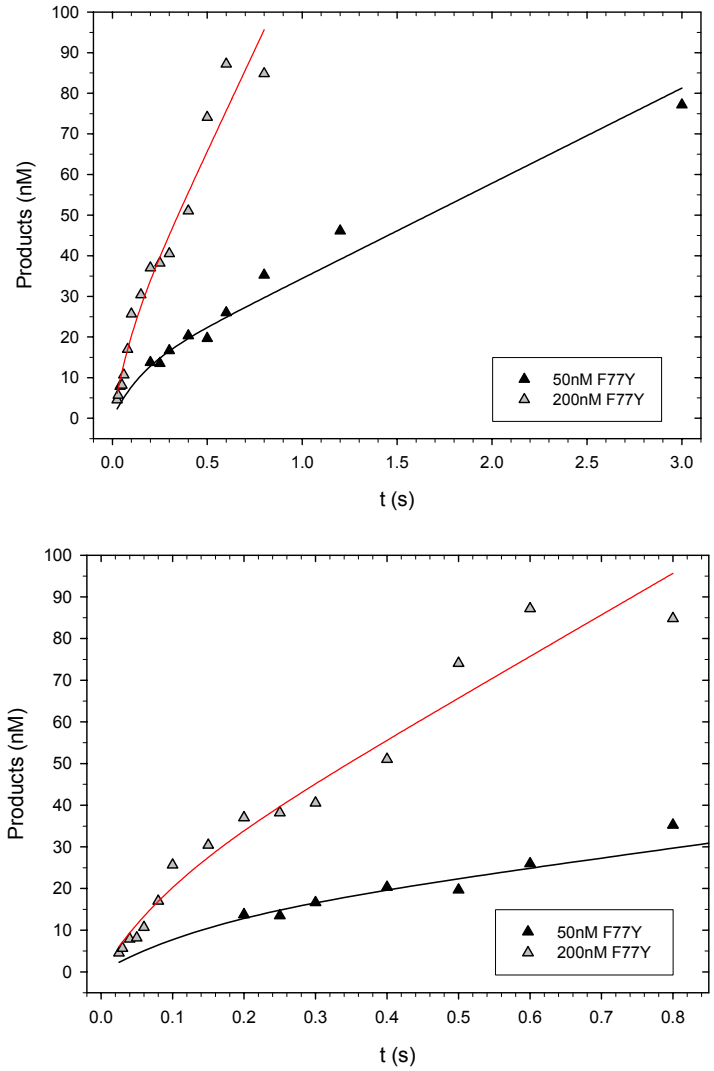

Figure 6-6. Presteady-state burst kinetics of F77Y UDG. Limiting amounts of F77Y UDG (50 nM and 200 nM) were reacted with excess dsDNA substrate (0.5 μM) AUA/A according to the protocol for the rapid quench glycosidic bond cleavage assay (Chapter 2). The data are fit with Eq. 2-3 to give the burst- and steady-state rate of the reactions (Table 6-2).

Table 6-2. Presteady-state burst kinetic constants for F77A and F77Y UDG

	50 nM F77A	100 nM F77A	50 nM F77Y	200 nM F77Y
Burst Amplitude (nM)	19	16	11	18
Burst rate (s^{-1})	ND	0.55	ND	8.9
Steady-state rate (nM/s)	1.5	2.9	23	96
k_{cat} (s^{-1})	0.03	0.03	0.46	0.48

The data in Figures 6-5 and 6-6 were fit with Eq. 2-3 to calculate the magnitude and rate of the product burst when limiting amounts of enzyme were reacted with substrate in excess (500 nM).

As discussed in Chapter 3, the burst amplitude is a function of the percent substrate bound, the net flux of the reaction, and the rate of product release. For F77A UDG k_{cat} is 50-fold slower than k_{max}, whereas for F77Y UDG it is only 20-fold slower. This difference should cause the presteady-state burst of F77A UDG to be larger than F77Y UDG at a given enzyme concentration. This is exactly the case as the burst amplitude of F77A UDG is almost double that of F77Y at the same enzyme and substrate concentrations. The burst amplitude of the 50 nM F77A UDG reaction shows that at least 38% of the enzyme bound substrate in the initial phase of the reaction. This value sets an upper-limit for the K_D for the substrate AUA/G at about 700 nM. Likewise the burst for the 50nM F77Y UDG reaction sets an upper-limit for the K_D of 2 μM for AUA/G. (These are only upper-limits and should not be over-interpreted as the burst amplitude is also affected by the rate of product release.) The burst rates of F77A and F77Y UDG are roughly 10- and 70-fold slower than the burst rate of wtUDG (38 s^{-1}), which is close to the damage factor these mutations have on k_{max} (Table 6-1). The

unresponsiveness of the burst amplitude to enzyme concentration for F77A UDG may reflect this mutant's lower affinity for substrate (relative to wild-type).

These burst kinetics confirm that product formation is faster than product release for F77A and F77Y UDG. These results also confirm the steady-state turnover numbers measured previously for these UDG variants (Table 5-1 pg. 80). However, the limited data density obtainable by these methods limits interpretation of the data. A reliable real-time technique, possibly some form of stopped-flow fluorescence that allows quantification of both free and bound products (so the burst could be detected), would be better suited to address this problem.

In summary, the trend of decreasing catalytic activity of the Phe77 mutants exhibited in the steady-state data of F77Y>F77A>F77N, was again duplicated in the single-turnover uracil excision measurements. The k_{max}/k_{cat} ratios for the Phe77 mutants indicated that despite a significant reduction in the rate of uracil excision for all mutants, there is still a step after chemistry that is rate limiting. The effects the mutations exhibited on reactions pathway steps before, during, and after bond cleavage indicate that the conserved Phe77 may play an important role in not only transition state stabilization, but also in substrate binding (especially in dsDNA substrates) and enzyme–product complex destabilization.

CHAPTER 7
STOPPED-FLOW TRYPTOPHAN FLUORESCENCE MEASRUEMENTS OF WILD-TYPE UDG AND PHE77 MUTANTS

The growing structural evidence documenting changes in structure between free and ligand bound proteins, clearly shows that ligand binding induces changes in protein conformation that are central to the biological function of the protein. Often, substrate binding to enzymes causes protein isomerizations that control the proper positioning of amino acids essential for specificity and catalysis. These substrate-induced isomerizations can be substantial and are frequently rate-limiting; therefore it is increasingly important to measure the kinetics of the changes in protein structure in order to establish their mechanistic significance.

An understanding of protein structural dynamics will undoubtedly advance our knowledge of enzymatic catalysis, much like observing a live organism yields vital information to a biologist unattainable in a fixed specimen. Crystal structures may be able to show us the anatomy of a protein, but they cannot tell us the nature of the beast. Unfortunately, due to a dearth of real time signals to detect the changes in protein structure that accompany ligand binding, the kinetics of such transitions have been measured in only a small fraction of the systems [230]. As luck would have it, UDG is one of the rare proteins with a robust tryptophan fluorescence signal that correlates with its catalytic cycle. Crystal structures of UDG in complex with substrate mimic and product duplex DNA ligands reveal that the enzyme has a movement upon binding substrate that causes two structural domains to come together and clamp down upon the

substrate (see Chapter 1 pg. 31 for a more detailed discussion) [193]. This movement is proposed to be the source of the tryptophan fluorescence changes of UDG, and has given us a rare window into the machinations of a powerful catalyst.

Controls for Trp fluorescence Stopped-Flow Measurements

The kinetic study of *E. coli* UDG by Stivers and coworkers was the first to demonstrate that the enzyme exhibited a quenching of its tryptophan fluorescence when mixed with DNAs containing the substrate mimic 2′-fluoro-2′-deoxyuridine (dfU) [153]. Subsequent stopped-flow fluorescence studies with deoxyuridine containing substrate oligos and *E. coli* UDG showed that the natural substrate could also cause a quenching of the enzyme's Trp fluorescence [202]. The Trp fluorescence quenching is proposed to be caused by an isomerization in UDG that allows it to "clamp down" upon substrate or substrate analog containing oligos [153]. Before an investigation into the effect the Phe77 mutations have upon the Trp fluorescence of UDG, a series of controls were performed to determine what features of the DNA substrates and products might possibly cause a change of the intrinsic Trp fluorescence of wild-type (His tagged) and mutant enzymes.

To ensure that the quenching of the Trp fluorescence of UDG was caused by the substrate and not any other ligand or artifact, the following series of controls were completed (see Chapter 2 for details on instrumental setup). These controls and all subsequent stopped-flow fluorescence measurements were performed in standard UDG reaction buffer that lacked BSA, because the tryptophan in BSA would be a source of interfering fluorescence. The tryptophan fluorescence of HisUDG (100 nM) was monitored on the millisecond time-scale either by itself or in combination with the standard set of ligands (Table 2-1 pg. 45): undamaged DNA that contains a central

mispair (ATA/G, 100 nM); deoxyuridine substrate DNA annealed with a proper pair (AUA/A, 200 nM) or annealed in a mispair (AUA/G, 200 nM); deoxypseudouridine substrate mimic DNA (AψA/G, 200 nM); and product mimic DNA (AXA/G, 200 nM). The Trp fluorescence traces are off-set arbitrarily from zero volts to prevent overlap in their display in a single graph shown in Figure 7-1.

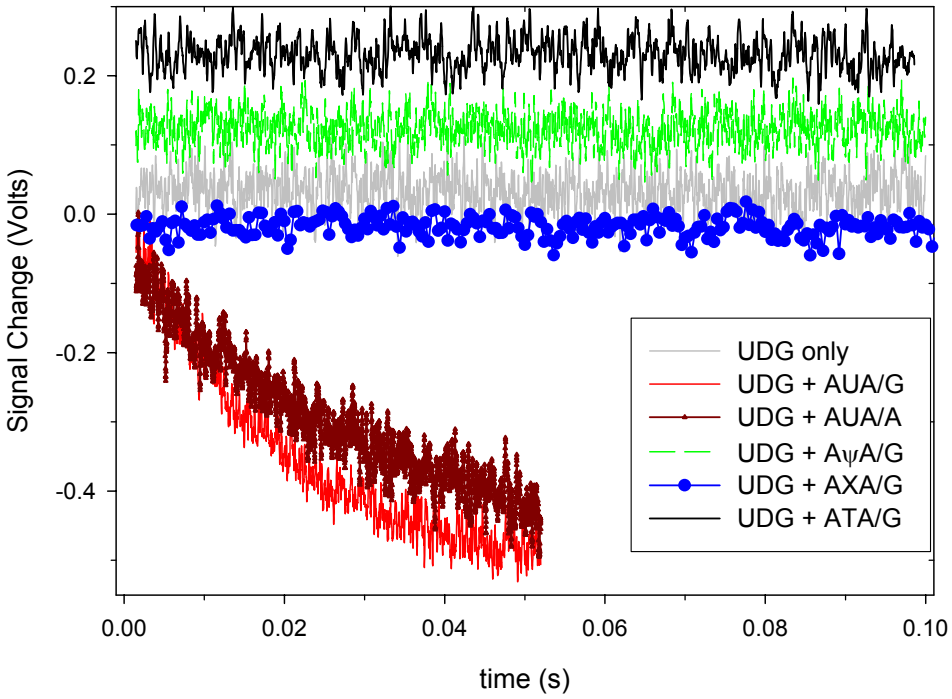

Figure 7-1. Trp fluorescence stopped-flow controls for HisUDG with various ligands. Only dU containing DNA triggered the quenching of the intrinsic Trp fluorescence of UDG (dark red and bright red traces). All the other DNA ligands (see figure legend) did not significantly change the Trp fluorescence of UDG and were off-set from UDG only (gray) for simultaneous display in this figure.

The UDG only trace (Fig. 7-1, gray solid line) shows that the enzyme's tryptophans do not photo-bleach, or fluctuate significantly during the course of the measurement, providing a steady baseline to compare changes in fluorescence. Of all the DNA ligands added to HisUDG, only the dU containing substrates (AUA/G and AUA/A) caused a

significant (6-fold; from -0.1 V to -0.6 V signal change) quenching in Trp fluorescence of the enzyme (Fig. 7-1, red solid line and dark red dotted line, respectively). A full description of this fluorescence change will be presented in the next section of this chapter.

The absence of a detectable change in the Trp fluorescence of HisUDG when mixed with the dψU substrate mimic containing double-stranded oligo is yet more proof that UDG does not interact with this ligand as it does the natural substrate (Fig. 7-1 dashed green line). This real-time measurement clearly shows that dψU does not induce Trp-quenching in UDG. One of the many possible interpretations for this result is that UDG cannot flip dψU when in solution, as it did in the crystal structure [187]. Knowing however, that the enzyme can flip and cleave other nucleotides when the steric constraints of the active site are relaxed [139] indicates that UDG samples other bases by flipping and makes this possibility seem unlikely.

A more probable explanation of the absence of a Trp-signal for dψU flipping is that the UDG–dψU complex is so transient that a population of molecules cannot remain in the nucleotide flipped state to supply a signal. This hypothesis is supported by our failed attempts to measure the nucleotide flipping rate of UDG. The experimental strategy we attempted was to design oligos containing a fluorescent reporter 2-AP nucleobase across from or adjacent to the dψU substrate mimic to measure the nucleotide flipping step. This strategy has been implemented successfully by several groups for this purpose (Chapter 1 pg. 29). Unfortunately, when wtUDG or the F77A UDG were mixed with this class of substrate mimic oligos the 2-AP fluorescent signal did not change significantly, therefore it was not possible to measure nucleotide flipping rate for any of the proteins

(data not shown). Thus, three independent fluorescent techniques (anisotropy, Trp fluorescence, and 2-AP fluorescence) have given results that imply that if the dψU nucleotide is flipped by the enzyme (as seen in the hUDG–dψU crystal structure), the resulting UDG–dψU complex is so transient that a population of molecules cannot remain in the nucleotide flipped state to supply a signal. (In addition, electrophoretic mobility shift assays with dψU containing ssDNA and dsDNA ligands did not detect significant binding by any UDG variant tested (Data not shown). Others groups have also reported this result [231]). This interpretation for this result with dψU agrees with the measurements with dT containing oligos, which also do not cause Trp-quenching in UDG. Therefore, UDG's interaction with dψU is indistinguishable from its interaction with normal DNA.

Since UDG can presumably flip dψU and there is no quenching of UDG's Trp fluorescence, it seems reasonable that the Trp-quenching in UDG is triggered only if dU or free uracil base can bind stably and deeply into the enzyme. Thus, the absence of dψU-induced Trp-quenching is indirect evidence that the Trp-quenching comes after nucleotide flipping. This series of reaction steps was first proposed by Wong and colleagues [202], and supported by subsequent research by other groups [194] (Chapter 1 pg. 31).

The Trp fluorescence measurements with tetrahydrofuran abasic-site product mimic containing dsDNA (AXA/G) showed this ligand did not cause any detectable change of the intrinsic Trp fluorescence of HisUDG (Fig. 7-1 dotted blue line). This result was surprising given that crystal structures of hUDG bound to abasic product DNA revealed that the enzyme had bound and flipped the deoxyribose product towards the substrate

binding pocket and had undergone a structural shift almost *identical* to that found in the substrate bound cocrystal structure [134, 187]; and unlike the dψU substrate mimic, the product mimic DNA is bound by UDG about 30-50 times stronger than a normal dsDNA of the same length and sequence, as measured via fluorescence anisotropy (Chapter 3 pg. 56). This result for abasic-site ligand agrees with the previous results for dψU, and suggests that the process that leads to the Trp-quenched state involves a step after nucleotide flipping, and only happens when substrate (specifically the uracil ring) can fully bind the active site.

These Trp fluorescence controls were also conducted with the Phe77 UDG mutants in the same manner. Like wt(His-tagged)UDG, the mutants exhibited Trp fluorescence quenching only for ligands that contained the true substrate deoxyuridine. Neither substrate or product mimic ligands, nor undamaged dsDNA caused the intrinsic Trp fluorescence of the Phe77 mutant UDGs to change in any detectable manner (data not shown).

This set of controls has defined the role various DNA ligands have in Trp fluorescence quenching of UDG and demonstrates that only oligos containing dU cause the fluorescence quenching. The fact that neither the uncleaveable substrate mimic dψU (AψA/G) and the product mimic (AXA/G) cause Trp-quenching, indicates that the presumed isomerization (if one exists) that causes this quenching happens only when the dU substrate is completely within the active site. The unambiguous assignment of the Trp fluorescence quenching as being solely caused by substrate lets us confidently assign the Trp fluorescence quenching and recovery phases in the reaction mechanisms of wild-type and mutant UDGs.

Stopped-Flow Trp fluorescence Measurements with wtUDG

The real-time Trp fluorescence change of wt(His-tagged)UDG during catalysis of the substrates AUA/G and ssAUA was recorded via fluorescence stopped-flow. The dependence of the quenching and recovery rates of HisUDG's intrinsic Trp fluorescence on the concentration of substrate was determined by titrating a fixed amount of HisUDG (0.1 μM) with increasing concentrations of substrate (0.3 μM to 3 μM). The full characterization of this Trp fluorescence change permits the assignment of the associated isomerization step in UDG's reaction scheme, and is the basis for comparisons with the Phe77 mutants Trp fluorescence kinetics.

Both single and double stranded substrates caused a 5-7 fold reduction (0.5– 0.7 volt signal change) in the Trp fluorescence of HisUDG (Fig. 7-2). The 5-7 fold change in the Trp fluorescence measured here is significantly greater than both the 1.8-fold (0.3 volt) quenching caused by dfU substrate mimic containing DNAs used in studies by Stivers and coworkers [153], and the 2-fold (0.2 volt) signal change measured by Wong et al [202]. This decay ranged from about 100 to 10 ms for 0.2 μM and 2.0 μM AUA/G substrate (compare traces *b* and *g* in Fig. 7-2A, left half of split time base). The data for these Trp-quenching phases was extracted and fit with Eq. 2-6 (black lines in Fig. 7-2A) to give a set of observed rate constants. Similar to the analytical strategy used in Chapter 6, these Trp-quenching rate constants were then graphed as a function of substrate concentration (AUA/G). Observed rate constants that lie on the linear portion of the concentration dependence of the reaction rates were fit separately by linear regression to provide initial estimates of the apparent second-order rate constant for association of the enzyme with the substrate (k_{on}, obtained from the slope), the rate of dissociation of enzyme from substrate (k_{off}, obtained from the of the *y*-intercept), and the

equilibrium dissociation constant (K_D) is the ratio of k_{off} over k_{on} [227]. These parameters were then used as constraints for a general hyperbolic expression representing two (or more)-step reversible binding (Equation 2-8). From Equation 2-8 the asymptotic value provides the observed rate constant for the maximal composite rate constant for reversible base flipping and substrate-induced isomerization (k_{quench}), k_{on} is derived from the product of K^*k_{quench}, and the *y*-intercept provides k_{off}. As stated in Chapter 6, the K_D from this analysis is independent of the number of intervening steps because it is the ratio of the composite dissociation constant (k_{off}) with the composite substrate binding constant (k_{on}). Equation 2-8 provides refinements for the values of k_{on}, k_{off}, k_{quench}, and K_D that will then be used as starting values to constrain simulations performed by globally fitting the kinetic traces to a single set of microscopic rate constants for a minimal UDG reaction mechanism (work in progress).

For wt(His-tagged)UDG k_{quench} is 650 s^{-1} and K_D is 34 nM for the substrate AUA/G. The observed rate constants and their fit with Equation 2-8 are displayed in Figure 7-3A, and collected in Table 7-1 (located at the end of this section). The dependence of the Trp fluorescence quenching on substrate concentration supplied another means of determining the equilibrium dissociation constant of UDG for the dsDNA substrate AUA/G. In Chapter 6 the dependence of uracil excision rates on the concentration of enzyme (pseudo-first order in enzyme, substrate concentration fixed) gave a K_D of 10 nM for AUA/G. This is not grossly different than the dissociation constant measured here with Trp fluorescence measurements that are pseudo-first order in substrate, with enzyme concentration fixed. Thus, these two very different methods have yielded similar results. The relatively low dissociation constant obtained from the curve fitting of the

fluorescence data is also qualitatively supported by the fact that the amplitude of the Trp fluorescence change is approximately the same through the entire substrate concentration range of the experiment (represented by the double-headed arrows in Fig. 7-2). This feature of the data indicates that HisUDG was saturated with substrate even at the lowest concentration (200nM AUA/G), in agreement with the high affinity for substrate obtained from the curve fitting. The K_D measured here with Trp fluorescence is very close to a dissociation constants measured for dfU containing DNA, also measured by Trp fluorescence stopped-flow [153]. The convergence of values from the different research groups validates the various methods used to study UDG.

The task of assigning a dissociation constant for the true substrate is difficult for enzymes that supposedly use two-steps to find their target, like UDG. The proposed reaction models (Fig. 8-1) have UDG forming a weak collision-complex with the DNA that leads to facilitated diffusion in the form of "hopping" along the DNA until the dU is found and flipped [153, 202]; after flipping, UDG isomerizes before catalysis. These three reversible steps form a complex series of interdependent microscopic rate constants that are most accurately assessed by global computer simulation of all the data sets simultaneously to obtain one concerted set of rate constants. We are currently working on global analysis of all the UDG data to further strengthen our kinetic models.

The maximal quenching rate constant of 650 s^{-1}, which supposedly reports on a isomerization of the protein that results in a "clamping" down upon the dU substrate, is several times faster than the maximal rate constant for uracil excision (k_{max} = 145 s^{-1}). Given these rates the proposed isomerization step must happen before glycosidic bond cleavage, which becomes rate-limiting under single-turnover conditions. The k_{quench} rate

constant is the sum of the forward and reverse rates for all the steps that uracil is in contact with the UDG active site. As such, a direct comparison with other modeled microscopic rate constants from other research cannot be made. However, our result of 650 s^{-1} is in the neighborhood of the maximal wtUDG Trp-quenching rate of ≈ 350 s^{-1} measured by Wong *et al.* for a 27mer dsDNA substrate similar to the 25mer (AUA/G) used in this work [202], and a maximal Trp-quenching rate for wtUDG of ≈ 400 s^{-1} for a duplex 11mer containing the substrate mimic dfU[194]. Both groups have also concluded that the isomerization represented by the quenching of the protein's intrinsic Trp fluorescence must come prior to the chemical step in the reaction pathway. The agreement between these three studies is convincing evidence that the phenomenon of UDG's substrate induced Trp fluorescence quenching is a faithful reporter on the substrate–enzyme interaction.

The decay phase of the Trp fluorescence traces plateaued and remained flat before entering the Trp fluorescence recovery phase for time durations that were dependent on the concentration of substrate utilized (compare traces *b* and *h*, Fig. 7-2A). The length of this phase in the Trp fluorescence kinetic traces was estimated by visual inspection and was found to be linearly dependent on the concentration of substrate (data not shown). The ratio of the length of the Trp-quenching plateau to the concentration of substrate revealed that UDG is in this fully quenched state for approximately half a millisecond per nanomolar of the initial substrate (AUA/G) concentration in the reaction. The same analysis with the single stranded substrate showed the same trend, except slightly faster (≈ 0.4 ms/nM ssAUA). This distinct phase in the Trp fluorescence kinetic traces of HisUDG is a build-up of enzyme molecules in the quenched state caused by the Trp

Figure 7-2. Tryptophan fluorescence kinetics of wt(His-tagged)UDG (see next page). (A) Trp fluorescence kinetic time courses of HisUDG (0.1 μM) recorded by stopped-flow (λ_{ex} = 290 nm, λ_{em} > 320 nm) after mixing with the dsDNA substrate AUA/G at 0.2, 0.3, 0.4, 0.6, 0.8, 1.6, and 3.0 μM (*traces b–h*, respectively). (B) stopped-flow Trp fluorescence kinetic traces acquired as in *A* for 0.1 μM HisUDG after mixing with the ssDNA substrate, ssAUA at 0.5, 1.0, 1.6, and 3.0 μM (*traces b–e*, respectively). All traces are shown offset from the baseline trace of enzyme only (0.1 μM) (*trace a* in A and B) by incremental amounts to facilitate their simultaneous display in the figures. Each trace displayed (A and B) represents an average of four to eight individual, oversampled acquisitions. The double-headed arrows (colored according to fluorescence kinetic trace) show the signal change (ΔV, the absolute value of difference between arrows) between fully quenched and fully recovered enzyme fluorescence. For HisUDG each concentration of substrate gave about the same ΔV (≈ -0.6; arrows are shown for first and last traces only). The solid lines through the colored data are the best fits to Eq. 2-6 and Eq. 2-7 to obtain the observed rate constants for Trp fluorescence quenching and recovery, respectively, used in the analysis presented in Figure 7-3.

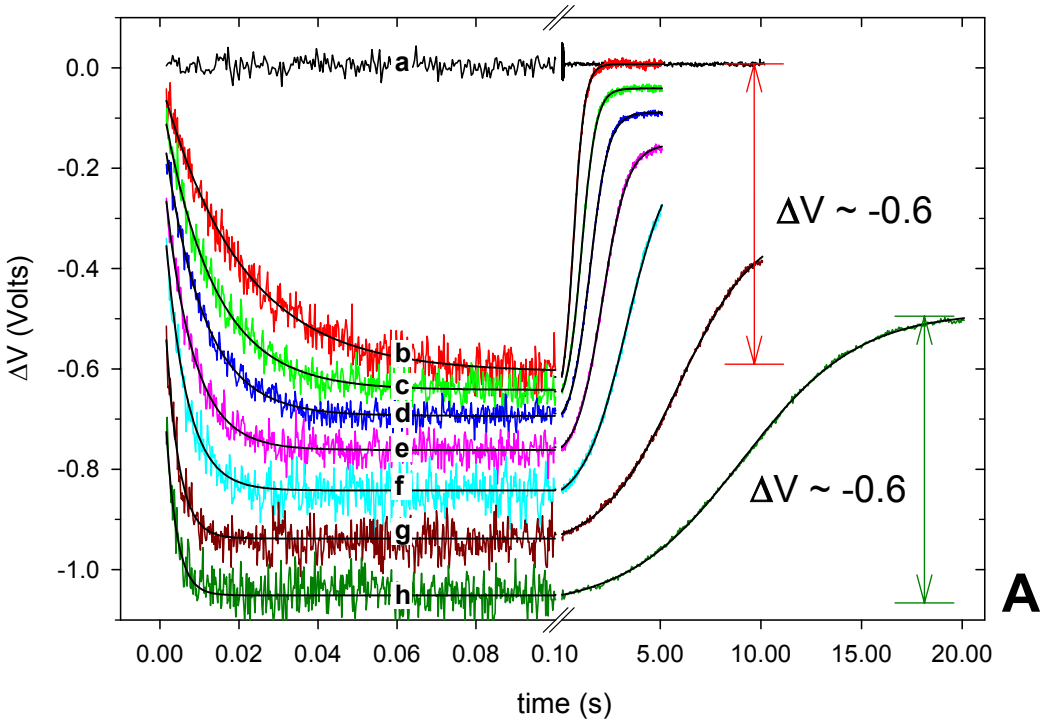
0.0
-0.2
-0.4
-0.6
-0.8
-1.0
ΔV (Volts)
a
b
c
d
e
f
g
h
ΔV ~ -0.6
ΔV ~ -0.6
0.00
0.02
0.04
0.06
0.08
0.10
5.00
10.00
15.00
20.00
time (s)
A

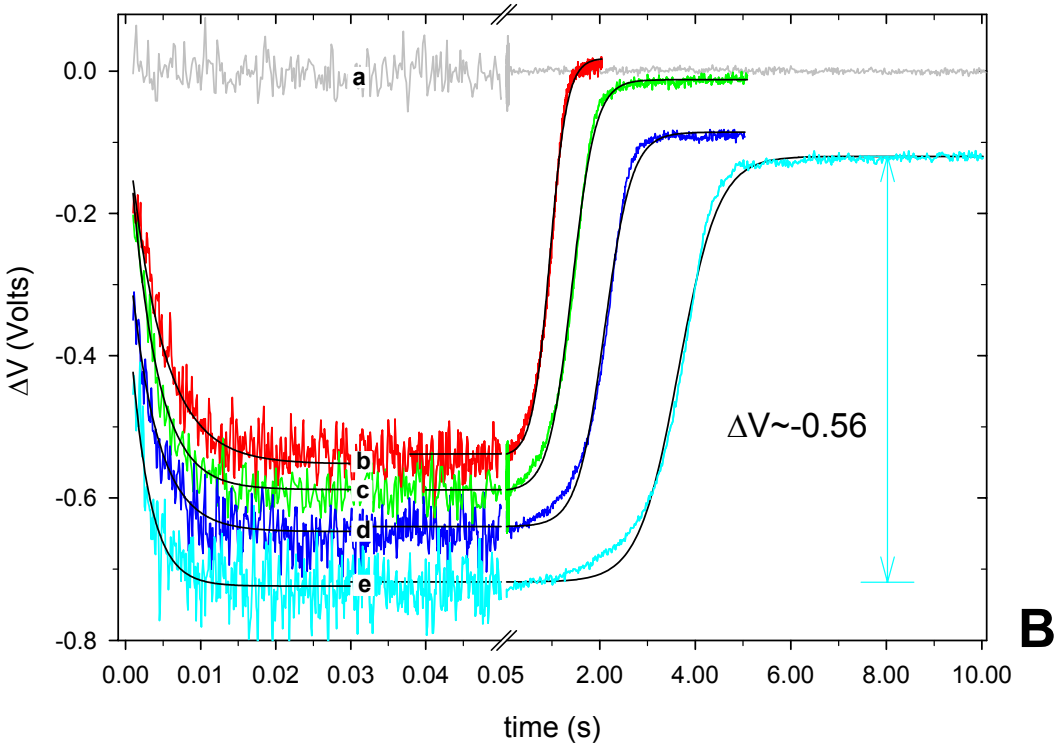
0.0
-0.2
-0.4
-0.6
-0.8
ΔV (Volts)
a
b
c
d
e
ΔV~-0.56
0.00
0.01
0.02
0.03
0.04
0.05
2.00
4.00
6.00
8.00
10.00
time (s)
B

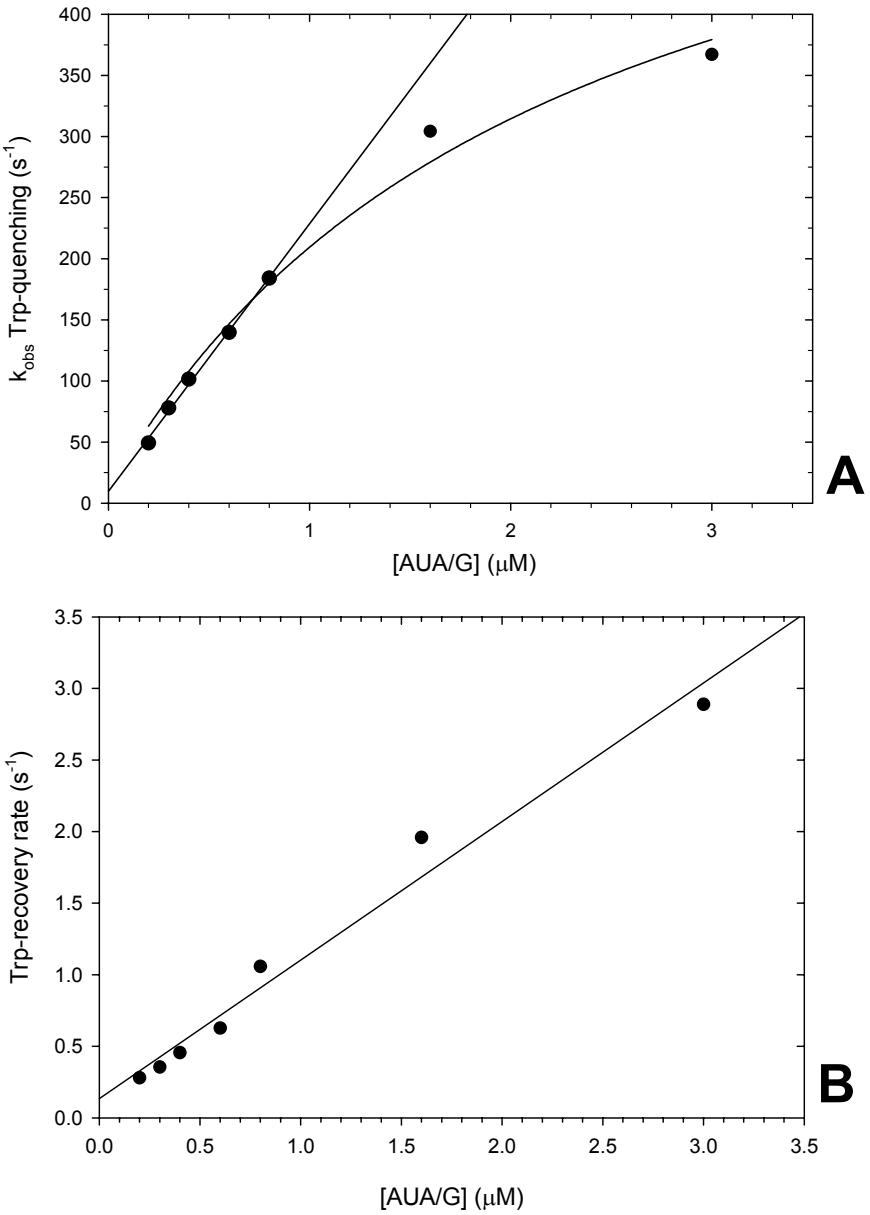

Figure 7-3. Curve fitting of the observed rates of HisUDG Trp fluorescence changes obtained from Fig. 7-2. (A) the observed rate constants (k_{obs}) from the nonlinear least squares single-exponential decay fits of the substrate induced HisUDG Trp-quenching (from Fig. 7-2A, left half of split time base; 0-100 ms) were plotted versus substrate concentration and fit with Eq. 2-8 to obtain best-fit parameters for the maximal Trp fluorescence quenching rate constant, k_{quench}, of 650 s^{-1} and apparent rate constants k_{off} and k_{on} (Table 7-1) (B) Trp fluorescence recovery rate constants (from Fig. 7-2A, right half of split time base; 0.1-20 s) graphed as a function of substrate concentration to reveal the linear dependence of the recovery rate on initial substrate concentration.

fluorescence recovery phase (discussed below) limiting the flux through this transition.

Following the maximal quenching plateau the intrinsic Trp fluorescence of UDG begins to recover (Fig 7-2A and B, right half of split time base). As expected for an isomerization related to catalysis, substrate induced Trp-quenching is completely reversible. Because the Trp fluorescence recovery phase has a noticeable lag which gives it a sigmoidal shape, these data needed to be fit with a 4 parameter sigmoid (Eq. 2-7) to obtain the Trp-recovery rates. A plot of the observed Trp-recovery rate constants versus substrate concentration reveals that Trp-recovery (k_{recov}) rates are linearly dependent on substrate concentration. Dividing k_{recov} by initial concentration of substrate gives a series of values that are the same within error with the steady-state turnover rate measured for the substrate AUA/A (1.4 s^{-1}; Fig. 7-3B). A small deviation of the Trp-recovery rate causing it to be slightly slower at higher enzyme concentrations is most likely the effect of product inhibition, since larger initial substrate concentrations will create more abasic site product DNA which has a K_D^{Ap} for this ligand of ≈ 140 nM (Table 4-1). Thus the Trp fluorescence of UDG fully recovered on a timescale that coincided with the complete conversion of substrate to product in accordance with the steady-state activity for HisUDG (Table 7-1). Therefore the processes that lead to the Trp-quenched state have much faster rates than the processes that reverse the quenching.

The dependence of the Trp-recovery on initial substrate concentration and excellent correlation between steady-state uracil excision and Trp-recovery rates are strong indicators that both techniques are measuring the same step, the rate-limiting release of products. Therefore, we propose that recovery of Trp fluorescence is coincident with the release of the abasic DNA and free uracil base products (and possibly caused by the

reversal of the conformational clamping proposed to be the cause of the Trp-quenching). However, this data does not totally exclude alternative scenarios in which Trp-recovery happens independently of product release.

The Trp-recovery rate constants observed in these experiments are in stark contrast to the results published by Wong and coworkers. Whereas Trp-quenching rates were comparable between these two bodies of work, the Trp fluorescence recovery rates measured by Wong et al. were much greater (15 s^{-1} versus 1.4 s^{-1}), while the recovery of Trp fluorescence was only "partial" in their reactions of wtUDG with a 27mer duplex substrate [202]. This rate is ten-fold faster than the steady-state turnover rate, prompting Wong et al. to add a second reversible isomerization following uracil excision to their model of UDG's reaction pathway; they proposed this extra step was the retraction of the enzyme's leucine finger from the abasic product DNA.

It is troubling that Trp fluorescence kinetic traces shown here and in the work of Jiang et al. demonstrate that UDG's intrinsic fluorescence should recover completely after the reaction [194], which was not observed in the fluorescence traces of Wong and cohorts. There are several differences between experimental methods employed in this work and the study by Wong et al. that could be the basis for the aforementioned discrepancies.

The first is the choice stopped-flow instruments and optics. This work uses an Applied Photo Physics Stopped-flow instrument equipped with a 150 W xenon arc lamp and a 320 nm cuton filter (Chapter 2) while Wong et al. employ an KinTek SF 2001 stopped-flow spectrophotometer fitted with either a 75-watt xenon arc lamp and a 325 nm cuton filter. The weaker lamp and different optics may have lead to a reduced signal

which does not allow for the full range of the Trp fluorescence change to be acquired (i.e., the noise buries features of the kinetic traces like the sigmoidal shape).

A more likely source of error is the different amount of enzyme and substrate used in the experiments. The experiments reported here use 10-fold more enzyme and substrate than those of Wong et al. Using low levels of enzyme endangers the accuracy of the data by both decreasing the signal to noise ratio and increasing the effects of fluorescence bleaching. Fluorescence bleaching is the irreversible destruction of a fluorophore's light emitting abilities, which tryptophan, like most fluorophores, is also susceptible. The percentage of signal bleached away increases at lower concentrations of UDG introducing more error into the measurement. During very long acquisitions there was a noticeable bleaching of UDG's Trp fluorescence even at the higher protein concentrations used here (data not shown). We believe the use of higher enzyme concentrations in this work supplies the greater signal to noise ratio needed to fully define the Trp fluorescence kinetics of UDG.

In summary, the apparent dissociation constant for the substrate AUA/G measured by the dependence of Trp fluorescence quenching of UDG agrees well with previous reports that also used Trp fluorescence stopped-flow to assess UDG. The maximum Trp-quenching rate constant for wt(His-tagged)UDG roughly agrees with previous findings and is greater than the rate constant for the chemical step and therefore must proceed it. The maximum Trp-recovery rate is approximately equal to the steady-state turnover rate, indicating that Trp-recovery happens concurrently with the release of products, which is the rate-limiting step in the steady-state.

Table 7-1. Trp fluorescence kinetics of wt(His-tagged)UDG and Phe77 mutants

Enzyme	k_{quench} (s^{-1})	k_{on} ($\mu M^{-1}s^{-1}$)	k_{off} (s^{-1})	K_D (nM)	K	k_{recov} (s^{-1})	k_{cat} (s^{-1})
wt(His)UDG	650 ± 40	290 ± 9	10 ± 2	34 ± 2	0.45 ± 0.03	1.4	1.4
F77A*	ND	ND	ND	ND	ND	0.05	0.06
F77N	670 ± 34	355 ± 18	50 ± 10	140 ± 10	0.53 ± 0.03	0.005	0.0096
F77Y	480 ± 20	290 ± 12	55 ± 5	190 ± 20	0.61 ± 0.04	0.22	0.5

Errors represent the deviation of the data from the fits and are only reported for the data presented in this chapter. The values of k_{recov} are extrapolations to the y-axis from the plotted data and therefore do not have error estimates. * due to a poor Trp signal for F77A UDG accurate quenching rates could not be determined.

Stopped-Flow Trp fluorescence Measurements with Phe77 Mutant UDGs

To determine if the mutations of Phe77 affected UDG's isomerization, fluorescence stopped-flow was employed as before for wt(His-tagged)UDG to acquire the real-time Trp fluorescence kinetics of the Phe77 mutants (0.1 μM) during reactions with increasing concentrations of AUA/G (0.2–3.0 μM). As stated previously, the Phe77 mutant UDGs, like His-tagged wtUDG, only exhibit changes in their intrinsic Trp fluorescence when mixed with deoxyuridine containing oligos. Therefore, the Trp fluorescence of these proteins can also serve as a probe into the conformational changes these proteins undergo during their catalytic cycle.

Tryptophan Fluorescence Kinetics of F77A UDG

Due to limitations in reagents, the Trp fluorescence kinetics of the Phe77 mutants were only rigorously explored with the double-stranded substrate, AUA/G. Like wt(His-tagged)UDG, reactions of F77A UDG with the ssDNA substrate did not show any significant differences in the shape of the Trp fluorescence kinetic traces, only faster kinetics, as compared with reactions with AUA/G (data not shown).

The Trp fluorescence kinetic traces of F77A UDG were noisy and ill-defined in the quenching phase (Fig. 7-4, left half of split time base). The magnitude of the Trp fluorescence signal changes of F77A UDG were reduced to about one-third that of HisUDG. The much larger amplitude of the recovery phase as compared to the quenching phase indicates that the most of the quenching phase is complete before the machine can acquire the first data points. Nevertheless, the quenching phases of the Trp fluorescence kinetic traces were fit with exponential decays (Eq. 2-6) that revealed that the quenching rates (k_{quench}) did not increase with increasing substrate concentration, but remained around 41 s^{-1}.

Because the Trp fluorescence signal of F77A UDG was less than 20% that of HisUDG, several measurements were made with double the amount of enzyme (0.2 μM) to confirm that this result was not an artifact caused by a less robust data set. Doubling F77A UDG did double the signal as expected, and it confirmed that the quenching was happening faster than the deadtime of the machine and was not an artifact (data not shown). This inability to accurately measure quenching rates as a function of substrate concentration, prevented measurement of a K_D for AUA/G as performed for HisUDG in the previous section. However, unlike wtUDG, the amplitude of the signal change (ΔV; Fig. 7-4 double-headed arrows) was not saturated and generally increased with increasing amount of substrate added. Qualitatively then, this indicates that F77A UDG was not saturated with substrate in this experiment as normal UDG was, implying that the affinity of this mutant for substrate must be at least several fold weaker than wtUDG. This qualitative observation from the Trp fluorescence data agrees with the dissociation constant for substrate measured by single-turnover titration ($K_D \approx 140$ nM; Fig. 6-5).

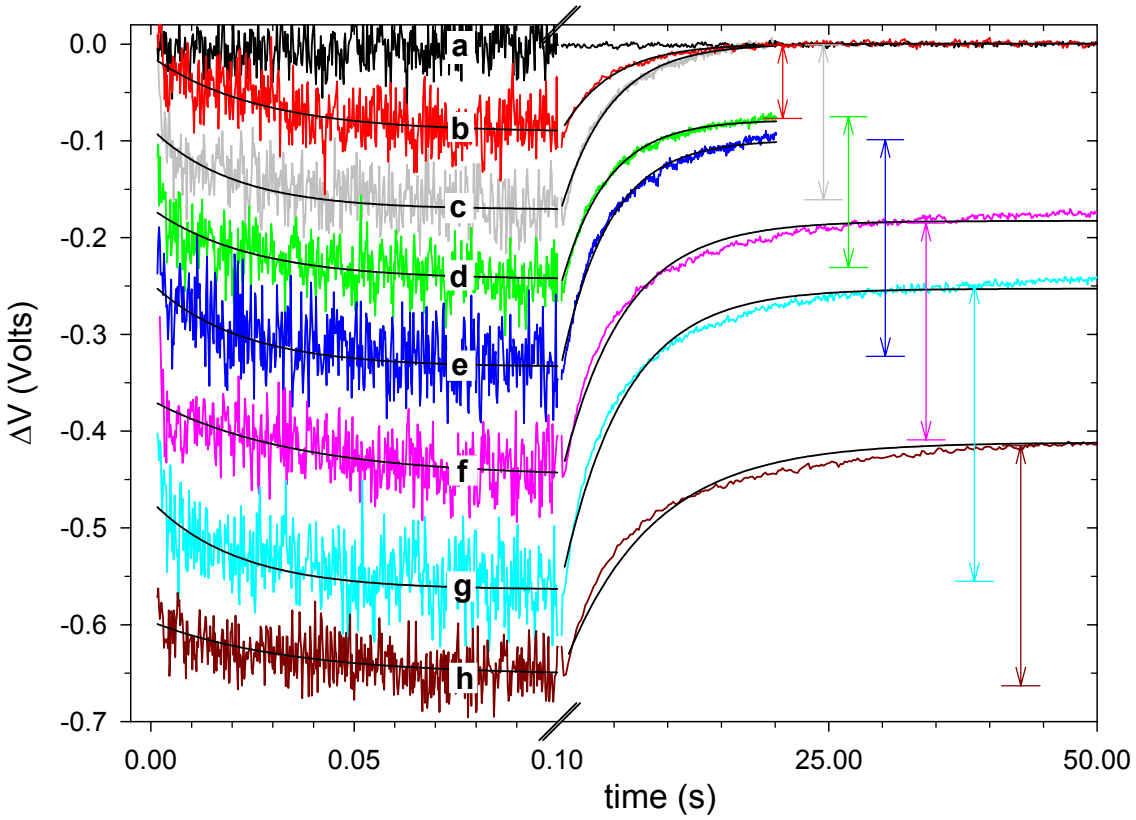

Figure 7-4. Tryptophan fluorescence kinetics of F77A UDG. (A) Trp fluorescence kinetic time courses of F77A UDG (0.1 μM) after mixing with the dsDNA substrate AUA/G at 0.3, 0.4, 0.6, 1.0, 1.5, 2.0 and 3.0 μM (traces b–h, respectively) as described in Chapter 2. Each trace displayed represents an average of four to eight individual, oversampled acquisitions and are shown offset from the baseline trace (*a*) of enzyme only (0.1 μM) by incremental amounts to facilitate their simultaneous display in the figure. The double-headed arrows (colored according to fluorescence kinetic trace) show the signal change (ΔV) between fully quenched and fully recovered enzyme fluorescence for each trace. Increasing substrate concentration caused F77A UDG to have an increasingly larger signal change (ΔV ranged from -0.07 to -0.3 V). This indicates that the magnitude of Trp-quenching of F77A UDG was increasing with increasing substrate. The solid lines are the best fits to Eq. 2-6 and 2-2 to obtain the observed rate constants for Trp fluorescence quenching and recovery presented in Figure 7-5.

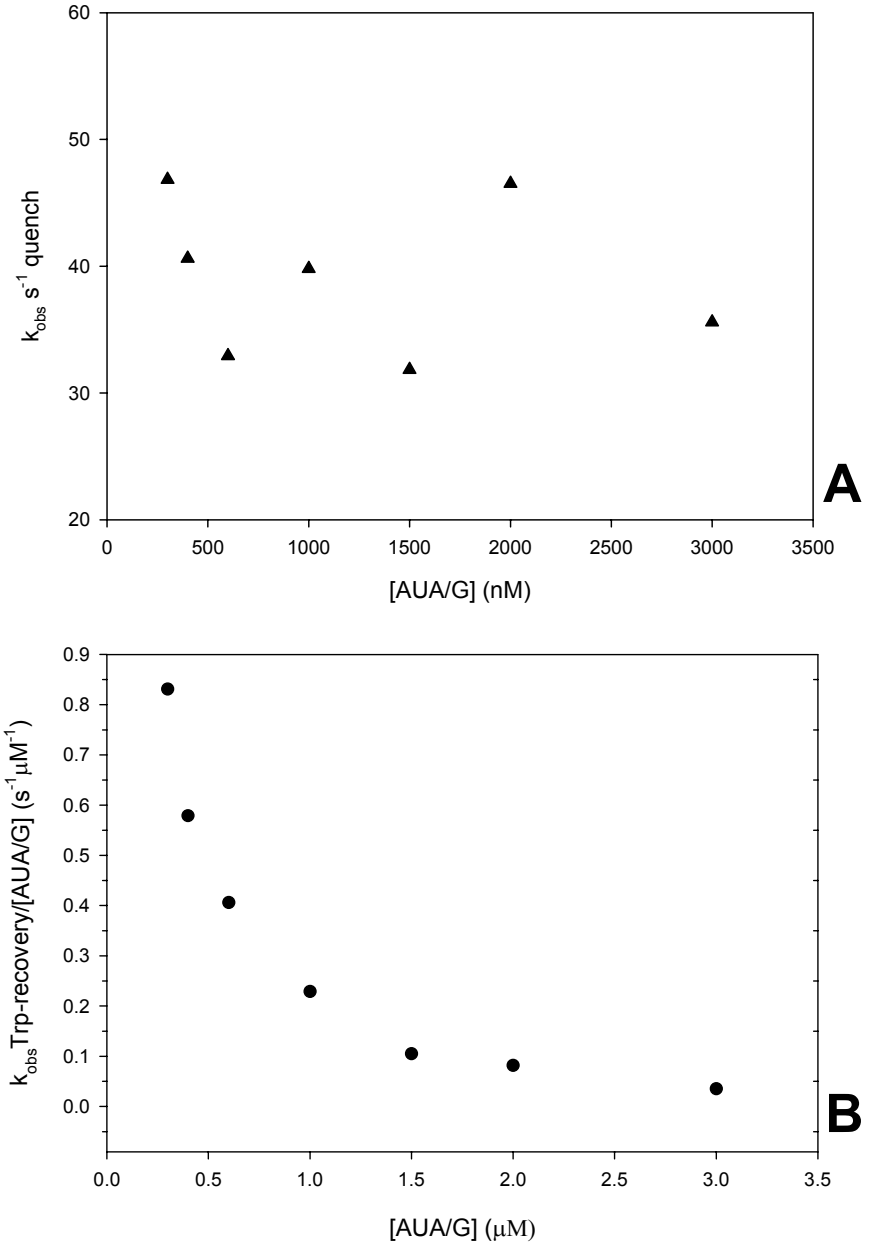

Figure 7-5. Analysis of the observed Trp fluorescence rates of F77A UDG. (A) The observed rate constants (k_{obs}) from the fits of the substrate induced F77A UDG Trp-quenching (Fig. 7-2A, left half of split time base; 0-100 ms) is graphed as a function of substrate (AUA/G) concentration. (B) Trp-recovery rates divided by the initial substrate concentration of each reaction (Fig. 7-2A, right half of split time base; 0.1-50 s) are plotted versus substrate concentration. The Trp-recovery of F77A plateaus at about k_{cat} for dsDNA ($\approx 0.05\ s^{-1}$; Table 7-1).

The recovery phase of the Trp fluorescence kinetic traces of F77A was better defined, and like HisUDG, proceeded at a rate that approximated the steady-state rate of glycosidic bond cleavage of dU by F77A (≈ 0.02 s^{-1} as compared to a k_{cat} of 0.05 s^{-1}). Yet unlike HisUDG, the recovery phase did not have a sigmoidal shape, but was exponential without a noticeable lag (figure 7-4, right half of split time base). The implications of this Trp-recovery trace line shape will be discussed in the summary of the Trp fluorescence data for all the Phe77 mutants.

Interpretation of the Trp-quenching data for F77A UDG is difficult due to the lack of a response to substrate concentration, but several possible hypotheses will be discussed here. The magnitude of the Trp-recovery phases indicates that F77A UDG is quenched by substrate, but at a rate too fast to be measured by the methods employed here. This data may indicate that replacement of Phe77 with alanine may impair the isomerization that leads to conformational clamping upon the substrate. Alternatively, the isomerization may not be impaired, only the Trp fluorescence signal for that particular change in UDG's structure may have been negated. The reduced affinity as compared to wild-type (K_D ≈ 140 nM) of F77A UDG for substrate DNA measured via single-turnover uracil excision kinetics may be the result of damage to the isomerization that leads to an induced fit for dU within the active-site, which supports the first hypothesis. This would mean that the attenuation in the Trp-quenching signal is correlated with the loss of the isomerization that leads to conformational clamping of substrate. Given that the majority of the quenching phase expired in the deadtime of the stopped-flow, precluding an accurate measurement of quenching rates, other techniques (e.g., NMR) would need to be employed to determine if F77A UDG still undergoes conformational clamping.

Tryptophan Fluorescence Kinetics of F77N UDG

The Trp fluorescence kinetic traces of F77N UDG were strikingly different from those of the alanine mutant. The Trp-quenching phase of F77N Trp fluorescence stopped-flow traces had a better signal change than F77A UDG which was about 50% that of HisUDG. Also in contrast to F77A UDG, the Trp-quenching phase was could be measured and was hyperbolically dependent on substrate concentration (Fig. 7-6, left half of split time base; Fig. 7-7A). The observed Trp-quenching rates acquired from fits of the data with Eq. 2-5 (black solid lines in Fig. 7-6) were analyzed just as in the earlier analysis of HisUDG, and gave an K_D of $\approx$ 140 nM and an asymptotic maximal limit for the observed Trp-quenching rate (k_{quench}) of approximately 670 s^{-1} (Fig. 7-6; Table 7-1).

The k_{quench} for F77N UDG is equivalent within error to the value for wt(His-tagged)UDG (650 s^{-1}). This is somewhat surprising given the asparagine mutation causes a 1600-fold reduction in the maximal uracil excision rate ($k_{max} \approx 0.08$ s^{-1}) as compared to HisUDG (Table 7-1). It seems then that the asparagine mutation does not interfere with substrate binding and flipping, or cripple UDG's supposed isomerization.

The $K_D \approx 140$ nM determined for F77N UDG's affinity for the substrate AUA/G measured via Trp fluorescence are greater than values measured for wt(His-tagged)UDG ($K_D \approx 0.034$ μM) and imply that the observed rates of Trp-quenching are not the result of anomalous binding of the substrate by this mutant. However, these data do not exclude the possibility that the free nucleobase uracil product is bound with a greater affinity to the asparagine mutant, and that this binding is contributing to the Trp-quenching of F77N UDG skewing the results. A measurement of the equilibrium binding of free uracil to F77N UDG would be needed to resolve this ambiguity. The amplitude of the signal change reached a maximum at 600 nM substrate ($\Delta V \approx -0.3$ Volts), which is in

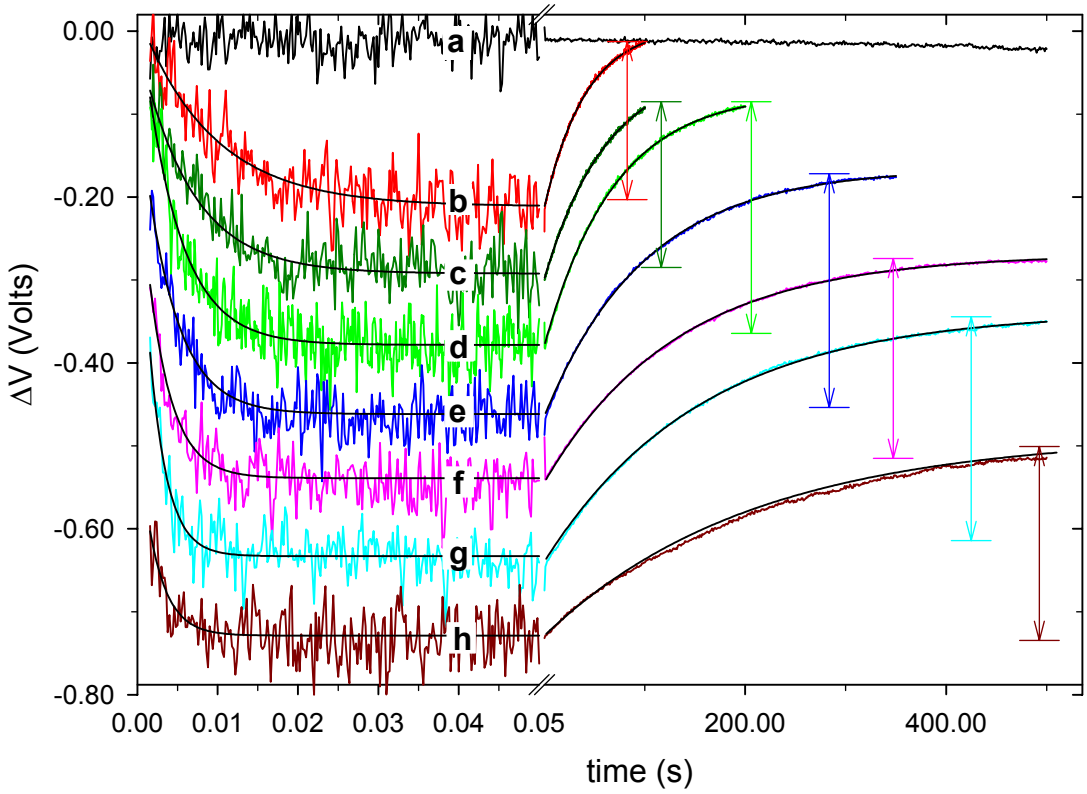

Figure 7-6. Tryptophan fluorescence kinetics of F77N UDG. Trp fluorescence kinetic time courses of F77N UDG (0.1 μM) after mixing with the dsDNA substrate AUA/G at 0.3, 0.4, 0.6, 1.0, 1.5, 2.0 and 3.0 μM (*traces b–h*, respectively) as described in Chapter 2. Each trace displayed represents an average of four to eight individual, oversampled acquisitions and are shown offset from the baseline trace of enzyme only (0.1 μM) (*trace a*) by incremental amounts to facilitate their simultaneous display in the figure. The double-headed arrows (colored according to fluorescence kinetic trace) show the signal change (ΔV) between fully quenched and fully recovered enzyme fluorescence for each trace. The signal change for F77N UDG plateaued (600 nM ΔV of ≈ -0.3 V) indicating this enzyme became fully saturated with substrate. The solid lines are the best fits to Eq. 2-5 to obtain the observed rate constants for Trp fluorescence quenching and recovery presented in Figure 7-7A and B.

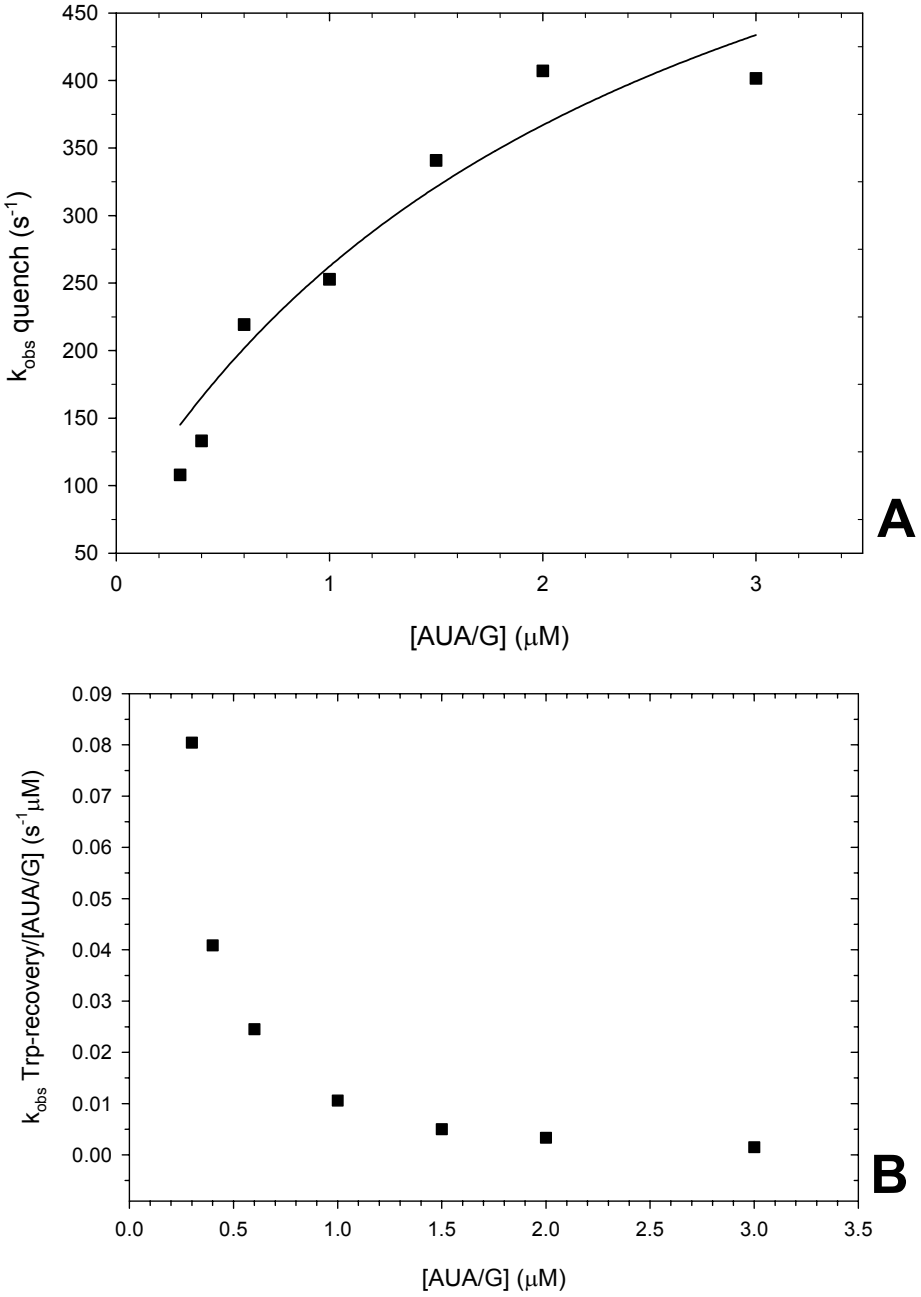

Figure 7-7. Analysis of the observed Trp fluorescence rates of F77N UDG. (A) The observed rate constants (k_{obs}) from the fits of the substrate induced F77N UDG Trp-quenching (Fig. 7-6, left half of split time base; 0-50 ms) is graphed as a function of substrate (AUA/G) concentration. As in Fig 7-6A linear regression (not shown) was used to obtain the initial constraints for fitting with Eq. 2-8. (B) Trp-recovery rates divided by the initial substrate concentration of each reaction (Fig. 7-6, right half of split time base; 0.05-500 s) are plotted versus substrate concentration. The Trp-recovery of F77N plateaus at about k_{cat} for dsDNA (≈ 0.005 s^{-1}; Table 7-1).

qualitative agreement with the K_D of F77N UDG for substrate obtained from the curve fitting. Full Trp-quenching at 600nM AUA/G, which implies that it requires at least a 6:1 ratio of substrate to protein to fully saturate this reaction step, also qualitatively agrees with the over 4-fold greater K_D of F77N UDG for AUA/G as compared to wtUDG (K_D's of 140 nM and 34 nM, respectively).

Like the F77A mutant, the Trp fluorescence recovery phase of the stopped-flow data for F77N UDG was exponential without a noticeable lag (Fig. 7-6, right half of split time base). Apparent Trp-recovery rate constants were obtained by the same analysis method as performed for F77A UDG, by fitting the stopped-flow data with Eq. 2-5 (solid black lines in Fig 7-6). As with His-tagged and F77A UDG, a plot of the observed Trp-recovery rate constants from these fits divided by concentration of substrate as a function of substrate concentration revealed that Trp fluorescence recovery of F77N UDG had a maximal rate of $\approx 0.005\ s^{-1}$, which is close to the steady-state rate of glycosidic bond cleavage of the substrate AUA/G (Fig. 7-7B; Table 7-1).

Tryptophan Fluorescence Kinetics of F77Y UDG

The stopped-flow kinetic traces of F77Y UDG Trp fluorescence are very close in amplitude and shape to those of the asparagine mutant. Similar to F77N UDG, the Trp-quenching phase was hyperbolically dependent on substrate concentration (Fig. 7-8, left half of split time base; Fig. 7-9A) and had a signal change which was also about 50% that of HisUDG. Data analysis was performed exactly as conducted for the previous enzymes. Fitting of the observed Trp-quenching rate constants (Fig. 7-9A & B) revealed that k_{quench} reached an asymptotic maximal limit of approximately 480 s^{-1} and that F77Y UDG has an apparent K_D of approximately 190 nM for the substrate AUA/G (Table 7-1).

The value of the maximal Trp-quenching rate constants for F77Y and wt(His-tagged) UDG are relatively close (480 s^{-1} versus 650 s^{-1}). Therefore, it appears that the addition of a hydroxyl group to the phenyl ring does not hamper the binding and flipping of the substrate, or the putative isomerization of the enzyme to an appreciable extent. However, the facts that the signal change is only 50% that of HisUDG and that the K_D measured by the Trp fluorescence response to AUA/G concentration is over 3 times that of the K_D wt(His-tagged UDG) measured the same way, indicates that the tyrosine mutation has affected the substrate interaction of the enzyme in some other unknown way. Thus, the differences that are responsible for the subtle reduction in activity caused by the F77Y mutation are subtle themselves, as to be expected. It is also important to note that the amplitude of the signal change (double-headed arrows) maximized at around the same concentration of substrate (600 nM AUA/G) as required by F77N UDG to saturate its Trp signal. This aspect of the F77N and F77Y UDG data sets is congruent with the close dissociation constants (140 nM versus 190 nM, respectively) determined for these proteins from the curve fitting.

Like the other mutants, the Trp fluorescence recovery phase rate was dependent on substrate concentration and was exponential (Fig. 7-6A, right half of split time base). Also like all the other Phe77 variants of UDG, a plot of the observed Trp-recovery rate constants versus substrate concentration revealed the fluorescence recovery rate plateaued at approximately the same value as the previously measured steady-state turnover of the substrate (Fig. 7-6C; Table 7-1). It appears then that the Trp-recovery of the F77Y happens concurrently with the steady-state rate-limiting release of product, the same as the other UDGs.

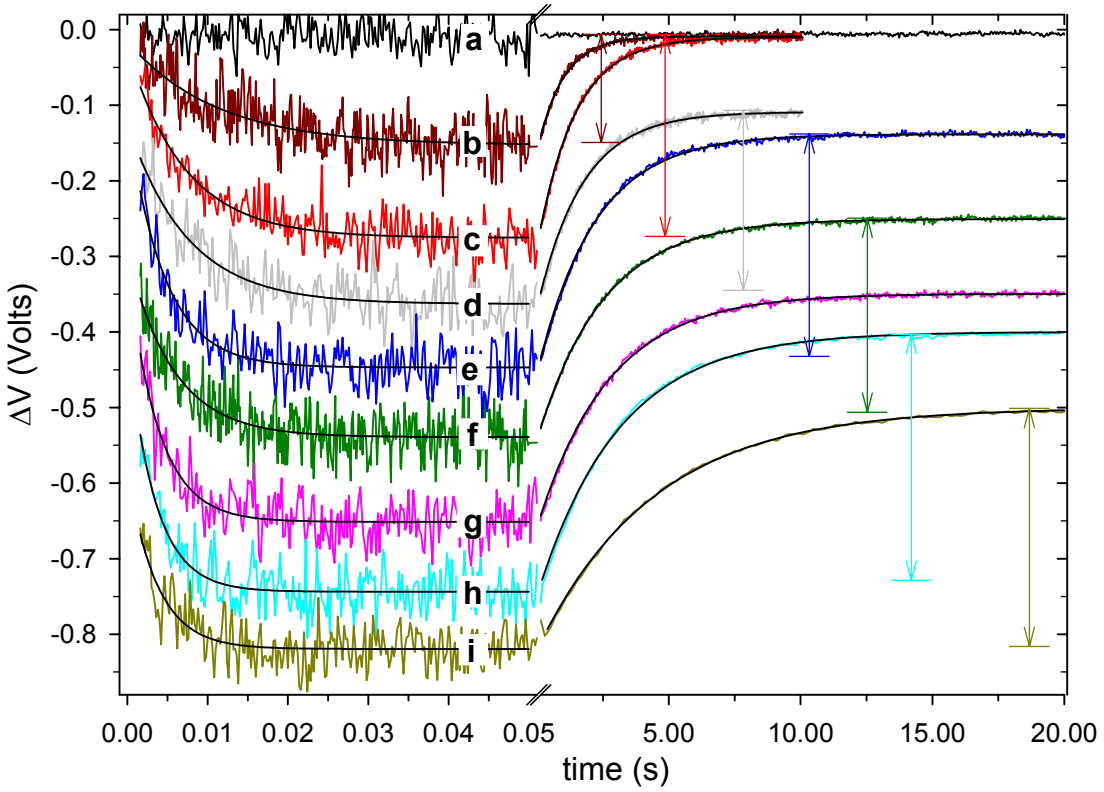

Figure 7-8. Tryptophan fluorescence kinetics of F77Y UDG. Trp fluorescence kinetic time courses of F77Y UDG (0.1 μM) after mixing with the substrate AUA/G at 0.2, 0.3, 0.4, 0.6, 0.8, 1.0, 1.5, and 2.0 μM (traces b–i, respectively) as described in Chapter 2. Each trace displayed represents an average of four to eight individual, oversampled acquisitions and are shown offset from the baseline trace of enzyme only (0.1 μM) (trace a) by incremental amounts to facilitate their simultaneous display in the figure. The double-headed arrows (colored according to fluorescence kinetic trace) show the signal change (ΔV) between fully quenched and fully recovered enzyme fluorescence for each trace. The maximal signal change for F77Y UDG plateaued at 600 nM substrate with a ΔV of ≈ -0.33 V. The black solid lines are the best fits to Eq. 2-5 to obtain the observed rate constants for Trp fluorescence quenching and recovery presented in Figure 7-9A and B.

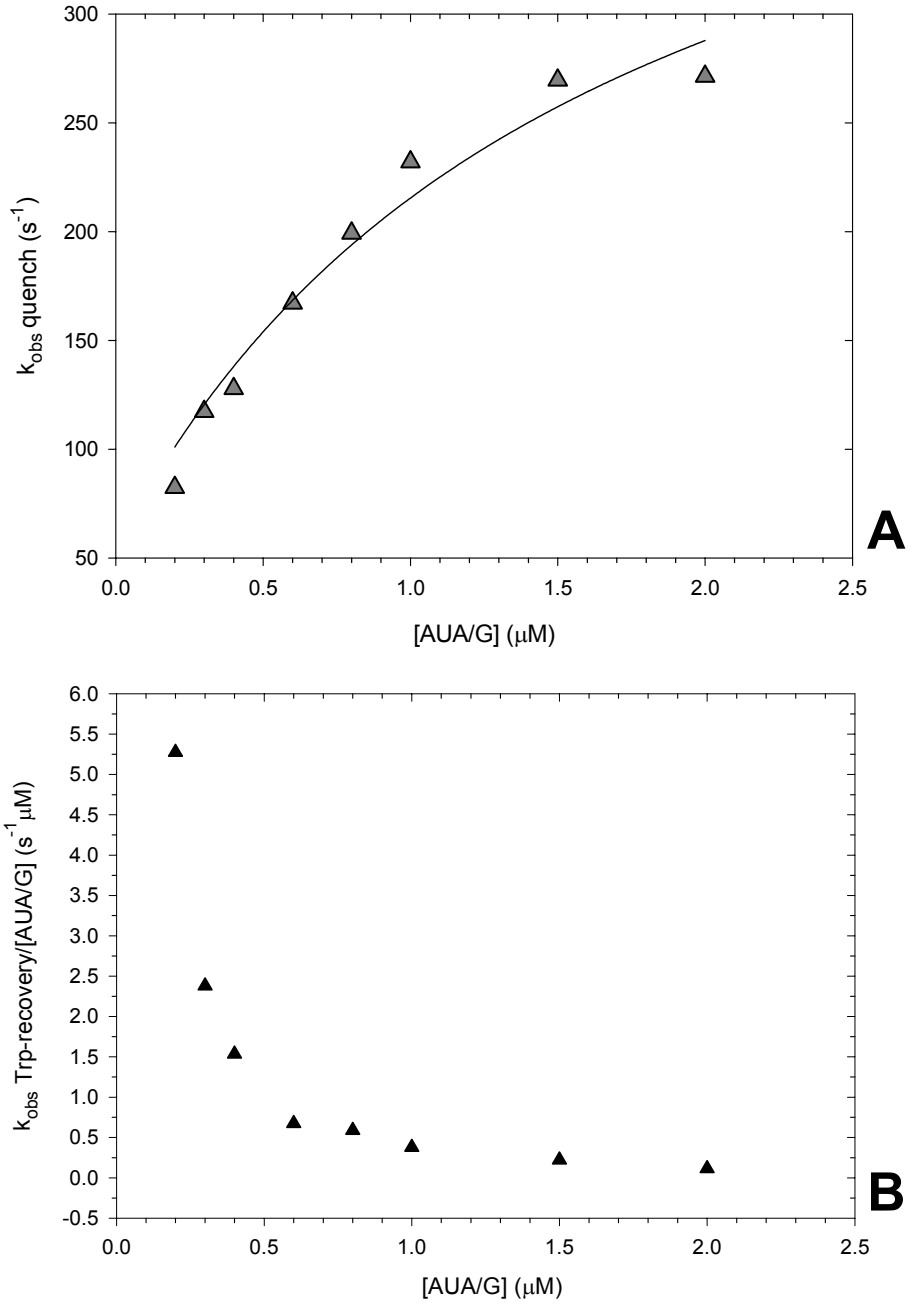

Figure 7-9. Analysis of the observed Trp fluorescence rates of F77Y UDG. (A) The observed rate constants (k_{obs}) from the fits of the substrate induced F77Y UDG Trp-quenching (Fig. 7-8, left half of split time base; 0-50 ms) is graphed as a function of substrate (AUA/G) concentration. As before, linear regression (not shown) provided the initial constraints for fitting with Eq. 2-8. (B) Trp-recovery rates divided by the initial substrate concentration of each reaction (Fig. 7-8, right half of split time base; 0.05-15 s) are plotted versus substrate concentration. The Trp-recovery of F77Y UDG also plateaus at around k_{cat} for dsDNA (≈ 0.22 s^{-1}; Table 7-1).

In summary, substrate induced Trp fluorescence quenching is dependent on substrate concentration for all UDGs studied except F77A UDG, which seemingly has a Trp-quenching rate faster than the deadtime of the measurement, preventing interpretation of this phase of F77A Trp kinetics. The Trp-quenching happens at rates that are faster than the maximal glycosidic bond cleavage rate, indicating as previously proposed, that the first isomerization comes before chemistry in the reaction pathways of all the UDG variants studied. Unexpectedly, the F77N mutation did not reduce the substrate induced isomerization as evidenced through the equivalent Trp-quenching rate constant with respect to HisUDG. The Trp fluorescence signal changes of the proteins became maximal at substrate concentrations that were in qualitative agreement with the dissociation constants for interaction of the respective UDGs with AUA/G determined from the curve fitting analysis.

The recovery phase of the Trp fluorescence kinetic traces was dependent on substrate concentration and saturated at rates that were, within error, identical to the steady-state turnover numbers for each of the proteins investigated. The strong correlation between Trp-recovery and steady-state catalytic rates implies Trp-recovery is reporting on the rate-limiting step of product release. The line shape of the Trp-recovery phase was exponential for all the Phe77 mutants, but was sigmoidal for HisUDG. The reason for this difference between line shapes may be due to the much faster rate of glycosidic bond cleavage wtUDG exhibits as compared to the Phe77 mutants (10-fold over the fastest mutant), which could cause a build-up of unreleased products that result in an increased half-life for the Trp-quenched enzyme population. This longer

Trp-quenched state would manifest itself in the fluorescence kinetic traces as a lag before the exponential Trp-recovery phase giving the traces their sigmoidal shape.

The Trp fluorescence kinetic measurements reported here provide a window into the conformational dynamics of UDG during its catalytic cycle and show how slight changes in an active-site can affect an enzyme's inner workings. These results also lay the ground work for a deeper understanding of the cause of the UDG Trp signal. Someday soon advances in computational studies of dynamics in protein structure along with full characterization of the tryptophans involved in the signal (discussed in detail in Chapter 8) will allow the accurate prediction of which specific tryptophans are involved in fluorescence changes during UDG's catalytic cycle. Knowing these residues would then help in the mapping of the possible changes in the enzyme's structure during catalysis, giving us a largely complete picture of how subtle changes in structure help this protein attain its remarkable catalytic prowess.

CHAPTER 8
CONCLUSIONS AND FUTURE DIRECTIONS

Summary of Results and Discussion

This study has addressed the role of the conserved active-site phenylalanine of *E. coli* UDG during the enzyme's catalytic cycle. This was accomplished by constructing and characterizing three site-directed mutations of Phe77: F77A, F77N and F77Y. The rigorous assessment of the effects of Phe77 substitution required the kinetic characterization of wild-type and His-tagged UDG, which in turn has yielded data that can contribute to the understanding of the normal UDG catalytic cycle.

Comparison of UDG Reaction Mechanisms

Two other groups have conducted detailed kinetic studies of *E. coli* UDG which have led to similar proposals for the reaction pathway (Fig. 8-1). The rates in the models are largely in agreement except for the on rates for the initial enzyme–DNA complex and the glycosidic bond cleavage rate. Both models contain the same sequence of steps (DNA association, dU flipping, conformational clamping, dU cleavage, product release; see the legend of Fig. 8-1 for the symbolic abbreviations) except that the model by Wong et al. includes an additional step for "retraction of the leucine finger" [202]. Glycosidic bond cleavage is irreversible and product release is rate-limiting in both models.

So how do the rate constants measured here for wt(His-tagged)UDG match up to these previous analyses? Unfortunately, because the deoxypsuedouridine substrate mimic did not supply a usable signal for nucleotide flipping (*ES*↔*EF*), we could not measure flipping rates for any of the proteins (represented as "?" in Fig. 8-1).

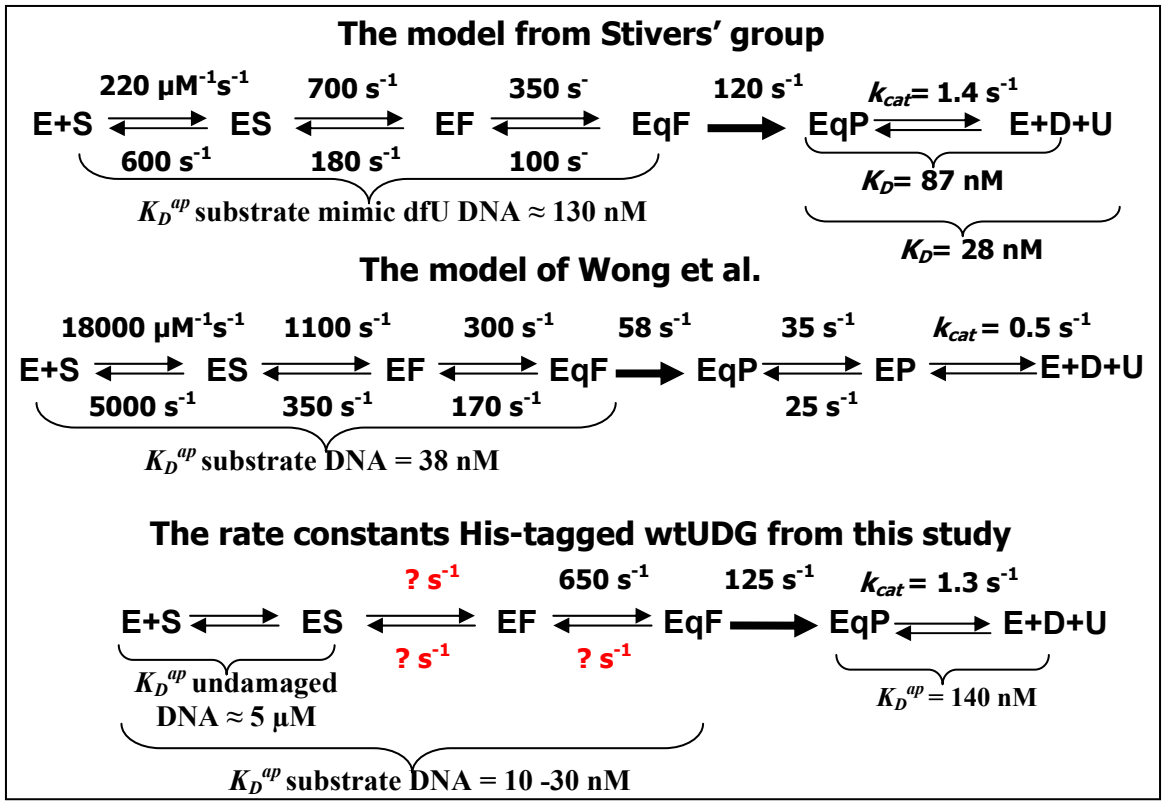

Figure 8-1. Comparison of the proposed kinetic models for wild-type UDG from *E. coli*. The steps represented by in the mechanisms are: formation of the initial UDG–DNA collision complex ($E+S \leftrightarrow ES$); deoxyuridine flipping ($ES \leftrightarrow EF$); first UDG isomerization leading to Trp quenching ($EF \leftrightarrow EqF$); irreversible glycosidic bond cleavage ($EqF \rightarrow EqP$); reverse protein isomerization as in leucine finger retraction –only in the model by Wong et al.– ($EqP \leftrightarrow EP$); product release ($EqP \leftrightarrow E+D+U$ or $EP \leftrightarrow E+D+U$ where D = abasic site DNA and U = free uracil). The models and latest rate constants are from [194, 202]. Red question marks represent rate constants that were not experimentally accessible with our methods.

Without data for the nucleotide flipping steps global fitting of a concerted set of rate constants to the reaction mechanisms was not feasible. Therefore the values of k_{on} and k_{off} measured via single-turnover titration are composite rate constants reflecting all the microscopic rates of the $ES \leftrightarrow EF \leftrightarrow EqF \rightarrow EqP$ steps. Likewise, the value of k_{quench} is a composite of $EF \leftrightarrow EqF \rightarrow EqP \leftrightarrow E+D+U$ steps involved in the state of intrinsic Trp fluorescence of UDG. This precludes a rigorous comparison of this data with the

proposed mechanisms for UDG. It must be conceded then that some of the differences between models may be due to the various methods employed in data fitting (e.g., the rates in the model of Wong et al. have been globally fitted while the others have not).

However, we can ask if our results provide reasonable constraints for the next kinetic analysis step, computational analysis for the complete reaction pathway. To this end we were able to measure the apparent dissociation constant for dsDNA substrate, which supplies the overall equilibrium of this interaction. The K_D^{Ap} of 34 nM obtained for the dsDNA substrate AUA/G is in excellent agreement with the values reported for a similar substrate (U paired with 2AP) and the dfU substrate analogue.

The rate of the Trp fluorescence quenching, and by association the supposed isomerization that leads to conformational clamping onto substrate, was faster than chemistry, putting this step ahead of glycosidic bond cleavage. The maximal rate of the chemical reaction (k_{max}) measured in this study was close to values reported by Stivers' group, but were larger than those modeled by Wong et al. The Trp fluorescence recovery phase of the stopped-flow kinetic traces support a model in which the reverse isomerization is concerted with product release, which is in contrast to the model of Wong and coworkers. Even if such an isomerization does not exist, the Trp-recovery definitely reports on the steady-state rate-limiting step of product release. This is a novel way (from the enzyme's perspective) to measure the steady-state kinetics of UDG and could prove useful to other researchers.

Summary of the Characterization of Phe77 UDG Mutants

The kinetic characterization of the Phe77 mutants involved the following steps: measuring the steady-state uracil excision kinetics of the mutants within single and double stranded DNA contexts; equilibrium binding measurements via fluorescence

anisotropy of the mutants with undamaged, substrate mimic deoxypsuedouridine (dψU), and product mimic containing duplex DNAs; presteady-state single-turnover uracil excision kinetic measurements; and an assessment of the substrate-induced Trp fluorescence change of the UDGs through fluorescence stopped-flow. The rate and equilibrium constants measured for the Phe77 mutants are mapped onto the reaction mechanism for wtUDG as a qualitative way to easily compare the effects of these changes at each particular step of the reaction (Fig. 8-2).

The steady-state glycosidic bond cleavage assays revealed that the F77A, F77N and F77Y mutations reduced the turnover number by about 23-, 150-, and 3-fold, respectively, as compared to the His-tagged wtUDG turnover number (k_{cat}) for the substrate AUA/A (Table 5-1). The effects on the turnover of the single-stranded substrate (ssAUA) were of the same relative magnitude except for the F77A mutation which was mitigated by this substrate (only 3-fold reduction in k_{cat} as compared to 23 fold for dsDNA), which hints that the dU flipping of F77A UDG may be impaired. This effect of the F77A mutation is also reflected in the specificity constants (k_{cat}/K_M) for AUA/A and ssAUA, which is reduced 200-fold for AUA/A, in contrast to the slight 0.6-fold reduction for ssAUA as compared to wtUDG. However, the F77N mutant reduced k_{cat}/K_M by 800-fold for the substrate AUA/A, and therefore was the most damaging.

The equilibrium binding measurements by fluorescence anisotropy gave approximately the same apparent dissociation constants for undamaged DNA (ATA/G, $K_D^{Ap} \approx 5.0$ μM) and abasic-site product mimic DNA (AXA/G, $K_D^{Ap} \approx 140$ nM) for all versions of UDG studied (Table 5-2). This result was expected because the mutations are

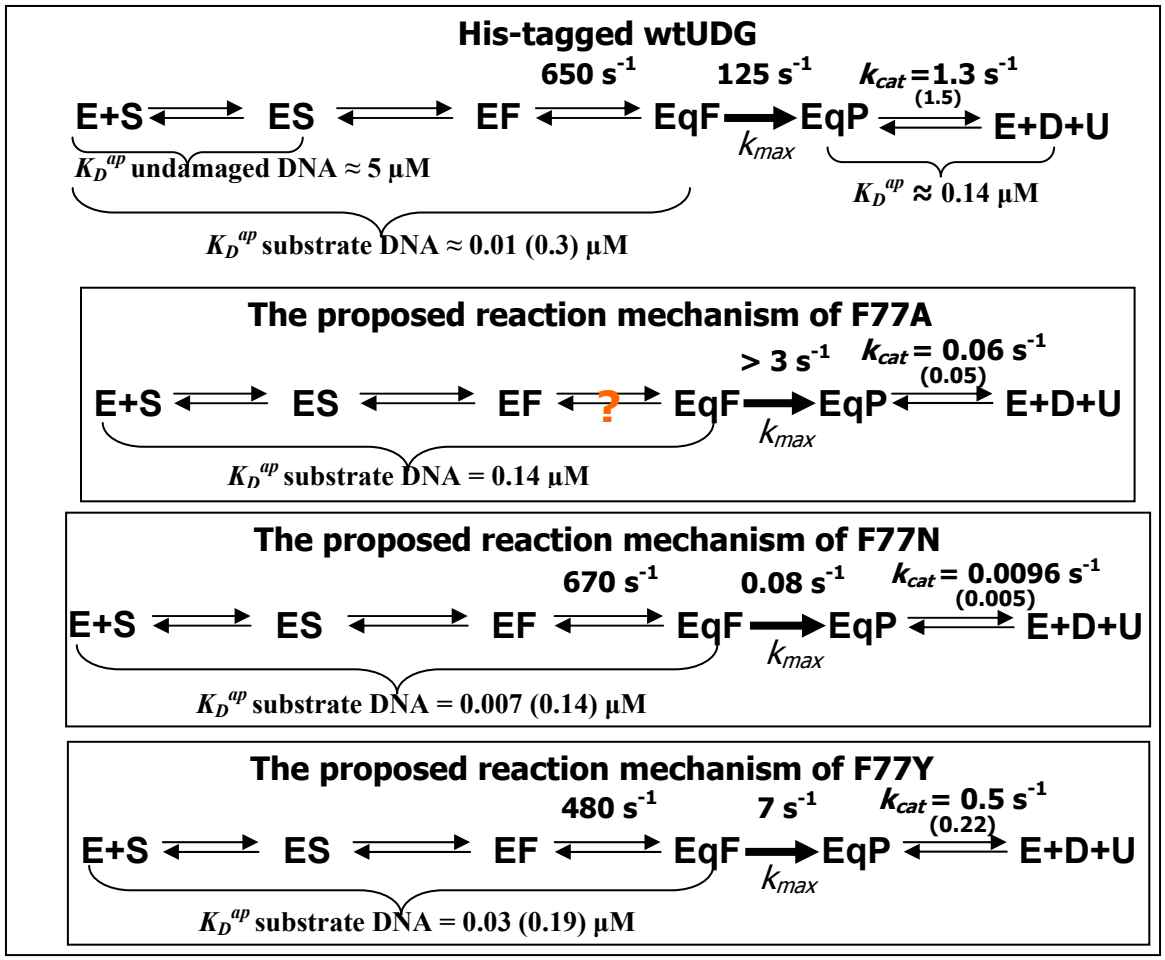

Figure 8-2. Qualitative constraints for proposed kinetic mechanisms for the Phe77 mutant UDGs. Comparison of the preliminary reaction mechanisms of the Phe77 mutants with His-tagged wtUDG. The reaction steps are represented exactly as in Fig. 8-1. Numbers in parentheses are values obtained for the same parameter through analysis of Trp fluorescence data. All Phe77 mutants have apparent dissociation constants for undamaged and product mimic DNA that are roughly equivalent to His-tagged wtUDG so these values have been omitted from the graphic.

deep within the protein and should not affect the DNA binding loops. The substrate analogue, deoxypseudouridine (dψU), was not bound appreciably tighter by the enzymes than undamaged DNA, except for the F77N mutant which had a slightly higher affinity (AψA/G, $K_D^{Ap} \approx 1.0$ µM) for this ligand, although still in the micromolar range. This result was interpreted as meaning wild-type, and mutant UDGs could not attain a stable,

deeply bound enzyme–dψU complex, and by association the supposed induced fit onto the dψU nucleotide would also be impeded (later supported by Trp fluorescence data).

The concentration independent maximal single-turnover uracil excision rates (k_{max}) reveal that the F77A, F77N and F77Y mutants have 30-, 1100-, and 15-fold slower uracil excision rates, respectively, relative to wt(His-tagged)UDG for the substrate AUA/G (Table 6-1; Fig 8-2). For comparison with other active-site mutations, these effects can be converted into free energy differences between the activation barriers for catalysis by the wild-type and mutant enzymes with the equation: $\Delta\Delta G = -RT\ ln\ (k_{max}^{wt}/k_{max}^{mut})$. The F77A and F77Y mutations have mild 2.0 and 1.6 kcal/mol destabilizing effects on the activation barrier of glycosidic bond cleavage, respectively. Therefore, the active-site phenylalanine has a small, but significant, contribution to transition state stabilization as demonstrated by the ablation of the phenyl group, or addition of a hydroxyl to the phenyl group. Changing Phe77 into asparagine destabilizes the glycosidic bond cleavage reaction by a surprisingly large 4.2 kcal/mol, which is close to the effect removal of the conserved histidine (important in the stabilization of the oxacarbenium reaction intermediate) has on lowering the activation barrier of the reaction (4.8 kcal/mol) [205].

The dependence of the single-turnover rate constants on the concentration of substrate allowed an apparent dissociation constant for the cleavable substrate (AUA/G) to be calculated. Only the F77A UDG had a drastically lower affinity ($K_D \approx 0.14$ μM) as determined from single turnover titration for the substrate AUA/G as compared to wt(His-tagged)UDG ($K_D \approx 0.01$ μM). This result indicates the phenyl group contributes a favorable interaction to binding substrate, and therefore can be considered a base "pulling" group.

The enzyme–substrate interactions of wild-type and Phe mutants with a mispaired duplex DNA substrate (AUA/G) was followed through changes in the intrinsic tryptophan fluorescence of the proteins. Immediately upon mixing with substrate, all UDG variants showed a reduction, or quenching, of their Trp fluorescence. The magnitude of the Trp-quenching was reduced relative to wt(His-tagged)UDG for all Phe77 mutants, with the F77A mutation having the most severe attenuation in the signal. The rate of Trp-quenching showed a hyperbolic dependence on substrate concentration for all enzymes except for the F77A mutant, which remained constant within the substrate concentration range of these experiments do to fluorescence kinetics to fast to measure by these stopped-flow methods. Although this limitation prevented a K_D for the substrate AUA/G from being determined for F77A UDG through the dependence of Trp-quenching rates on substrate concentration, the Trp fluorescence signal did not achieve a clear maximum in the concentration range of this experiment, which qualitatively indicates a lower affinity for substrate for the F77A mutant as compared to wild-type. The maximal rate of Trp-quenching was faster than the concentration independent rate of glycosidic bond cleavage for all the UDG variants. The F77N and F77Y mutants maximal Trp-quenching rates (670 s^{-1} and 480 s^{-1}, respectively) compare well to wt(His-tagged)UDG value (k_{quench} = 650 s^{-1}) (Table 7-1; Fig. 8-2).

The recovery of Trp fluorescence proceeded at rates that were approximately equal to the steady-state turnover rates of substrate to products for the respective UDG versions. This result implies that the steady-state rate-limiting step of product release, and possibly the reversal of the conformational clamping, happen concurrently. The line shape of the recovery phase of the Trp fluorescence for the Phe77 mutants is exponential,

while for wt(His-tagged)UDG it is sigmoidal. This difference between the shapes of the Trp fluorescence kinetic traces may be caused by the much faster chemical step of the wild-type enzyme, which creates a build-up of product bound UDG as compared to the mutants. Overall the Phe mutations seem to have affected UDG's catalytic cycle at both substrate binding, and surprisingly, at product release steps, in addition to the affects on glycosidic bond cleavage. These results show the importance of the active site phenylalanine in the catalytic cycle of UDG.

Wild Speculation on the Causes of Phe77 Mutational Effects

To my knowledge, this is the first report of a mutational analysis of the conserved active-site phenylalanine of UDG from any source. All known DNA-glycosylases that recognize neutral bases [232], even those from other structural families, and many other DNA interacting proteins have an aromatic amino acid that stacks directly on top of the base. Are these enzymes taking advantage of a favorable π-π stacking energy during binding, or is the aromatic ring just a convenient structural feature and good water excluding surface in an active-site? Some speculation on the causes of the Phe77 mutational effects may provide some insight into this question.

Active-Site Dielectric Effects of Phe77 Mutations

Certainly the fact that the asparagine mutation, the substitution that is the most hydrophilic, is the most damaging implicates the dielectric constant of the UDG active site as an important factor for catalytic functioning. Heteronuclear NMR and Raman studies [197, 206] have shown the surprising finding that UDG lowers the N1 pK_a of the uracil leaving group by 3.4 units as compared to that in aqueous solution, resulting in uracil existing as a stable anionic species in the active site at neutral pH. Further NMR measurements [158, 205] have found that the histidine (His187) that stabilizes the

developing enolate on uracil O2 is neutral in the catalytically active state of the enzyme. This suggests His187 has a $pK_a < 5.5$, which is lower than the normal histidine pK_a of 6.0.

Characterization of the transition state of the UDG reaction as dissociative with charged intermediates led to the proposal that the UDG active-site environment most likely has a low dielectric constant [141, 232]. At first thought, the stabilization of charged intermediates by a hydrophobic active site may seem paradoxical. However, Werner and Stivers propose the decrease in the pK_a of the N1 position of uracil, and delocalization of the electron density to uracil O2, would serve to diminish the reactivity of N1 as a nucleophile, thereby increasing the lifetime of the intermediate. Stivers and coworkers also hypothesize that UDG facilitates charge migration onto the pyrimidine base, by forming hydrogen bonds that are weak in the ground state and become increasingly stronger as the transition state is approached. When there is a large pK_a mismatch between donor and acceptor groups in the ground state there would be weak hydrogen bonding, which becomes stronger hydrogen bonding as the anionic transition state is approached, and the pK_a values become more closely matched [233, 234]. In this instance, uracil O2 (pK_a -3) accepts a hydrogen bond from the NH^{ε} donor of His187 ($pK_a \approx 14$) creating a pK_a mismatch of 17 units in the UDG ground state. These researchers claim this pK_a mismatch would be reversed in the transition state when the O2 pK_a increases by 10 pK_a units (pK_a O2 $^{imidol} \approx 7$), where a significant amount of charge has resonated onto the O2 atom of the leaving group. The authors claim, "[s]uch effects can be energetically amplified in an enzyme active site of low dielectric as compared to water because of the stronger Coulombic attractive forces between acceptor and donor groups

with matched pK_a values." [232 p. 2749]. Jiang and Stivers point out that UDG binds the neutral uracil base 500 times more weakly than the N1-O2 imidate form, and removal of His187 by mutagenesis destabilizes the transition state of the reaction by 4.2 kcal/mol without affecting ground-state substrate binding, consistent with their model. Not only would the hydrogen bond between the catalytic histidine and uracil benefit from a low dielectric active site, but a hydrophobic environment would also lower the pK_a of the N1 position of uracil reducing its ability to reform a bond with the carbenium on the deoxyribose. In summary, it seems it is more proper (less confusing) to say that the implied low dielectric constant in the UDG active site stabilizes the broken glycosidic bond which happens to result in charged intermediates, rather than stabilization of the charged intermediates themselves.

Therefore it seems highly logical that introducing a hydrophilic group like asparagine, which could even bring water into the active site, would disrupt achievement of the transition state leading to the large observed mutagenic effect. Yet to jump to the conclusion that the only parameter the Phe77 mutations affected was the dielectric constant of the active-site would over-simplify the effects, ignoring the electronic and structural changes intertwined with these side chain substitutions. In the absence of dielectric measurements of the UDG active-site or structural information on the Phe77 UDG mutants, a comparison with other mutational studies and structural models is the only means to further our understanding of the data presented here.

Although this is the first mutational study of a phenylalanine in UDG, it is not the first such study for other enzymes. There are many mutational studies of conserved phenylalanines, but most are in transmembrane proteins, so the phenylalanine is on the

exterior of the protein. However, I have come across a recent study that involved a phenylalanine in an active-site of 4-oxalocrotonate tautomerase [235]. Czerwinski and coworkers were trying to find the factors that cause the catalytic proline of the tautomerase to have a perturbed pK_a (3 units below normal). The study by Czerwinski et al. also chose to mutate the target Phe into four different amino acids, two of which were a tyrosine and an alanine, similar to the work presented here.

Also similar to the data presented here, Czerwinski et al. found that the Tyr mutation had a very mild effect as opposed to the Ala mutation, which was more damaging to the enzyme's activity. The relevant data to the discussion here from the tautomerase research were the estimates of the dielectric constant in the active-sites of their Phe mutants. As expected, the alanine mutant increased the dielectric constant of the active-site by approximately 7 units, indicating this mutation greatly increased the solvent accessibility of the active-site. However, the same analysis with the Tyr mutant revealed that the dielectric constant had actually become slightly *lower* (more hydrophobic) than that of the wild-type tautomerase. If the same, almost non-effect on the dielectric constant upon substituting Tyr for Phe in the UDG active-site can be expected, then it can be argued that there must be some other factor that causes the F77Y mutation to reduce the k_{max} by almost 15-fold. This relatively large mutational effect for such a seemingly small change in UDG hints at complicated combination of changes effected within the active site by the Phe77 mutations that is clearly more than just changes in the dielectric environment in the active site. An examination of the possible structural changes caused by these mutations must also be taken into account.

Structural Implications of Phe77 Mutations: Base Twisting Effects?

As noted in Chapter 1 (pg. 41), the side chain of the active-site asparagine responsible for cytosine/uracil discrimination is not fixed in space by H-bonds to any other part of the protein. Comparison of the free and dψU bound hUDG crystal structures shows this side chain has some conformational of freedom (Fig 8-3). Therefore, it is conceivable then that removal of Phe77 in the F77A mutant (and possibly the F77N mutation) has allowed the flipped dU to retain more of its normal, energetically favored *anti*-conformation. In other words, the uracil ring may not be twisted the full 90˚ relative to the sugar, as seen in the hUDG-dψU complex, during catalysis with F77A UDG.

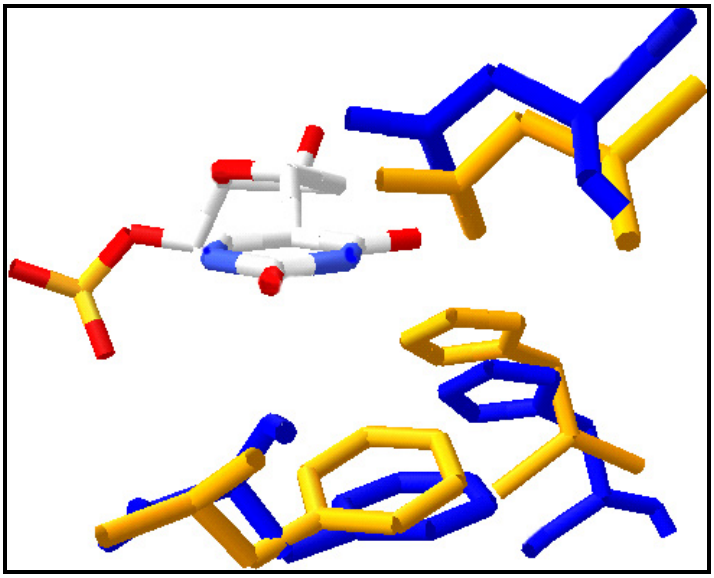

Figure 8-3. Comparison of major uracil ring interacting groups in free and dψU bound hUDG crystal structures. The free hUDG structure is blue and the dψU bound is orange. Upon binding substrate mimic or abasic site DNA product these active site residues close in: Asn from the top, His approaches O2 of uracil, and Phe from underneath. Generated with ExPasy and PBD ID 1AKZ and 1EMH.

A recent study [236] has noted that the process of base twisting in binding nucleotides is a general phenomenon in observed directly in several DNA glycosylase, and glycosylase-like proteins. These authors cite that base twisting favors the formation of oxacarbenium ion transition states in furanose sugars, such as ribose and deoxyribose. Not only has the twisting of a target, extrahelical base been directly observed in cocrystals of hUDG–dψU complex, but also in the structure of the broadspecificity human enzyme alkyladenine DNA glycosylase (AAG) bound to DNA containing 1,N6-ethenoadenine [237], and the functionally homologous HhH glycosylase AlkA [238]. Mol et al. propose that for enzymes which do not make specific contacts to DNA base functional groups and are able to excise a wide range of DNA bases, the physical twisting of the target base may be the primary means for enhancing catalysis. Base twisting is also present in the structure of purine nucleoside phosphorylase (PNP), which is not a DNA glycosylase, but catalyzes the reversible phosphorolysis of hypoxanthine or guanine ribonucleosides and 2′-deoxyribonucleosides to the free purine bases and the corresponding α-D-ribosyl 1-phosphates; a chemical reaction similar to that catalyzed by the DNA glycosylases [239]. Interestingly, PNP like UDG, also has a transition state for catalysis that proceeds via a primarily dissociative oxacarbenium ion transition state. These structures implicate physical twisting of normal bases (i.e., nucleotides that have a stable glycosidic bond) as an important component of the active site chemistry that allows these enzymes to efficiently remove these bases (e.g., uracil and mispaired thymine). Given the implied role of substrate distortion in the catalysis of UDG, we need to ask how may have the Phe mutations affected the conformation of bound substrate in the UDG active site?

Removal of the phenyl group in F77A UDG caused a 30-fold reduction in k_{max} for bond scission (only 3% of wtUDG activity). Could this in part be a result of this assumed perturbation in uracil ring orientation as compared to the normal active-site? The proposed structure-based reaction mechanism of Parikh et al. (Chapter 1 pg. 46) states the activation barrier for glycosidic bond cleavage is lowered mainly by enzyme enforced stereoelectronic cooperativity between the anomeric and σ-π aromatic effects which aligns pairs of atomic orbitals so the electrons can flow from the deoxyribose C1′ to the uracil O2, facilitating formation of the oxacarbenium and uracil anion intermediates. An idea of the magnitude of these proposed stereoelectronic effects can help us decide whether or not they are an important part of the F77A phenotype.

Analysis of supposed stereoelectronic effects in a number of enzyme reactions have led to the suggestion that commonly these effects contribute, at most, 1-2 kcal/mol towards lowering the activation barrier during catalysis [190]. Coincidentally the F77A mutational effect was calculated to destabilize the transition state by 2 kcal/mol as compared to wild-type. This is hardly convincing evidence, but luckily Mismatch Uracil DNA Glycosylase (MUG or a.k.a. DUG) can be compared to the Phe77 UDG mutants to help further ascertain how important base twisting is in the functioning of UDG. The MUG–substrate mimic cocrystal structure naturally contains some of the structural features that are possibly present in the F77A UDG–substrate complex.

UDG and MUG Comparison Offers Insights into the Importance of Phe77

The only active site amino acid that interacts with the substrate that is common to both UDG and MUG is a phenylalanine (Phe30 in MUG) [144]. MUG is missing all of the catalytic machinery that is used by Ung family UDGs. In addition, MUG also lacks the determinates that allow UDG to discern uracil from cytosine and thymine, namely the

asparagine that forms H-bonds which match with uracil but not cytosine, and the tyrosine that blocks the methyl group of thymine (Fig. 1-6). Therefore, MUG not only can remove uracil (but only efficiently from U:G mismatches), it can also remove 3,N^4-ethenocytosine (εC) and thymine along with a range of similarly substituted pyrimidines [138].

The crystal structure of MUG bound to DNA containing the substrate analogue, dfU [240], is similar to the UDG complex with dψU containing DNA, but contains some key differences. MUG, like any glycosylase, flips the target base into its active site by rotating the nucleotide 180˚. The sugar pucker of the flipped nucleotide is in a nearly identical 3′-exo conformation as seen in UDG, suggesting MUG uses a similar sugar preorganization strategy. Also in the MUG structure, there is a rotation of the uracil ring around the glycosidic bond, but importantly, it is only about 50° as compared to the 90° rotation in the UDG-dψU structure (Fig. 8-4).

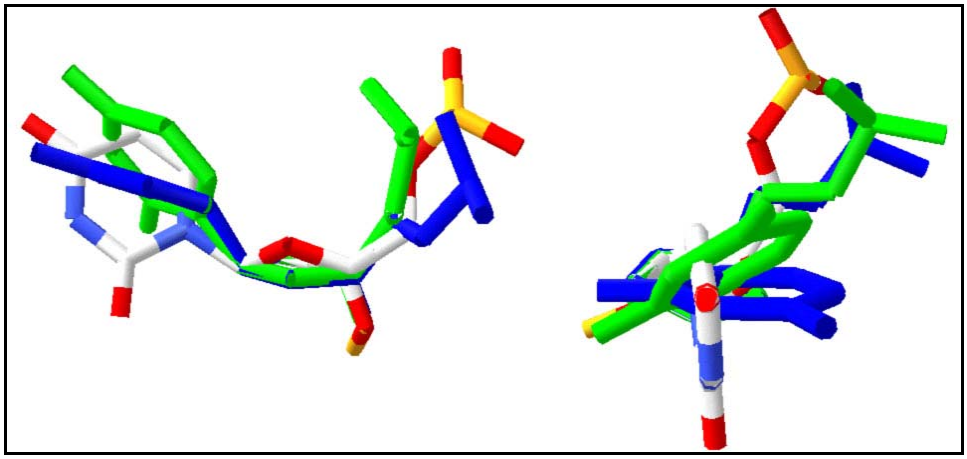

Figure 8-4. Enzyme-induced rotation of the uracil base about the glycosidic bond. Crystal structures of the substrate mimics dψU (blue) and dfU (green) bound to UDG and MUG are aligned with dU (CPK coloring) from dsDNA to show the magnitude of the glycosylase-induced sugar flattening and uracil ring rotation relative to the undistorted substrate. The structure alignment on the right is a head-on view of the structure on the left. Generated with SwissProt PDB Viewer and PDB structures 1EMH [187] and 1MWJ [240].

Aligning the secondary structural elements of MUG and UDG that are bound to substrate mimics (Fig. 8-5) reveals that the active site phenylalanines lie directly within the same plane! It is quite perplexing that phenylalanine, which by the data presented here has a relatively small contribution to stabilizing the transition state of the reaction, is the only active site group that is conserved between UDG and MUG (and is almost conformationally identical!). Since both MUG and UDG have an active site Phe but not an Asn, it would appear that the Phe is sufficient to rotate the ring significantly. Thus, the active site Asn could work in concert with the Phe to achieve full 90˚ rotation of the uracil ring as seen in UDG–dψU complex.

Does the orientation of the uracil base with respect to the sugar in the DUG active site allow the coupling of the σ-π aromatic and anomeric stereoelectronic effects as proposed for UDG? This is a difficult question to answer as direct comparisons between UDG and MUG cannot be made because the catalytic mechanisms of these glycosylases may be different. However, MUG has a kmax of 0.037 s-1for dU in a U/G mispair [138], which translates into an appreciable reduction in the activation barrier for dU cleavage of about 10.3 kcal/mol (as compared to 15.2 kcal/mol for UDG). The fact that MUG has a channel to the active site from the opposite side that admits water, rules out the structural duty of Phe30 as preventing water from entering MUG. Since MUG lacks the groups UDG uses to stabilize the transition state by electrostatic interactions it is tempting to think that substrate distortion plays a prominent role in the transition state of the MUG reaction. Mutational analysis of Phe30 in MUG is needed to discern the role of substrate distortion in MUG catalysis. Such a study may unravel the paradox of why the phenylalanine has been so strictly maintained in these glycosylases.

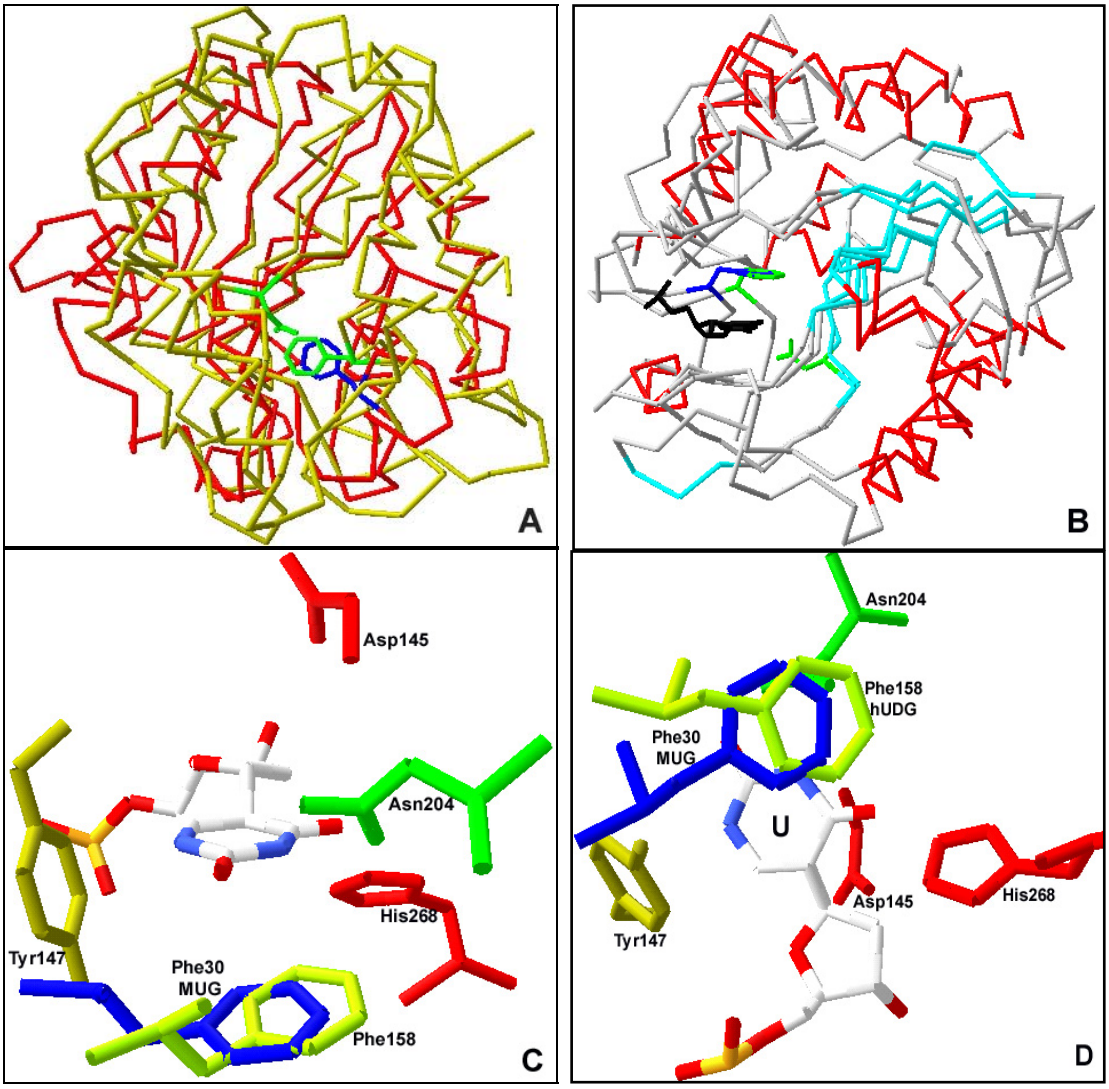

Figure 8-5. Comparison of Phe position in dψU–hUDG and dfU–MUG crystal structures. (A) Alpha carbon backbone traces of UDG (gold) and MUG (red) aligned by secondary structural elements. Phe 30 of MUG (blue) and Phe and Asn (green) of UDG delineate the active sites. (B) The alignment becomes clearer when the C^{α} traces are colored by secondary structure: α-helix in red, β-sheet in cyan, and coil in gray. Active site amino acids are colored as in A and dψU is black. (C and D) Side and bottom views, respectively, of dψU (CPK coloring) and UDG active site groups with Phe30 from MUG (blue). Active site groups involved in catalysis are colored in red. Generated with ExPasy and PDB ID 1EMH and 1MWJ.

In this section structural comparisons were made to guess at the conformation of dU within F77A UDG. There are a small number of putative members of the MUG (a.k.a. DUG)/TDG family that have a leucine or similar hydrophobic residue instead of the active site phenylalanine [136]. The substitution of tyrosine for phenylalanine is common in other UDG superfamily members. Unfortunately, these glycosylases are currently uncharacterized. It would be interesting to see if these UDGs were similar to the mutants created in this work. Of course, the question of what substrate conformation exists within F77A UDG can only be directly answered by a structure of dψU bound to this protein. Even if such a structure showed a fully relaxed dψU within the active site of F77A UDG, concluding that stereoelectronic effects are indeed the basis of the alanine mutational effects is again, highly speculative. What is needed is a full computational simulation of the F77A reaction mechanism.

To be successful the computational simulation of the transition state of the F77A UDG reaction would require the replacement of crystal packing forces with an aqueous environment, the assessment of the substrate and mutated active-site structure by simulated annealing, the incorporation of the isotope effects measured for wtUDG, and an accurate estimate of the dielectric constant within the active site. As there currently is no estimate of the dielectric constant with wtUDG, let alone F77A UDG, and no facile means of attaining these constants, meaningful computational simulation of the Phe77 mutants is not possible.

Simple structural modeling of F77A UDG reveals little as the alanine does not hydrogen bond. However, both the tyrosine and asparagine can possibly H-bond to other

groups in the active site. Structural modeling of these changes to UDG reveals possible new H-bonding patterns within these mutants.

Modeling of F77N and F77Y UDG Structures

Because the asparagine and tyrosine side chains are both bulky and can hydrogen bond they may effect the conformations of other nearby side chains. Therefore a computational search of the possible rotamers of these mutated side chains was performed and the possible new H-bonding interactions computed with the Swiss-PDB Viewer program and the structural coordinates from the hUDG–dψU complex (PDB ID 1EMH). Energy minimization with the GROMOS96 force field implementation of the Swiss-PDB Viewer did little to change the protein structures, and could not be implemented on the nucleic acid portion of the model because there are no energy topologies for nucleotides built into the program yet.

Figure 8-6 shows the modeling results for F77N UDG. The computed rotamer of the amide side chain predicts that this group could form a new H-bond with the active site Tyr that provides the steric barrier to the methyl group of thymine. This H-bond could keep the Asn side chain up and away from the bound substrate if the substrate is kept in the same distorted conformation within F77N UDG as it is in wild-type human UDG. It does not appear that this new H-bond between the amide group and the hydroxyl of the Tyr would significantly alter the conformation of its phenol group as it can still form an H-bond with a backbone carbonyl. Therefore, this basic structural modeling predicts that the mutant Asn would not clash sterically with incoming substrate and the substrate might have space to take on a more relaxed conformation (Fig. 8-4).

The same structural modeling was performed for F77Y UDG (Fig. 8-7). The model predicts that the phenol side chain will remain stacked upon the uracil ring, just as

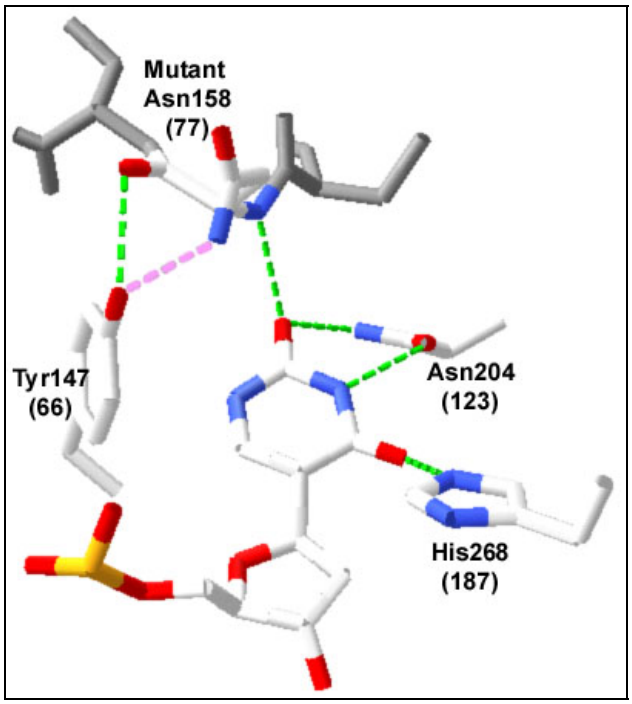

Figure 8-6. Structural model of F77N UDG. Using the Swiss-PDB Viewer and structural coordinates for the hUDG–dψU crystal structure (PDB ID 1EMH) the target Phe was mutated and the lowest energy rotamer of the new Asn side chain selected. Computed H-bonds: expected = green dashed line; new = pink dashed line. Active site amino acids (CPK coloring) are labeled according to hUDG with the number for the corresponding group in *E. coli* UDG in parentheses.

the phenyl group is normally in wtUDG. This conformation puts the tyrosine hydroxyl group within H-bonding distance of both the N^{ε} (2.71 Å) and the N^{δ} (2.78 Å) of the imidazole of the catalytic histidine (which donates an important H-bond to uracil O2 to pull electron density away from the N-glycosidic bond). This histidine to uracil H-bond has been investigated extensively by NMR [158] and was found to be a short strong hydrogen bond that donates an estimated 2.2 kcal/mol to stabilization of the transition state. Could the introduced Tyr be directing a proton at the N^{ε} of the catalytic histidine that directly interferes with the H-bond to Uracil O2? Or alternatively an H-bond to the N^{δ} of the imidazole may disrupt the function of the catalytic His by causing it to be

misaligned. It is hypothesized that a H-bond from the peptide backbone nitrogen of Ser270 (Ser 189 in eUDG) to the N^{δ} keeps the imidazole in the $N^{\varepsilon 2}$-tautomer, ready for H-bonding to uracil [205]. It is intriguing that the added hydroxyl group may exert its larger than expected (1.6 kcal/mol) mutational effect through a partial disruption of the H-bond that aids in leaving group activation.

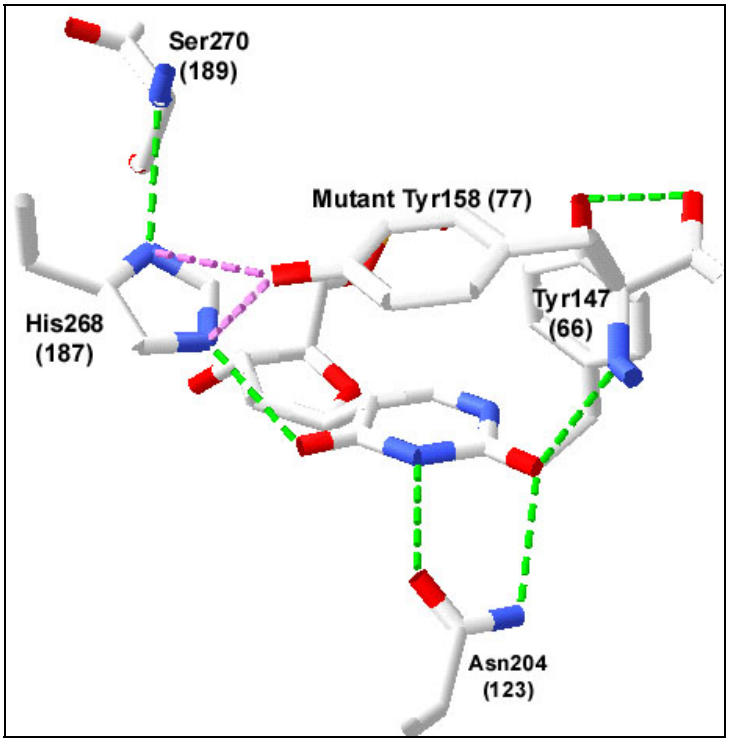

Figure 8-7. Structural model of F77Y UDG. As is Fig. 8-6 the target Phe in the hUDG–dψU crystal structure (PDB ID 1EMH) was mutated and the lowest energy rotamer of the new Tyr side chain selected. Computed H-bonds: expected = green dashed line; new = pink dashed line. Active site amino acids (CPK coloring) are labeled according to hUDG with the number for the corresponding group in *E. coli* is in parentheses.

In this section I have presented arguments for the most likely sources of the mutational effects exhibited by the changes to Phe77 of *e*UDG. In summary, the effects exhibited by switching Phe77 into alanine are probably at least in part, or maybe wholly, caused by the accompanying change in the dielectric constant of the active site that

removing the phenyl group likely causes (as has been shown in 4-oxalocrotonate tautomerase). The alanine mutation also impaired Trp fluorescence quenching and lowered the enzyme's affinity for substrate, which implies the mechanics of binding and conformational clamping to dU in this mutant are also damaged. Switching Phe77 with asparagine in all likelihood also caused a change in the dielectric constant of the UDG active site that at least in part caused the large reduction in the maximal glycosidic bond cleavage rate. Basic structural modeling and the uninhibited substrate-induced Trp fluorescence quenching of F77N UDG imply that the Asn side chain does not interfere with substrate binding, and therefore exerts its effects at the chemical step or after. Structural modeling and the similar Trp fluorescence kinetics for F77Y UDG also suggest that the tyrosine substitution does not sterically clash with the bound substrate. One intriguing possibility for the larger than expected mutational effect of adding a hydroxyl to the end of Phe77 is that this hydroxyl may be directing a proton at the catalytic histidine; interfering with the H-bond that draws electron density onto the O2 of uracil in the transition state. With the alanine and asparagine mutations, the possibility that the substrate no longer docks into the active site in an alignment that would fully take advantage of hypothesized stereoelectronic effects created by base twisting should also be taken into consideration.

Structural Dynamics of UDG

For decades biochemists have sought to explain enzymatic catalysis by a summation of mutagenesis effects with little success. Recent advances in computational methods have led to the discovery of some previously unappreciated features in the reaction mechanisms of various enzymes, but more often are seriously flawed or fail to adequately explain these catalytic mechanisms. Examples of computational studies with

UDG emphasize this point. One study predicted that the protonation state of the catalytic His changed during the course of the enzymatic reaction and that this residue activates a water molecule to act as a proton donor to the uracil [241]; results that are exactly opposed to experiment. Computational simulation by Dinner et al. [208] correctly predicted the phosphodiester backbone charges would aid in the stabilization of the transition state in the UDG reaction mechanism, but grossly overestimated their effects.

Sources for the deviation between experiment and computation could be any vast number of parameters, from an inaccurate computational estimation of the effective dielectric constant for the enzyme active site, to improper treatment of the solvent. Just as with mutagenesis, the simple summation of computed energetic effects often does not add up to a complete understanding of enzymatic catalysis. I believe one major hurdle to the accurate modeling of enzyme catalysis is the proper simulation of global protein dynamics through the entire reaction. Only by accounting for the global structural changes, and not just the positions of a limited number of side chains, can the full effects of ligand docking be appreciated.

It was once thought that the major function of the peptide backbone of a protein catalyst was to serve mainly as a static scaffold to ensure the proper constellation of amino acids for catalysis. It is now known that just as life needs to be flexible to allow for adaptation, enzymes take advantage of the flexibility in their structures. There are numerous examples of ligand-induced structural changes that are vital to enzyme function. From molecular motors that utilize conformational changes to produce a force for movement [242] to receptors that are triggers for changes in protein structure that are propagated over long distances to transmit a signal. To accurately determine the

dynamics of these structural changes and their mechanistic role, these protein dynamics need to be measured during the course of the reaction in real time [230].

Data presented in Chapter 7 demonstrated the utility of an intrinsic signal that can report on specific events (in this case substrate docking) in real time. The tryptophan fluorescence changes of *e*UDG has made us aware that the subtle structural differences between the substrate mimic bound and free enzyme crystal structures could in fact be a real event in the catalytic cycle of UDG. This invaluable natural tool has been used extensively to measure the substrate-induced isomerization, yet the basis behind these Trp fluorescence changes remains a mystery.

Proposed Experiments to Decipher the Origin of Trp-Quenching in UDG

Full analysis of the intrinsic fluorescence of *e*UDG would require the site-directed mutagenesis of each of the six tryptophans separately into phenylalanine and the spectroscopic characterization of each of the six new UDG variants. This spectroscopic characterization would entail measuring the excitation and emission spectra of each protein along with the fluorescence lifetimes. After this initial spectroscopic characterization, chemical fluorescence quenchers iodide and acrylamide could be used to asses the fractional accessibility of the various tryptophans to the solvent. Iodide being an ionic species will only quench the fluorescence of Trp residues that are located in more hydrophilic environments (surface), while acrylamide readily penetrates into the hydrophobic interior and quenches fluorescence emission of Trp residues throughout the entire protein [228]. By comparing the efficiency of quenching of iodide and acrylamide, the molecular environment of each Trp residue can be ascertained. Emission spectra and Trp fluorescence lifetime measurements with chemical quenchers may reveal alterations in Trp spectra due to protein conformational changes, even when the conformational

changes are small and local. Finally, the real time substrate-dependent Trp fluorescence kinetics of each Trp mutant should be performed as described in Chapter 7. Hopefully, someday someone will use these techniques to deconstruct the intrinsic Trp fluorescence of UDG. In the absence of such a detailed spectroscopic analysis of UDG, I will use what has been discovered about the nature of Trp fluorescence and the substrate-induced conformational change of UDG to try to dissect the mechanism of Trp fluorescence quenching in UDG.

Fluorescence quenching is a general term used to describe any process that leads to nonradiative decay to the ground state from the excited state of a molecule that would normally decay by emission of a photon. Tryptophan fluorescence is affected by a complex set of factors, but in general the most influential is the dielectric environment in the immediate vicinity of the indole side chain, which in turn is a function of solvent accessibility and the proximity of charged groups. (Trp is not the only amino acid that is quenched by charge. As tyrosine is deprotonated, its fluorescence is also quenched [243].) A number of recent studies involving wide range of techniques, including two-photon excitation and hybrid quantum mechanical molecular dynamics [228, 244], have provided new details on the nature of the electronic transition that leads to fluorescence from the indole group. Upon absorption of a photon, tryptophan can enter into its two lowest excited states termed ^1L_a and ^1L_b. The quantum mechanical studies have predicted that electron density is shifted from the pyrole ring to the benzene ring of indole upon excitation to the ^1L_a state, and that it is from this state that the majority of photons are emitted. This means that negative dipoles or charges near the benzene end of

the indole could reduce the population of the ^1L_a state, and hence quench the Trp fluorescence [245].

Proposed Mechanism for Substrate-Induced UDG Trp-Quenching

If we assume that the human and *E. coli* enzymes have the same isomerizations during catalysis (a safe assumption due to the very small differences between these proteins), we can use the crystal structures of free hUDG and hUDG bound to substrate mimic and product ligands to ascertain whether there are structural changes in the enzyme that would change the electrostatic environment of the tryptophans. Of the six tryptophans that are in *e*UDG, four overlap almost perfectly with seven Trp residues in hUDG, with a fifth pair one amino acid apart. The tryptophans that are not conserved between the enzymes are spread out on the side opposite the DNA binding cleft on the protein's surface, which makes it unlikely that these residues participate in substrate-induced fluorescence quenching. Of the four Trp pairs that are in the same conformation in both UDGs, one is about 12 Å below the active site, while the three remaining pairs form a network above the active site with the closest residue being only about 4.5 Å away (Fig. 8-8). Because the Trp-quenching is substantial and substrate-dependent, it must involve multiple tryptophans that are likely in close proximity to the active site. These constraints make the three tryptophans above the active site the most likely source of the intrinsic fluorescence signal of UDG.

Because these three residues are conserved positionally between *E. coli* and human, we can overlay the hUDG free and dψU bound crystal structures (this is necessary because a *e*UDG–dψU structure is not available) to determine if substrate mimic binding induces changes in the conformations of the tryptophans. This structural comparison (accomplished with Swiss PDB Viewer) is presented in Figure 8-8. The dark gray amino

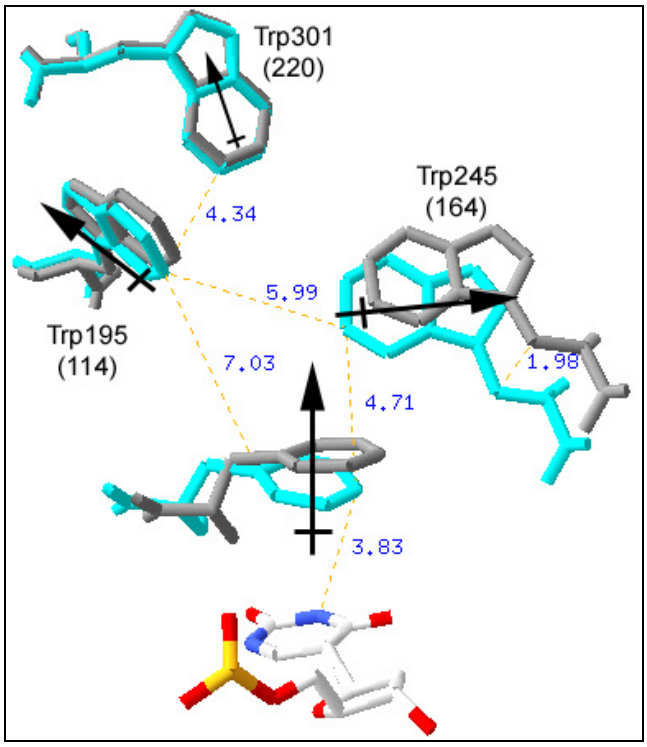

Figure 8-8. The conserved tryptophans proposed to quench during substrate docking. The enzyme only hUDG structure (PDB ID 1AKZ; gray) was overlaid with the dψU–hUDG cocrystal (PDB ID 1EMH; cyan) to show the changes in Trp position. Distances between groups (yellow dashed lines with blue numbers) are in angstroms. The black crossed arrows represent the theoretical dipoles uracil binding/anion formation may cause (see text for details).

acids are from free enzyme and the groups in cyan are from the dψU–hUDG structure. The overlay shows that Trp245 (164 in eUDG) is the only Trp that undergoes a significant structural change. This group shifts about 2 Å down towards the active site Phe (which also shifts towards the uracil ring) and almost 1 Å toward Trp195. Since both Trp245 and the active site Phe shift in the same direction, they remain almost equidistant. Is this relatively slight change in spacing between groups upon substrate mimic binding the source of the quenching? This structural change appears to be too small to account for the large change in the tryptophans environment the fluorescence data suggest. The other possibility of charged side chains drastically rearranging to approach the

tryptophans (instead of the tryptophans rearranging) is ruled out because mapping of these groups revealed that none of them (including histidines that can quench Trp fluorescence in neutral form) approach the Trp residues upon dψU binding.

Phenylalanine has been suspected of being able to quench nearby tryptophans, but through an irregular H-bond between the benzene ring and the indole nitrogen [246]. The closest tryptophan (Trp245) to the active site Phe of UDG is in the wrong conformation for formation of this type of interaction (and does not become closer to the Phe as both groups shift downward upon dψU binding). The absence of drastic structural changes in the environments of these tryptophans implies that the substrate-induced quenching must occur through a different mechanism.

I propose that the source of the substrate-induced Trp fluorescence quenching of UDG is the induction of a dipole caused by uracil stacking on top of the active site Phe, pushing its π-electron cloud up towards the benzene ring portion of the indole side chains of the two closest tryptophans (Fig. 8-8). This would in turn induce a dipole in these tryptophans that would disrupt there ^1L_a excited states thereby quenching their fluorescence. The third Trp may quench as a result of Trp-Trp resonance energy transfer, which has been found to occur efficiently at distances up to 14 Å [228], or it may also be quenched by this induced dipole. In fact any of the tryptophans could quench by homotransfer of resonance energy to a quenched Trp with a shifted spectrum (resonance energy transfer from Trp to Phe is energetically uphill and therefore unlikely) [228]. This model implies that Trp-quenching in UDG is not just a function of the isomerization into the conformational docking of substrate, but is also linked to the charged intermediates of the reaction.

This model of UDG Trp-quenching can explain the variability in the amount of wtUDG quenching seen with different substrate mimics and the differences in the quenching of the Phe77 mutants. Formation of a uracil anion in the active site would be expected to increase the induced Phe dipole and lead to increased Trp quenching. This would explain why under very similar conditions the amount of Trp quenching caused by the dfU substrate mimic is not as large (about 6-fold less) as the quenching caused by dU which gives a negatively charged reaction intermediate [153, 194]. The ability of wtUDG to stabilize the uracil anion could also explain why there is a lag in the fluorescence recovery of wtUDG during the reaction. The lag in the Trp fluorescence kinetics of UDG would then be in part caused by build up of the charged product in the UDG active site. Because the Phe77 mutants probably cannot stabilize the uracil anion as well as wtUDG, they do not exhibit this lag in their Trp fluorescence kinetics. In addition, because the Phe mutants lack or have a disrupted phenyl group, the propagation of the substrate induced dipole to the tryptophans would also be reduced, which predicts the Trp signal change should be reduced by the Phe mutations. This is exactly what transpires as F77N and F77Y UDG have over 50% smaller signal changes and the F77A mutation causes a huge 90% reduction in Trp signal.

In this section I have proposed a mechanism for the substrate-induced Trp fluorescence quenching in UDG. The model suggests that quenching is caused by uracil binding inducing a dipole in the active site phenyl group which is directed toward three conserved tryptophans above the active site. This dipole would become larger upon conversion of substrate into an anionic intermediate, causing stronger more prolonged quenching. This model can explain various features of the Trp fluorescence kinetics of

wild-type and mutant UDGs, including the lag in Trp fluorescence recovery with wtUDG and the reduced Trp signal of the Phe mutants. An important feature of the model is that although Trp-quenching and the proposed conformational clamping may be concurrent, they are not dependent on each other. This explains why abasic site DNA product binding, which also induces an isomerization in hUDG that is indistinguishable from the substrate mimic induced conformational change, does not cause Trp-quenching. The UDG Trp-quenching model makes predictions that can be tested. It predicts that any ligand that could stably associate with the UDG active site Phe and cause an dipole directed towards the proximal tryptophans would cause Trp-quenching (free uracil binding does cause Trp quenching in UDG [159]). To my knowledge this is the first attempt to explain the mechanism of substrate-induced Trp-quenching of UDG. In light of these conclusions it would seem prudent not to over-interpret the Trp fluorescence kinetics of UDG as there currently is very little data that directly links the conformational change seen in the crystal structure with the Trp quenching.

Further Experiments to Aid in Understanding the Phe77 Mutants

What possible experiments might help unravel the role phenylalanine 77 plays in the mechanics of UDG? Given the wide range of developed techniques and advances in technology, experimental design is often more limited by imagination (and fiscal considerations) than by practical applications. I have divided ideas for future studies into two categories: experiments that could have been performed with currently accessible materials and equipment (intra-lab), and approaches that would require outside materials and equipment (inter-lab).

In the intra-lab category of experiments are the Trp fluorescence quenching characterization and kinetic measurements discussed in the previous section. In addition,

there are some relatively simple stopped-flow experiments that would augment the results reported here. Trp fluorescence kinetics of UDG association with the proteinaceous inhibitor Ugi (Chap 1 pg. 34) would be interesting in several ways. Ugi inserts an uncharged group into UDG (although not deeply), so if Ugi causes Trp-quenching it would disprove my proposed quenching mechanism. If there was a usable Trp signal for Ugi–UDG association, how each of the Phe77 mutants responds to the Ugi inhibitor would tell us about the role Phe77 has in inhibitor binding. Comparing Trp fluorescence kinetics with Ugi of both wild-type and mutant proteins could tell us more about how the mutations may have affected the supposed conformational clamping step.

Another use of Ugi would be as a non-denaturing quench to study the kinetic partitioning between reactants and products of the Phe77 mutants as previously performed by Wong et al. [202] for *E. coli* UDG. Comparing the single-turnover uracil excision kinetics of a denaturing quench which instantaneously stops the reaction, with the non-denaturing Ugi quench which allows bound substrate to either go to products or dissociate, provides a measure of the flux of the reaction. In this way the forward commitment to catalysis can be determined for the Phe77 mutants, further defining the role of the active site Phe in glycosidic bond cleavage.

The chemical rescue method applied by Jiang and colleagues [198, 199] in their studies of *E. coli* UDG would provide a means to ascertain if the Phe77 mutations affected the nucleotide flipping abilities of the enzyme. The chemical rescue uses a pyrene wedge incorporated into an oligo to force the opposing nucleotide (dU in this case) in the complimentary DNA strand to become extra-helical. This means the dU is preorganized in the flipped conformation. By contrasting the uracil excision kinetics

with and without pre-flipped dU the role of Phe77 in nucleotide flipping could be firmly established.

As for inter-lab studies, the most obvious need is for crystal structures of the Phe77 mutants bound to the dψU substrate mimic. Structures of the Phe77 mutants would be invaluable aids in the interpretation of the kinetics data. Perhaps someday when protein crystallization is almost fully automated, some curious person (possibly myself) will program their robot to solve these structures to compare with this project.

Other inter-lab experiments could use other forms of spectroscopy. Raman spectroscopy is a technique that has been shown to be able to specifically assign a signal to Phe77 that changes when UDG associates with the substrate mimic dfU [197]. Comparison of Raman spectrums of wtUDG to the Phe77 mutants with the substrate mimic could provide information on perturbations in the interaction of the Phe77 mutants with DNA.

Isothermal titration microcalorimetry (ITC) has been used to study the binding interactions between protein and DNA. ITC measurements can provide direct determinations of the number of binding sites of the protein, the enthalpy of binding, and the equilibrium dissociation constant of the interaction. From measurements of the dissociation constant, the free energy of binding can be calculated, and hence the entropy of binding determined. Thus, ITC measurements can determine the complete thermodynamics of protein–DNA binding. This technique could be used to fully characterize the thermodynamics of UDG–DNA (or mutant UDG–DNA) interactions, such as if UDG really can flip dψU substrate mimic nucleotide.

Future Directions

The catalytic power of UDG and its ability to flip a nucleotide from a double helix tempt biochemists to dream of novel uses for this enzyme. Already, in an important proof of concept, UDG has been engineered into a glycosylase that is specific for extra-helical cytosine [247]. It is not hard to imagine that someday glycosylases could be designed to be able to flip a target nucleotide and perform a reaction that would change its coding properties. In fact, the targeting of these engineered glycosylases to DNA sequences could be achieved by linking them to sequence specific zinc fingers as previously accomplished with the restriction endonuclease Fok I [248-250]. Matching DNA sequence specific proteins with a general endonuclease has created chimeras that can stimulate homologous recombination [251] and identify transcription factor binding sites [252]. Site-specific glycosylases designed in the same manner could be able to fix deleterious single nucleotide polymorphisms in vivo. Understanding the function of active site groups and their role in substrate recognition and catalysis is the first step towards a new generation of drugs (enzymes) that fix the disease instead of just alleviating the symptoms.

In hindsight, it seems obvious that an enzyme as old as UDG would be recruited in important roles in other processes, not just DNA repair. In humans, somatic hypermutation of antibody variable domains is accomplished by directed cytosine deamination and recruited UDG (Chapter 1 pg. 9). Several viruses, some of which infect humans, have incorporated UDG into their genomes for roles in mutation avoidance [165, 253], DNA replication and virulence [162, 163, 166, 254], and latency [161]. Thus UDG is not just catalyst, but is also structural cog in the machinery of viruses. Future UDG research not only will focus on the *in vivo* functioning of uracil-initiated base excision

repair, but also the understanding of the other tasks UDG has been recruited to, and those yet to be discovered.

Final Thoughts on the Role of Aromatics in DNA Metabolizing Enzymes

As discussed earlier, many DNA glycosylases contain an active site aromatic group; phenylalanine in many such cases. For example, members of the helix-hairpin-helix family of glycosylases such as Human 3-Methyladenine DNA Glycosylase (homologue to *E. coli* AlkA) sandwich the target damaged base between His and Tyr [237]. Human 8-oxoguanine DNA glycosylase (OGG1) also has an aromatic (Phe319) that stacks with the 8-oxoguanine damage [255]. Amazingly, a stacking phenylalanine is the major direct (and discriminating) contact with the pyrimidine base as visualized in structures of various bound mismatches cocrystallized with MutS glycosylase, a member of the mismatch excision repair pathway [256-258]. Some DNA glycosylases even intercalate an aromatic side chain in between bases of duplex DNA (e.g., Formamidopyrimidine DNA Glycosylase intercalates a Phe [259]) like many other DNA binding and metabolizing enzymes. Why is this common motif not that important to the catalytic function of UDG? Maybe because UDG is such a powerful catalyst taking the Phe out does little to impair it. Car enthusiasts and mechanical engineers know that very small changes, or "tweaks", often can have profound effects on the power generated by combustion engines. UDG is the corvette of glycosylases; nature has tweaked every bit catalytic power it could from this peptide frame. The phenylalanine in the UDG active site might just be a tweak for optimum performance. Yet, other glycosylases that are not as endowed as UDG might show much more catastrophic effects if their active site aromatic group was mutated.

Yet, there is a paradox between the extreme conservation of the active site Phe in Ung family UDGs and conservation in other UDG families, notably MUG, and the mild mutational effect caused by its removal as seen in the F77A mutant. Given this paradox, maybe the role of the active site Phe is to improve the long-term stability of the protein *en vivo*. Or maybe a catalytic enhancement of 2 kcal/mol becomes a strong selective pressure for an enzyme as important to genome stability as UDG. In his review [190] of stereoelectronic effects in enzymatic reactions, Benner states that stereoelectronic effects are often only 1-2 kcal/mol in magnitude, which may be argued is negligible when compared to the 17 kcal/mol (12 orders of magnitude) rate enhancements that are not uncommon in enzymatic reactions. It might be argued that natural selection is unlikely to be influenced by them. On the other hand, if selection-pressure refines the active site quite highly, it may be that "perfect" enzymes will follow stereoelectronic rules that would be lost in the selection "noise" in normal chemical reactions. Uracil DNA glycosylase may just be an example of a perfect enzyme.

Even though the results of this work do not strongly support it, I still believe that the general trend of aromatic base stacking in active sites of DNA metabolizing enzymes (especially glycosylases) hints at an important facet in the substrate specificity and catalysis of these proteins. Hopefully, this work might cause other biochemists to take a second look at these aromatics. Then whether this trend is just a structural convenience, adds to the stability of the protein, or has true mechanistic importance could be revealed.

LIST OF REFERENCES

1. **Benner, S.A. and A.D. Ellington**, *The last ribo-organism.* Nature, 1987. 329(6137): p. 295-6.

2. **Joyce, G.F.**, *The antiquity of RNA-based evolution.* Nature, 2002. 418(6894): p. 214-21.

3. **Zintzaras, E., M. Santos, and E. Szathmary**, *"Living" under the challenge of information decay: the stochastic corrector model vs. hypercycles.* J Theor Biol, 2002. 217(2): p. 167-81.

4. **Dworkin, J.P., A. Lazcano, and S.L. Miller**, *The roads to and from the RNA world.* J Theor Biol, 2003. 222(1): p. 127-34.

5. **White, H.B.I.**, *Evolution of coenzymes and the origin of pyridine nucleotides.*, in *The Pyridine Nucleotide Coenzymes.*, J. Everse, Anderson, B., You, K.-S., Editor. 1982, Academic Press: New York. p. 1–17.

6. **Lazcano, A., R. Guerrero, L. Margulis, and J. Oro**, *The evolutionary transition from RNA to DNA in early cells.* J Mol Evol, 1988. 27(4): p. 283-90.

7. **Benner, S.A., A.D. Ellington, and A. Tauer**, *Modern metabolism as a palimpsest of the RNA world.* Proc Natl Acad Sci U S A, 1989. 86(18): p. 7054-8.

8. **Poole, A., D. Penny, and B.M. Sjoberg**, *Confounded cytosine! Tinkering and the evolution of DNA.* Nat Rev Mol Cell Biol, 2001. 2(2): p. 147-51.

9. **Shapiro, R. and R.S. Klein**, *The deamination of cytidine and cytosine by acidic buffer solutions. Mutagenic implications.* Biochemistry, 1966. 5(7): p. 2358-62.

10. **Mosbaugh, D.W. and S.E. Bennett**, *Uracil-excision DNA repair.* Prog Nucleic Acid Res Mol Biol, 1994. 48: p. 315-70.

11. **Lindahl, T. and B. Nyberg**, *Heat-induced deamination of cytosine residues in deoxyribonucleic acid.* Biochemistry, 1974. 13(16): p. 3405-10.

12. **Ehrlich, M., X.Y. Zhang, and N.M. Inamdar**, *Spontaneous deamination of cytosine and 5-methylcytosine residues in DNA and replacement of 5-methylcytosine residues with cytosine residues.* Mutat Res, 1990. 238(3): p. 277-86.

13. **Lindahl, T.**, *Instability and decay of the primary structure of DNA.* Nature, 1993. 362(6422): p. 709-15.

14. **Frederico, L.A., T.A. Kunkel, and B.R. Shaw**, *A sensitive genetic assay for the detection of cytosine deamination: determination of rate constants and the activation energy.* Biochemistry, 1990. 29(10): p. 2532-7.

15. **Frederico, L.A., T.A. Kunkel, and B.R. Shaw**, *Cytosine deamination in mismatched base pairs.* Biochemistry, 1993. 32(26): p. 6523-30.

16. **Richards, R.G., L.C. Sowers, J. Laszlo, and W.D. Sedwick**, *The occurrence and consequences of deoxyuridine in DNA.* Adv Enzyme Regul, 1984. 22: p. 157-85.

17. **Sowers, L.C., B.R. Shaw, M.L. Veigl, and W.D. Sedwick**, *DNA base modification: ionized base pairs and mutagenesis.* Mutat Res, 1987. 177(2): p. 201-18.

18. **Beletskii, A. and A.S. Bhagwat**, *Correlation between transcription and C to T mutations in the non-transcribed DNA strand.* Biol Chem, 1998. 379(4-5): p. 549-51.

19. **Morey, N.J., C.N. Greene, and S. Jinks-Robertson**, *Genetic analysis of transcription-associated mutation in Saccharomyces cerevisiae.* Genetics, 2000. 154(1): p. 109-20.

20. **Green, P., B. Ewing, W. Miller, P.J. Thomas, and E.D. Green**, *Transcription-associated mutational asymmetry in mammalian evolution.* Nat Genet, 2003. 33(4): p. 514-7.

21. **Sono, M., Y. Wataya, and H. Hayatsu**, *Role of bisulfite in the deamination and the hydrogen isotope exchange of cytidylic acid.* J Am Chem Soc, 1973. 95(14): p. 4745-9.

22. **Chen, H. and B.R. Shaw**, *Kinetics of bisulfite-induced cytosine deamination in single-stranded DNA.* Biochemistry, 1993. 32(14): p. 3535-9.

23. **Lough, J., M. Jackson, R. Morris, and R. Moyer**, *Bisulfite-induced cytosine deamination rates in E. coli SSB:DNA complexes.* Mutat Res, 2001. 478(1-2): p. 191-7.

24. **Murata-Kamiya, N., H. Kamiya, H. Kaji, and H. Kasai**, *Glyoxal, a major product of DNA oxidation, induces mutations at G:C sites on a shuttle vector plasmid replicated in mammalian cells.* Nucleic Acids Res, 1997. 25(10): p. 1897-902.

25. **Murata-Kamiya, N., H. Kamiya, H. Kaji, and H. Kasai**, *Mutational specificity of glyoxal, a product of DNA oxidation, in the lacI gene of wild-type Escherichia coli W3110.* Mutat Res, 1997. 377(2): p. 255-62.

26. **Murata-Kamiya, N., H. Kamiya, H. Kaji, and H. Kasai**, *Methylglyoxal induces G:C to C:G and G:C to T:A transversions in the supF gene on a shuttle vector plasmid replicated in mammalian cells.* Mutat Res, 2000. 468(2): p. 173-82.

27. **Moncada, S., R.M. Palmer, and E.A. Higgs**, *Nitric oxide: physiology, pathophysiology, and pharmacology.* Pharmacol Rev, 1991. 43(2): p. 109-42.

28. **Prior, J.J. and D.V. Santi**, *On the mechanism of the acid-catalyzed hydrolysis of uridine to uracil. Evidence for 6-hydroxy-5,6-dihydrouridine intermediates.* J Biol Chem, 1984. 259(4): p. 2429-34.

29. **Burney, S., J.L. Caulfield, J.C. Niles, J.S. Wishnok, and S.R. Tannenbaum**, *The chemistry of DNA damage from nitric oxide and peroxynitrite.* Mutat Res, 1999. 424(1-2): p. 37-49.

30. **Caulfield, J.L., J.S. Wishnok, and S.R. Tannenbaum**, *Nitric oxide-induced deamination of cytosine and guanine in deoxynucleosides and oligonucleotides.* J Biol Chem, 1998. 273(21): p. 12689-95.

31. **Vigny, J.C.P.**, *Bioorganic Photochemistry*, ed. H. Morrison. Vol. 1. 1990, New York: Wiley. 1.

32. **Rahn, M.H.P.R.O.**, *Photochemistry and Photobiology of Nucleic Acids*, ed. S.Y. Wang. Vol. 2. 1976, New York: Academic Press. 35.

33. **Liu, F.T. and N.C. Yang**, *Photochemistry of cytosine derivatives. 2. Photohydration of cytosine derivatives. Proton magnetic resonance study on the chemical structure and property of photohydrates.* Biochemistry, 1978. 17(23): p. 4877-85.

34. **Boorstein, R.J., T.P. Hilbert, R.P. Cunningham, and G.W. Teebor**, *Formation and stability of repairable pyrimidine photohydrates in DNA.* Biochemistry, 1990. 29(46): p. 10455-60.

35. **Jiang, N. and J.S. Taylor**, *In vivo evidence that UV-induced C-->T mutations at dipyrimidine sites could result from the replicative bypass of cis-syn cyclobutane dimers or their deamination products.* Biochemistry, 1993. 32(2): p. 472-81.

36. **Barak, Y., O. Cohen-Fix, and Z. Livneh**, *Deamination of cytosine-containing pyrimidine photodimers in UV-irradiated DNA. Significance for UV light mutagenesis.* J Biol Chem, 1995. 270(41): p. 24174-9.

37. **Tu, Y., R. Dammann, and G.P. Pfeifer**, *Sequence and time-dependent deamination of cytosine bases in UVB-induced cyclobutane pyrimidine dimers in vivo.* J Mol Biol, 1998. 284(2): p. 297-311.

38. **Glickman, B.W., R.M. Schaaper, W.A. Haseltine, R.L. Dunn, and D.E. Brash**, *The C-C (6-4) UV photoproduct is mutagenic in Escherichia coli.* Proc Natl Acad Sci U S A, 1986. 83(18): p. 6945-9.

39. **Franklin, W.A. and W.A. Haseltine**, *The role of the (6-4) photoproduct in ultraviolet light-induced transition mutations in E. coli.* Mutat Res, 1986. 165(1): p. 1-7.

40. **Horsfall, M.J. and C.W. Lawrence**, *Accuracy of replication past the T-C (6-4) adduct.* J Mol Biol, 1994. 235(2): p. 465-71.

41. **Schaaper, R.M., R.L. Dunn, and B.W. Glickman**, *Mechanisms of ultraviolet-induced mutation. Mutational spectra in the Escherichia coli lacI gene for a wild-type and an excision-repair-deficient strain.* J Mol Biol, 1987. 198(2): p. 187-202.

42. **Horsfall, M.J., A. Borden, and C.W. Lawrence**, *Mutagenic properties of the T-C cyclobutane dimer.* J Bacteriol, 1997. 179(9): p. 2835-9.

43. **Peng, W. and B.R. Shaw**, *Accelerated deamination of cytosine residues in UV-induced cyclobutane pyrimidine dimers leads to CC-->TT transitions.* Biochemistry, 1996. 35(31): p. 10172-81.

44. **Fix, D.F.**, *Thermal resistance of UV-mutagenesis to photoreactivation in E. coli B/r uvrA ung: estimate of activation energy and further analysis.* Mol Gen Genet, 1986. 204(3): p. 452-6.

45. **Hutchinson, F.**, *Induction of tandem-base change mutations.* Mutat Res, 1994. 309(1): p. 11-5.

46. **Burger, A., D. Fix, H. Liu, J. Hays, and R. Bockrath**, *In vivo deamination of cytosine-containing cyclobutane pyrimidine dimers in E. coli: a feasible part of UV-mutagenesis.* Mutat Res, 2003. 522(1-2): p. 145-56.

47. **Shen, J.C., W.M. Rideout, 3rd, and P.A. Jones**, *High frequency mutagenesis by a DNA methyltransferase.* Cell, 1992. 71(7): p. 1073-80.

48. **Ahmad, I. and D.N. Rao**, *Chemistry and biology of DNA methyltransferases.* Crit Rev Biochem Mol Biol, 1996. 31(5-6): p. 361-80.

49. **Zingg, J.M., J.C. Shen, A.S. Yang, H. Rapoport, and P.A. Jones**, *Methylation inhibitors can increase the rate of cytosine deamination by (cytosine-5)-DNA methyltransferase.* Nucleic Acids Res, 1996. 24(16): p. 3267-75.

50. **Zingg, J.M., J.C. Shen, and P.A. Jones**, *Enzyme-mediated cytosine deamination by the bacterial methyltransferase M.MspI.* Biochem J, 1998. 332 (Pt 1): p. 223-30.

51. **Sharath, A.N., E. Weinhold, and A.S. Bhagwat**, *Reviving a dead enzyme: cytosine deaminations promoted by an inactive DNA methyltransferase and an S-adenosylmethionine analogue.* Biochemistry, 2000. 39(47): p. 14611-6.

52. **Shen, J.C., J.M. Zingg, A.S. Yang, C. Schmutte, and P.A. Jones**, *A mutant HpaII methyltransferase functions as a mutator enzyme.* Nucleic Acids Res, 1995. 23(21): p. 4275-82.

53. **Yang, A.S., J.C. Shen, J.M. Zingg, S. Mi, and P.A. Jones**, *HhaI and HpaII DNA methyltransferases bind DNA mismatches, methylate uracil and block DNA repair.* Nucleic Acids Res, 1995. 23(8): p. 1380-7.

54. **Yang, A.S., M.L. Gonzalgo, J.M. Zingg, R.P. Millar, J.D. Buckley, and P.A. Jones**, *The rate of CpG mutation in Alu repetitive elements within the p53 tumor suppressor gene in the primate germline.* J Mol Biol, 1996. 258(2): p. 240-50.

55. **Gonzalgo, M.L. and P.A. Jones**, *Mutagenic and epigenetic effects of DNA methylation.* Mutat Res, 1997. 386(2): p. 107-18.

56. **Faili, A., S. Aoufouchi, Q. Gueranger, C. Zober, A. Leon, B. Bertocci, J.C. Weill, and C.A. Reynaud**, *AID-dependent somatic hypermutation occurs as a DNA single-strand event in the BL2 cell line.* Nat Immunol, 2002. 3(9): p. 815-21.

57. **Harris, R.S., S.K. Petersen-Mahrt, and M.S. Neuberger**, *RNA editing enzyme APOBEC1 and some of its homologs can act as DNA mutators.* Mol Cell, 2002. 10(5): p. 1247-53.

58. **Harris, R.S., J.E. Sale, S.K. Petersen-Mahrt, and M.S. Neuberger**, *AID is essential for immunoglobulin V gene conversion in a cultured B cell line.* Curr Biol, 2002. 12(5): p. 435-8.

59. **Rada, C., G.T. Williams, H. Nilsen, D.E. Barnes, T. Lindahl, and M.S. Neuberger**, *Immunoglobulin isotype switching is inhibited and somatic hypermutation perturbed in UNG-deficient mice.* Curr Biol, 2002. 12(20): p. 1748-55.

60. **Yamanaka, S., K.S. Poksay, M.E. Balestra, G.Q. Zeng, and T.L. Innerarity**, *Cloning and mutagenesis of the rabbit ApoB mRNA editing protein. A zinc motif is essential for catalytic activity, and noncatalytic auxiliary factor(s) of the editing complex are widely distributed.* J Biol Chem, 1994. 269(34): p. 21725-34.

61. **Petersen-Mahrt, S.K. and M.S. Neuberger**, *In vitro deamination of cytosine to uracil in single-stranded DNA by APOBEC1.* J Biol Chem, 2003.

62. **Yamanaka, S., M.E. Balestra, L.D. Ferrell, J. Fan, K.S. Arnold, S. Taylor, J.M. Taylor, and T.L. Innerarity**, *Apolipoprotein B mRNA-editing protein induces hepatocellular carcinoma and dysplasia in transgenic animals.* Proc Natl Acad Sci U S A, 1995. 92(18): p. 8483-7.

63. **Tye, B.K., J. Chien, I.R. Lehman, B.K. Duncan, and H.R. Warner**, *Uracil incorporation: a source of pulse-labeled DNA fragments in the replication of the Escherichia coli chromosome.* Proc Natl Acad Sci U S A, 1978. 75(1): p. 233-7.

64. **Warner, H.R., B.K. Duncan, C. Garrett, and J. Neuhard**, *Synthesis and metabolism of uracil-containing deoxyribonucleic acid in Escherichia coli.* J Bacteriol, 1981. 145(2): p. 687-95.

65. **Dube, D.K., T.A. Kunkel, G. Seal, and L.A. Loeb**, *Distinctive properties of mammalian DNA polymerases.* Biochim Biophys Acta, 1979. 561(2): p. 369-82.

66. **Focher, F., P. Mazzarello, A. Verri, U. Hubscher, and S. Spadari**, *Activity profiles of enzymes that control the uracil incorporation into DNA during neuronal development.* Mutat Res, 1990. 237(2): p. 65-73.

67. **Kunkel, T.A. and L.A. Loeb**, *On the fidelity of DNA replication. Effect of divalent metal ion activators and deoxyrionucleoside triphosphate pools on in vitro mutagenesis.* J Biol Chem, 1979. 254(13): p. 5718-25.

68. **Warner, H.R., R.B. Thompson, T.J. Mozer, and B.K. Duncan**, *The properties of a bacteriophage T5 mutant unable to induce deoxyuridine 5'-triphosphate nucleotidohydrolase. Synthesis of uracil-containing T5 deoxyribonucleic acid.* J Biol Chem, 1979. 254(16): p. 7534-9.

69. **Goulian, M., B. Bleile, and B.Y. Tseng**, *The effect of methotrexate on levels of dUTP in animal cells.* J Biol Chem, 1980. 255(22): p. 10630-7.

70. **Mosbaugh, D.W.**, *Purification and characterization of porcine liver DNA polymerase gamma: utilization of dUTP and dTTP during in vitro DNA synthesis.* Nucleic Acids Res, 1988. 16(12): p. 5645-59.

71. **O'Donovan, G.A., G. Edlin, J.A. Fuchs, J. Neuhard, and E. Thomassen**, *Deoxycytidine triphosphate deaminase: characterization of an Escherichia coli mutant deficient in the enzyme.* J Bacteriol, 1971. 105(2): p. 666-72.

72. **Reichard, P.**, *Interactions between deoxyribonucleotide and DNA synthesis.* Annu Rev Biochem, 1988. 57: p. 349-74.

73. **Rampazzo, C., M. Johansson, L. Gallinaro, P. Ferraro, U. Hellman, A. Karlsson, P. Reichard, and V. Bianchi**, *Mammalian 5'(3')-deoxyribonucleotidase, cDNA cloning, and overexpression of the enzyme in Escherichia coli and mammalian cells.* J Biol Chem, 2000. 275(8): p. 5409-15.

74. **Shlomai, J. and A. Kornberg**, *Deoxyuridine triphosphatase of Escherichia coli. Purification, properties, and use as a reagent to reduce uracil incorporation into DNA.* J Biol Chem, 1978. 253(9): p. 3305-12.

75. **Cedergren-Zeppezauer, E.S., G. Larsson, P.O. Nyman, Z. Dauter, and K.S. Wilson**, *Crystal structure of a dUTPase.* Nature, 1992. 355(6362): p. 740-3.

76. **el-Hajj, H.H., H. Zhang, and B. Weiss**, *Lethality of a dut (deoxyuridine triphosphatase) mutation in Escherichia coli.* J Bacteriol, 1988. 170(3): p. 1069-75.

77. **Tye, B.K., P.O. Nyman, I.R. Lehman, S. Hochhauser, and B. Weiss**, *Transient accumulation of Okazaki fragments as a result of uracil incorporation into nascent DNA.* Proc Natl Acad Sci U S A, 1977. 74(1): p. 154-7.

78. **Warner, H.R. and B.K. Duncan**, *In vivo synthesis and properties of uracil-containing DNA.* Nature, 1978. 272(5648): p. 32-4.

79. **Nilsen, H., I. Rosewell, P. Robins, C.F. Skjelbred, S. Andersen, G. Slupphaug, G. Daly, H.E. Krokan, T. Lindahl, and D.E. Barnes**, *Uracil-DNA glycosylase (UNG)-deficient mice reveal a primary role of the enzyme during DNA replication.* Mol Cell, 2000. 5(6): p. 1059-65.

80. **Adleman, L.M.**, *Computing with DNA.* Scientific American, 1998: p. 54-61.

81. **Nilsen, H. and H.E. Krokan**, *Base excision repair in a network of defence and tolerance.* Carcinogenesis, 2001. 22(7): p. 987-98.

82. **Scharer, O.D. and J. Jiricny**, *Recent progress in the biology, chemistry and structural biology of DNA glycosylases.* Bioessays, 2001. 23(3): p. 270-81.

83. **Memisoglu, A. and L. Samson**, *Base excision repair in yeast and mammals.* Mutat Res, 2000. 451(1-2): p. 39-51.

84. **Lindahl, T.**, *Suppression of spontaneous mutagenesis in human cells by DNA base excision-repair.* Mutat Res, 2000. 462(2-3): p. 129-35.

85. **Krokan, H.E., H. Nilsen, F. Skorpen, M. Otterlei, and G. Slupphaug**, *Base excision repair of DNA in mammalian cells.* FEBS Lett, 2000. 476(1-2): p. 73-7.

86. **Lindahl, T. and R.D. Wood**, *Quality control by DNA repair.* Science, 1999. 286(5446): p. 1897-905.

87. **Marnett, L.J. and J.P. Plastaras**, *Endogenous DNA damage and mutation.* Trends Genet, 2001. 17(4): p. 214-21.

88. **Marnett, L.J., J.N. Riggins, and J.D. West**, *Endogenous generation of reactive oxidants and electrophiles and their reactions with DNA and protein.* J Clin Invest, 2003. 111(5): p. 583-93.

89. **Atamna, H., I. Cheung, and B.N. Ames**, *A method for detecting abasic sites in living cells: age-dependent changes in base excision repair.* Proc Natl Acad Sci U S A, 2000. 97(2): p. 686-91.

90. **Loeb, L.A. and B.D. Preston**, *Mutagenesis by apurinic/apyrimidinic sites.* Annu Rev Genet, 1986. 20: p. 201-30.

91. **Podlutsky, A.J., Dianova, II, S.H. Wilson, V.A. Bohr, and G.L. Dianov**, *DNA synthesis and dRPase activities of polymerase beta are both essential for single-nucleotide patch base excision repair in mammalian cell extracts.* Biochemistry, 2001. 40(3): p. 809-13.

92. **Gros, L., M.K. Saparbaev, and J. Laval**, *Enzymology of the repair of free radicals-induced DNA damage.* Oncogene, 2002. 21(58): p. 8905-25.

93. **Piersen, C.E., A.K. McCullough, and R.S. Lloyd**, *AP lyases and dRPases: commonality of mechanism.* Mutat Res, 2000. 459(1): p. 43-53.

94. **Sandigursky, M., A. Yacoub, M.R. Kelley, Y. Xu, W.A. Franklin, and W.A. Deutsch**, *The yeast 8-oxoguanine DNA glycosylase (Ogg1) contains a DNA deoxyribophosphodiesterase (dRpase) activity.* Nucleic Acids Res, 1997. 25(22): p. 4557-61.

95. **Sobol, R.W., R. Prasad, A. Evenski, A. Baker, X.P. Yang, J.K. Horton, and S.H. Wilson**, *The lyase activity of the DNA repair protein beta-polymerase protects from DNA-damage-induced cytotoxicity.* Nature, 2000. 405(6788): p. 807-10.

96. **Weiss, B.**, *Endonuclease II of Escherichia coli is exonuclease III.* J Biol Chem, 1976. 251(7): p. 1896-901.

97. **Mol, C.D., D.J. Hosfield, and J.A. Tainer**, *Abasic site recognition by two apurinic/apyrimidinic endonuclease families in DNA base excision repair: the 3' ends justify the means.* Mutat Res, 2000. 460(3-4): p. 211-29.

98. **Chan, E. and B. Weiss**, *Endonuclease IV of Escherichia coli is induced by paraquat.* Proc Natl Acad Sci U S A, 1987. 84(10): p. 3189-93.

99. **Weiss, B.**, *Endonuclease V of Escherichia coli prevents mutations from nitrosative deamination during nitrate/nitrite respiration.* Mutat Res, 2001. 461(4): p. 301-9.

100. **Demple, B., T. Herman, and D.S. Chen**, *Cloning and expression of APE, the cDNA encoding the major human apurinic endonuclease: definition of a family of DNA repair enzymes.* Proc Natl Acad Sci U S A, 1991. 88(24): p. 11450-4.

101. **Robson, C.N. and I.D. Hickson**, *Isolation of cDNA clones encoding a human apurinic/apyrimidinic endonuclease that corrects DNA repair and mutagenesis defects in E. coli xth (exonuclease III) mutants.* Nucleic Acids Res, 1991. 19(20): p. 5519-23.

102. **Chen, D.S., T. Herman, and B. Demple**, *Two distinct human DNA diesterases that hydrolyze 3'-blocking deoxyribose fragments from oxidized DNA.* Nucleic Acids Res, 1991. 19(21): p. 5907-14.

103. **Hadi, M.Z. and D.M. Wilson, 3rd**, *Second human protein with homology to the Escherichia coli abasic endonuclease exonuclease III.* Environ Mol Mutagen, 2000. 36(4): p. 312-24.

104. **Lieber, M.R.**, *The FEN-1 family of structure-specific nucleases in eukaryotic DNA replication, recombination and repair.* Bioessays, 1997. 19(3): p. 233-40.

105. **Gary, R., K. Kim, H.L. Cornelius, M.S. Park, and Y. Matsumoto**, *Proliferating cell nuclear antigen facilitates excision in long-patch base excision repair.* J Biol Chem, 1999. 274(7): p. 4354-63.

106. **Dogliotti, E., P. Fortini, B. Pascucci, and E. Parlanti**, *The mechanism of switching among multiple BER pathways.* Prog Nucleic Acid Res Mol Biol, 2001. 68: p. 3-27.

107. **Sandigursky, M., G.A. Freyer, and W.A. Franklin**, *The post-incision steps of the DNA base excision repair pathway in Escherichia coli: studies with a closed circular DNA substrate containing a single U:G base pair.* Nucleic Acids Res, 1998. 26(5): p. 1282-7.

108. **Sung, J.S. and D.W. Mosbaugh**, *Escherichia coli Uracil- and Ethenocytosine-Initiated Base Excision DNA Repair: Rate-Limiting Step and Patch Size Distribution.* Biochemistry, 2003. 42(16): p. 4613-25.

109. **Mohrenweiser, H.W., D.M. Wilson, and I.M. Jones**, *Challenges and complexities in estimating both the functional impact and the disease risk associated with the extensive genetic variation in human DNA repair genes.* Mutat Res, 2003. 526(1-2): p. 93-125.

110. **Fortini, P., B. Pascucci, E. Parlanti, R.W. Sobol, S.H. Wilson, and E. Dogliotti**, *Different DNA polymerases are involved in the short- and long-patch base excision repair in mammalian cells.* Biochemistry, 1998. 37(11): p. 3575-80.

111. **Nash, R.A., K.W. Caldecott, D.E. Barnes, and T. Lindahl**, *XRCC1 protein interacts with one of two distinct forms of DNA ligase III.* Biochemistry, 1997. 36(17): p. 5207-11.

112. **Marintchev, A., A. Robertson, E.K. Dimitriadis, R. Prasad, S.H. Wilson, and G.P. Mullen**, *Domain specific interaction in the XRCC1-DNA polymerase beta complex.* Nucleic Acids Res, 2000. 28(10): p. 2049-59.

113. **Dimitriadis, E.K., R. Prasad, M.K. Vaske, L. Chen, A.E. Tomkinson, M.S. Lewis, and S.H. Wilson**, *Thermodynamics of human DNA ligase I trimerization and association with DNA polymerase beta.* J Biol Chem, 1998. 273(32): p. 20540-50.

114. **Montecucco, A., R. Rossi, D.S. Levin, R. Gary, M.S. Park, T.A. Motycka, G. Ciarrocchi, A. Villa, G. Biamonti, and A.E. Tomkinson**, *DNA ligase I is recruited to sites of DNA replication by an interaction with proliferating cell nuclear antigen: identification of a common targeting mechanism for the assembly of replication factories.* Embo J, 1998. 17(13): p. 3786-95.

115. **Bennett, R.A., D.M. Wilson, 3rd, D. Wong, and B. Demple**, *Interaction of human apurinic endonuclease and DNA polymerase beta in the base excision repair pathway.* Proc Natl Acad Sci U S A, 1997. 94(14): p. 7166-9.

116. **Sobol, R.W., J.K. Horton, R. Kuhn, H. Gu, R.K. Singhal, R. Prasad, K. Rajewsky, and S.H. Wilson**, *Requirement of mammalian DNA polymerase-beta in base-excision repair.* Nature, 1996. 379(6561): p. 183-6.

117. **Srivastava, D.K., B.J. Berg, R. Prasad, J.T. Molina, W.A. Beard, A.E. Tomkinson, and S.H. Wilson**, *Mammalian abasic site base excision repair. Identification of the reaction sequence and rate-determining steps.* J Biol Chem, 1998. 273(33): p. 21203-9.

118. **Sanderson, R.J., S.E. Bennett, J.S. Sung, and D.W. Mosbaugh**, *Uracil-initiated base excision DNA repair synthesis fidelity in human colon adenocarcinoma LoVo and Escherichia coli cell extracts.* Prog Nucleic Acid Res Mol Biol, 2001. 68: p. 165-88.

119. **Bennett, S.E., J.S. Sung, and D.W. Mosbaugh**, *Fidelity of uracil-initiated base excision DNA repair in DNA polymerase beta-proficient and -deficient mouse embryonic fibroblast cell extracts.* J Biol Chem, 2001. 276(45): p. 42588-600.

120. **Pascucci, B., G. Maga, U. Hubscher, M. Bjoras, E. Seeberg, I.D. Hickson, G. Villani, C. Giordano, L. Cellai, and E. Dogliotti**, *Reconstitution of the base excision repair pathway for 7,8-dihydro-8-oxoguanine with purified human proteins.* Nucleic Acids Res, 2002. 30(10): p. 2124-30.

121. **Sattler, U., P. Frit, B. Salles, and P. Calsou**, *Long-patch DNA repair synthesis during base excision repair in mammalian cells.* EMBO Rep, 2003. 4(4): p. 1-5.

122. **Sung, J.S., S.E. Bennett, and D.W. Mosbaugh**, *Fidelity of uracil-initiated base excision DNA repair in Escherichia coli cell extracts.* J Biol Chem, 2001. 276(3): p. 2276-85.

123. **Jiricny, J. and M. Nystrom-Lahti**, *Mismatch repair defects in cancer.* Curr Opin Genet Dev, 2000. 10(2): p. 157-61.

124. **Osheroff, W.P., H.K. Jung, W.A. Beard, S.H. Wilson, and T.A. Kunkel**, *The fidelity of DNA polymerase beta during distributive and processive DNA synthesis.* J Biol Chem, 1999. 274(6): p. 3642-50.

125. **Nilsen, H., T. Lindahl, and A. Verreault**, *DNA base excision repair of uracil residues in reconstituted nucleosome core particles.* Embo J, 2002. 21(21): p. 5943-52.

126. **Lindahl, T.**, *An N-glycosidase from Escherichia coli that releases free uracil from DNA containing deaminated cytosine residues.* Proc Natl Acad Sci U S A, 1974. 71(9): p. 3649-53.

127. **Chung, J.H., E.K. Im, H.Y. Park, J.H. Kwon, S. Lee, J. Oh, K.C. Hwang, J.H. Lee, and Y. Jang**, *A novel uracil-DNA glycosylase family related to the helix-hairpin-helix DNA glycosylase superfamily.* Nucleic Acids Res, 2003. 31(8): p. 2045-55.

128. **Lindahl, T.**, *New class of enzymes acting on damaged DNA.* Nature, 1976. 259(5538): p. 64-6.

129. **Gallinari, P. and J. Jiricny**, *A new class of uracil-DNA glycosylases related to human thymine-DNA glycosylase.* Nature, 1996. 383(6602): p. 735-8.

130. **Haushalter, K.A., M.W. Todd Stukenberg, M.W. Kirschner, and G.L. Verdine**, *Identification of a new uracil-DNA glycosylase family by expression cloning using synthetic inhibitors.* Curr Biol, 1999. 9(4): p. 174-85.

131. **Sandigursky, M. and W.A. Franklin**, *Thermostable uracil-DNA glycosylase from Thermotoga maritima a member of a novel class of DNA repair enzymes.* Curr Biol, 1999. 9(10): p. 531-4.

132. **Sartori, A.A., S. Fitz-Gibbon, H. Yang, J.H. Miller, and J. Jiricny**, *A novel uracil-DNA glycosylase with broad substrate specificity and an unusual active site.* Embo J, 2002. 21(12): p. 3182-91.

133. **Starkuviene, V. and H.J. Fritz**, *A novel type of uracil-DNA glycosylase mediating repair of hydrolytic DNA damage in the extremely thermophilic eubacterium Thermus thermophilus.* Nucleic Acids Res, 2002. 30(10): p. 2097-102.

134. **Parikh, S.S., C.D. Mol, G. Slupphaug, S. Bharati, H.E. Krokan, and J.A. Tainer**, *Base excision repair initiation revealed by crystal structures and binding kinetics of human uracil-DNA glycosylase with DNA.* EMBO J., 1998. 17(17): p. 5214-26.

135. **Putnam, C.D., M.J. Shroyer, A.J. Lundquist, C.D. Mol, A.S. Arvai, D.W. Mosbaugh, and J.A. Tainer**, *Protein mimicry of DNA from crystal structures of the uracil-DNA glycosylase inhibitor protein and its complex with Escherichia coli uracil-DNA glycosylase.* J Mol Biol, 1999. 287(2): p. 331-46.

136. **Aravind, L. and E.V. Koonin**, *The alpha/beta fold uracil DNA glycosylases: a common origin with diverse fates.* Genome Biol, 2000. 1(4): p. 0007.1 - .8.

137. **Pearl, L.H.**, *Structure and function in the uracil-DNA glycosylase superfamily.* Mutat Res, 2000. 460(3-4): p. 165-81.

138. **O'Neill, R.J., O.V. Vorob'eva, H. Shahbakhti, E. Zmuda, A.S. Bhagwat, and G.S. Baldwin**, *Mismatch uracil glycosylase from Escherichia coli: A general mismatch or a specific DNA glycosylase?* J Biol Chem, 2003.

139. **Kavli, B., G. Slupphaug, C.D. Mol, A.S. Arvai, S.B. Peterson, J.A. Tainer, and H.E. Krokan**, *Excision of cytosine and thymine from DNA by mutants of human uracil-DNA glycosylase.* Embo J, 1996. 15(13): p. 3442-7.

140. **Varshney, U. and J.H. van de Sande**, *Specificities and kinetics of uracil excision from uracil-containing DNA oligomers by Escherichia coli uracil DNA glycosylase.* Biochemistry, 1991. 30(16): p. 4055-61.

141. **Werner, R.M. and J.T. Stivers**, *Kinetic isotope effect studies of the reaction catalyzed by uracil DNA glycosylase: evidence for an oxocarbenium ion-uracil anion intermediate.* Biochemistry, 2000. 39(46): p. 14054-64.

142. **Jiang, Y.L., Y. Ichikawa, F. Song, and J.T. Stivers**, *Powering DNA repair through substrate electrostatic interactions.* Biochemistry, 2003. 42(7): p. 1922-9.

143. **Jiang, Y.L. and J.T. Stivers**, *Reconstructing the substrate for uracil DNA glycosylase: tracking the transmission of binding energy in catalysis.* Biochemistry, 2001. 40(25): p. 7710-9.

144. **Liu, P., A. Burdzy, and L.C. Sowers**, *Substrate recognition by a family of uracil-DNA glycosylases: UNG, MUG, and TDG.* Chem Res Toxicol, 2002. 15(8): p. 1001-9.

145. **Ford, A.J.G.a.R.A.**, *The Chemist's Companion: A handbook of Practical Data, Techniques, and References*. 1972, New York: Wiley-Interscience.

146. **Winter, M.**, *WebElements*, http://www.webelements.com/webelements/elements/text/O/radii.html

147. **Hatahet, Z., Y.W. Kow, A.A. Purmal, R.P. Cunningham, and S.S. Wallace**, *New substrates for old enzymes. 5-Hydroxy-2'-deoxycytidine and 5-hydroxy-2'-deoxyuridine are substrates for Escherichia coli endonuclease III and formamidopyrimidine DNA N-glycosylase, while 5-hydroxy-2'-deoxyuridine is a substrate for uracil DNA N-glycosylase.* J Biol Chem, 1994. 269(29): p. 18814-20.

148. **Zastawny, T.H., P.W. Doetsch, and M. Dizdaroglu**, *A novel activity of E. coli uracil DNA N-glycosylase excision of isodialuric acid (5,6-dihydroxyuracil), a major product of oxidative DNA damage, from DNA.* FEBS Lett, 1995. 364(3): p. 255-8.

149. **Dizdaroglu, M., A. Karakaya, P. Jaruga, G. Slupphaug, and H.E. Krokan**, *Novel activities of human uracil DNA N-glycosylase for cytosine-derived products of oxidative DNA damage.* Nucleic Acids Res, 1996. 24(3): p. 418-22.

150. **Verri, A., P. Mazzarello, S. Spadari, and F. Focher**, *Uracil-DNA glycosylases preferentially excise mispaired uracil.* Biochem J, 1992. 287 (Pt 3): p. 1007-10.

151. **Nilsen, H., S.P. Yazdankhah, I. Eftedal, and H.E. Krokan**, *Sequence specificity for removal of uracil from U.A pairs and U.G mismatches by uracil-DNA glycosylase from Escherichia coli, and correlation with mutational hotspots.* FEBS Lett, 1995. 362(2): p. 205-9.

152. **Panayotou, G., T. Brown, T. Barlow, L.H. Pearl, and R. Savva**, *Direct measurement of the substrate preference of uracil-DNA glycosylase.* J Biol Chem, 1998. 273(1): p. 45-50.

153. **Stivers, J.T., K.W. Pankiewicz, and K.A. Watanabe**, *Kinetic mechanism of damage site recognition and uracil flipping by Escherichia coli uracil DNA glycosylase.* Biochemistry, 1999. 38(3): p. 952-63.

154. **Bellamy, S.R.W. and G.S. Baldwin**, *A kinetic analysis of substrate recognition by uracil-DNA glycosylase from herpes simplex virus type 1.* Nucl. Acids. Res., 2001. 29(18): p. 3857-63.

155. **Otterlei, M., E. Warbrick, T.A. Nagelhus, T. Haug, G. Slupphaug, M. Akbari, P.A. Aas, K. Steinsbekk, O. Bakke, and H.E. Krokan**, *Post-replicative base excision repair in replication foci.* Embo J, 1999. 18(13): p. 3834-44.

156. **Lindahl, T., S. Ljungquist, W. Siegert, B. Nyberg, and B. Sperens**, *DNA N-glycosidases: properties of uracil-DNA glycosidase from Escherichia coli.* J Biol Chem, 1977. 252(10): p. 3286-94.

157. **Slupphaug, G., I. Eftedal, B. Kavli, S. Bharati, N.M. Helle, T. Haug, D.W. Levine, and H.E. Krokan**, *Properties of a recombinant human uracil-DNA glycosylase from the UNG gene and evidence that UNG encodes the major uracil-DNA glycosylase.* Biochemistry, 1995. 34(1): p. 128-38.

158. **Drohat, A.C. and J.T. Stivers**, *Escherichia coli uracil DNA glycosylase: NMR characterization of the short hydrogen bond from His187 to uracil O2.* Biochemistry, 2000. 39(39): p. 11865-75.

159. **Jiang, Y.L., Y. Ichikawa, and J.T. Stivers**, *Inhibition of uracil DNA glycosylase by an oxacarbenium ion mimic.* Biochemistry, 2002. 41(22): p. 7116-24.

160. **Bharati, S., H.E. Krokan, L. Kristiansen, M. Otterlei, and G. Slupphaug**, *Human mitochondrial uracil-DNA glycosylase preform (UNG1) is processed to two forms one of which is resistant to inhibition by AP sites.* Nucleic Acids Res, 1998. 26(21): p. 4953-9.

161. **Pyles RB, T.R.**, *Evidence that the herpes simplex virus type 1 uracil DNA glycosylase is required for efficient viral replication and latency in the murine nervous system.* J Virol, 1994. 68(8): p. 4963-72.

162. **Ellison, K.S., W. Peng, and G. McFadden**, *Mutations in active-site residues of the uracil-DNA glycosylase encoded by vaccinia virus are incompatible with virus viability.* Journal Of Virology, 1996. 70(11): p. 7965-73.

163. **Prichard, M., G. Duke, and E. Mocarski**, *Human cytomegalovirus uracil DNA glycosylase is required for the normal temporal regulation of both DNA synthesis and viral replication.* J. Virol., 1996. 70(5): p. 3018-25.

164. **Courcelle, C.T., J. Courcelle, M.N. Prichard, and E.S. Mocarski**, *Requirement for uracil-DNA glycosylase during the transition to late-phase cytomegalovirus DNA replication.* Journal Of Virology, 2001. 75(16): p. 7592-601.

165. **Priet, S., J.M. Navarro, N. Gros, G. Querat, and J. Sire**, *Functional Role of HIV-1 Virion-associated Uracil DNA Glycosylase 2 in the Correction of G:U Mispairs to G:C Pairs.* J Biol Chem, 2003. 278(7): p. 4566-71.

166. **Chen, R., H. Wang, and L.M. Mansky**, *Roles of uracil-DNA glycosylase and dUTPase in virus replication.* J Gen Virol, 2002. 83(Pt 10): p. 2339-45.

167. **Ladner, R.D.**, *The role of dUTPase and uracil-DNA repair in cancer chemotherapy.* Curr Protein Pept Sci, 2001. 2(4): p. 361-70.

168. **Scharer, O.D., H.M. Nash, J. Jiricny, J. Laval, and G.L. Verdine**, *Specific Binding of a Designed Pyrrolidine Abasic Site Analog to Multiple DNA Glycosylases.* J. Biol. Chem., 1998. 273(15): p. 8592-7.

169. **Focher, F., A. Verri, S. Spadari, R. Manservigi, J. Gambino, and G.E. Wright**, *Herpes simplex virus type 1 uracil-DNA glycosylase: isolation and selective inhibition by novel uracil derivatives.* Biochem J, 1993. 292 (Pt 3): p. 883-9.

170. **Sun, H., C. Zhi, G.E. Wright, D. Ubiali, M. Pregnolato, A. Verri, F. Focher, and S. Spadari**, *Molecular modeling and synthesis of inhibitors of herpes simplex virus type 1 uracil-DNA glycosylase.* J Med Chem, 1999. 42(13): p. 2344-50.

171. **Sekino, Y., S.D. Bruner, and G.L. Verdine**, *Selective Inhibition of Herpes Simplex Virus Type-1 Uracil-DNA Glycosylase by Designed Substrate Analogs.* J. Biol. Chem., 2000. 275(47): p. 36506-8.

172. **Marmur, I.T.J.**, *Replacement of thymidylic acid by deoxyuridylic acid in the deoxyribonucleic acid of a transducing phage for Bacillus subtilis.* Nature, 1963. 197: p. 794–5.

173. **Cone, R., T. Bonura, and E.C. Friedberg**, *Inhibitor of uracil-DNA glycosylase induced by bacteriophage PBS2. Purification and preliminary characterization.* J Biol Chem, 1980. 255(21): p. 10354-8.

174. **Wang, Z. and D.W. Mosbaugh**, *Uracil-DNA glycosylase inhibitor gene of bacteriophage PBS2 encodes a binding protein specific for uracil-DNA glycosylase.* J Biol Chem, 1989. 264(2): p. 1163-71.

175. **Wang, Z.G., D.G. Smith, and D.W. Mosbaugh**, *Overproduction and characterization of the uracil-DNA glycosylase inhibitor of bacteriophage PBS2.* Gene, 1991. 99(1): p. 31-7.

176. **Acharya, N., S. Roy, and U. Varshney**, *Mutational analysis of the uracil DNA glycosylase inhibitor protein and its interaction with Escherichia coli uracil DNA glycosylase.* J Mol Biol, 2002. 321(4): p. 579-90.

177. **Handa, P., S. Roy, and U. Varshney**, *The role of leucine 191 of Escherichia coli uracil DNA glycosylase in the formation of a highly stable complex with the substrate mimic, ugi, and in uracil excision from the synthetic substrates.* J Biol Chem, 2001. 276(20): p. 17324-31.

178. **Mol, C.D., A.S. Arvai, G. Slupphaug, B. Kavli, I. Alseth, H.E. Krokan, and J.A. Tainer**, *Crystal structure and mutational analysis of human uracil-DNA glycosylase: structural basis for specificity and catalysis.* Cell, 1995. 80(6): p. 869-78.

179. **Ravishankar, R., M. Bidya Sagar, S. Roy, K. Purnapatre, P. Handa, U. Varshney, and M. Vijayan**, *X-ray analysis of a complex of Escherichia coli uracil DNA glycosylase (EcUDG) with a proteinaceous inhibitor. The structure elucidation of a prokaryotic UDG.* Nucleic Acids Res, 1998. 26(21): p. 4880-7.

180. **Savva, R. and L.H. Pearl**, *Nucleotide mimicry in the crystal structure of the uracil-DNA glycosylase-uracil glycosylase inhibitor protein complex.* Nat Struct Biol, 1995. 2(9): p. 752-7.

181. **Xiao, G., M. Tordova, J. Jagadeesh, A.C. Drohat, J.T. Stivers, and G.L. Gilliland**, *Crystal structure of Escherichia coli uracil DNA glycosylase and its complexes with uracil and glycerol: structure and glycosylase mechanism revisited.* Proteins, 1999. 35(1): p. 13-24.

182. **Savva, R., K. McAuley-Hecht, T. Brown, and L. Pearl**, *The structural basis of specific base-excision repair by uracil-DNA glycosylase.* Nature, 1995. 373(6514): p. 487-93.

183. **Slupphaug, G., C.D. Mol, B. Kavli, A.S. Arvai, H.E. Krokan, and J.A. Tainer**, *A nucleotide-flipping mechanism from the structure of human uracil-DNA glycosylase bound to DNA.* Nature, 1996. 384(6604): p. 87-92.

184. **Klimasauskas, S., S. Kumar, R.J. Roberts, and X. Cheng**, *HhaI methyltransferase flips its target base out of the DNA helix.* Cell, 1994. 76(2): p. 357-69.

185. **Reinisch, K.M., L. Chen, G.L. Verdine, and W.N. Lipscomb**, *The crystal structure of HaeIII methyltransferase convalently complexed to DNA: an extrahelical cytosine and rearranged base pairing.* Cell, 1995. 82(1): p. 143-53.

186. **Mol, C.D., S.S. Parikh, C.D. Putnam, T.P. Lo, and J.A. Tainer**, *DNA repair mechanisms for the recognition and removal of damaged DNA bases.* Annu Rev Biophys Biomol Struct, 1999. 28: p. 101-28.

187. **Parikh, S.S., G. Walcher, G.D. Jones, G. Slupphaug, H.E. Krokan, G.M. Blackburn, and J.A. Tainer**, *Uracil-DNA glycosylase-DNA substrate and product structures: Conformational strain promotes catalytic efficiency by coupled stereoelectronic effects.* PNAS, 2000. 97(10): p. 5083-8.

188. **Kirby, A.J.**, *The Anomeric Effect and Related Stereoelectronic Effects at Oxygen*. 1983, New York: Springer-Verlag.

189. **Banavali, N.K. and A.D. MacKerell, Jr.**, *Reevaluation of stereoelectronic contributions to the conformational properties of the phosphodiester and N3'-phosphoramidate moieties of nucleic acids.* J Am Chem Soc, 2001. 123(28): p. 6747-55.

190. **Benner, S.A.**, *Stereoelectronic Analysis of Enzymatic Reactions*, in *Mechanistic Principles of Enzyme Activity*, J.F. Liebman and A. Greenberg, Editors. 1988, VCH: New York. p. 27–74.

191. **Perrin, C.L.**, *Is there stereoelectronic control in formation and cleavage of tetrahedral intermediates?* Acc Chem Res, 2002. 35(1): p. 28-34.

192. **Dunathan, H.C.**, *Conformation and reaction specificity in pyridoxal phosphate enzymes.* Proc Natl Acad Sci U S A, 1966. 55(4): p. 712-6.

193. **Saikrishnan, K., M. Bidya Sagar, R. Ravishankar, S. Roy, K. Purnapatre, P. Handa, U. Varshney, and M. Vijayan**, *Domain closure and action of uracil DNA glycosylase (UDG): structures of new crystal forms containing the Escherichia coli enzyme and a comparative study of the known structures involving UDG.* Acta Crystallogr D Biol Crystallogr, 2002. 58(Pt 8): p. 1269-76.

194. **Jiang, Y.L. and J.T. Stivers**, *Mutational analysis of the base-flipping mechanism of uracil DNA glycosylase.* Biochemistry, 2002. 41(37): p. 11236-47.

195. **Higley, M. and R.S. Lloyd**, *Processivity of uracil DNA glycosylase.* Mutat Res, 1993. 294(2): p. 109-16.

196. **Bennett, S.E., R.J. Sanderson, and D.W. Mosbaugh**, *Processivity of Escherichia coli and rat liver mitochondrial uracil-DNA glycosylase is affected by NaCl concentration.* Biochemistry, 1995. 34(18): p. 6109-19.

197. **Dong, J., A.C. Drohat, J.T. Stivers, K.W. Pankiewicz, and P.R. Carey**, *Raman spectroscopy of uracil DNA glycosylase-DNA complexes: insights into DNA damage recognition and catalysis.* Biochemistry, 2000. 39(43): p. 13241-50.

198. **Jiang, Y.L., K. Kwon, and J.T. Stivers**, *Turning On Uracil-DNA Glycosylase Using a Pyrene Nucleotide Switch.* J. Biol. Chem., 2001. 276(45): p. 42347-54.

199. **Jiang, Y.L., J.T. Stivers, and F. Song**, *Base-flipping mutations of uracil DNA glycosylase: substrate rescue using a pyrene nucleotide wedge.* Biochemistry, 2002. 41(37): p. 11248-54.

200. **Werner, R.M., Y.L. Jiang, R.G. Gordley, G.J. Jagadeesh, J.E. Ladner, G. Xiao, M. Tordova, G.L. Gilliland, and J.T. Stivers**, *Stressing-out DNA? The contribution of serine-phosphodiester interactions in catalysis by uracil DNA glycosylase.* Biochemistry, 2000. 39(41): p. 12585-94.

201. **Johnson, K.A.**, *Rapid quench kinetic analysis of polymerases, adenosinetriphosphatases, and enzyme intermediates.* Methods Enzymol, 1995. 249: p. 38-61.

202. **Wong, I., A.J. Lundquist, A.S. Bernards, and D.W. Mosbaugh**, *Presteady-state analysis of a single catalytic turnover by Escherichia coli uracil-DNA glycosylase reveals a "pinch-pull-push" mechanism.* J Biol Chem, 2002. 277(22): p. 19424-32.

203. **Schramm, V.L.**, *Enzymatic transition-state analysis and transition-state analogs.* Methods Enzymol, 1999. 308: p. 301-55.

204. **Berti, P.J.**, *Determining transition states from kinetic isotope effects.* Methods Enzymol, 1999. 308: p. 355-97.

205. **Drohat, A.C., G. Xiao, M. Tordova, J. Jagadeesh, K.W. Pankiewicz, K.A. Watanabe, G.L. Gilliland, and J.T. Stivers**, *Heteronuclear NMR and crystallographic studies of wild-type and H187Q Escherichia coli uracil DNA glycosylase: electrophilic catalysis of uracil expulsion by a neutral histidine 187.* Biochemistry, 1999. 38(37): p. 11876-86.

206. **Drohat, A.C., J. Jagadeesh, E. Ferguson, and J.T. Stivers**, *Role of electrophilic and general base catalysis in the mechanism of Escherichia coli uracil DNA glycosylase.* Biochemistry, 1999. 38(37): p. 11866-75.

207. **Jiang, Y.L., A.C. Drohat, Y. Ichikawa, and J.T. Stivers**, *Probing the limits of electrostatic catalysis by uracil DNA glycosylase using transition state mimicry and mutagenesis.* J Biol Chem, 2002. 277(18): p. 15385-92.

208. **Dinner, A.R., G.M. Blackburn, and M. Karplus**, *Uracil-DNA glycosylase acts by substrate autocatalysis.* Nature, 2001. 413(6857): p. 752-5.

209. **Parkin, D.W., B.A. Horenstein, D.R. Abdulah, B. Estupinan, and V.L. Schramm**, *Nucleoside hydrolase from Crithidia fasciculata. Metabolic role, purification, specificity, and kinetic mechanism.* J Biol Chem, 1991. 266(31): p. 20658-65.

210. **Shapiro, R. and S. Kang**, *Uncatalyzed hydrolysis of deoxyuridine, thymidine, and 5-bromodeoxyuridine.* Biochemistry, 1969. 8(5): p. 1806-10.

211. **Goodman, M.F.**, *Hydrogen bonding revisited: geometric selection as a principal determinant of DNA replication fidelity.* Proc Natl Acad Sci U S A, 1997. 94(20): p. 10493-5.

212. **Fix, D.F. and B.W. Glickman**, *Asymmetric cytosine deamination revealed by spontaneous mutational specificity in an Ung- strain of Escherichia coli.* Mol Gen Genet, 1987. 209(1): p. 78-82.

213. **Duncan, B.K. and J.H. Miller**, *Mutagenic deamination of cytosine residues in DNA.* Nature, 1980. 287(5782): p. 560-1.

214. **Duncan, B.K. and B. Weiss**, *Specific mutator effects of ung (uracil-DNA glycosylase) mutations in Escherichia coli.* J Bacteriol, 1982. 151(2): p. 750-5.

215. **Fix, D.F. and B.W. Glickman**, *Differential enhancement of spontaneous transition mutations in the lacI gene of an Ung- strain of Escherichia coli.* Mutat Res, 1986. 175(2): p. 41-5.

216. **Viswanathan, A., J. Liu, and P.W. Doetsch**, *E. coli RNA polymerase bypass of DNA base damage. Mutagenesis at the level of transcription.* Ann N Y Acad Sci, 1999. 870: p. 386-8.

217. **Haug, T., F. Skorpen, P.A. Aas, V. Malm, C. Skjelbred, and H.E. Krokan**, *Regulation of expression of nuclear and mitochondrial forms of human uracil-DNA glycosylase.* Nucleic Acids Res, 1998. 26(6): p. 1449-57.

218. **Nagelhus, T.A., G. Slupphaug, T. Lindmo, and H.E. Krokan**, *Cell cycle regulation and subcellular localization of the major human uracil-DNA glycosylase.* Exp Cell Res, 1995. 220(2): p. 292-7.

219. **Radany, E.H., K.J. Dornfeld, R.J. Sanderson, M.K. Savage, A. Majumdar, M.M. Seidman, and D.W. Mosbaugh**, *Increased spontaneous mutation frequency in human cells expressing the phage PBS2-encoded inhibitor of uracil-DNA glycosylase.* Mutat Res, 2000. 461(1): p. 41-58.

220. **Kavli, B., O. Sundheim, M. Akbari, M. Otterlei, H. Nilsen, F. Skorpen, P.A. Aas, L. Hagen, H.E. Krokan, and G. Slupphaug**, *hUNG2 is the major repair enzyme for removal of uracil from U:A matches, U:G mismatches, and U in single-stranded DNA, with hSMUG1 as a broad specificity backup.* J Biol Chem, 2002. 277(42): p. 39926-36.

221. **Satoh, M.S., C.J. Jones, R.D. Wood, and T. Lindahl**, *DNA excision-repair defect of xeroderma pigmentosum prevents removal of a class of oxygen free radical-induced base lesions.* Proc Natl Acad Sci U S A, 1993. 90(13): p. 6335-9.

222. **Duncan, B.K. and J.A. Chambers**, *The cloning and overproduction of Escherichia coli uracil-DNA glycosylase.* Gene, 1984. 28(2): p. 211-9.

223. **Varshney, U., T. Hutcheon, and J.H. van de Sande**, *Sequence analysis, expression, and conservation of Escherichia coli uracil DNA glycosylase and its gene (ung).* J Biol Chem, 1988. 263(16): p. 7776-84.

224. **Bennett, S.E. and D.W. Mosbaugh**, *Characterization of the Escherichia coli uracil-DNA glycosylase.inhibitor protein complex.* J Biol Chem, 1992. 267(31): p. 22512-21.

225. **Fasman, G.D.**, *Handbook of Biochemistry and Molecular Biology: Nucleic Acids*. 3rd ed, ed. G.D. Fasman. Vol. 1. 1975, Boca Raton, Fl: CRC Press.

226. **Mazumder, A., J.A. Gerlt, M.J. Absalon, J. Stubbe, R.P. Cunningham, J. Withka, and P.H. Bolton**, *Stereochemical studies of the beta-elimination reactions at aldehydic abasic sites in DNA: endonuclease III from Escherichia coli, sodium hydroxide, and Lys-Trp-Lys.* Biochemistry, 1991. 30(4): p. 1119-26.

227. **Johnson, K.A.**, *Transient-state kinetic analysis of enzyme reaction pathways.*, in *The Enzymes*. 1992. p. 1-61.

228. **Lakowicz, J.R.**, *Principles of fluorescence spectroscopy*. 2nd ed. 1999, New York: Plenum Publishers. 10013.

229. **Shroyer, M.J., S.E. Bennett, C.D. Putnam, J.A. Tainer, and D.W. Mosbaugh**, *Mutation of an active site residue in Escherichia coli uracil-DNA glycosylase: effect on DNA binding, uracil inhibition and catalysis.* Biochemistry, 1999. 38(15): p. 4834-45.

230. **Johnson, K.A.**, *Advances in transient-state kinetics.* Curr Opin Biotechnol, 1998. 9(1): p. 87-9.

231. **Stivers, J.T. and A.C. Drohat**, *Uracil DNA Glycosylase: Insights from a Master Catalyst.* Archives of Biochemistry and Biophysics, 2001. 396(1): p. 1-9.

232. **Stivers, J.T. and Y.L. Jiang**, *A mechanistic perspective on the chemistry of DNA repair glycosylases.* Chem Rev, 2003. 103(7): p. 2729-59.

233. **Shan, S.O., S. Loh, and D. Herschlag**, *The energetics of hydrogen bonds in model systems: implications for enzymatic catalysis.* Science, 1996. 272(5258): p. 97-101.

234. **Shan, S.O. and D. Herschlag**, *The change in hydrogen bond strength accompanying charge rearrangement: implications for enzymatic catalysis.* Proc Natl Acad Sci U S A, 1996. 93(25): p. 14474-9.

235. **Czerwinski, R.M., T.K. Harris, M.A. Massiah, A.S. Mildvan, and C.P. Whitman**, *The structural basis for the perturbed pKa of the catalytic base in 4-oxalocrotonate tautomerase: kinetic and structural effects of mutations of Phe-50.* Biochemistry, 2001. 40(7): p. 1984-95.

236. **Mol, C.D., A.S. Arvai, T.J. Begley, R.P. Cunningham, and J.A. Tainer**, *Structure and activity of a thermostable thymine-DNA glycosylase: evidence for base twisting to remove mismatched normal DNA bases.* J Mol Biol, 2002. 315(3): p. 373-84.

237. **Lau, A.Y., M.D. Wyatt, B.J. Glassner, L.D. Samson, and T. Ellenberger**, *Molecular basis for discriminating between normal and damaged bases by the human alkyladenine glycosylase, AAG.* Proc Natl Acad Sci U S A, 2000. 97(25): p. 13573-8.

238. **Hollis, T., Y. Ichikawa, and T. Ellenberger**, *DNA bending and a flip-out mechanism for base excision by the helix-hairpin-helix DNA glycosylase, Escherichia coli AlkA.* Embo J, 2000. 19(4): p. 758-66.

239. **Fedorov, A., W. Shi, G. Kicska, E. Fedorov, P.C. Tyler, R.H. Furneaux, J.C. Hanson, G.J. Gainsford, J.Z. Larese, V.L. Schramm, and S.C. Almo**, *Transition state structure of purine nucleoside phosphorylase and principles of atomic motion in enzymatic catalysis.* Biochemistry, 2001. 40(4): p. 853-60.

240. **Barrett, T.E., O.D. Scharer, R. Savva, T. Brown, J. Jiricny, G.L. Verdine, and L.H. Pearl**, *Crystal structure of a thwarted mismatch glycosylase DNA repair complex.* EMBO J., 1999. 18(23): p. 6599-609.

241. **Luo, N., E. Mehler, and R. Osman**, *Specificity and catalysis of uracil DNA glycosylase. A molecular dynamics study of reactant and product complexes with DNA.* Biochemistry, 1999. 38(29): p. 9209-20.

242. **Purich, D.L.**, *Enzyme catalysis: a new definition accounting for noncovalent substrate- and product-like states.* Trends Biochem Sci, 2001. 26(7): p. 417-21.

243. **Li, Y.K., A. Kuliopulos, A.S. Mildvan, and P. Talalay**, *Environments and mechanistic roles of the tyrosine residues of delta 5-3-ketosteroid isomerase.* Biochemistry, 1993. 32(7): p. 1816-24.

244. **Callis, P.R.**, *1La and 1Lb transitions of tryptophan: applications of theory and experimental observations to fluorescence of proteins.* Methods Enzymol, 1997. 278: p. 113-50.

245. **Vivian, J.T. and P.R. Callis**, *Mechanisms of tryptophan fluorescence shifts in proteins.* Biophys J, 2001. 80(5): p. 2093-109.

246. **Rouviere, N., M. Vincent, C.T. Craescu, and J. Gallay**, *Immunosuppressor binding to the immunophilin FKBP59 affects the local structural dynamics of a surface beta-strand: time-resolved fluorescence study.* Biochemistry, 1997. 36(24): p. 7339-52.

247. **Kwon, K., Y.L. Jiang, and J.T. Stivers**, *Rational engineering of a DNA glycosylase specific for an unnatural Cytosine:pyrene base pair.* Chem Biol, 2003. 10(4): p. 351-9.

248. **Kim, Y.G. and S. Chandrasegaran**, *Chimeric restriction endonuclease.* Proc Natl Acad Sci U S A, 1994. 91(3): p. 883-7.

249. **Chandrasegaran, S. and J. Smith**, *Chimeric restriction enzymes: what is next?* Biol Chem, 1999. 380(7-8): p. 841-8.

250. **Smith, J., M. Bibikova, F.G. Whitby, A.R. Reddy, S. Chandrasegaran, and D. Carroll**, *Requirements for double-strand cleavage by chimeric restriction enzymes with zinc finger DNA-recognition domains.* Nucleic Acids Res, 2000. 28(17): p. 3361-9.

251. **Bibikova, M., D. Carroll, D.J. Segal, J.K. Trautman, J. Smith, Y.G. Kim, and S. Chandrasegaran**, *Stimulation of homologous recombination through targeted cleavage by chimeric nucleases.* Mol Cell Biol, 2001. 21(1): p. 289-97.

252. **Ruminy, P., C. Derambure, S. Chandrasegaran, and J.P. Salier**, *Long-range identification of hepatocyte nuclear factor-3 (FoxA) high and low-affinity binding sites with a chimeric nuclease.* J Mol Biol, 2001. 310(3): p. 523-35.

253. **Pyles, R.B. and R.L. Thompson**, *Mutations in accessory DNA replicating functions alter the relative mutation frequency of herpes simplex virus type 1 strains in cultured murine cells.* Journal Of Virology, 1994. 68(7): p. 4514-24.

254. **De Silva, F.S. and B. Moss**, *Vaccinia virus uracil DNA glycosylase has an essential role in DNA synthesis that is independent of its glycosylase activity: catalytic site mutations reduce virulence but not virus replication in cultured cells.* J Virol, 2003. 77(1): p. 159-66.

255. **Bruner, S.D., D.P. Norman, and G.L. Verdine**, *Structural basis for recognition and repair of the endogenous mutagen 8-oxoguanine in DNA.* Nature, 2000. 403(6772): p. 859-66.

256. **Natrajan, G., M.H. Lamers, J.H. Enzlin, H.H. Winterwerp, A. Perrakis, and T.K. Sixma**, *Structures of Escherichia coli DNA mismatch repair enzyme MutS in complex with different mismatches: a common recognition mode for diverse substrates.* Nucleic Acids Res, 2003. 31(16): p. 4814-21.

257. **Obmolova, G., C. Ban, P. Hsieh, and W. Yang**, *Crystal structures of mismatch repair protein MutS and its complex with a substrate DNA.* Nature, 2000. 407(6805): p. 703-10.

258. **Lamers, M.H., A. Perrakis, J.H. Enzlin, H.H. Winterwerp, N. de Wind, and T.K. Sixma**, *The crystal structure of DNA mismatch repair protein MutS binding to a G x T mismatch.* Nature, 2000. 407(6805): p. 711-7.

259. **Gilboa, R., D.O. Zharkov, G. Golan, A.S. Fernandes, S.E. Gerchman, E. Matz, J.H. Kycia, A.P. Grollman, and G. Shoham**, *Structure of formamidopyrimidine-DNA glycosylase covalently complexed to DNA.* J Biol Chem, 2002. 277(22): p. 19811-6.

BIOGRAPHICAL SKETCH

Ryan Shaw was born on Feb. 21, 1974 in Sandusky, Ohio. He received a B.S. in Chemistry/Biochemistry from Ohio University in 1998. He first attended graduate school at Arizona State University. During his appointment there, he came under the guidance of Dr. Linda Bloom and started his research on Uracil DNA glycosylase. At ASU Ryan was also awarded a fellowship training grant to study the application of biomolecular devices. In the summer of 1999, Ryan moved with Dr. Bloom and her lab to the University of Florida where he finished his doctorate in Biochemistry.